UNIVERSITY OF THE
WITWATERSRAND,
JOHANNESBURG

The Design, Synthesis and Structure-Activity Relationship of Antitubercular Lassomycin Derivatives

Ntombizanele Ngqinayo

Supervisor: Dr. Maya Makatini

DECLARATION

I hereby confirm that the work presented in this thesis is my original work, and to the best of my knowledge, it has not been submitted previously or concurrently for any degree at any other institution. This entire work was conducted by me under the supervision of Dr. Maya Makatini. It is submitted for examination for the degree of Doctor of Philosophy at the University of Witwatersrand

9/11/2023 

DEDICATION

I dedicate this thesis to my parents: my late mom, Bongiswa Olayi Ngqinayo, who had invested in my academic life from the very beginning; and my dad Sabelo Bennedict Ngqinayo, my all-time support system.

ACKNOWLEDGMENTS

First and foremost, I would like to acknowledge and thank my Lord and Saviour Jesus Christ, for carrying, strengthening and sustaining me throughout this process. May Your Name be glorified. Through Him, all things were made possible, and there are not enough words to express my gratitude.

I would like to thank and appreciate my supervisor, Dr. Maya M. Makatini, for going beyond and above for me. You have been my mentor, my supervisor, my support system, and there's nothing you have not done to help me throughout my post-graduate career and personal life. I thank you for helping me when I was on the brink of giving up my PhD. I thank you for all your crucial advice, motivation, financial help, academic help, constructive criticism, and especially your patience with me. You truly have been the best supervisor I could hope for.

I would also like to thank my current and former peptide group colleagues for their input, assistance, friendship, and support: Priscilla Nyembe, Thabo Peme, Sinazo Cobongela, Khanani Machumele, Refilwe Moepya, Thapelo Mbele, and Ntlama Lesotho. I would like to give a special thanks to Thandokuhle Ntombela for taking his time to double-check my work and giving well-thought feedback and constructive criticism.

I would like to apricate the organic group members, including Mudzuli Maphupha, Josephine Maboya, Aneesa Gani, and Nompumelelo Mathebula, for always lending a hand when needed. I thank the Wits School of Chemistry department for academic support and the stores department.

I would like to acknowledge the National Research Foundation (NRF)-DAAD for financial support throughout the years.

Lastly, I would like to thank my family for all their support, patience, and motivation: my dad, Sabelo Bennedict Ngqinayo, and my sisters Nombutho and Thobeko Ngqinayo; and Ntombizodwa Mpthuthi (née Ngqinayo). I would also like to thank my special mom, Poppy E. Mawela, and her late husband for all their support.

ABSTRACT

Tuberculosis (TB) is a potentially fatal infectious disease caused by *Mycobacterium tuberculosis* (*Mtb*) and is a global health risk responsible for over 1.5 million deaths worldwide annually. Tuberculosis is treated with a combinatory regimen of approved first-line drugs such as rifampicin and isoniazid as well as second-line anti-TB drugs such as fluoroquinolones, most of which use similar mechanisms to cause cell death. The formation of multidrug resistance (MDR) TB strains, biofilms, and dormant persister cells (non-replicating cells) are some factors that prolong TB treatment and hence the need for developing novel antitubercular agents with a different mode of action. Furthermore, the emergence of multidrug resistance TB poses a challenge in controlling and eradicating tuberculosis.

Lassomycin is a novel antimicrobial peptide (AMP) that has garnered much interest across various research groups due to its ability to effectively target and kill *Mtb,* including MDR strains and latent TB, with a potency that is similar to that of rifampicin. Lassomycin is highly basic and targets the highly acidic *N*-terminal domain (NTD) of the caseinolytic enzyme that forms part of the caseinolytic protease crucial for *Mtb* cell survival. Lassomycin has an unusual mode of action that causes *Mtb* cell death by disrupting the highly controlled and tightly regulated proteolysis by inhibiting proteolytic activities as well as increasing unfoldase activities. Thus, lassomycin shows great potential as a candidate for drug development.

This study aimed to design lassomycin derivatives with improved stability and potency; and synthesize them using shorter and cost-effective synthetic routes. Peptide modifications includes **(i)** replacing the macrolactam ring in the peptide sequence with a disulfide bridge via a simpler ring-formation method resulting in an enlarged cyclic ring; **(ii)** replacing 'difficult' arginine residues with less basic lysine residues; **(iii)** forming cationic derivatives by increasing the number of basic lysine residues to enhance selectivity for the bacterial membrane; **(iv)** conjugating peptide derivatives to lipophilic molecules including palmitic acid and 1-adamantane carboxylic acid to improve bacterial cell penetration and binding; **(v)** conjugating the peptides to silver nanoparticles for improved drug delivery and antimicrobial effect; **(vi)** incorporating *N*-methylated residues to improve peptide stability; **(vii)** making non-polar peptide derivatives by replacing all basic amino acids with alanine to investigate the importance of the basic residues and study structure activity relationship (SAR) **(viii)**

synthesizing linear derivatives in order to investigate the effect of the ring and (**ix**) shortening the peptide sequences to include only the cyclic ring or the tail sequence portions in order to shorten the synthetic route.

Peptides were synthesized via the Fluorenylmethyloxycarbonyl (Fmoc) solid phase peptide synthesis strategy (SPPS) and purified using a semi-preparative High-Performance Liquid Chromatogram (prep-HPLC). They were then analysed using High-Performance Liquid Chromatography Mass Spectrometry (HPLC-MS), Circular Dichroism (CD), and nuclear magnetic resonance (NMR) spectroscopy. Silver nanoparticles and the peptide conjugates were characterized using ultraviolet-visible (UV-Vis) spectrophotometry and transmission electron microscopy (TEM) imaging. Two-dimensional (2D) Nuclear magnetic resonance (NMR) spectroscopy, including [^{1}H, ^{1}H] COSY, [^{1}H, ^{1}H] TOCSY, [^{1}H, ^{13}C] HSQC, [^{1}H, ^{1}H] HMBC and [^{1}H, ^{1}H] ROESY were used to determine the structural conformation of Pep-2-NN, a lassomycin derivative that has activity against tuberculosis. Furthermore, the secondary structure of selected derivatives was examined using circular dichroism (CD) spectroscopy. Computational studies were utilized to determine the structure of the active lassomycin derivatives, Pep-2-NN and Pep-2-NNA.

All the peptide derivatives were successfully synthesized, including non-polar, short-chained, and those conjugated to silver nanoparticles and lipophilic molecules. The disulfide bridge was successfully added to replace the lactam bridge of the parent lassomycin peptide by oxidising sidechain thiol groups of two cysteine residues inserted at appropriate positions in the sequences. All the peptides were purified to varying degrees of success, and their behaviour was analysed to investigate structure-activity relationships. The silver nanoparticles were successfully synthesized in-house and conjugated to Pep-2-NN. Transmission Electron Microscopy (TEM) imaging revealed that the silver nanoparticles have a spherical morphology at sizes that ranged between 7 nm and 9 nm whilst peptide conjugated nanoparticles were between 9 – 12 nm.

Caseinolytic protease (ClpP1P2 or ClpP) assay studies revealed that the peptides display inhibiting and activating properties when screened against the protease, including lassomycin derivatives with shortened chains such as Ring-2-NNA-Ada, Ring-2-NN, and Tail-2-NN.

The secondary structure of selected lassomycin derivatives was studied using circular dichroism (CD), revealing that the structures are comprised of anti-parallel beta- (β) sheets at slightly higher proportions followed by alpha- (α) helix and, to some extent, β-turn motif.

Computational studies were conducted on selected derivatives to predict their secondary structure and revealed that the peptides form stable α-helical conformations.

NMR revealed that Pep-2-NN formed a 'knotted' structure, where the tail sequence was threaded inside the cyclic ring with a curved loop, and certain residues in the ring acted as 'steric plugs' to prevent unthreading.

In conclusion, the insertion of the disulfide bridge remains an effective alternative to the lactam bond found originally on lassomycin and can result in the formation of biologically active derivatives with the desired stable 'lasso' conformation.

Keywords: *Lassomycin, tuberculosis, caseinolytic enzyme, ClpC1, Caseinolytic protease, ClpP, silver nanoparticles.*

OUTLINE

Herein, the study is presented in six parts. The first part of the thesis introduces the study and expands on the cause, history, impact, and treatment of tuberculosis. The development of novel anti-tuberculosis agents, including lassomycin, is also tackled and explained in detail. A research article (to be submitted) is presented and discussed in the second part of the thesis, including the synthesis of lassomycin-amide derivatives with various structural modifications, including cationic, non-polar, and N-methylated peptides.

The third and fourth parts of the thesis discuss the conjugation of lassomycin-amide derivatives with large lipophilic moieties such as palmitic acid and 1-adamantane carboxylic acid. High-Performance Liquid Chromatography (HPLC) and Mass Spectrometry (MS) were used to study the behaviour of the derivatives of various chain lengths, including longer-chained peptides (Pep-1-NNA and Pep-2-NNA) and shorter-chained peptides (Ring-2-NN, Ring-2-NNA, and Tail) when conjugated to lipophilic groups. Circular Dichroism (CD) studies were used to determine the secondary structures of the peptide derivatives, which revealed that they are predominantly stabilized by anti-parallel beta sheets, followed by an alpha helix. Lastly, a protease assay study was conducted on the derivatives against the caseinolytic protease (ClpP1P2 or ClpP), revealing that the peptides (Pep-2-NN, Ring-2-NNA-Ada, Tail-2-NN, and Compound X) possess anti-proteolytic activities. Interestingly, Ring-2-NN was able to activate proteolytic activity.

The fifth section discusses the successful synthesis of silver nanoparticles and their conjugation to lassomycin-amide derivative, Pep-2-NN, as well as the use of Transmission electron microscopy (TEM) and Ultraviolet-Visible spectrophotometry techniques for analysis.

Part six explores the use of two-dimensional Nuclear Magnetic Resonance (NMR) spectroscopy techniques for structural elucidation of Pep-2-NN, revealing that the peptide possibly comprises a lasso structure with the tail portion of the sequence threaded inside the ring. Computational studies revealed that Pep-2-NN and Pep-2-NNA peptides were stabilized predominantly by alpha-helical conformation, and the length of the disulfide bond formed in the ring portion to replace the lactam bond found in the natural lassomycin peptide was within the acceptable range. Furthermore, the studies revealed that the C-terminus amino acid (isoleucine) of Pep-2-NN was in close proximity to the phenylalanine of the ring portion, thus suggesting a possible threaded ‘lasso’ conformation.

In conclusion, lassomycin derivatives were successfully synthesized and conjugated to lipophilic acid molecules and silver nanoparticles. Furthermore, lassomycin derivatives demonstrated the ability to kill *Mycobacterium tuberculosis* and possess inhibiting and activating properties against the caseinolytic protease. Also, the structure of Pep-2-NN was shown to be knotted, where the tail is threaded inside the ring. Thus, replacing the lactam bond with a disulfide bridge and the amidation of the C-terminus, in addition to other modifications, does not negatively impact the structure and function of lassomycin.

LIST OF TABLES

LIST OF SCHEMES

LIST OF FIGURES

LIST OF GRAPHS

LIST OF ABBREVIATIONS

AgNPs	Silver nanoparticles
AIDS	Acquired immunodeficiency syndrome
Ala	Alanine
AMP	Antimicrobial peptide
Arg	Arginine
Asn	Asparagine
Asp	Aspartic acid
ATPase	Adenosine triphosphatase
B. subtilis	*Bacillus subtilis*
BCG	Bacille Calmette-Guérin
CDC	Centers for Disease Control and Prevention
Clp	Caseinolytic protease complex
ClpC1	Caseinolytic enzyme
ClpP1P2 or ClpP	Caseinolytic protease
COSY	COrrelated SpectroscopY
COVID-19	Corona virus disease-2019
Cys	Cysteine
DCM	Dichloromethane
DIC	*N, N′*-Diisopropylcarbodiimide
Dipea	*N, N*-Diisopropylethylamine
DMF	Dimethylformamide
DMSO	Dimethylsulfoxide
EDT	1,2-Ethanedithiol
Fmoc	Fluorenylmethyloxycarbonyl
Gln	Glutamine
Gly	Glycine
HATU	Hexafluorophosphate Azabenzotriazole Tetramethyl Uronium
HBCs	High burden countries
HBTU	2-(1H-benzotriazole-1-yl)-1,1,3,3-tetramethyluronium hexafluorophosphate
HIV	Human Immuno-deficiency Virus

HMBC	Heteronuclear Multiple Bond Correlation
HOBt	Hydroxybenzotriazole
HPLC	High-Performance Liquid Chromatography
HSQC	Heteronuclear Single Quantum Coherence
Ile	Isoluecine
Leu	Leucine
LMICs	Low-to-middle income countries
Lys	Lysine
MBHA	4-methylbenzhydrylamine
MDR	Multidrug resistance
MIC	Minimum inhibitory concentration
Mtb	*Mycobacterium tuberculosis*
NMR	Nuclear Magnetic Resonance spectroscopy
NOE	Nuclear Overhauser Effect
NOESY	Nuclear Overhauser Effect Spectroscopy
NTD	*N*-terminal domain
Oxyma Pure	ethyl (hydroxyimino)cyanoacetate
Phe	Phenylalanine
ROESY	Rotating frame Overhauser Enhancement Spectroscopy
SPPS	Solid Phase Peptide Synthesis
SPR	Surface plasmon resonance
TB	Tuberculosis
TEM	Transmission electron microscopy
TFA	Trifluoroacetic acid
TIS	Triisopropylsilane
TOCSY	Total correlation spectroscopy
UV-Vis	Ultraviolet-Visible
Val	Valine
WHO	World Health Organization
XDR	Extensively drug resistant

TABLE OF CONTENTS

Chapter 1

Introduction

1.1. Background information about tuberculosis

1.1.1. A brief history of tuberculosis

Tuberculosis (TB) is one of the oldest diseases that have been affecting humankind for centuries and has been killing people for at least 9000 years.[1] *Mycobacterium tuberculosis* (*Mtb*) is the causative agent of TB and is believed to have been around for over 150 million years. The origins of *Mtb* are not yet known and were initially thought to have been from *Mycobacterium bovis* (*M. bovis*), which was transferred from domesticated cattle and passed on to humans. However, it was later realized that both *Mtb* and *M. bovis* originated around the same time and possibly from another *mycobacterium* species.

Mtb was discovered by Dr. Robert Koch in 1882, but the evidence of tuberculosis-like infections dates back thousands of years.[2] The first recorded documents about human infection with TB date back to 3300 years (in India) and 2300 years ago (in China),[2-4] furthermore, TB-afflicted skeletons preserved for 4000 years were discovered in Europe and the Middle East.[2, 5] Before the scientific discovery of *Mtb* by Dr. Koch, tuberculosis was referred to as the "king's evil" (or scrofula, cervical tuberculous lymphadenitis) around the Middle Ages, where it was believed healing came from the king's hand touch, which years later graduated to consumption. Consumption was diagnosed form observing symptoms such as wasting away of the body, chest pains and coughing with blood in the sputum.[2]

1.1.2. The transmission, spread, and symptoms of tuberculosis

Tuberculosis is a leading cause of death from a single infectious disease across the world and is caused by *Mycobacterium tuberculosis* (*Mtb*), a highly contagious pathogen that is transmitted primarily through the air from a person who is ill with the disease (active TB).[2-3, 6] TB is transmitted when bacillus-filled droplets are expelled to the air through sneezing and coughing and are inhaled by the next person and settle in the lungs. Moreover, prolonged or

repeated exposure increases the chances of spreading the disease.[7-10] Lungs remain the most commonly affected body organ by TB, and the infection may result in pus-filled cavities and permanent tissue scarring. The lung infection is also referred to as pulmonary TB and is highly contagious.[10-11] Persons with active TB may show symptoms such as coughing blood, chest pains, night sweats, excessive weight loss, and wasting away of muscle that may be caused by malnutrition.[1, 12]

Extra-pulmonary TB (EPTB) develops when the bacillus migrates from the lungs to other body parts, including the skin, kidneys, bones, and brain (TB meningitis) which is the most severe form that affects about 10% of active TB cases and is most common in HIV-infected people and young children.[13] Some of the symptoms of EPTB include personality changes and stroke for spinal and brain TB; the presence of blood in the urine in kidney TB; absences, back pain, and deformities in bones and spinal TB[14]; and lesions in skin TB. EPTB is mostly non-contagious, with a few exceptions, such as when it is located in the oral cavity.[7]

Miliary TB occurs when *Mtb* enters the bloodstream and spreads to other body parts, simultaneously causing infection in multiple sites.[7] Lungs remain the most commonly affected body organ by TB; the infection may result in pus-filled cavities and permanent tissue scarring. The infection in the lungs is highly contagious.[10-11] The damage caused by TB can be devastating and irreversible and often lead to a diminished quality of life. TB with clinical symptoms is also known as active TB.

When a person with a strong immune system is infected with TB, the body can defend itself from *Mtb* invasion by trapping the bacilli inside antibodies which are white blood cells responsible for fighting against infections leading to the development of latent or inactive TB. Individuals infected with latent TB have no clinical symptoms and are non-contagious and do not risk infecting others.[10] Latent TB remains a threat to human life as it may be activated and progress to active TB. The reactivation risk of latent TB and progression to active TB is approximately 5 – 15% and is greatly increased by repetitive and prolonged interactions with a person with active TB and compromise in the immune system, such as becoming ill. TB co-infection with HIV further increases the risk to approximately 30%.[15-16]

Factors that can weaken a person's immune system include smoking, alcohol abuse, and not sleeping properly. Other immune-compromising situations include when the person develops life-threatening illnesses such as cancer or undergoing cancer chemotherapy.

1.1.3. TB statistics

Tuberculosis is a global health concern responsible for an estimated 1.8 billion infections (close to a quarter of the world's population) worldwide and the deaths of over a million people each year, killing 1 person every 21 seconds.[17] In 2022, an estimated 10.6 million people fell ill with TB, and half a million people got infected with resistant TB strains, according to the World Health Organization (WHO). Furthermore, an estimated 1.6 million people succumbed to TB, an increase from 1.5 million in the previous year (2021) attributed to the COVID-19 pandemic. Tuberculosis poses a very serious threat to human life, and as a result, over 4000 people lose their lives every day due to the disease. Tuberculosis is also responsible for causing an estimated 1.2 million children to fall ill annually worldwide.[18] In South Africa, TB remains the leading cause of death and is responsible for the deaths of an estimated 61,000 people, with about 328,000 people who fell ill. South Africa is one of the High TB Burden countries in the world, which mostly comprises low- to middle-income countries for the 2021–2025 period, according to the WHO (2022).[19] According to WHO, TB is an opportunistic infectious disease with a high mortality rate in patients co-infected with Human Immuno-deficiency Virus (HIV) and has resulted in 214,000 deaths in 2022 (a rise from 187,000 in 2021).[19]

1.1.4. High TB-burden countries

Tuberculosis is a poverty-driven disease and mostly impacts the poorest of the poor in impoverished communities. Moreover, a majority of all TB cases (about 90%) and deaths (about 95%) stem from low- to middle-income countries, and these are also referred to as High TB- burden countries (HBCs).[1, 12, 20] The construction of HBCs lists play an important role of directing focus and attention to burdened countries that require assistance in combating TB and the first global list of high TB burden countries was established in 1998.[21] The recently published HBC lists were determined by assessing the global tuberculosis burden data from over 200 countries.[19] South Africa is one of the world's hardest-hit countries that has been listed in all three categories of the HBCs lists, including 'TB,' 'HIV-associated TB (TB/HIV)' and 'multidrug TB (MDR/RR TB)' which were published by WHO's *Global Tuberculosis Report 2022*. The current list of High TB-burden countries is summarized in **Figure 1.1** below. Most impoverished communities are overcrowded and lack medical care resources, and this further exacerbates the spread of TB.[1, 12] Developed

countries are not burdened by TB as demonstrated by their combined incidence of less than 10 cases per 100,000 population per year, which is higher than that of LMICs (combined incidence of 183 cases per 100,000 population per year). Also, wealthier countries can access effective diagnostic measures for rapid detection and effective anti-TB drug treatments.

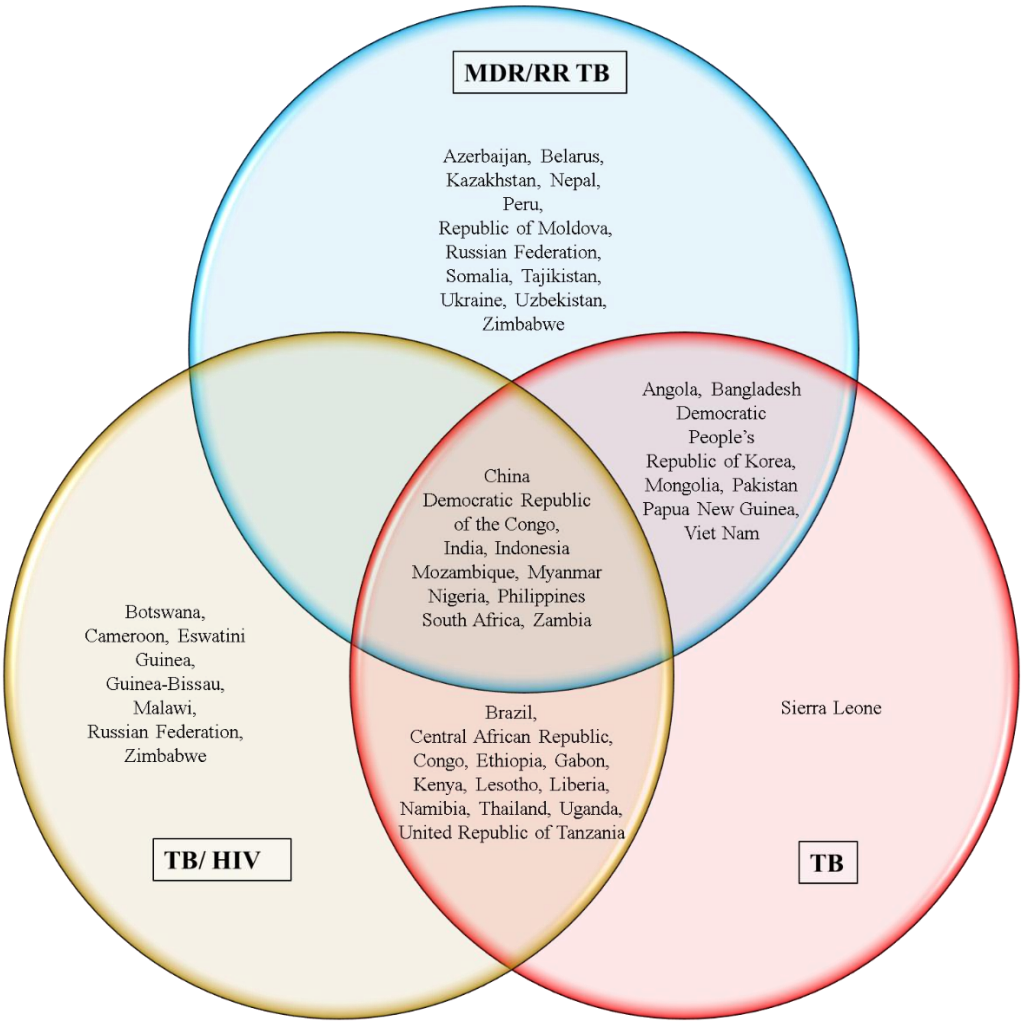

Figure 1.1: A diagram illustrating the lists of countries with a high burden of TB, TB/ HIV, and MDR/RR TB. Some countries like South Africa, India, and China are listed in all three TB burden categories. Data was obtained from the World Health Organization's Global Tuberculosis Report 2022.[21]

1.1.5. The impact of tuberculosis

The impact of tuberculosis on the finances, physical and mental health of the patients

In addition to patients' health, tuberculosis may impact their economic status, mental health, family, and social life. Tuberculosis negatively impacts the patient's quality of life as it

usually results in physical illness and various kinds of body deformities at the site of infection, which may cause the patients to be unable to work, thus resulting in job loss and poverty. TB mostly affects individuals from the most productive group aged between 15 – 49 years.[22-23] Although many countries often provide free TB diagnosis and treatment within public health services, this is usually not enough to ease the financial burden many TB patients and their families face. Furthermore, countries also incur costs when providing medical assistance services and thus rely on importing medication from developed western countries and donations from organizations such as the World Health Organization (WHO). Tuberculosis is a global emergency and has impacted the finances of the global community due to their attempts to eradicate TB. Also, WHO also reported that an extra $1.1 billion is needed every year to invest in developing better drugs and diagnostics and the ultimate eradication of TB.[1] Tuberculosis can also psychologically impact the lives of its victim, such as when they must isolate themselves to stop the spread of the disease, especially to their immediate families. [1] It is reported that TB patients and their families continue to face stigma and discrimination due to their status, and this often leads to feelings of shame, guilt, and resentment resulting in isolation from society.[23]

TB and HIV co-infection and the impact of COVID-19

The human immunodeficiency virus (HIV) and the coronavirus disease 2019 (COVID-19) pandemics have had an enormous negative impact on the control, prevention, and eradication of tuberculosis in varying proportions.

The human immunodeficiency virus weakens the immune system of infected persons and increases the likelihood of TB infection by 18 times and the progression of latent TB to active TB by 30%.[24] Furthermore, TB infection leads to the activation of the immune system, producing chemokine proteins that further stimulate HIV replication in co-infected patients and thus accelerate the progression to Acquired Immuno-deficiency Syndrome (AIDS). At the same time, HIV increases the risk of infection with multidrug-resistant TB strains.[25-27] Thus, HIV and TB are a deadly combination with a synergistic relationship where one disease speeds up the progression of the other, and tuberculosis is the leading cause of death in co-infected persons.[25, 28] The effects of HIV-TB co-infection are exacerbated by lack of patient compliance due to pill burden, cumulative drug toxicity, drug-drug interactions, and communication gaps in HIV and TB treatment programmes.[27] Antiretroviral therapy (ART) is

an effective measure that is used in preventing the progression to active TB in HIV-infected persons in addition to controlling the virus, with several studies reporting a reduction of up to 94% risk of TB infection.[28]

According to the WHO's *Global Tuberculosis Report 2020*, the emergence of the COVID-19 pandemic interrupted and reversed the progress that has been achieved in the fight against tuberculosis by disturbing essential programmes that were put in place to deal with TB.[19, 29] Furthermore, an estimated 10 years of progress in TB was lost due to COVID-19 resulting in a spike in TB incidence and mortality cases in 2021, an increase observed for the first time in years.[1] COVID-19 has also affected the plan to reduce TB mortality and incidence cases by 90% and 80%, respectively, as compared to 2015, through the WHO's End TB Strategy following United Nations (UN) Sustainable Development Goals (SDGs). The COVID-19 pandemic exacerbated TB, overwhelmed national health systems, made it impossible for many patients to receive treatment, and pushed more people into poverty.[16, 30]

1.1.6. The physiology of *Mtb* and the pathogenesis of tuberculosis

Mycobacterium tuberculosis is an aerobic, slow-growing bacteria and a member of the Mycobacterium Tuberculosis Complex (MTC), which are Gram-positive and acid-fast pathogens. Other members of MTC include *Mycobacterium laprae* (*M. laprae*), which causes leprosy, *Mycobacterium bovis* which causes TB in cattle, *Mycobacterium genavense*, *Mycobacterium ulcerans*, *Mycobacterium Africanum*, *Mycobacterium smegmantis* and *Mycobacterium paratuberculosis* amongst others. The *Mycobacterium* genus comprises over 100 closely related species based on their genetic material.[31]

Mycobacteria have irregular and rod-shaped cells with diameters ranging between 0.3 – 0.5 µm, and their cell envelope, which comprises the cell wall and an inner membrane, plays a crucial role in the protection and survival of the cell. The contents of the lipid-rich cell wall of *mycobacteria* include peptidoglycan-arabinogalactan co-polymers that are covalently bound to long-chained mycolic acids, lipids, and pore-forming proteins. Furthermore, the cell wall functions as a highly efficient permeability barrier for the *Mtb* cell.[31] Hence the mycobacterium cell wall and membrane have been a target of most anti-TB agents, especially approved anti-TB drugs.

Mycobacterium tuberculosis is an intracellular pathogen that usually resides and multiplies inside the phagolysosomes of alveolar macrophages, which are white blood cells that target and kill foreign microorganisms in the body and form part of a human's defense system.[9, 32] A person with a healthy immune system can fight off TB infection and prevent *Mtb* from multiplying and spreading through a process known as phagocytosis where the mycobacterium is engulfed and digested by the macrophages resulting in cell death.[9] However, *Mtb* is a highly complex and metabolically flexible pathogen that can evolve and adapt to any environmental change throughout infection, including inside the macrophages where the mycobacterium can remain dormant for years and give rise to latent TB.[1, 9, 31] *Mycobacteria* are opportunistic pathogens, and their detection is crucial to determine the treatment courses to be administered.[31]

1.2. Prevention, diagnosis, and treatment of tuberculosis

Tuberculosis is a preventable and curable disease that may result in death if not treated properly. Accurate and rapid diagnostics, TB preventative measures, and effective treatment are crucial in controlling and eradicating the disease.[33]

1.2.1. The prevention of tuberculosis

There are various measures that can be used to prevent the transmission and spread of tuberculosis, including vaccination, early diagnosis, self-isolation of people with clinically active TB, and receiving proper medical treatment.[33] Covering one's mouth when sneezing and coughing and avoiding overcrowded poor-ventilated areas are also practical actions that can be taken to prevent tuberculosis transmission. It is estimated that only 2.8 million people worldwide received preventive medication in 2020.[1]

Vaccination is considered one of the most powerful tools that can be employed in the prevention of communicable diseases, according to the Centers for Disease Control and Prevention (CDC).[34] Bacillus Calmette-Guerin (BCG) is the only available vaccination for tuberculosis and is unfortunately not good enough to stop the transmission of TB and is reportedly ineffective in adults.[1, 33] BCG is a live-attenuated vaccine of the *mycobacterium bovis* strain that was originally isolated in 1902 from a cow with tuberculosis and cultured for 13 years to generate a mutant strain with a weakened immune system but with high

immunogenicity.[34-36] The safety of BCG administration is a health concern, as vaccination may result in complications and side effects ranging from mild to severe such as hardening, swelling, suppuration, ulceration, and eventually crusting in the injection site, resulting in permanent scarring.[34-35]

Tuberculosis prevention can also be achieved by treating latent TB with a prophylactic treatment method known as Isoniazid prophylaxis therapy (IPT) as an effective measure to prevent the progression of latent TB to active TB.[33] IPT can also be used in combination with ART in persons co-infected with TB and HIV to prevent TB infection.[28, 37] The use of isoniazid, one of the leading anti-TB drugs, as a preventative measures is approved by WHO and is cost-effective with a treatment duration of at least 6 months.[1, 38] Rifampicin can also be used as a prevention therapy against TB, taken daily in a shorter treatment duration of 4 months.[38]

1.2.2. The diagnosis of tuberculosis

Early and rapid diagnosis of tuberculosis with accurate diagnostic measures is imperative to prevent the spread and progression of TB.[39] Despite the advances made thus far in TB diagnostics, there is still a need for rapid, cost-effective, and accurate TB diagnosis techniques, especially in low- to middle-income countries with a high TB burden.[39] Most diagnostic tools currently used for TB detection are considered unreliable and not simple enough, while others are inaccurate.[40] Other drawbacks of currently approved diagnostics include longer turnaround times (the waiting period from testing to receiving results); some devices are expensive, and others require trained medical care providers and complex laboratory facilities.[40] The type of specimen used to test for *Mtb* presence depends on the diagnostic technique used, including skin, sputum, blood, and urine. The cost, life span, and accuracy of a device are important factors to consider for determining the best technique.

Sputum-based TB tests, including smear, culture, and nucleic acid amplification (molecular) tests, are considered primary diagnostics for detecting *Mtb* in active TB cases. Sputum smear microscopy and culture tests are diagnostic tools used to detect acid-fast bacilli in the sputum, a thick mucus found in the lungs, to confirm TB infection. Culture is more sensitive and accurate than sputum smear, which is cost-effective. [39, 41] Sputum smears cannot distinguish between *Mtb* and nontuberculous mycobacteria which results in false positive tests, while

culture tests have longer turnaround times of about 4 weeks and even longer for TB resistance and require expensive equipment and trained medical care staff.[41-42] Several molecular tests such as Xpert MTB/RIF Assay (Cepheid, USA) have been approved by the WHO as first-line diagnostic tools for rapid and accurate detection of TB and resistant TB strains (mostly isoniazid and rifampicin-resistant) to minimize delays in starting appropriate TB treatment.[43-46] Line probe assays are molecular tests that can also detect drug resistance TB.[40, 47]

Other TB diagnostic tools include the tuberculin skin test (TST) technique which involves injecting a small amount of tuberculin into the skin to detect the presence of *Mtb*, whereby a positive TB test is confirmed upon observing swelling around the injection site.[16, 48] The Alere Determine Lipoarabinomannan (LAM) TB test, also known as the AlereLAM, is used to detect *Mtb* in the urine and is recommended for use in HIV-coinfected patients even with low CD4-cell counts.[17] LAM tests detect the mannose-capped lipoarabinomannan (ManLAM), a lipoglycan and a component of the *Mtb* cell wall shed during replication inside a host.[40] Serological tests are blood tests that are used to diagnose TB by detecting the presence of antibodies, however, they have been banned by many countries as they are unreliable due to their inaccuracy.[39] Interferon Gamma Release Assays (IGRAs) also require blood samples for diagnosis, however, they measure T-cell responses to detect the presence of TB, including latent TB, and cannot distinguish between the two tuberculosis forms.[49-50] Lastly, tuberculosis can be diagnosed by radiographical tools, including X-ray imaging plays which detect changes and abnormalities in tissues of different body organs, and this is especially important for extra-pulmonary TB infections.[10] Radiographical techniques that are used to diagnose TB include computer tomography (CT scans), ultrasonography, and magnetic resonance scanning (MRI scans).[10]

1.2.3. Treatment of tuberculosis using approved anti-TB drugs

Tuberculosis is curable, and rapid and effective TB treatment is crucial for controlling and preventing TB transmission.[39-40] New TB cases are treated using first-line anti-TB drugs that include a regimen of rifampicin, isoniazid, ethambutol, and pyrazinamide, which are taken together as a combination for 2 months, followed by a combinatorial intake of isoniazid and rifampicin for the last 4 months. Second-line anti-TB drugs are administered in multidrug-resistant (MDR) TB cases that develop when the *mycobacterium* has mutated and become

unresponsive towards rifampicin and isoniazid. MDR TB cases are more difficult to treat and require longer treatment courses (up to 2 years) with less effective drugs that are more toxic and expensive than first-line drugs.[51] Second-line drugs include a regimen of rifampicin, isoniazid, fluoroquinolones, and injectables, and further development of anti-TB drug treatment resistance leads to the development of extensively drug-resistant (XDR) TB, which is extremely difficult to treat.[47] Anti-TB drug-resistant strains are deadly and are responsible for a quarter of all TB, and unfortunately, the treatment for MDR- and XDR-TB strains have a low success rate of about 50% and 30%, respectively.[39-40] The mechanism of action, side-effects, and the development of drug resistance for first-line and second-line anti-TB drugs are presented in **Table 1.1** and **Table 1.2** below, respectively.

Table 1.1: The mode of action and side effects of first-line anti-TB drugs.

First-line Anti-TB drug	Mode of action, development of drug resistance, and side-effects
Rifampicin	• Rifampicin inhibits deoxyribonucleic acid (DNA), which in turn inhibits the synthesis of messenger ribonucleic acid (RNA) and proteins, thus resulting in cell death.[52-53] • Rifampicin resistance results from gene mutations in the RNA-polymerase. • Can cause hepatic toxicity
Isoniazid	• Isoniazid is activated and forms an adduct that inhibits the synthesis of mycolic acid by binding to a reductase enzyme (InhA) of the *Mtb*.[54] • Isoniazid resistance occurs due to genetic mutations in the katG and InhA enzymes. • Can cause neurotoxicity and hepatic toxicity.[54]
Ethambutol	• Emb targets the arabinosyltransferase enzyme and inhibits the synthesis of the arabinogalactan and thereby increasing cell wall permeability.[52, 55] • Ethambutol resistance occurs due to mutations in the emb gene responsible for coding arabinosyltransferase in the ribosome. • Can cause visual loss.[56]
Pyrazinamide	• Pyrazinamide inhibits processes that regulate the passage of solutes through the cell membrane and can decrease pH to highly acidic levels and thus causing damage to vital enzymes.[57] • When pyrazinamide is included in the first-line regimen, it increases treatment success rates to 95% in 6 months.[57] • TB resistance to pyrazinamide is caused by a genetic mutation in the *pncA* enzyme that is responsible for coding the pyrazinamidase enzyme that is responsible for activating pyrazinamide.[55] • Side effects include an upset gastrointestinal tract.

Table 1.2: Mechanism of second-line anti-TB drugs. [51, 58-59]

Second-line Anti-TB drug	Mode of action and side effects
Levofloxacin (Lfx) or Moxifloxacin (Mfx)	• Levofloxacin and moxifloxacin are fluoroquinolones that target the topoisomerase enzymes responsible for the supercoiling of DNA, where they inhibit DNA transcription and DNA replication.[60] • Side effects are associated with the central nervous system (CNS) and include psychosis, tremor, and convulsions.[61]
Bedaquiline (Bdq)	• Bedaquiline inhibits Adenosine triphosphate (ATP) synthesis, which is crucial for *Mtb* growth and survival in the dormant state.[62]
Linezolid (Lzd)	• Linezolid binds to the 50S ribosome and inhibits protein synthesis.[63] • Side effects may include bone marrow suppression, optic neuritis, and peripheral neuropathy.[40]
Clofazimine (Cfz)	• The mechanism of action of clofazimine involves the destabilization of the *Mtb* membrane and increasing reactive oxidative species, resulting in the deaths of persister cells.[64] • Cfz is effective against rifampicin resistance.[40]
Cycloserine (Cs) or Terizidone ((Trd)	• Cycloserine and its terizidone analogue target and inhibit cell wall synthesis by inhibiting the d-alanine racemase and d-alanine:d-alanine ligase enzymes, which results in the interruption of the peptidoglycan synthesis.[65]
Ethambutol (Emb)	• Ethambutol inhibits the biosynthesis of the cell wall.
Delamanid (Dlm)	• Delamanid is a pro-drug that inhibits the synthesis of *Mtb* cell wall by inhibiting mycolic acid production.[66]
Pyrazinamide (Z)	• Pyrazinamide inhibits processes that regulate the passage of solutes through the cell membrane.
Imipenem-cilastatin (Ipm-Cln) or Meropenem (Mpm)	• Imipenem binds to the penicillin-binding proteins (PBPs) to inhibit cell wall synthesis, while cilastatin prevents the degradation of imipenem in the kidneys.[67]
Amikacin (Am) or Streptomycin (S)	• Amikacin and streptomycin are aminoglycosides that inhibit protein synthesis.[68] • Side effects include ototoxicity (impacting hearing and balance) and nephrotoxicity (leading to rapid deterioration of kidney function).[68]
Ethionamide (Eto) or Prothionamide (Pto)	• Ethionamide and prothionamide are second-line injectables and may be nicotinamide adenine dinucleotide (NAD) biosynthesis inhibitors that inhibit the synthesis of mycolic acids, thus cell wall synthesis.[69-71]
p-aminosalicylic (PAS)	• p-aminosalicylic inhibits folic acid biosynthesis and iron intake.[65]

The mistreatment and inappropriate use of anti-TB drugs by patients, as well as non-compliance due to longer treatment durations and the use of ineffective drugs, greatly contribute to the development of resistant TB strains.[26, 72] Other factors contribute to long treatment duration, the formation of biofilms and persister cells, which are non-dividing, dormant cells with the same genetic makeup as the susceptible cells and are different from drug-resistant strains.[73] Biofilms are best described as mycobacterium cells that have "aggregated to form "bundles".[74] Persisters are formed when a small population of TB cells becomes tolerant and survive treatment with antibiotics and multiply, and they give rise to a new population of TB cells that possess the same susceptibility as the original one when treatment subsides. Persisters are characterized by a significantly lower growth rate that may be due to a global shutdown of processes essential for active cell growth, which increases tolerance towards antibiotics as they may no longer be subjected to inhibition.[72] In comparison to persisters, drug-resistant TB cells are non-responsive towards anti-TB treatment and survive treatment by mutating their genes, giving rise to a population of mutated TB cells with the same genetic modification.[75-76] **Figure 1.2** demonstrates the difference between the formation and persistence of persisters **(A)** and resistant TB cells **(B)**. The development of persisters, biofilms, and TB-resistant forms of TB demonstrates the resilience of *Mtb*, and this shows the complexity and 'intelligence' of tuberculosis and its drive for survival. Thus, TB is a deadly pathogen that needs to be eradicated.

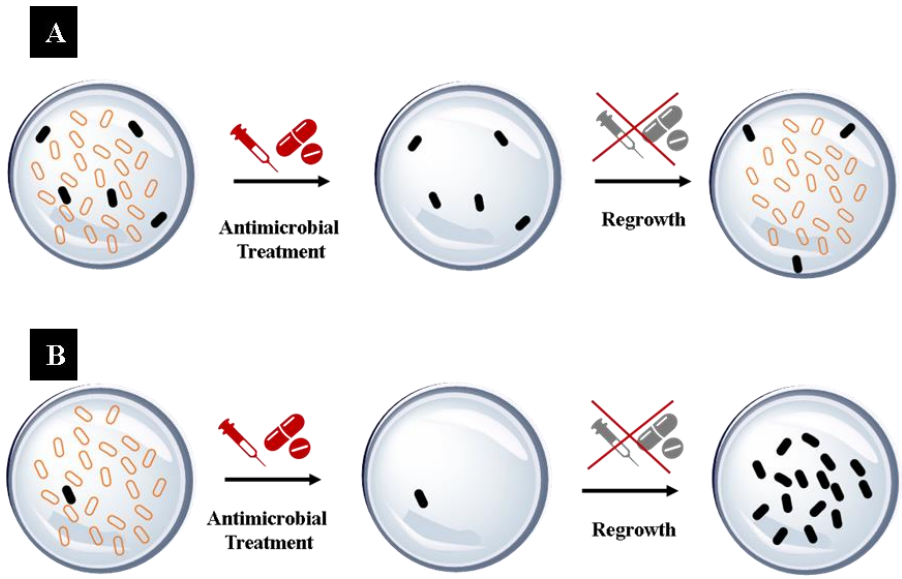

Figure 1.2: The demonstration of the mechanisms of persister cells **(A)** and TB-resistant cells **(B)** after treatment with antibiotics.

Currently, approved anti-TB treatments have not been able to eradicate or control the spread of tuberculosis, and therefore new leads that employ different modes of action are required, and antimicrobial peptides have been considered as a potential alternative source of new antibiotics.[77]

1.3. Antimicrobial peptides as potential antitubercular peptides

The interest in antimicrobial peptides (AMPs) as potential antitubercular leads is due to their attractive properties, such as their ability to kill anti-TB drug-resistance strains. Furthermore, AMPs have a low propensity for the development of drug resistance. Although antibacterial AMPs are the most studied peptides, AMPs are reported to target a wide range of microbial organisms including parasites, viruses, gram-positive and gram-negative bacteria as well as multi-drug resistant bacterial strains.[77-78]The interest in AMPs is driven need and urgency to control the spread of tuberculosis that has been exacerbated by the emergence of multidrug resistance.[79]

Antimicrobial peptides are produced by all life forms, including humans, animals, and microbes, as part of the innate immune system and thus act as the first line of defence against invading pathogens and can stop an infection before it progresses to cause symptoms.[80-81] Antimicrobial peptides usually consist of approximately 10 – 40 amino acid residues in their sequences and are generally cationic with a net positive charge, although some can be negatively charged. Moreover, the conformation of AMPs is stabilized by secondary structure, including alpha helices and beta sheets, which can be altered during their interaction with the cell membranes of their targets .[78, 82]

Contrary to antibiotics which target specific cellular activities such as the cell wall and DNA processes, most antimicrobial peptides are reported to target and cause disruption to the cell membrane of various microorganisms as a primary mechanism of action (membrane-action).[78, 83] However, not all AMPs can cause cell death by targeting the cell membrane as others can pass through the membrane to interact with the components of the cell to cause death.[78] Furthermore, AMPs can also cause cell death by interacting with intracellular components and inhibiting protein synthesis and DNA processes (non-membrane action).

AMPs interact with the bacterial cell envelope through electrostatic interactions with the negatively charged anionic surface of the mycobacterial membrane due to their cationic

nature via their side chains of basic amino acids such as arginine and lysine.[77, 80, 84] Furthermore, the side chains of bulky nonpolar amino acids such as proline and phenylalanine are thought to behave as lipophilic anchors that lead to membrane disruption.[77] This interaction causes the AMPs to accumulate in the bacterial membrane, forming pores, thinning, altered curvature, and modification of cell envelope electrostatics.[80] This action allows for the passage of the peptides into the cytoplasm, where they interact with various intracellular targets, including nucleic acids, enzymes, and organelles.[80]

The cationic nature of antimicrobial peptides causes them to have a low affinity for mammalian cells, which have membranes that are comprised zwitterionic phospholipids that result in a neutral charge.[80, 85] Furthermore, in contrast to microorganisms, mammalian cells have significant cholesterol content, stabilizing the phospholipid bilayer and thus decreasing the activity of AMPs.[78, 80] AMPs are, however, able to interact with mammalian cell membranes through due to weak hydrophobic interactions.[80]

1.3.1. The modification of antimicrobial peptides to improve pharmacological properties

Antimicrobial peptides can be reproduced by chemical synthesis or recombinant expression systems. This allows the peptides to be further designed and easily modified to improve their thermal and enzymatic stability.[78] AMPs are reported to result in a synergetic effect when combined with other antibiotic and delivery systems such as nanoparticles.[78] Despite their attractive properties and advances in peptide research, AMPs still face challenges in their application, such as potential toxicity to humans, susceptibility to proteases, folding issues of some larger peptides and high production costs.[78] In order to successfully design peptides, certain properties such as peptide length, net charge, size, charge, hydrophobicity, amphiphilicity, and solubility are taken into consideration as they play a crucial role in the activities and selectivity of AMPs.[78]

Numerous antimicrobial peptides have been explored and recognised as effective agents that use various mechanisms of action that result in *Mtb* cell death, and the caseinolytic protease of tuberculosis has emerged as a potential target for anti-TB therapeutics.

1.4. Caseinolytic protease complex as a potential antitubercular target

1.4.1. Background information

The caseinolytic protease complex (Clp) plays a crucial role in *Mtb's* survival, including maintaining *Mycobacterium* cells during infection by managing the stressful conditions within a host (such as phagocytosis) and protein quality control. Thus, the protease complex has been explored as a target for new anti-TB agents that utilize a different mechanism of action from currently approved anti-TB drugs. Furthermore, other pathogens, such as *Bacillus subtilis* (*B. subtilis*) and *Listeria monocytogenes* (*L. monocytogenes*) share a similar protease.

1.4.1.1. Role of the caseinolytic protease

The caseinolytic protease complex (Clp) comprises the caseinolytic enzyme (ClpC1) bound to the caseinolytic protease (ClpP1P2 or ClpP), and together they play an important role in protein quality control that involves the degradation of damaged misfolded and non-functional protein substrates. Most bacterial species, including *Escherichia coli*, *Bacillus subtilis*, and *Staphylococcus aureus*, contain the caseinolytic protease complex; however, they are non-essential for cell viability.[86] During this process, the ClpC1 binds to and unfolds substrates linked to a degradation tag and translocates them to the ClpP1P2 degradation chamber for proteolysis in an ATPase-dependent fashion were cleaved into smaller peptides. Furthermore, the resulting peptides are later recycled into functional protein substrates.[86-90] Waste protein degradation is a strictly regulated process to avoid targeting regular and functioning protein substrates, thus keeping the cell well maintained for survival.[86, 91]

ClpP1P2 is made of two heptameric rings of ClpP1 and ClpP2 subunits stacked together to form a tetradecamer that creates a channel housing a serine catalytic site made up of a triad of serine (Ser), histidine (His), and aspartic acid (Asp) residues which are accessible via the axial openings. The Ser residue is responsible for substrate cleavage, while the aspartic acid stabilizes the complex. Proteolysis occurs when the protease is in an extended conformation that forms when an adenosine triphosphate enzyme (ATPase) binds to the protease and when the protease is in a compressed state formed when the serine and histidine residues are further apart, and there is no substrate degradation. ClpC1 binds to the *N*-terminal region of the

ClpP1P2 through hydrophobic pockets. ClpC1 belongs to the AAA+ ATPases superfamily of chaperons in *Mtb* and is responsible for storing and providing the energy needed for substrate degradation. ClpP1P2, which is not bound to ClpC1, cannot degrade protein substrates and can only degrade peptides. The role of the caseinolytic protease complex in waste protein management, as illustrated in **Figure 1.3(a)** below.

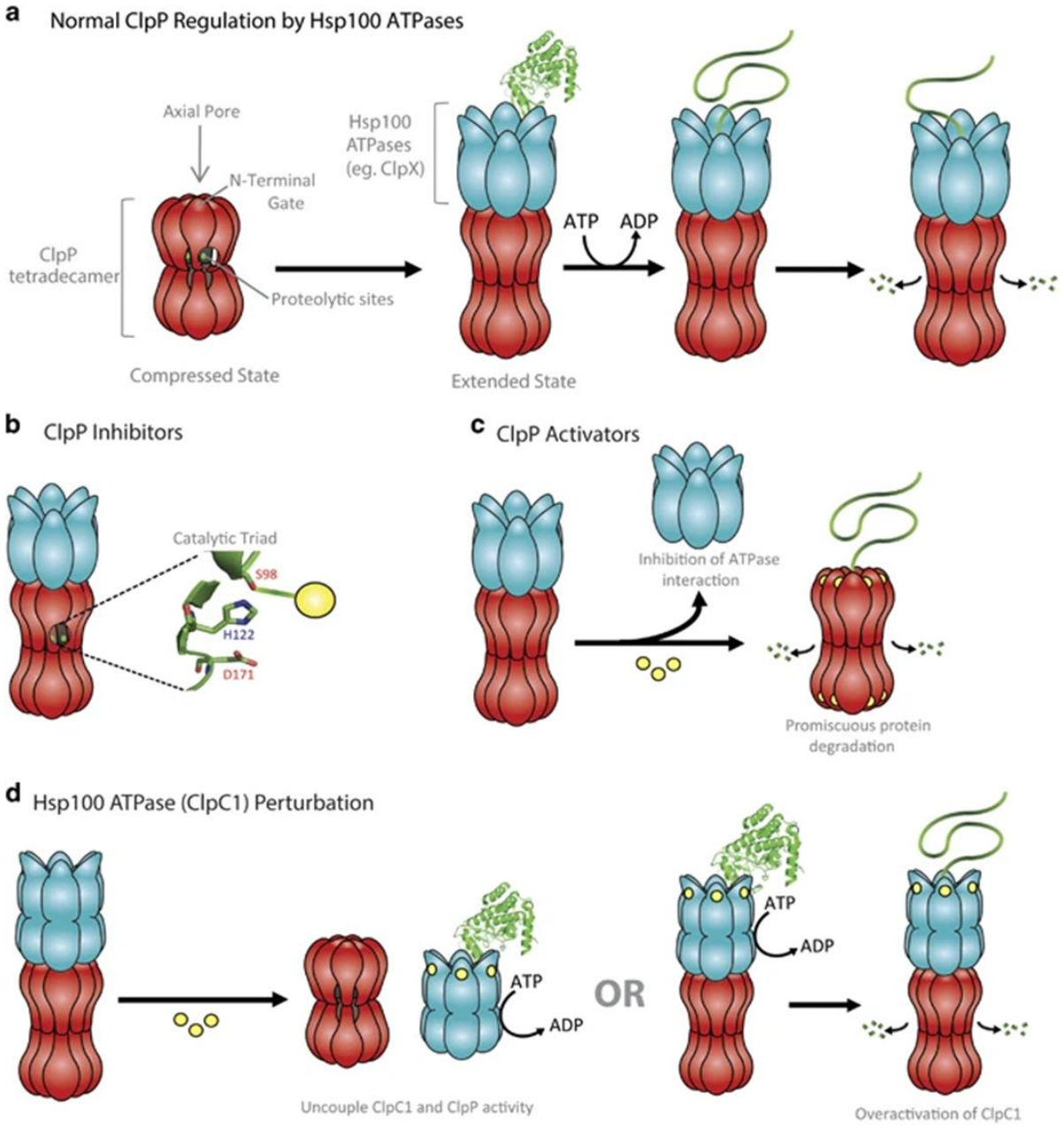

Figure 1.3: The illustration of **(a)** the role of the caseinolytic protease complex in protein degradation of damaged protein substrates in the absence of antitubercular agents and the mechanism of action of inhibitory **(b)**, activating **(c)** and **(d)** ClpC1-targeting molecules. Image is obtained under the Creative Commons Attribution 4.0 International License, CC BY 4.0.

The caseinolytic protease complex has garnered interest as a promising target for new anti-TB drug therapeutics with a different mode of action to currently approved drugs because it plays a crucial role in *Mtb* cell survival. Several anti-TB agents that cause *Mtb* cell death by inhibiting and/or activating the caseinolytic protease activities have been well-reported, and these include antimicrobial peptides, acyldepsipeptides (ADEPs), and Activators of Self-Compartmentalizing Proteases (ACPs).

1.4.1.2. Novel antitubercular agents that target the Clp complex

ClpP activators

Several molecules that target the caseinolytic protease complex and disrupt the tightly regulated proteolytic activities by either inhibiting and/or activating proteolytic activities to cause *Mtb* cell death have been well reported. These include acyldepsipeptides (ADEPs), Activators of Self-Compartmentalizing Proteases (ACPs), and sclerotiamide, which have been termed as ClpP activators as their action results in the activation of the proteolytic activities. The activation of ClpP results in unregulated proteolytic activity that leads to the indiscriminate degradation of protein substrates which can cause cell death in bacterial species that contain essential or non-essential.[86] Furthermore, this approach has been observed as a different mechanism to that of antibiotics whose action usually results in the inhibition of specific processes such as cell wall and protein synthesis. Furthermore, this unusual strategy of activation rather than inhibition may allow drugs to be effective against the development of drug-resistant strains, persister cells, and dormant persister cells that are attributed to the prolonged existence of tuberculosis. This is important since the mycobacterium has adapted and has become resistant to currently approved anti-TB treatments and therefore this offers a new measure to combat TB. ADEPs are a group of closely related compounds produced by a soil bacterium known as *Streptomyces hawaiiensis* NRRL15010.[86] ADEPs kill TB cells by mimicking ClpC1 through binding to the ClpP1P2 active site and activating it for the proteolytic activity, resulting in unregulated and non-selective proteolysis leading to cell death.[86] ADEPs have activity against the ClpP present in *Escherichia coli* (*E. coli*), *B. subtilis,* and *Neisseria meningitides* bacterial pathogens and the difficult-to-kill persister cells. Despite the attractive properties of Clp activators, ADEPs are associated with limitations such as poor water solubility as well as enzymatic and chemical instability, while ACPs and sclerotiamide are less effective than ADEPs.

ClpP inhibitors

Molecules that inhibit ClpP activities, such as the β-lactone inhibitors and phenyl esters, have also been investigated and were found to form covalent adducts with the active site of Clp that results in irreversible inhibition of proteolytic activity.[86] Interestingly, some enantiomers of phenyl esters possess the ability to decouple the ClpP1P2 oligomer into ClpP1 and ClpP2 heptamers and thus prohibit proteolysis.[86] Unfortunately, the molecular structure of β-lactones contains a cyclic ester which causes them to be vulnerable to rapid hydrolysis that results in rapid clearance and short-life, thus limiting their consideration for clinical development.[86, 92]

Molecules that target the caseinolytic enzyme (ClpC1)

The caseinolytic enzyme plays an important role in waste protein degradation since the ClpP depends on the ATPase to select and unfolds damaged substrates for degradation, and in its absence, the protease can only degrade peptides. Therefore, ClpC1 makes an attractive target for anti-TB drug development which can interrupt and deregulate the proteolytic process and cause mycobacterial cell death. Several antimicrobial peptides (AMPs) that target the caseinolytic enzyme have been well-reported over the years, and these were mainly discovered through screening natural extracts for anti-mycobacterium activities. *Mtb* was usually chosen for these studies as it contains ClpC1, essential for cell viability, in contrast to other bacteria that contain non-essential Clp.[86]

Lassomycin, cyclomarin A, and ecumicin are cyclic antimicrobial peptides from actinomycetes that target the acidic region of ClpC1 with high affinity but bind at slightly different sites to cause *Mtb* cell death.[93] Lassomycin reportedly binds to the most acidic region as it is highly basic due to the presence of several basic arginine amino acid residues in its sequence. Moreover, these peptides were active against growing dormant and resistant *Mtb* cells and inactive against mammalian cells.[94] Lassomycin and ecumicin utilize a similar action of inhibiting protein degradation by decoupling ClpC1 from the protease resulting in cytotoxicity due to the accumulation of waste protein while increasing unfoldase (ATPase) activities.[94] However, cyclomarin A has the opposite effect as it activates uncontrollable protein degradation without increasing ATPase activity.[94-95] Rufomycin is a short-chain cyclic peptide that also targets ClpC1 to cause *Mtb* cell death by significantly decreasing proteolytic activity without affecting the unfoldase activity.[91] Optimization of

pharmacological properties of the peptides is required for further development due to limitations such as poor solubility of ecumicin and poor enzymatic stability of cyclomarin A.

The mechanisms of action of the molecules that cause ClpP inhibition or activation and those that target the caseinolytic enzyme are illustrated in **Figure 1.3(b) – (d)** above.

1.5. Lassomycin as a promising anti-TB agent targeting the caseinolytic enzyme (ClpC1)

1.5.1. Background information

Lassomycin (shown in **Figure 1.4a**) is a highly basic, antitubercular peptide that was discovered in 2014 by the Lewis group during a screening process and was found to effectively and selectively target and kill *Mtb* with a potency that is similar to rifampicin, one of the leading anti-TB drugs. [87] Lassomycin is classified as a member of lasso peptides, which are ribosomally synthesized and posttranslationally modified peptides (RiPPs).[96] The structure of lassomycin is unique from other cyclic peptides such as ecumicin and cyclomarin A and is characterized by the threading of the peptide chain (Gln15-Ile16) into the macrolactam ring that is connected via an isopeptide bond formed by the N-terminus Gly1 and Asp8. The constricted structure of lasso peptides reportedly results in increased stability against enzymatic and thermal degradation.[97] Lassomycin is a class II lasso peptide due to the absence of disulfide bridges for structure stabilization, and it, therefore, relies on sterically demanding amino acid residues (also known as 'steric plugs' that hold the threaded C-terminal tail above and below the ring to prevent it from unthreading. The 'steric plugs' for lassomycin are postulated to be Arg13 and Asp15.

Lassomycin is potent against *Mtb*, including the MDR and XDR- resistant TB strains and latent TB with a minimum inhibitory concentration (MIC) range of 0.8 – 3 μg/mL.[87] Lassomycin was found to be active against other mycobacteria, including *Mycobacterium avium* and *Mycobacterium smegmatis*. Lassomycin shows great potential to be considered and developed as a first-line anti-TB drug.

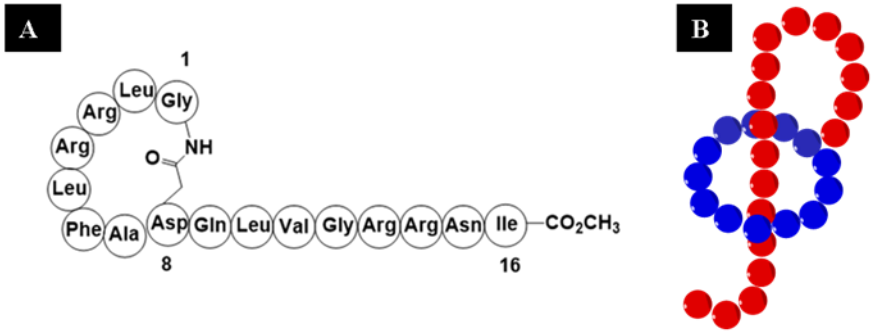

Figure 1.4: The structure of lassomycin showing the amino acid sequence **(A)** and an illustration of the threaded lasso conformation **(B)**.

1.5.2. The biosynthesis of lassomycin

1.5.2.1. General biosynthesis of lasso peptides

According to the literature, the biosynthesis of lasso peptides is not exact for all the peptides but most share similar pathways. In general, the biosynthesis of lasso peptides involves a set pathway with essential gene-encoding components to generate a precursor peptide (A), a gene to encode a cysteine protease (B), and a gene for an ATP-dependent macrolactam synthetase (C).[73] **Figure 1.5** below illustrates the general biosynthetic pathway of lasso peptides. Lassomycin and other lasso peptides, such as the lariatins, further split the B protein into B1 and B2 clusters.[73]Although the biosynthesis of lassomycin is not yet published thus far[73], it is proposed to follow a similar route to that of lariatin.[87]

In order to assemble a folded lasso peptide, a linear precursor peptide consisting of an N-terminal leader region and a C-terminal core to form the structural backbone of peptides is first generated from the ribosome.[98] The B1 protein binds to the leader peptide and is transported to the B2 protein for processing and then transferred to the C protein for assembling to form the mature lasso peptide and remove the leader peptide.[73] The C protein is suggested to be responsible for the formation of the isopeptide bond (macrolactam bridge), and the D protein is responsible for the export of mature lasso peptides.[73] The O-methyltransferase responsible for the C-terminal methylation of lassomycin is located downstream of the ABC transport.[73]

It is suggested that it is highly unlikely that the tail portion of the lasso peptide would thread into the ring before it is cyclized due to steric hindrance, and therefore the tail is suggested to be pre-folded in a manner that would allow the isopeptide bond to form around it.[98]

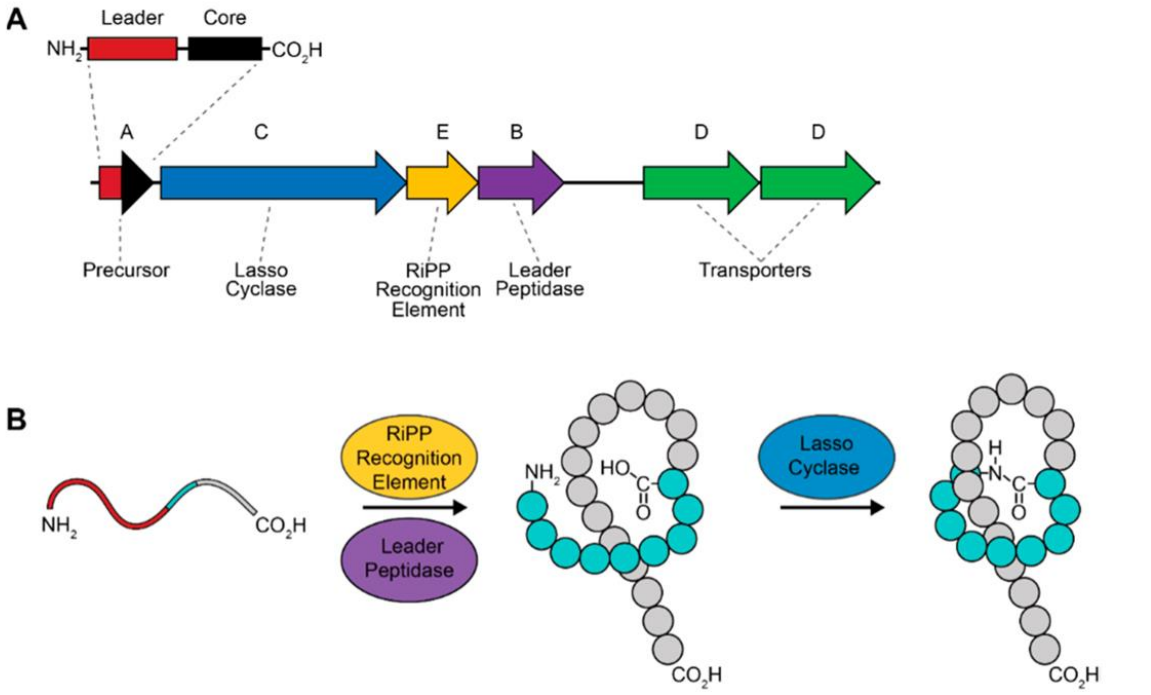

Figure 1.5: Illustrating the general biosynthetic pathway of lasso peptides. Modified Image obtained under the Creative Commons Attribution 4.0 International License, CC BY 4.0.[99]

1.5.2.2. Proposed biosynthetic pathway for lassomycin

It is suggested that lassomycin follows a similar biosynthetic route as lariatin, where the precursor peptide is predicted to be encoded by the *lasA* gene. The proposed route by the Lewis group is presented in **Figure 1.6** below.[100] For lariatin, the precursor peptide is believed to be cleaved by LarD and converted to a mature lasso peptide by LarB, which is then transported by LarE. At the same time, the function of LarC is unknown but is suggested to be important for antibiotic activity.[87] LasF is proposed to be responsible for the formation of the methyl ester on the mature lasso structure of the lassomycin peptide.

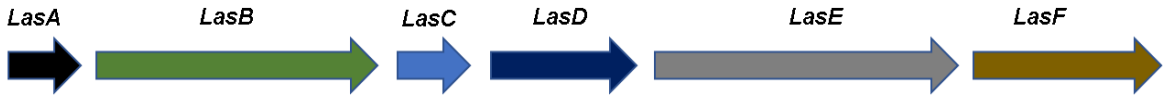

Figure 1.6: The proposed lassomycin biosynthesis pathway.

1.5.3. Lassomycin mechanism of action

Lassomycin binds to the highly acidic region of the N-terminal domain (NTD) of ClpC1, which causes the enzyme to be uncoupled from the ClpP1P2 protease, resulting in the

inhibition of proteolytic activity that leads to cell death. ClpP1P2 that is decoupled from ClpC1 cannot perform substrate degradation processes, resulting in the accumulation of damaged substrates that lead to cytotoxicity. In addition, there is an excessive increase in the unfoldase activity when lassomycin is bound to ClpC1. This is due to uncontrolled and non-selective unfolding of protein substrates that result in loss of function and thus result in cell death.[87-88] Ultimately, lassomycin disrupts the highly regulated and controlled proteolytic activity of the caseinolytic protease complex. As of now (2023), it is unknown which of the two above-mentioned actions by lassomycin, excessive unfoldase activity versus inhibition of proteolysis, is the primary cause of *Mtb* death.

The four arginine residues in the sequence of lassomycin are responsible for the highly basic nature of the peptide and are reported to participate in binding to the acidic region of ClpC1.[94] Also, the docking studies obtained by the Gavrish group revealed that ClpC1 uses glutamine (Gln17) to interact with lassomycin through hydrogen bonding and is necessary for binding.[86, 100] Also, lassomycin binds allosterically to ClpC1 since the protein can unfold the protein substrates in the presence of the peptide.

The nature of lassomycin, its potency, and its highly unusual mode of action show that lassomycin has the potential to be further developed into a potent anti-TB drug that can play a role in combating TB. Unfortunately, even though lassomycin was discovered about 8 years ago, there has been limited published research about its chemical synthesis of lassomycin and derivatives. This has led to hiatus in further advancement in related work. A couple of research groups that attempted to synthesize lassomycin and its derivatives have reported challenges reproducing the peptide, which resulted in extremely low bactericidal activity against *Mtb* and no potency in some instances. The reported loss of activity may have been due to the absence of the characteristic lasso structure in the peptides.[101]

1.6. Way forward

The discovery of lassomycin received significant attention as a novel antitubercular peptide displaying an unusual mode of action to target and kill TB, including the latent and tolerant forms and resistant TB strains. Lassomycin, therefore, has the potential to be developed into a first-line anti-TB drug for TB treatment, control, and eradication. Unfortunately, many AMPs

display clinically unfavourable properties, including relatively high inhibitory concentrations, sensitivity to salts, and cytotoxicity effects.[77]

1.7. Aim and objectives

1.7.1. Aim

The project aim was to design and synthesize novel lassomycin derivatives to target the caseinolytic enzyme and inhibit its protease activities.

1.7.2. Objectives

- To shorten the synthetic route by replacing the lactam bridge with a disulfide bridge.
- To investigate the importance of the basic residues by replacing the basic amino acids with alanine.
- To reduce the synthesis cost by shortening the peptide sequences and synthesizing only the cyclic ring or the tail part of the peptide.
- To increase the cell membrane penetration of the lassomycin by attaching highly lipophilic moieties such as adamantane and palmitic acid.
- To investigate the effect of the cyclic ring by synthesizing non-cyclized peptides without the disulfide bridge.
- To employ nuclear magnetic resonance (NMR) spectroscopy to determine the structure of active lassomycin derivatives.
- To conjugate lassomycin derivatives to metallic nanoparticles in order to improve potency.

1.8. Hypothesis

Lassomycin shows noticeable antibiotic activity against *Mtb*. Until now, several research groups that have attempted to synthesize the peptide and its derivatives have reported a loss of activity against TB cells and unthreaded structural conformations. Lassomycin derivatives such as Pep-2-NN that were synthesized in-house during a Master's degree study (2019) showed promising activity that was comparable to the activity of the commercially available ethambutol. The substitution of the lactam bridge and arginine residues with the disulfide bridge and lysine residues, respectively in Pep-2-NN, may have improved the potency of the peptide. The disulfide bridge is formed after the synthesis of the whole peptide chain like in nature while during the chemical synthesis of the lactam bridge in the lab the bridge is formed first and then the tail portion of the peptide is added. This restricts the number of conformations that can form.

Hence we hypothesize that introduction of the disulfide bridge enables the peptides to assume the threaded conformation which is necessary for biological activity. The structural elucidation study of Pep-2-NN will provide information about the conformation of the chemically synthesized active peptide structures, which will be used to determine structure activity relationship.

References

1. Moutinho, S., The Oldest Pandemic. *Scientific American* **2022,** *326* (6), S16-S20.

2. Jordao, L.; Vieira, O. V., Tuberculosis: new aspects of an old disease. *International Journal of Cell Biology* **2011,** *2011*.

3. Barberis, I.; Bragazzi, N. L.; Galluzzo, L.; Martini, M., The history of tuberculosis: from the first historical records to the isolation of Koch's bacillus. *Journal of Preventive Medicine and Hygiene* **2017,** *58* (1), E9.

4. Lin, P. L.; Pawar, S.; Myers, A.; Pegu, A.; Fuhrman, C.; Reinhart, T. A.; Capuano, S. V.; Klein, E.; Flynn, J. L., Early events in Mycobacterium tuberculosis infection in cynomolgus macaques. *Infection and Immunity* **2006,** *74* (7), 3790-3803.

5. Smith, I., Mycobacterium tuberculosis pathogenesis and molecular determinants of virulence. *Clinical Microbiology Reviews* **2003,** *16* (3), 463-496.

6. Ducati, R. G.; Ruffino-Netto, A.; Basso, L. A.; Santos, D. S., The resumption of consumption: a review on tuberculosis. *Memórias do Instituto Oswaldo Cruz* **2006,** *101*, 697-714.

7. https://www.cdc.gov/tb/education/corecurr/pdf/chapter2.pdf (accessed 20 January 2023).

8. Fogel, N., Tuberculosis: a disease without boundaries. *Tuberculosis* **2015,** *95* (5), 527-531.

9. Schäfer, G.; Jacobs, M.; Wilkinson, R. J.; Brown, G. D., Non-opsonic recognition of Mycobacterium tuberculosis by phagocytes. *Journal of Innate Immunity* **2009,** *1* (3), 231-243.

10. Alshoabi, S. A.; Almas, K. M.; Aldofri, S. A.; Hamid, A. M.; Alhazmi, F. H.; Alsharif, W. M.; Abdulaal, O. M.; Qurashi, A. A.; Aloufi, K. M.; Alsultan, K. D., The Diagnostic Deceiver: Radiological Pictorial Review of Tuberculosis. *Diagnostics* **2022,** *12* (2), 306.

11. Hanekom, S.; Pharaoh, H.; Irusen, E.; Daniels, K. J., Post-tuberculosis health-related quality of life, lung function and exercise capacity in a cured pulmonary tuberculosis population in the Breede Valley District, South Africa. *South African Journal of Physiotherapy* **2019,** *75* (1), 1-8.

12. Gupta, K. B.; Gupta, R.; Atreja, A.; Verma, M.; Vishvkarma, S., Tuberculosis and nutrition. *Lung India: official organ of Indian Chest Society* **2009,** *26* (1), 9.

13. Bourgi, K.; Fiske, C.; Sterling, T. R., Tuberculosis meningitis. *Current Infectious Disease Reports* **2017,** *19* (11), 1-9.

14. Leonard Jr, M. K.; Blumberg, H. M., Musculoskeletal tuberculosis. *Microbiology spectrum* **2017,** *5* (2), 28.

15. Kiazyk, S.; Ball, T., Tuberculosis (TB): Latent tuberculosis infection: An overview. *Canada Communicable Disease Report* **2017,** *43* (3-4), 62.

16. Sharma, S. K.; Mohanan, S.; Sharma, A., Relevance of latent TB infection in areas of high TB prevalence. *Chest* **2012,** *142* (3), 761-773.

17. García, J. I.; Kelley, H. V.; Meléndez, J.; de León, R. A. A.; Castillo, A.; Sidiki, S.; Yusoof, K. A.; Nunes, E.; Téllez, C. L.; Mejía-Villatoro, C. R., Improved Alere Determine Lipoarabinomannan Antigen Detection Test for the diagnosis of human and bovine tuberculosis by manipulating urine and milk. *Scientific Reports* **2019,** *9* (1), 18012.

18. https://www.tballiance.org/why-new-tb-drugs/global-pandemic (accessed 15 February 2023).

19. Bagcchi, S., WHO's Global Tuberculosis Report 2022. *The Lancet Microbe* **2023,** *4* (1), e20.

20. Chandra, T. J.; Selvaraj, R.; Sharma, Y., Same day sputum smear microscopy for the diagnosis of pulmonary tuberculosis: Ziehl-Neelsen versus fluorescent staining. *Journal of Family Medicine and Primary Care* **2015,** *4* (4), 525.

21. *Global tuberculosis report 2022*; 2022.

22. Ukwaja, K.; Modebe, O.; Igwenyi, C.; Alobu, I., The economic burden of tuberculosis care for patients and households in Africa: a systematic review. *The International Journal of Tuberculosis and Lung Disease* **2012,** *16* (6), 733-739.

23. Goyal-Honavar, A.; Markose, A. P.; Chhakchhuakk, L.; John, S. M.; Joy, S.; Kumar, S. D.; Saha, S. K.; Palathinkal, J. R.; Bula, S. S.; Yalamanchili, S., Unmasking the human face of TB-The impact of tuberculosis on the families of patients. *Journal of Family Medicine and Primary Care* **2020,** *9* (10), 5345.

24. Adhikari, N.; Bhattarai, R. B.; Basnet, R.; Joshi, L. R.; Tinkari, B. S.; Thapa, A.; Joshi, B., Prevalence and associated risk factors for tuberculosis among people living with HIV in Nepal. *Plos ONE* **2022,** *17* (1), e0262720.

25. Pinto, C. M.; Carvalho, A. R., The HIV/TB coinfection severity in the presence of TB multi-drug resistant strains. *Ecological Complexity* **2017,** *32*, 1-20.

26. Monin, L.; Khader, S. A. In *Chemokines in tuberculosis: the good, the bad and the ugly*, Seminars in immunology, Elsevier: 2014; pp 552-558.

27. Ramesh, G.; MacLean, A. G.; Philipp, M. T., Cytokines and chemokines at the crossroads of neuroinflammation, neurodegeneration, and neuropathic pain. *Mediators of Inflammation* **2013,** *2013*.

28. Briggs, M. A.; Emerson, C.; Modi, S.; Taylor, N. K.; Date, A., Use of isoniazid preventive therapy for tuberculosis prophylaxis among people living with HIV/AIDS: a review of the literature. *Journal of Acquired Immune Deficiency Syndromes (1999)* **2015,** *68* (Suppl 3), S297.

29. Silva, S.; Arinaminpathy, N.; Atun, R.; Goosby, E.; Reid, M., Economic impact of tuberculosis mortality in 120 countries and the cost of not achieving the Sustainable Development Goals tuberculosis targets: a full-income analysis. *The Lancet Global Health* **2021,** *9* (10), e1372-e1379.

30. Blumberg, H. M.; Ernst, J. D., The challenge of latent TB infection. *Journal of the American Medical Association* **2016,** *316* (9), 931-933.

31. Cook, G. M.; Berney, M.; Gebhard, S.; Heinemann, M.; Cox, R. A.; Danilchanka, O.; Niederweis, M., Physiology of mycobacteria. *Advances in Microbial Physiology* **2009,** *55*, 81-319.

32. Vergne, I.; Chua, J.; Singh, S. B.; Deretic, V., Cell biology of *Mycobacterium tuberculosis* phagosome. *Annual Review of Cell and Developmental Biology*. **2004,** *20*, 367-394.

33. Caws, M.; Marais, B.; Heemskerk, D.; Farrar, J., *Tuberculosis in adults and children*. Springer Nature: 2015.

34.http://www.vacfa.uct.ac.za/news/bcg-vaccine-covid-19-implications-south-africa (accessed 14 February 2023).

35. Arts, R. J.; Moorlag, S. J.; Novakovic, B.; Li, Y.; Wang, S.-Y.; Oosting, M.; Kumar, V.; Xavier, R. J.; Wijmenga, C.; Joosten, L. A., BCG vaccination protects against experimental viral infection in humans through the induction of cytokines associated with trained immunity. *Cell Host & Microbe* **2018,** *23* (1), 89-100. e5.

36. Li, J.; Zhan, L.; Qin, C., The double-sided effects of Mycobacterium Bovis bacillus Calmette–Guérin vaccine. *NPJ Vaccines* **2021,** *6* (1), 14.

37. Al-Darraji, H.; Kamarulzaman, A.; Altice, F., Isoniazid preventive therapy in correctional facilities: a systematic review. *The International Journal of Tuberculosis and Lung Disease* **2012,** *16* (7), 871-879.

38. Kendall, E. A.; Hussain, H.; Kunkel, A.; Kubiak, R. W.; Trajman, A.; Menzies, R.; Drain, P. K., Isoniazid or rifampicin preventive therapy with and without screening for subclinical TB: a modeling analysis. *BMC Medicine* **2021,** *19* (1), 1-16.

39. Walzl, G.; McNerney, R.; du Plessis, N.; Bates, M.; McHugh, T. D.; Chegou, N. N.; Zumla, A., Tuberculosis: advances and challenges in development of new diagnostics and biomarkers. *The Lancet Infectious Diseases* **2018,** *18* (7), e199-e210.

40. Wang, A.; MacNeil, A.; Maloney, S., Comparison and lessons learned from neglected tropical diseases and tuberculosis. *Plos Global Public Health* **2021,** *1* (10), e0000027.

41. Shuaib, Y. A.; Khalil, E. A.; Schaible, U. E.; Wieler, L. H.; Bakheit, M. A.; Mohamed-Noor, S. E.; Abdalla, M. A.; Homolka, S.; Andres, S.; Hillemann, D., Smear microscopy for diagnosis of pulmonary tuberculosis in eastern Sudan. *Tuberculosis research and treatment* **2018,** *2018*.

42. https://www.cdc.gov/tb/education/corecurr/pdf/chapter4.pdf (accessed 22 February 2023).

43. Ulrich, M.; Christensen, D.; Coyne, S.; Craw, P.; Henchal, E.; Sakai, S.; Swenson, D.; Tholath, J.; Tsai, J.; Weir, A., Evaluation of the Cepheid GeneXpert® system for detecting Bacillus anthracis. *Journal of Applied Microbiology* **2006,** *100* (5), 1011-1016.

44. Suárez, I.; Fünger, S. M.; Kröger, S.; Rademacher, J.; Fätkenheuer, G.; Rybniker, J., The diagnosis and treatment of tuberculosis. *Deutsches Aerzteblatt International* **2019,** *116* (43).

45. Meaza, A.; Tesfaye, E.; Mohamed, Z.; Zerihun, B.; Seid, G.; Eshetu, K.; Amare, M.; Sinshaw, W.; Dagne, B.; Mollalign, H., Diagnostic accuracy of Truenat Tuberculosis and Rifampicin-Resistance assays in Addis Ababa, Ethiopia. *Plos ONE* **2021,** *16* (12), e0261084.

46. Ngangue, Y. R.; Mbuli, C.; Neh, A.; Nshom, E.; Koudjou, A.; Palmer, D.; Ndi, N. N.; Qin, Z. Z.; Creswell, J.; Mbassa, V., Diagnostic accuracy of the truenat MTB plus assay and comparison with the Xpert MTB/RIF assay to detect tuberculosis among hospital outpatients in Cameroon. *Journal of Clinical Microbiology* **2022,** *60* (8), e00155-22.

47. Hemhongsa, P.; Tasaneeyapan, T.; Swaddiwudhipong, W.; Danyuttapolchai, J.; Pisuttakoon, K.; Rienthong, S.; McCarthy, K.; Varma, M. J.; Whitmore, J.; Varma, J. K., TB, HIV-associated TB and multidrug-resistant TB on Thailand's border with Myanmar, 2006–2007. *Tropical Medicine & International Health* **2008,** *13* (10), 1288-1296.

48. Kliegman, R. M.; Behrman, R. E.; Jenson, H. B.; Stanton, B. M., *Nelson textbook of pediatrics e-book*. Elsevier Health Sciences: 2007.

49. Banaei, N.; Gaur, R. L.; Pai, M., Interferon gamma release assays for latent tuberculosis: what are the sources of variability? *Journal of Clinical Microbiology* **2016,** *54* (4), 845-850.

50. Burbelo, P. D.; Keller, J.; Wagner, J.; Klimavicz, J. S.; Bayat, A.; Rhodes, C. S.; Diarra, B.; Chetchotisakd, P.; Suputtamongkol, Y.; Kiertiburanakul, S., Serological diagnosis of pulmonary *Mycobacterium tuberculosis* infection by LIPS using a multiple antigen mixture. *BMC Microbiology* **2015,** *15*, 1-9.

51. Rendon, A.; Tiberi, S.; Scardigli, A.; D'Ambrosio, L.; Centis, R.; Caminero, J. A.; Migliori, G. B., Classification of drugs to treat multidrug-resistant tuberculosis (MDR-TB): evidence and perspectives. *Journal of Thoracic Disease* **2016,** *8* (10), 2666.

52. Arbex, M. A.; Varella, M. d. C. L.; Siqueira, H. R. d.; Mello, F. A. F. d., Antituberculosis drugs: drug interactions, adverse effects, and use in special situations-part 1: first-line drugs. *Jornal Brasileiro de Pneumologia* **2010,** *36*, 626-640.

53. Rana, F., Rifampicin—an overview. *International Journal of Pharmacy and Chemistry* **2013,** *3* (1), 83-7.

54. Jena, L.; Nayak, T.; Deshmukh, S.; Wankhade, G.; Waghmare, P.; Harinath, B., Isoniazid with multiple mode of action on various mycobacterial enzymes resulting in drug resistance. *J Infect Dis Ther* **2016,** *4* (5), 2332-0877.1000297.

55. Jnawali, H. N.; Ryoo, S., First-and second-line drugs and drug resistance. *Tuberculosis-Current Issues in Diagnosis and Management* **2013,** *20*, 163-80.

56. Organization, W. H., Ethambutol efficacy and toxicity: literature review and recommendations for daily and intermittent dosage in children. **2006**.

57. Momekov, G.; Dilyan, F.; Yulian, V.; Georgi, S.; Plamen, P., Pyrazinamidepharmaceutical, biochemical and pharmalogical properties and reapraisal of its role in the chemotherapy of tuberculosis. Pharmacia: 2014.

58. Organization, W. H., *WHO consolidated guidelines on drug-resistant tuberculosis treatment*. World Health Organization: 2019.

59. https://tbfacts.org/second-line-drugs/ (accessed 08 March 2023).

60. Joshi, S.; Yadav, D.; Yadav, R., Fluoroquinolones: a review on anti-tubercular activity. *Monatshefte für Chemie-Chemical Monthly* **2021,** *152* (8), 881-894.

61. Moorthy, N.; Raghavendra, N.; Venkatarathnamma, P., Levofloxacin-induced acute psychosis. *Indian Journal of Psychiatry* **2008,** *50* (1), 57.

62. Sarathy, J. P.; Gruber, G.; Dick, T., Re-understanding the mechanisms of action of the anti-mycobacterial drug bedaquiline. *Antibiotics* **2019,** *8* (4), 261.

63. Bal, A. M., Linezolid. **2021**.

64. Gopal, M.; Padayatchi, N.; Metcalfe, J.; O'Donnell, M., Systematic review of clofazimine for the treatment of drug-resistant tuberculosis. *The International Journal of Tuberculosis and Lung Disease* **2013,** *17* (8), 1001-1007.

65. Kolyva, A. S.; Karakousis, P. C., Old and new TB drugs: mechanisms of action and resistance. *Understanding Tuberculosis-New Approaches to Fighting against Drug Resistance* **2012**.

66. Xavier, A. S.; Lakshmanan, M., Delamanid: A new armor in combating drug-resistant tuberculosis. *Journal of Pharmacology and Pharmacotherapeutics* **2014,** *5* (3), 222-224.

67. Rodloff, A.; Goldstein, E.; Torres, A., Two decades of imipenem therapy. *Journal of Antimicrobial Chemotherapy* **2006,** *58* (5), 916-929.

68. Padda, I. S.; Reddy, K. M., Antitubercular medications. In *StatPearls [Internet]*, StatPearls Publishing: 2021.

69. Rohde, K. H.; Sorci, L., The prospective synergy of antitubercular drugs with NAD biosynthesis inhibitors. *Frontiers in Microbiology* **2021,** *11*, 634640.

70. Ushtanit, A.; Kulagina, E.; Mikhailova, Y.; Makarova, M.; Safonova, S.; Zimenkov, D., Molecular determinants of Ethionamide resistance in clinical isolates of mycobacterium tuberculosis. *Antibiotics* **2022,** *11* (2), 133.

71. Belete, T. M., Recent Progress in the Development of Novel Mycobacterium Cell Wall Inhibitor to Combat Drug-Resistant Tuberculosis. *Microbiology Insights* **2022,** *15*, 11786361221099878.

72. Babamahmoodi, F.; Mahdavi, M. R.; Jalali, H.; Talebi, B.; Roshan, P.; Mahdavi, M., Evaluation of gene mutations involved in drug resistance in Mycobacterium tuberculosis strains derived from tuberculosis patients in Mazandaran, Iran, 2013. *International Journal of Molecular and Cellular Medicine* **2014,** *3* (3), 190.

73. Zhu, S.; Su, Y.; Shams, S.; Feng, Y.; Tong, Y.; Zheng, G., Lassomycin and lariatin lasso peptides as suitable antibiotics for combating mycobacterial infections: current state of biosynthesis and perspectives for production. *Applied Microbiology and Biotechnology* **2019,** *103* (10), 3931-3940.

74. Esteban, J.; García-Coca, M., Mycobacterium biofilms. *Frontiers in Microbiology* **2018,** *8*, 2651.

75. Lewis, K., Persister cells, dormancy and infectious disease. *Nature Reviews Microbiology* **2007,** *5* (1), 48-56.

76. Fauvart, M.; De Groote, V. N.; Michiels, J., Role of persister cells in chronic infections: clinical relevance and perspectives on anti-persister therapies. *Journal of Medical Microbiology* **2011,** *60* (6), 699-709.

77. Liu, Z.; Brady, A.; Young, A.; Rasimick, B.; Chen, K.; Zhou, C.; Kallenbach, N. R., Length effects in antimicrobial peptides of the (RW) n series. *Antimicrobial Agents and Chemotherapy* **2007,** *51* (2), 597-603.

78. Bahar, A. A.; Ren, D., Antimicrobial peptides. *Pharmaceuticals* **2013,** *6* (12), 1543-1575.

79. Oliveira, G. S.; Costa, R. P.; Gomes, P.; Gomes, M. S.; Silva, T.; Teixeira, C., Antimicrobial peptides as potential anti-tubercular leads: a concise review. *Pharmaceuticals* **2021,** *14* (4), 323.

80. Mehta, K.; Sharma, P.; Mujawar, S.; Vyas, A., Role of Antimicrobial Peptides in Treatment and Prevention of Mycobacterium Tuberculosis: A Review. *International Journal of Peptide Research and Therapeutics* **2022,** *28* (5), 132.

81. Artur Schmidtchen, M. P., Martin Malmsten, Effect of hydrophobic modifications in antimicrobial peptides. *Advances in Colloid and Interface Science* **2013**.

82. Niidome, T.; Matsuyama, N.; Kunihara, M.; Hatakeyama, T.; Aoyagi, H., Effect of chain length of cationic model peptides on antibacterial activity. *Bulletin of the Chemical Society of Japan* **2005,** *78* (3), 473-476.

83. Strøm, M. B.; Haug, B. E.; Skar, M. L.; Stensen, W.; Stiberg, T.; Svendsen, J. S., The pharmacophore of short cationic antibacterial peptides. *Journal of Medicinal Chemistry* **2003,** *46* (9), 1567-1570.

84. Malina, A.; Shai, Y., Conjugation of fatty acids with different lengths modulates the antibacterial and antifungal activity of a cationic biologically inactive peptide. *Biochemical Journal* **2005,** *390* (3), 695-702.

85. Avrahami, D.; Shai, Y., A new group of antifungal and antibacterial lipopeptides derived from non-membrane active peptides conjugated to palmitic acid. *Journal of Biological Chemistry* **2004,** *279* (13), 12277-12285.

86. Culp, E.; Wright, G. D., Bacterial proteases, untapped antimicrobial drug targets. *The Journal of Antibiotics* **2017,** *70* (4), 366-377.

87. Gavrish, E.; Sit, C. S.; Cao, S.; Kandror, O.; Spoering, A.; Peoples, A.; Ling, L.; Fetterman, A.; Hughes, D.; Bissell, A., Lassomycin, a ribosomally synthesized cyclic peptide, kills Mycobacterium tuberculosis by targeting the ATP-dependent protease ClpC1P1P2. *Chemistry & Biology* **2014,** *21* (4), 509-518.

88. Parish, T., Targeting mycobacterial proteolytic complexes with natural products. *Chemistry & Biology* **2014,** *21* (4), 437-438.

89. Malik, I. T.; Brötz-Oesterhelt, H., Conformational control of the bacterial Clp protease by natural product antibiotics. *Natural Product Reports* **2017,** *34* (7), 815-831.

90. Zhang, S.; Chen, J.; Shi, W.; Cui, P.; Zhang, J.; Cho, S.; Zhang, W.; Zhang, Y., Mutation in clpC1 encoding an ATP-dependent ATPase involved in protein degradation is associated with pyrazinamide resistance in Mycobacterium tuberculosis. *Emerging Microbes & Infections* **2017,** *6* (1), 1-2.

91. Choules, M. P.; Wolf, N. M.; Lee, H.; Anderson, J. R.; Grzelak, E. M.; Wang, Y.; Ma, R.; Gao, W.; McAlpine, J. B.; Jin, Y.-Y., Rufomycin targets ClpC1 proteolysis in Mycobacterium tuberculosis and M. abscessus. *Antimicrobial Agents and Chemotherapy* **2019,** *63* (3), e02204-18.

92. Di, L.; Kerns, E. H.; Hong, Y.; Chen, H., Development and application of high throughput plasma stability assay for drug discovery. *International Journal of Pharmaceutics* **2005,** *297* (1-2), 110-119.

93. Xu, X.; Zhang, L.; Yang, T.; Qiu, Z.; Bai, L.; Luo, Y., Targeting caseinolytic protease P and its AAA1 chaperone for tuberculosis treatment. *Drug Discovery Today* **2023**, 103508.

94. Lee, H.; Suh, J.-W., Anti-tuberculosis lead molecules from natural products targeting Mycobacterium tuberculosis ClpC1. *Journal of Industrial Microbiology and Biotechnology* **2016,** *43* (2-3), 205-212.

95. Schmitt, E. K.; Riwanto, M.; Sambandamurthy, V.; Roggo, S.; Miault, C.; Zwingelstein, C.; Krastel, P.; Noble, C.; Beer, D.; Rao, S. P., The natural product cyclomarin kills Mycobacterium tuberculosis by targeting the ClpC1 subunit of the caseinolytic protease. *Angewandte Chemie International Edition* **2011,** *50* (26), 5889-5891.

96. Cheng, C.; Hua, Z.-C., Lasso peptides: heterologous production and potential medical application. *Frontiers in Bioengineering and Biotechnology* **2020,** *8*, 571165.

97. Hanna, C. C.; Hermant, Y. O.; Harris, P. W.; Brimble, M. A., Discovery, Synthesis, and Optimization of Peptide-Based Antibiotics. *Accounts of Chemical Research* **2021,** *54* (8), 1878-1890.

98. Duan, Y.; Niu, W.; Pang, L.; Bian, X.; Zhang, Y.; Zhong, G., Unusual Post-Translational Modifications in the Biosynthesis of Lasso Peptides. *International Journal of Molecular Sciences* **2022,** *23* (13), 7231.

99. Tan, S.; Moore, G.; Nodwell, J., Put a bow on it: knotted antibiotics take center stage. *Antibiotics* **2019,** *8* (3), 117.

100. Churchyard, G. J.; Fielding, K. L.; Lewis, J. J.; Coetzee, L.; Corbett, E. L.; Godfrey-Faussett, P.; Hayes, R. J.; Chaisson, R. E.; Grant, A. D., A trial of mass isoniazid preventive therapy for tuberculosis control. *New England Journal of Medicine* **2014,** *370* (4), 301-310.
101. Harris, P. W.; Cook, G. M.; Leung, I. K.; Brimble, M. A., An Efficient Chemical Synthesis of Lassomycin Enabled by an On-Resin Lactamisation–Off-Resin Methanolysis Strategy and Preparation of Chemical Variants. *Australian Journal of Chemistry* **2016,** *70* (2), 172-183.

Chapter 2

Journal Research Article Manuscript (to be submitted)

Title: Design and Synthesis of Disulfide-Bridge Substituted Lassomycin-Amide derivatives

Ntombizanele Ngqinayo[1], Bhavna G. Gordhan[2], Maya M. Makatini[1]

[1]Molecular Sciences Institute, School of Chemistry, University of the Witwatersrand, Johannesburg, South Africa

[2]Department of Science and Technology/National Research Foundation Centre of Excellence for Biomedical TB Research, School of Pathology, Faculty of Health Sciences, University of the Witwatersrand and the National Health Laboratory Service, Johannesburg, South Africa

Correspondence:

University of the Witwatersrand
School of Chemistry
Humphrey Raikes Building
Private Bag Wits 2050
+27 (0) 11 717 6708
Email: maya.makatini@wits.ac.za

Abstract:

Tuberculosis (TB) is a global health concern, claiming over a million lives each year worldwide. The emergence of *Mycobacterium tuberculosis* (*Mtb*) multidrug-resistant (MDR) strains which are non-responsive towards approved anti-TB drug treatment, has led researchers to develop novel anti-TB agents that employ different mechanisms of action that do not target the cell wall synthesis and DNA metabolism. Lassomycin is a highly basic lasso peptide that was recently discovered to target and kill *Mtb* by selectively binding to the acidic *N*-terminal domain (NTD) of the caseinolytic enzyme (ClpC1) and decouples it from the caseinolytic protease (ClpP1P2) to disrupt the essential, tightly regulated proteolytic process. This study focuses on the design and synthesis of lassomycin derivatives with some of the following modifications: N-methylated amino acids to improve stability and cationic amino acids to enhance penetration into the *Mtb* cell envelope. Peptide derivatives were successfully synthesized via the Fmoc Solid State Peptide Synthesis (SPPS) strategies and purified using semi-preparative high-performance liquid chromatography (HPLC) and analyzed using liquid

chromatography coupled to mass spectrometry (LC-MS). The peptide derivatives were also tested for bactericidal activity against *Mtb*, and Pep-2-NN showed potent activity comparable to ethambutol. Pep-Lys-NN (cationic derivative) was found to be selectively active against the *Bacillus subtillis*, which also contains ClpC1 targeted by lassomycin.

Keywords:

Lassomycin, *Mycobacterium tuberculosis*, tuberculosis, caseinolytic enzyme, ClpC1, caseinolytic protease

2.1. Introduction

Tuberculosis (TB) is a preventable and curable disease caused by the *Mycobacterium tuberculosis* (*Mtb*) pathogen and is potentially fatal if not treated properly. TB has become a global challenge, infecting an estimated 1.8 billion people (about a quarter of the world's population) and has caused about 1.5 million deaths each year across the world. Low- to middle-income countries bore most of the TB burden with high incidence cases (about 90% of all TB cases) and high mortality rates (about 95% of all TB deaths). [1-3]

2.1.1. Challenges with currently approved anti-TB drugs

New TB cases that are susceptible to anti-TB drugs are treated with a combination of rifampicin, isoniazid, ethambutol, and pyrazinamide, which are taken together for 2 months, followed by isoniazid and rifampicin for the last 4 months. Second-line anti-TB drug treatment regimens are administered when *Mtb* has become unresponsive to any 2 of the first-line drugs simultaneously, giving rise to multidrug-resistant (MDR) strains that are more difficult to treat.[4] Second-line drugs, including levofloxacin, moxifloxacin, bedaquiline, delamanid, and linezolid, are more expensive and toxic than first-line drugs. Multidrug-resistant TB is one of the leading causes of death in TB-infected persons, with cases found mostly in developing countries.[4] Multidrug-resistant TB is exacerbated by poor chemotherapy[5] that results from patient non-compliance due to prolonged treatment durations and toxicity due to drug treatment. Although TB is prevalent in developing countries, it remains a global challenge due to its presence in every country. Therefore, effective measures are needed to control and prevent the spread of TB.

Most currently approved anti-TB drugs use a similar mode of action to target and kill TB, including inhibiting cell wall synthesis and DNA processes. TB has, however, adapted, evolved, and mutated against these anti-TB drugs, thus resulting in the development and emergence of resistant TB strains. Developing new and novel anti-TB drugs that utilize different modes of action to target and kill *Mtb* is one of the measures that can be employed to combat TB. Lassomycin is a highly basic and novel antimicrobial peptide (AMP) that was discovered from a soil bacterium and was found to effectively target and kill *Mtb* using a unique mode of action. Lassomycin has the ability also to kill latent TB as well as resistant anti-TB strains.

2.1.2. Lassomycin as a potential anti-TB drug agent

The target of lassomycin (**Figure 2.1**) is the caseinolytic enzyme (ClpC1), an unfoldase hexameric protein of the AAA family of chaperones. ClpC1 couples to the caseinolytic protease (ClpP1P2) tetradecamer to form the caseinolytic protease complex (Clp) responsible for maintaining *Mtb* cells through a tightly-regulated protein quality control.[6-7] During the quality control process, damaged and non-functional protein substrates with a degradation tag are located and bound to the ClpC1, which further translocates them to the ClpP1P2 degradation chamber for proteolysis in an ATPase dependent-fashion. During the proteolytic process, the damaged and non-functional protein substrates are cleaved into smaller peptides which are later recycled into functional protein substrates.[8-12] Clp also plays a role in the survival of *Mtb*, especially during stressful processes such as phagocytosis encountered during infection. Lassomycin binds to the acidic *N*-terminal domain (NTD) of ClpC1 and decouples it from the ClpP1P2 protease, resulting in the inhibition of proteolytic activity that leads to the accumulation of damaged substrates, resulting in cell death caused by cytotoxicity. Also, in the presence of lassomycin, the unfoldase activity of ClpC1 increases by up to 10-fold due to uncontrolled and non-selective unfolding of protein substrates resulting in loss of function and thus resulting in cell death.[8-9] To the best of our knowledge, it is unknown whether the actual *Mtb* cell death is caused by the inhibition of proteolysis or the excessive increase of unfoldase activity. Lassomycin is highly potent against *Mtb* and was reported to have a minimum inhibitory concentration (MIC) range of 0.8 – 3 μg/mL.[8]

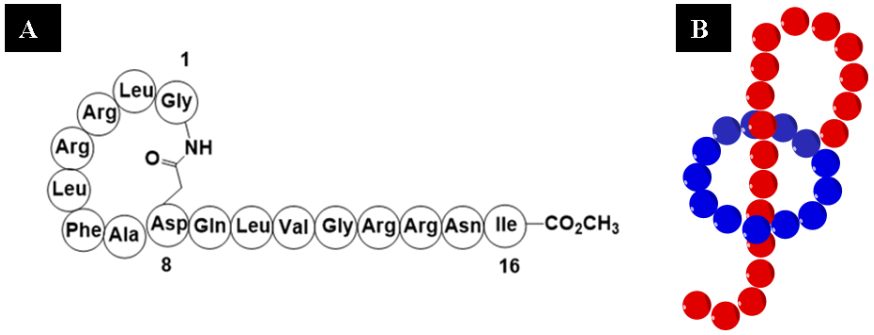

Figure 2.1: (**A**) The structure of lassomycin showing the amino acid sequence and (**B**) an illustration of the threaded lasso conformation.

The lasso structure of lassomycin is constructed by the threading of the peptide chain (Gln17-Ile18) into the 8 amino acids long ring (loop) connected through an isopeptide bond formed by the N-terminus Gly1 and Asp8. This important feature results in a constricted peptide shape with increased stability against enzymatic and thermal degradation.[13] The lasso structure of lassomycin is stabilized by sterically demanding amino acid residues (also known as 'steric plugs') that hold the threaded C-terminal tail above and below the ring to prevent it from unthreading. The basicity of lassomycin is due to the presence of 4 arginine (Arg) amino acid residues postulated to bind to ClpC1. Due to its highly unusual mode of action and potency, it is apparent that lassomycin shows potential to be developed into a potent anti-TB drug that can play a role in combating TB. However, advancements in lassomycin-based research have dwindled in the past few years. Since the discovery of lassomycin about 8 years ago, there has been limited published work about the attempts to synthesize and re-produce lassomycin and its derivatives. A couple of research groups (Brimble and Lear groups) that attempted to synthesize lassomycin and its derivatives encountered challenges in reproducing the peptide, resulting in diminished-to-no bactericidal activity against *Mtb*. The loss of activity may have been due to the absence of the distinctive lasso structure of the peptides, as the tail (linear chain) was not threading inside the cyclic ring as postulated by the Brimble research group.[14] The Lear research group also reached the same realization, thus concluding that the natural lassomycin initially isolated by the Gavrish group may be of a lasso structure instead of the reported *C*-terminal tail being tightly packed near the ring.[8, 14-15] This paper focuses on the design and synthesis of drug-like lassomycin derivatives with improved membrane permeability and enzyme stability. The modifications performed include **(i)** replacing the macrolactam ring with a disulfide bridge which in turn results in an enlarged cyclic ring; shorter and cost-effective synthetic routes **(ii)** substituting 'difficult' arginine

residues with less basic lysine residues; **(iii)** increasing the number of lysine derivatives to make the peptide more cationic and selective for the bacterial membrane; **(iv)** incorporation of *N*-methylated residues to improve peptide stability, and lastly **(v)** making non-polar peptide derivatives by replacing all basic amino acids with alanine to investigate the importance of the basic residues. The challenges encountered with the chemical synthesis of the peptide derivatives using the Fmoc solid-state peptide synthesis (SPPS) strategy are discussed at length as well as possible solutions. Chemical synthesis of peptides is usually selected over biosynthesis due to the ease of modifying the sequences during synthesis. Lastly, we discuss biological activities for some lassomycin derivatives that were synthesized and subjected to biological activities against *Mtb* and other pathogens.

2.2. Materials and methods

2.2.1. Materials

2.2.1.1. Solvents and reagents

The reagents used to synthesize lassomycin derivatives included rink amide MBHA resin, Fmoc protected amino acids, coupling reagents such as Hexafluorophosphate Azabenzotriazole Tetramethyl Uronium (HATU), Hydroxybenzotriazole (HOBt) purchased from DLD Scientific. Diisopropylethylamine (Dipea), piperidine, trifluoroacetic acid (TFA), triisopropylsilane (TIS), formic acid, *N, N'*-Diisopropylcarbodiimide (DIC), thionyl chloride, 1,2-Ethanedithiol (EDT), and acetic acid (AcOH) were purchased from Sigma Aldrich and Pyramid Scientific. Solvents such as dimethylformamide (DMF), dimethyl sulfoxide (DMSO), diethyl ether, methanol, and acetonitrile were purchased from Sigma Aldrich, Radchem, and Pyramid Scientific. Other chemicals used were part of the broader organic research laboratory, such as dichloromethane (DCM), which was dried upon distillation over calcium hydride, triethyl silane (TES), iodine, ascorbic acid, bromoacetic acid, aluminium trichloride ($AlCl_3$), paraformaldehyde, p-toluenesulfonic acid, hexane, chloroform ($CHCl_3$), ethyl acetate, toluene and acetone, sodium hydrogen carbonate ($NaHCO_3$), magnesium sulphate ($MgSO_4$).

2.2.2. Methods

2.2.2.1. Peptide synthesis

All the peptides were synthesized via the Fluorenylmethyloxycarbonyl (Fmoc-) solid phase peptide synthesis (SPPS) strategy on the Fmoc-protected Rink Amide 4-methylbenzhydrylamine (MBHA) resin as a solid support.[16] The rink resin was first pre-swelled in dimethyl formamide (DMF) for 3 hours before use. The resin was then transferred to a reaction vessel fitted with a fritted resin support and washed twice with DMF/ DCM/DMF, and the solvent was removed by vacuum filtration.

2.2.2.2. Fmoc removal

The resin was treated with 20% piperidine solution in DMF (v/v) for 2 x 5 min. The reagents were removed by filtration under vacuum. The piperidine solution is used to irreversibly cleave the base-labile Fmoc- group and expose the free amino group (NH_2) to allow aminoacylation with incoming amino acid. The resin was then washed with DMF/DCM/DMF to remove contaminants and side products.

2.2.2.3. Attachment of the first amino acid to the resin

Fmoc-protected isoleucine (Fmoc-Ile-OH, 0.2M) is the first amino acid attached to the resin in all the synthesized peptide derivatives. Fmoc-Ile-OH was first activated into an active ester by mixing with 2-(1H-benzotriazole-1-yl)-1,1,3,3-tetramethyluronium hexafluorophosphate and diisopropylethylamine (0.19 M HBTU/ 1M Dipea) and then transferred to the reaction vessel and attached to resin-linker for 40 min.

2.2.2.4. Peptide chain elongation

The resin-Ile-Fmoc was treated with 20% piperidine and washed with DMF. The second amino acid, 0.2 M asparagine (Fmoc-ASN(Trt)-OH, 1.2 mmol), was mixed with HBTU (0.19 M, 0.87 g) and 1M Dipea and attached to give Fmoc-Asn(Trt)-Ile-Resin. Amino acid attachment and Fmoc removal steps were repeated until all the amino acids in the peptide sequence were added, resulting in 18 amino acid-long peptide derivatives. Washings with

DMF and DCM were performed in-between steps. Peptide derivatives were initially synthesized using a peptide synthesizer, and due to the presence of impurities, manual synthesis was then employed. Hexafluorophosphate Azabenzotriazole Tetramethyl Uronium (HATU) was used instead of HBTU in some derivatives to improve yields. The coupling reaction times were decreased to 30 minutes, but double coupling (2 x 30 min) was done for all amino acid residues to ensure successful coupling to the growing chain.

2.2.2.5. Cyclization using iodine

After all the amino acids were coupled, a disulfide bridge was formed between two cysteine (Cys, C) residues in each derivative by treating the peptides with a dilute solution of iodine in DMF/water (4:1) for a maximum of 40 min. The mass of the iodine used for cyclization was 0.102 g as determined by the calculations: Loading capacity (mmols/g) x 10 equivalence x iodine molar mass (253.81 g/mol). Iodine simultaneously cleaves the cysteine triphenylmethyl (Trt) protecting group and oxidizes the cysteine residues to form a disulfide bond. The iodine also acts as a scavenger for the Trt carbocations. A dilute iodine solution was used to ensure that the disulfide bridge formed is intra-molecular (taking place within a molecule) and not intermolecular (taking place between molecules). After cyclization, the peptidyl resin was washed with DMF (2 x 10 mL), and excess iodine was quenched with 2% ascorbic acid in DMF until the golden-brown color in the washing solvent was no longer observed, and the reagents were filtered by vacuum.

2.2.2.6. The TFA-cleavage of the permanent protecting groups

After cyclization, the peptides were thoroughly washed with DCM and dried under a vacuum. Peptides were cleaved from the resin linker, and permanent protecting groups were removed by acidolysis with a 94% trifluoroacetic acid (TFA) cocktail with 1% triisopropylsilane (TIS), 2.5% 1,2-ethanedithiol (EDT) and 2.5% water. The peptides were precipitated using diethyl ether, and the supernatant was decanted after centrifuging. The peptides were then washed four times with ether. TIS, water, and EDT function as scavengers for the cleaved protecting groups as they can irreversibly attack the peptide backbone and alkylate it, resulting in the formation of impurities and low yields. The cleavage time for each peptide was at least 3 hours.

2.2.2.7. Synthesis of *N*-methylated amino acids

The *N*-methylated amino acids were synthesized in 2 parts and according to literature procedures. The first part involved synthesizing 5-oxazolidinones precursors, which were then used to synthesize the *N*-methylated amino acids.

(a) Synthesis of 5-oxazolidinones

To synthesize 5-oxazolidinones, Fmoc- protected amino acids (5 mM, 15 mmol) were mixed with paraformaldehyde (0.3 M, 3 g) and *p*- toluenesulfonic acid (0.3 M, 300 mg) in toluene (100 mL). The mixture was refluxed overnight in a Dean-Stark setup at a temperature of 110°C. Thin Layer Chromatography (TLC), (CHCl /MeOH/AcOH 97.05:2:0.5) was used to monitor the reaction until the starting materials were no longer detected. After cooling, the solution was washed with saturated sodium hydrogen carbonate ($NaHCO_3$) to remove the excess acid and dried over anhydrous magnesium sulfate ($MgSO_4$). The mixture was then concentrated *in vacuo* to give the crude product. In some cases, re-crystallization was used to purify the products. Commercially purchased Fmoc-Val-OH, Fmoc-Leu-OH, and Fmoc-Ala-OH amino acids were chosen for *N*-methylation. HPLC-MS was used to analyze the results.

(b) Synthesis of N-methylated Fmoc-protected amino acids

To synthesize the *N*-methylated amino acids, triethylsilane (2 eq) was added to a solution containing the 5-oxazolidinone (1 eq) and aluminum trichloride ($AlCl_3$, 2 eq) in dry DCM. The reaction was stirred overnight at room temperature, and TLC (Ethyl acetate/hexane 1:3) was used to monitor the reaction until the starting materials were no longer detected. The mixture was then washed with 1 M hydrochloric acid (HCl), and the organic layer containing the final product was dried over anhydrous $MgSO_4$. The product was then concentrated *in vacuo* and solidified upon cooling. The crude products were purified by re-crystallization, and characterization analysis was done using NMR spectroscopic analysis.

2.2.2.8. Peptide analysis using High Performance Liquid Chromatography coupled to Mass Spectroscopy (HPLC-MS)

A small amount of each derivative was dissolved in HPLC-grade solvents and analyzed using HPLC-MS to determine successful synthesis. A Thermo Scientific Dionex Ultimate 3000 UHPLC instrument coupled to a Bruker Compact Q-TOF mass spectrometer was used to

analyze the results and determine purity. The compounds were separated using a Phenomenex C18 column (5 µm, 100 Å, 250 mm × 21.2 mm), and mass spectrometry analysis was done using a positive mode electrospray ionization source (ESI).

2.2.2.9. Purification using Preparatory High-Performance Liquid Chromatography (Prep-HPLC)

All synthesized peptide derivatives were subjected to purification using semi-preparative HPLC, carried out on an Agilent 1260 Infinity semi-preparative instrument via reverse phase chromatography. A Phenomenex Kinetex XB-C18 column (5 µm, 100 Å, 250 mm × 21.2 mm) was used to separate the compounds with a 15 mL/min flow rate. The compounds were detected at wavelengths of 215 nm and 254 nm. For the mobile phase, a two-buffer system consisting of 0.1 % formic acid/H_2O (v/v) (Buffer A) and 0.1 % formic acid/acetonitrile (v/v) (Buffer B) was utilized. The peptide derivatives were eluted using a gradient method of 5 – 95 % Buffer B in 10 min, unless stated otherwise.

2.2.2.10. Screening for biological activities and cytotoxicity studies

After purification, some peptide derivatives were subjected to biological screening against the *Mtb* as well as cytotoxicity testing. All tests were performed using external sources. The biological screening was done at the National Health Laboratory Service (NHLS). The toxicity screening for Pep-2-NN was done at Mintek-Advance Material Division as a dose-response study against Human T cells (MT4 cells). Screening was conducted at 20 µL and 100 µL as well as a dose-response experiment. Cytotoxicity evaluation was done on the HIV growth supporting human T-cell line, MT4 (Human T-cell leukaemia).

On the day of cytotoxicity testing, cells were counted and seeded at 1 x 106 cells per mL. A total of 100 µL of cells were added to each well of a 96-well cell culture plate for testing. The plate was placed into the incubator to equilibrate to 37°C and 5 % CO_2. During this time, test compounds were made up of 10% RPMI solution in the desired concentration. A total of 100 µL compound was added to wells containing cells and mixed to ensure the solution was homogeneous with the cells. The plate was placed into the 37°C incubator for 5 days. On the 5^{th} day, 10 µL of MTS was added and mixed. The plates were then incubated for a further four hours and read at 450 nm (xMARK™, Bio-Rad, USA.).

2.3. Results and discussion

2.3.1. Design of lassomycin derivatives

There is a growing interest in designing new peptides that are based on the sequences of naturally occurring antimicrobial peptides in order to enhance antimicrobial activities, improve potency and increase stability against proteolytic and enzymatic degradation.[17-18] Although lassomycin has significant potency and is novel, the peptide is not ready for immediate use in its natural state. In this section, all modifications done on lassomycin are discussed, and the list of the peptide derivatives is summarized in **Table 2.1**.

Table 2.1: A summary of all the peptide derivatives discussed in this article. The letters in each sequence represent an amino acid residue. The residues of interest, where modifications were done, are highlighted with purple for arginine (R), blue for lysine (K), and red for asparagine (N).

Peptide number:	Peptide derivative	Sequence
1	Lassomycin	IN**RR**GVLQDAFL**RR**LG
2	Pep-1-NNA	IN**RR**GVLQCDAFL**RR**LGC
3	Pep-1-NN	IN**RR**GVLQC**N**GL**RR**LFAC
4	Pep-2-NNA	IN**KK**GVLQCDAFL**KK**LGC
5	Pep-2-NN	IN**KK**GVLQC**N**GL**KK**LFAC
2a	Pep-1-NNA-Lys	IN**RR**G**KK**QCDAF**KRRK**GC
3a	Pep-1-NN-Lys	IN**RR**G**KK**QC**N**G**KRRK**FAC
4a	Pep-Lys-NNA	IN**KK**G**KK**QCDAF**KKKK**GC
5a	Pep-Lys-NN	IN**KK**G**KK**QC**N**G**KKKK**FAC

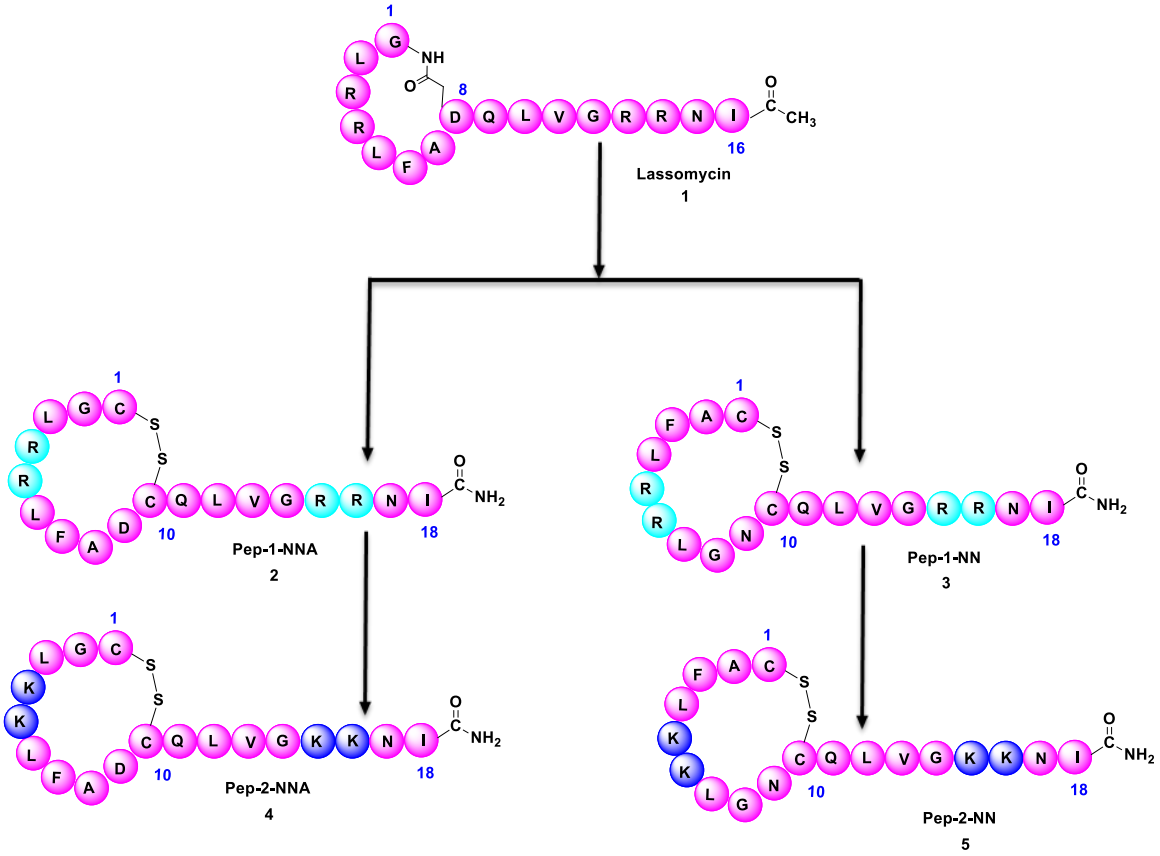

Figure 2.2: A mapping of the modifications done to design lassomycin derivatives from parent peptide **(1)** to form Pep-1-NNA **(2)** and Pep-1-NN **(3)** by replacing the macrolactam bridge with a disulfide bridge and the ester *C*-terminal with an amide group. Pep-2-NNA **(4)** and Pep-2-NN **(5)** compounds were derived from **(2)** and **(3)**, respectively, by substituting arginine amino acids with lysine residues.

2.3.1.1. Replacing macrolactam bridge with a disulfide bridge

Unfortunately, previous attempts by other research groups to synthesize lassomycin and like-derivatives have been challenging due to poor anti-microbial activities against *Mtb* that do not come close to those observed for the natural lassomycin. Since the natural lassomycin showed good antimicrobial activity against TB, the poor-to-no bactericidal activity observed by the Lear research group can be attributed to the lasso structure.[8, 14-15] The disulfide bridge enables cyclization occurrence after the whole peptide has formed and taken the correct conformation.

2.3.1.2. Amidation of the C – terminal ending of lassomycin

The C-terminal of all the peptides was modified by replacing the ester with an amide ending, and this was done in order to improve enzymatic stability against peptidases (compounds **(2)**

– **(5)** in **Figure 2.2** and all compounds in **Figure 2.3**). C-terminal amides in peptides are known to participate in intramolecular hydrogen bonding that further reinforces the stability of the secondary structure, which is not usually observed in peptides with an ester *C*-terminal ending.[19] In order to achieve amidation, the peptides were synthesized using a rink amide MBHA resin as a solid support which allows the amide ending to be exposed upon the cleavage of the peptides when treated with a TFA cocktail solution. The insertion of a disulfide bridge and the amidation of the C-terminal ending of lassomycin resulted in the direct formation of Pep-1-NNA **(2)**. Pep-1-NN was constructed to follow an anti-clockwise direction from aspartic acid (D) to alanine (A); also, aspartic acid was substituted with asparagine (N) which resulted in the formation of Pep-1-NN **(5)**. This resulted in the formation of a ring with (C10)-NGLRRLFA-(C1) sequence instead of the expected (C10)-DAFLRRLG-(C1), enclosed by a disulfide bond formed by C1 and C10. This resulted in the formation of derivatives that were categorized to fall under the -NN sequence series which is attached at the end of each compound name. Some derivatives from the -NN series that were tested for biological activities were found to be active against *Mtb*, thus resulting in the continuation of this series.

2.3.1.3. Arginine-based lassomycin derivatives

Pep-1-NNA **(2)** and Pep-1-NN **(3)** are arginine-rich, basic peptides that were successfully synthesized via Fmoc SPPS strategy and were obtained at very low yields, and this may have been due to the presence of four arginine (R) residues. Arginine residues are known to be "difficult" amino acids because of the challenges they pose during synthesis, such as the formation of incomplete sequences due to steric hindrance caused by the bulky guanidin sidechain. Furthermore, each arginine residue sidechain guanidino is protected by a bulky 2,2,4,6,7-pentamethyldihydrobenzofuran-5-sulfonyl (pbf) that also increases steric hindrance. Therefore, Pep-1-NN and Pep-1-NNA peptide derivatives were synthesized using longer reaction times, with each amino acid double-coupled to ensure successful aminoacylation. The presence of asparagine (N) and glutamine (Q) residues which are both protected with the bulky trityl (Trt) group, which is known to cause steric hindrance, may have also contributed to poor yields. White precipitates were observed during the cleavage step with trifluoroacetic acid (TFA) for Pep-1-NN and Pep-1-NNA to release the peptides from permanent protecting groups. These white precipitates were suggested to have been salt precipitates formed through the interaction between the guanidino groups with concentrated TFA. Guanidino side

chains are basic with a pKa of ≈ 12.5, behave like organic bases, and are likely to have reacted with a deprotonated anionic TFA. Therefore, the peptides' cleavage time was extended overnight instead of the standard 4 hours to ensure sufficient reaction time for complete deprotection. The formation of TFA salts and steric hindrance may have resulted in numerous impurities observed when the peptides were analyzed via LC-MS. After purification with prep-HPLC, the Pep-1-NNA product was obtained at 92% purity (28% yield), and Pep-1-NN was obtained at over 95% purity (15% yield), respectively. Due to the difficulty of synthesizing arginine-rich peptides, the derivatives were further modified by replacing the arginine groups with lysine groups giving rise to Pep-2-NNA (from Pep-1-NN) and Pep-2-NN (from Pep-2-NN).

2.3.1.4. Substitution of arginine amino acid residues with lysine

Since lassomycin binds to the acidic NTD region of ClpC1, the presence of arginine amino acid residues may play a significant role during the interaction and binding to the enzyme. Arginine amino acids were substituted with slightly less basic lysine (K) residues to investigate arginine's role and importance when binding to ClpC1. One of the reported advantages of replacing arginine with lysine is that the product yield improves due to eliminating some difficulties encountered with arginine while maintaining some basicity. Substituting arginine with lysine also decreases the overall molecular mass, which may improve bioavailability (absorption) in the human body. Pep-2-NNA **(4)** and Pep-2-NN **(5)** derivatives are lysine-substituted peptides that were successfully synthesized and purified with over 95% purity. Two distinct peaks were eluted at different retention times (T_{R1} = 7.3 min and T_{R2} = 7.7 min) and collected during the purification of Pep-2-NNA using semi-preparatory. Each of the two peaks was observed to have the desired peptide mass (1975.1 mDa) upon analysis using HPLC coupled to mass spectrometry (MS). The fractions collected, which were labelled as Pep-2-NNA_Conf1 for T_{R1} and Pep-2-NNA_Conf2 for T_{R2} for better clarity, were observed as conformational isomers since the HPLC column that was used for separation was non-chiral. Also, to ensure that the derivatives synthesized were protected against racemization, shorter coupling-reaction times (30 min) and a good coupling reagent (HATU) were used.[20] Although the yields obtained for both peptide derivatives were poor, it is taken into consideration that purity and yield decrease with increasing peptide chain length (all the peptides discussed are 18 amino acids longer unless stated otherwise). Pep-2-NN had a better yield of 18.20% than both Pep-2-NNA_conf1 (5% yield) and Pep-2-

NNA_conf2 (8.6% yield). The yields were determined using the loading capacity of the derivatives.

Screening for biological activities against Mtb

Pep-2-NN and Pep-2-NNA conformers (1&2) were subjected to a biological screening study against *Mtb*, revealing that all peptide derivatives were potent against the mycobacterium. During the screening process, TB cells were incubated in the presence of each peptide derivative, upon which the Minimum Inhibitory Concentration (MIC_{99}) was determined after 7 days and after 14 days in order to study the bactericidal behavior of lassomycin derivatives. First-line antibiotics rifampicin (RIF), isoniazid (INH) and ethambutol (EMB) were used as control. **Table 2.2** summarizes the results obtained during the biological screening of lassomycin peptides against TB cells. However, all the peptides showed potency against TB cells after 7 days of incubation at varying degrees. Pep-2-NN was more potent than both conformers of Pep-2-NNA at a MIC of 9.87 µg/mL. The potency of Pep-2-NN was comparable to that of ethambutol (MIC = 12.5 µg/mL). Interestingly Pep-2-NN is part of the derivative series (-NN) that was mistakenly synthesized to have an inverted cyclic ring sequence and does not follow that of the lassomycin parent peptide. Although Pep-2-NN is more potent than both Pep-2-NNA conformers, Pep-2-NNA_conf2 (MIC = 39.5 µg/mL) required a lower concentration to kill and hinder the growth of TB cells and was, therefore, more potent than Pep-2-NNA_Conf1(MIC = 79.0 µg/mL). After 14 days of incubation, both Pep-2-NN and Pep-2-NNA_Conf2 derivatives lost activity against *Mtb* (MIC > 632 µg/mL) and could no longer be able to hinder the growth of the bacterium. Meanwhile, Pep-2-NNA_Conf1 maintained some activity after 14 days of incubation, requiring more concentration to hinder the growth of *Mtb*. Because all the peptides were able to kill the TB cells within the first 7 days, it is apparent that the peptide derivatives have no restrictions in entering the mycobacterium cells; however, the mycobacterium was able to adapt and get stronger in the presence of the derivatives. Although Pep-2-NNA_conf2 shares the same peptide sequence with Pep-2-NNA_cofn1, it behaves more like Pep-2-NN as both derivatives are observed to have better bactericidal activities after 7 days of incubation, and both lost activity after 14 days. Meanwhile, Pep-2-NNA_Conf1 showed poor potency after 7 days of incubation and maintained some bactericidal activity after 14 days. Since Pep-2-NN was more potent than both Pep-2-NNA conformers, it may initially seem that antimicrobial

activity *Mtb* is influenced by the nature and position of amino acids in the sequence. However, this may be disputed as Pep-2-NNA-Conf2, which has a different peptide sequence, inhibits the growth of *Mtb* like that of Pep-2-NN. Also, although the Pep-2-NNA conformers share a similar sequence, they behaved differently based on their activity against *Mtb*. Therefore, the arrangement of amino acids in the peptide sequence might not play a huge role, and what matters could be the structural conformation. Pep-2-NN and Pep-2NNA_Conf2 may have a similar structural shape and conformation. The lasso conformation has been determined to be the active form of lassomycin, and the difference in the bactericidal activities in the Pep-2-NNA isomers may be due to this effect. The major cause of the knotting effect is the arrangement of the sterically demanding amino acid residues holding the linear chain (tail) above and below the ring, distinct from lasso peptides. Incorporating asparagine (N) in place of aspartic acid (D) in Pep-2-NN may also have enhanced cell permeability as amide functional groups have been reported to increase membrane permeability[21]. Pep-2-NN and Pep-2-NNA isomers are more active than those reported by other groups[14-15]; however, more studies and modifications are needed to improve potency further. The bactericidal lassomycin peptide was reported with a MIC of 0.3 – 8 µg/mL against *Mtb*[8].

Table 2.2: Summary of the results obtained from screening Pep-2-NN and Pep-2-NNA_conf1&2 lassomycin derivatives for biological activities against *Mtb*. All derivatives screened showed reasonable bactericidal activities against the mycobacterium pathogen. Rifampicin (RIF), isoniazid (INH) and ethambutol (EMB) were used as control.

Entry	Compound	MIC_{99} (µg/mL) 7 days	MIC_{99} (µg/mL) 14 days
1	Pep-2-NNA_conf1	79.0	316
2	Pep-2-NNA_conf2	39.5	> 632
3	Pep-2-NN	9.87	> 632
Control			
4	RIF	0.008	
5	INH	0.054	
6	EMB	12.5	

Cytotoxicity studies of Pep-2-NN

Pep-2-NN was also subjected to a dose-response cytotoxicity screening study to determine toxicity against Human T-cells. The cytotoxicity of Pep-2-NN was observed to increase with increasing peptide concentration (**Table 2.3**). The cytotoxicity studies show that at the active concentration, more than 50% of the cells are viable and, therefore, worth looking into as a lead for exploration and further development as a potential antitubercular agent. The natural lassomycin has very low cytotoxicity against human liver cells (at a half-maximal inhibitory concentration of 350 μg/mL) and does not cause red blood cells to rupture, which may be attributed to poor penetration to mammalian cells.

Table 2.3: A dose-response study to determine the cytotoxicity of Pep-2-NN against human T cells. The cytotoxicity of the peptide against the human cells was observed to increase with concentration.

Entry	Concentration/ (μg/mL)	Toxicity (%)
1	100	58.54
2	50	55.93
3	25	45.57
4	12.5	35.50
5	6.25	36.22
6	3.125	18.63
7	1.56	34.45

2.3.1.5. Cationic lassomycin derivatives

Modified cationic lassomycin-amide derivatives (**2a**, **3a**, **4a,** and **5a** in **Figure 2.3**) were derived from compounds **(2)** – **(5)** in **Figure 2.2**, in which all valine (V) and leucine (L) amino acid residues were substituted with lysine (K). Non-polar amino acid residues, leucine, and valine residues were selected for substitution with lysine over glycine (G) and alanine (A) due to their bulkiness (steric hindrance) and that they are prone to aggregation during synthesis. Not all non-polar amino acids were chosen for substitution with lysine in order to keep the peptide balanced. Also, polar uncharged residues asparagine (N), aspartic acid (D),

and glutamine (Q) were excluded from the list of lysine substituted residues as they may be considered for future work. Peptide cationic modifications also increased the basicity of the derivatives, which may improve the interaction with and penetration to the mycobacterium cell wall and improve potency. Also, increasing cationic residues and the basicity of peptides lead to an increase in the ability of the peptide to cause cell rupture once inside the cell. Lysine-based cationic peptides were preferably synthesized over the more potent arginine-based derivatives in an effort to minimize the inherent challenges encountered during the synthetic procedures (discussed in previous sections). All the peptide derivatives were successfully synthesized (**2a**, **3a**, **4a,** and **5a** in **Figure 2.3**). Pep-Lys-NN (38% yield) was obtained at 90% purity after purification with prep-HPLC. While the purity of Pep-Lys-NNA (69.1% yield) was not easily determined by ultra-violet (UV) detection. Pep-1-NN-Lys was obtained at over 95% purity but with a very low yield. Much like the arginine-rich derivatives **2** and **3**, both Pep-1-NN-Lys and Pep-1-NNA-Lys (also arginine-rich) formed salt precipitates with TFA during cleavage which were observed as a white precipitate on the resin, and these salts were formed at a much faster rate and a greater amount which may have been due to increased basicity.

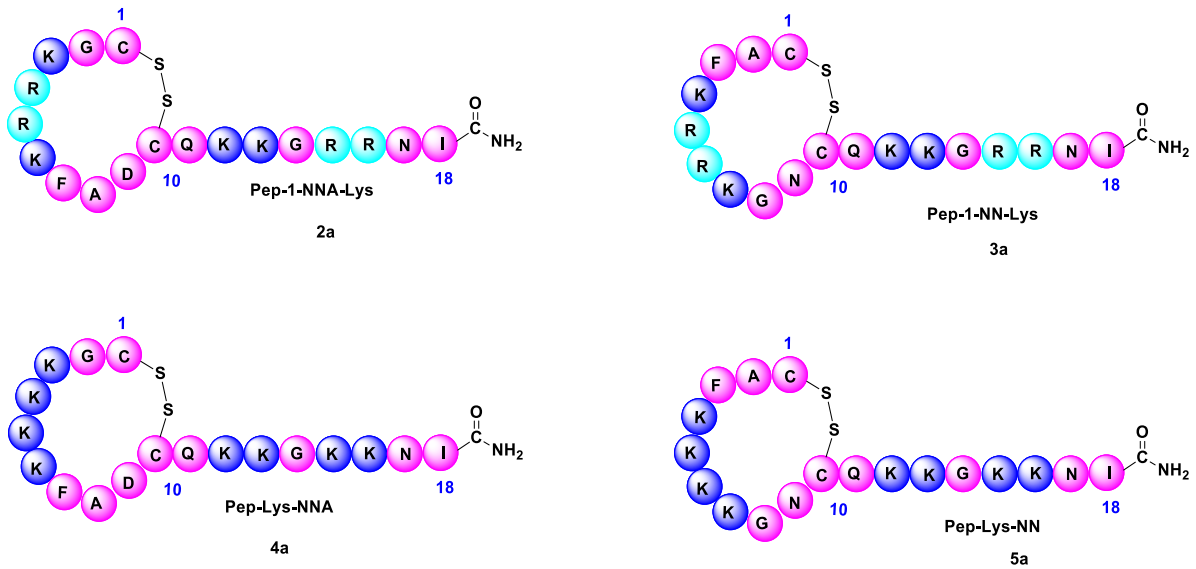

Figure 2.3: Cationic lassomycin derivatives were formed by replacing valine (V) and leucine (L) residues with lysine (K). Pep-1-NNA-Lys **(2a)** was derived from Pep-1-NNA **(2)**, Pep-1-NN-Lys **(3a)** was derived from Pep-1-NN **(3)**, Pep-Lys-NNA **(4a)** was derived from Pep-2-NNA **(4)** and Pep-Lys-NN **(5a)** was derived from Pep-2-NN **(5)**.

Biological activities of cationic lassomycin derivatives

The cationic peptide, Pep-Lys-NN, was subjected to a screening test against several bacterial strains, including *Escherichia coli* (*E. coli*), *Pseudomonas aeruginosa* (*P. aeruginosa*), *Staphylococcus aureus* (*S. aureus*) and *Bacillus subtilis* (*B. subtilis*) to test for antimicrobial activities. The results from the screening tests are reported and summarized in **Table 2.4**. Of all the pathogens tested, Pep-Lys-NN was only active against the *B. subtilis* ATCC 2002 strain, and this may be because *B. subtilis* shares a similar caseinolytic protease to *Mtb* that is targeted by lassomycin. The *E. coli*, *P. aeruginosa*, and *S. aureus* pathogens did not contain ClpC1 and were not killed by the peptide. This is supported by the results obtained in a study by the Gavrish group, which showed that *E. coli* and *S. aureus* (along with other organisms that do not share the ClpC1 enzyme) were not targeted by lassomycin[8]. This adds to the narrative that lassomycin is highly selective against ClpC1. *B. subtilis* is found naturally in the human body, but its caseinolytic protease and its AAA+ ATPases are non-essential for cell viability compared to those found in the *Mtb*.[11] In the future, a pool of pathogens tested against lassomycin derivatives may be expanded to further understand the lassomycin's characteristics and mechanisms. Unfortunately, when Pep-Lys-NN was tested again for activity against *Mtb* using an Alamar blue assay, along with Pep-Lys-NNA and Pep-1-NN, the peptides precipitated in the media. When the Alarmar blue dye was added to the samples, the color turned pink to indicate that the derivatives were inactive against the mycobacterium (**Figure 2.4**). The growth of the mycobacterium was milky and spread out, which was not expected. Therefore, the Alarmar blue assay may not be the best technique to test for the activity of the peptide derivatives against *Mtb*.

Table 2.4: Results from screening the cationic peptide, Pep-Lys-NN, with a small pool of different organisms. The peptide only showed activity against *B. subtilis*, the only organism in the list that shares the same caseinolytic protease as *Mtb*.

		Minimum inhibitory concentration (µg/mL) for different organisms			
Compound	Starting concentration/ (µg/mL)	*E. coli* ATCC25922	*P. aeruginosa* ATCC 27853	*S. aureus* ATCC29913	*B. subtilis* ATCC 2002
Pep-Lys-NN	256	>256	>256	>256	256

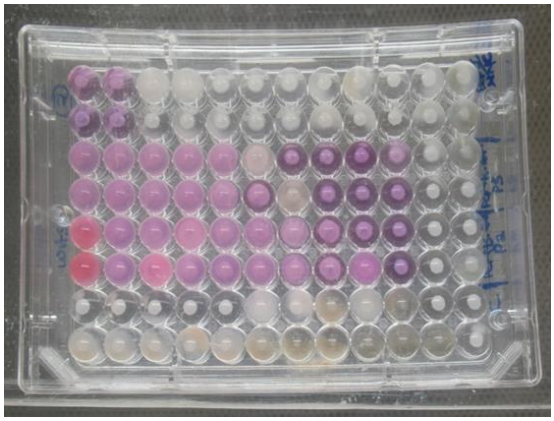

Figure 2.4: The Alarmar blue assay that was used to test the activity of Pep-Lys-NN, Pep-Lys-NNA, and Pep-1-NN against *Mtb*. When the Alarmar blue dye was added to the samples, the color turned pink to indicate that the derivatives were inactive against the mycobacterium.

2.3.1.6. *N*-methylation of Pep-2-NN and Pep-2-NNA lassomycin derivatives

Lassomycin shows great potential for the treatment of tuberculosis, however, because natural peptides are inherently prone to poor chemical and physical stabilities such as enzymatic degradation, therefore further development may be required.[11, 22] Currently, to the best of our knowledge, there is no available published work about the stability of lassomycin in physiological conditions. In this study, *N*-methylated amino acids were incorporated into the Pep-2-NN and Pep-2-NNA lassomycin peptide derivatives to improve stability. This strategy also increases the hydrophobicity of the peptide and thereby increasing bioavailability. One of the major drawbacks of peptide *N*-methylation modifications is that the degree of purity decreases with increasing peptide chain length and the number of *N*-methylated amino acids. This phenomenon was observed and better demonstrated in a study by F. Albericio and colleagues (2005).[23]

The synthesis of *N*-methylated valine (Fmoc-*N*-Me-Val-OH), leucine (Fmoc-*N*-Me-Leu-OH) and alanine (Fmoc-*N*-Me-Ala-OH)

N-methylated valine, leucine, and alanine amino acids were synthesized using according to the Freidinger synthetic route, which was chosen from a wide range of available α-*N*-methylation methods due to racemization-free reactions, and any Fmoc- protected amino can be used[24]. To synthesize the *N*-methylated amino acid residues, a 2-step procedure was followed, and this included the synthesis of 5-oxazolidinone precursors, which will then be

used in the second and final step to form the final product. To make the amino acid 5-oxazolidinone precursors (compound **6**, **Scheme 2.1**), a mixture of the appropriate Fmoc amino acid and paraformaldehyde was heated under reflux in toluene. *P*-toluenesulfonic acid was used as a catalyst to activate the paraformaldehyde to become more electrophilic to better react with the Fmoc-amino acid and form oxazolidinones. Fmoc-protected valine (V), leucine (L), and alanine (A) amino acids were chosen for *N*-methylation. Upon successful synthesis, 5-oxazolidinones were purified by recrystallization and were obtained as crystalline substances. Each *N*-methylated amino acid was synthesized according to **Scheme 2.2** and pre-concentrated *in vacuo* after purification to form a gel-like substance that crystallized upon cooling. Fmoc-*N*-Me-Leu-OH (84% yield) and Fmoc-*N*-Me-Ala-OH (31% yield) were obtained as slightly yellow crystals, and Fmoc-*N*-Me-Val-OH (70% yield) product was a white amorphous mixture. Analysis with HPLC-MS and Nuclear Magnetic Resonance Spectroscopy (NMR) showed that *N*-methylation of the amino acids was successful, with purity greater than 95% for all amino acids. The melting points of Fmoc-*N*-Me-Leu-OH and Fmoc-*N*-Me-Ala-OH were similar to those commercially purchased from Sigma-Aldrich. However, the melting point of Fmoc-*N*-Me-Val-OH was slightly greater, which may be due to the presence of minor impurities. **Table 2.5** summarizes the results of synthesized *N*-methylated amino acids.

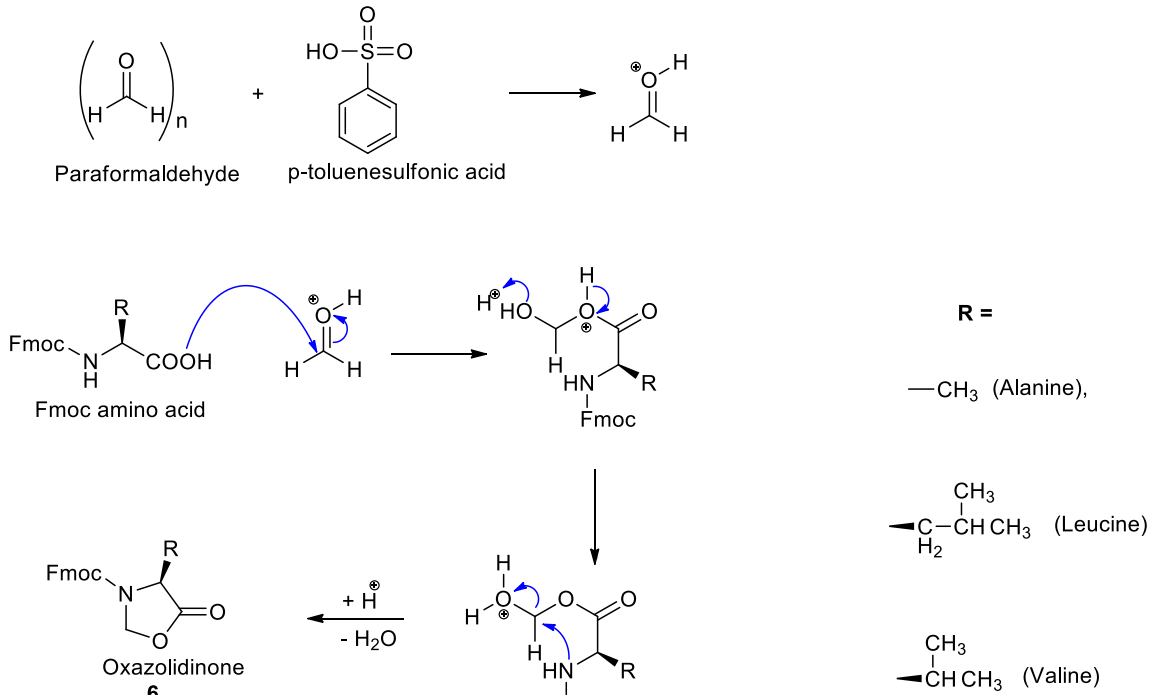

Scheme 2.1: The mechanism of synthesizing the 5-oxazolidinones from Fmoc-protected amino acids. R represents the side chain of the amino acid.

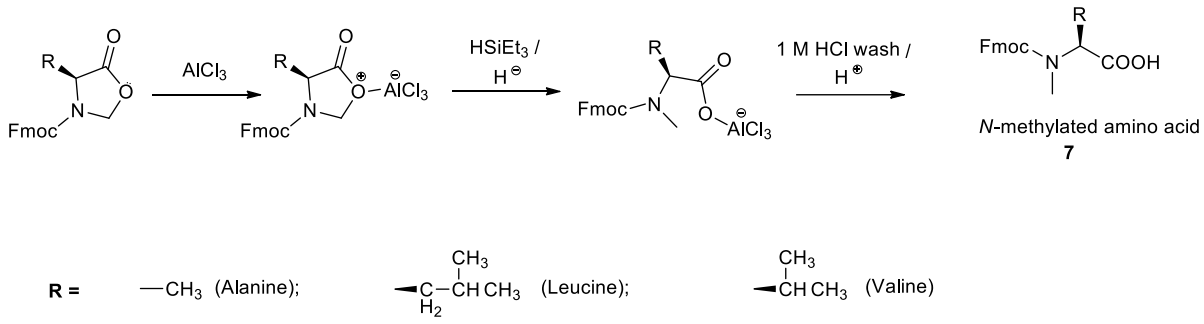

Scheme 2.2: The synthesis of *N*-methylated Fmoc- protected amino acids from the 5- oxazolidinone precursors. R represents the side chain of the amino acid.

Table 2.5: Summary of the data obtained for the synthesized Fmoc *N*-methylated amino acids Fmoc-*N*-Me-Ala-OH, Fmoc-*N*-Me-Leu-OH, and Fmoc-*N*-Me-Val-OH, and these include the melting point and selected NMR data. Ala = Alanine (A), Leu = Leucine (L) and Val = Valine (V)

***N*- methylated amino acid**	**% Yield**	**% Purity**	**Theoretical M.P (°C)**	**Actual M.P (°C)**	**$^{\alpha}$*N*-C$\underline{H}_3$ (ppm) ^{1}H NMR**	**$^{\alpha}$*N*-$\underline{C}H_3$ (ppm) ^{13}C NMR**
Fmoc-*N*-Me-Ala-OH	31	> 95	140	145	2.91 (3H, s, N-CH_3)	30.50 (C, s, N-CH_3)
Fmoc-*N*-Me-Leu-OH	84	> 95	113 -116	114	2.86 (3H, s, N-CH_3)	30.33 (C, s, N-CH_3)
Fmoc-*N*-Me-Val-OH	70	> 95	140 -145	> 150	2.90 (3H, s, N-CH_3)	27.43 (C, s, N-CH_3)

Synthesis of N-methylated Pep-2-NNA and Pep-2-NNA peptide derivatives

Pep-2-NN and Pep-2-NNA were further derivatized by incorporating *N*-methylated amino acids in place of alanine (A), leucine (L), and valine (V) for each peptide. Pep-2-NN and Pep-2-NNA were selected because they showed relatively good biological activities when screened against *Mtb*. To minimize impurities and to ensure successful and complete incorporation of the *N*-methylated amino acids into the peptide chain, ethyl (hydroxyimino) cyanoacetate (Oxyma Pure) and HOBt were used as coupling reagents during synthesis. Furthermore, the coupling time of *N*-methylated amino acids was increased to 1 hour with double coupling and washings in-between with DMF/DCM solvents. The *N*-methylated Pep-2-NN and Pep-2-NNA derivatives were successfully synthesized as determined by analysis with HPLC-MS and were purified using semi-prep HPLC. However, they were not successfully separated and isolated from impurities that co-eluted with the derivatives. It is

not uncommon for some peptidic impurities to be co-eluted with the parent peptide, as has been observed for most of the previously discussed peptides. It was impossible to determine the product yields due to poor separation and isolation of *N*-methylated Pep-2-NN from impurities during purification. When several *N*-methylated amino acids are coupled consecutive to each other, they cause the *N*-methyl-rich peptides to be vulnerable to impurities such as deletion sequence, which are observed when some amino acid residues appear to be missing in the final product. Other impurities encountered with *N*-methylated Pep-2-NN were incomplete sequences that were usually terminated after adding an *N*-methylated amino acid. Impurities of terminated sequences included INKKGV(Me), INKKGV(Me)L(Me)QCNGL(Me), and INKKGV(Me)L(Me). Termination of sequences arising after coupling *N*-methylated amino acids may have resulted from the blockage of aminoacylation by the *N*-methyl groups, also the deprotection of the Fmoc of *N*-methylated amino acids may have been slow and incomplete, resulting in incomplete sequences. For future purposes, the deprotection solution or method may be modified by adding the non-nucleophilic 1,8-Diazabicyclo[5.4.0]undec-7-ene (DBU) to ensure complete Fmoc deprotection and thus improve yields. DBU is more sterically hindered than piperidine, and in lower concentrations, it has been found to result in fewer impurities, and this may be attributed to its bulky nature.[25]

2.3.1.7. Non-polar lassomycin peptide derivatives

Non-polar lassomycin derivatives Pep-Ala-NNA and Pep-Ala-NNA, derived from replacing all lysine amino acids with alanine in Pep-2-NNA and Pep-2-NN, respectively, were also synthesized in order to investigate the importance of basicity in the binding and potency of lassomycin. The structures of Pep-Ala-NN and Pep-Ala-NNA are shown in **Figure 2.5**. Alanine was chosen because it is a small amino acid over glycine because of its ability to stabilize the 3D structure (folding). The results which may be obtained from using alanine over glycine are expected not to differ significantly. Replacing all lysine residues with alanine causes the peptide to be neutral with poor water solubility.

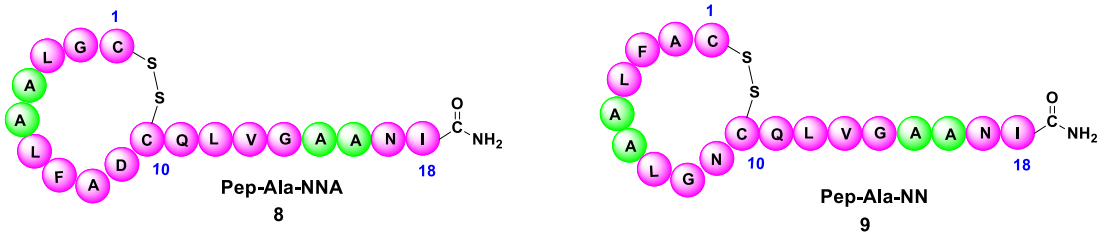

Figure 2.5: The structures of Pep-Ala-NNA **(8)** and Pep-Ala-NN **(9)** by replacing all the lysine residues in Pep-2-NNA and Pep-2-NN, respectively.

Challenges with purifications:

Pep-Ala-NNA and Pep-Ala-NN were successfully synthesized, as confirmed with HPLC-MS analysis, however, difficulties were encountered during purification, which may be due to the highly non-polar nature of the peptides. Unlike the previously discussed peptide, the alanine-based peptides were not soluble in water and had to be dissolved in small amounts of DMSO. However, they would precipitate out of the solution upon adding water or acetonitrile to decrease the concentration of DMSO for purification with prep-HPLC. Upon storage, the peptides also form a gel-like solution which may be due to intense aggregation and 3-D structure formation.

2.4. Conclusion

Lassomycin is a significantly potent and highly selective antimicrobial peptide that kills *Mtb* with bactericidal activity that is comparable to rifampicin.[8] However, the loss of bactericidal activity encountered by research groups that attempted to synthesize the peptide inspired our group to synthesize lassomycin derivatives using different strategies. Several challenges were encountered during peptide modification and synthesis especially for arginine-rich peptides (compounds **2**, **2a**, **3,** and **3a**), *N*-methylated peptides, and non-polar alanine-rich peptides, resulting in poor yields and purity. However, these should not deter any future interest in expanding on these areas in order to further study and improve the potency of lassomycin and its derivatives. Lysine-based peptide derivatives, Pep-2-NNA **(4)** and Pep-2-NN **(5)** had better results concerning purity and yield; furthermore, they had antimicrobial activity against *Mtb* upon screening. Also, the cationic highly lysine-rich Pep-Lys-NN **(5a)** showed potency and selectivity for *B. subtilis*, which shares a similar protease as *Mtb* that is targeted by lassomycin. Therefore, this further demonstrates that lassomycin is worth looking into as a

potential anti-TB agent to be further developed as a drug to combat TB. Interestingly, the two isolated conformers of Pep-2-NNA interact differently towards *Mtb,* and these can be further studied in order to determine the active conformation of lassomycin when bound to ClpC1 as it is not yet known. In addition to the bactericidal effects of the modified lassomycin derivatives and the selectivity demonstrated by Pep-Lys-NN, the cytotoxicity studies revealed that at the active concentration of Pep-2-NN, more than 50% of human cells remained viable. Therefore disulfide-bridge substituted lassomycin-amide peptide derivatives are worth exploring as lead anti-TB agents for further development into antitubercular drug treatment. In conclusion, substituting the macrolactam bridge with a disulfide bond seems to produce potent derivatives against mycobacterium instead of attempting to keep the macrolactam bond during chemical synthesis. Future work involves 3D structure elucidation using NMR spectroscopy to understand the activity of Pep-2-NN, after which further derivatives will be synthesized.

References:

1. Moutinho, S., The Oldest Pandemic. *Scientific American* **2022,** *326* (6), S16-S20.

2. Gupta, K. B.; Gupta, R.; Atreja, A.; Verma, M.; Vishvkarma, S., Tuberculosis and nutrition. *Lung India: Official Organ of Indian Chest Society* **2009,** *26* (1), 9.

3. Chandra, T. J.; Selvaraj, R.; Sharma, Y., Same day sputum smear microscopy for the diagnosis of pulmonary tuberculosis: Ziehl-Neelsen versus fluorescent staining. *Journal of Family Medicine and Primary Care* **2015,** *4* (4), 525.

4. Babamahmoodi, F.; Mahdavi, M. R.; Jalali, H.; Talebi, B.; Roshan, P.; Mahdavi, M., Evaluation of gene mutations involved in drug resistance in Mycobacterium tuberculosis strains derived from tuberculosis patients in Mazandaran, Iran, 2013. *International Journal of Molecular and Cellular Medicine* **2014,** *3* (3), 190.

5. Joshi, J. M., Tuberculosis chemotherapy in the 21st century: Back to the basics. *Lung India* **2011,** *28* (3), 193-200.

6. Caño-Muñiz, S.; Anthony, R.; Niemann, S.; Alffenaar, J.-W. C., New approaches and therapeutic options for Mycobacterium tuberculosis in a dormant state. *Clinical Microbiology Reviews* **2018,** *31* (1), e00060-17.

7. Lupoli, T. J.; Vaubourgeix, J.; Burns-Huang, K.; Gold, B., Targeting the proteostasis network for mycobacterial drug discovery. *American Chemical Society infectious diseases* **2018,** *4* (4), 478-498.

8. Gavrish, E.; Sit, C. S.; Cao, S.; Kandror, O.; Spoering, A.; Peoples, A.; Ling, L.; Fetterman, A.; Hughes, D.; Bissell, A., Lassomycin, a ribosomally synthesized cyclic peptide, kills Mycobacterium tuberculosis by targeting the ATP-dependent protease ClpC1P1P2. *Chemistry & Biology* **2014,** *21* (4), 509-518.

9. Parish, T., Targeting mycobacterial proteolytic complexes with natural products. *Chemistry & Biology* **2014,** *21* (4), 437-438.

10. Malik, I. T.; Brötz-Oesterhelt, H., Conformational control of the bacterial Clp protease by natural product antibiotics. *Natural Product Reports* **2017,** *34* (7), 815-831.

11. Culp, E.; Wright, G. D., Bacterial proteases, untapped antimicrobial drug targets. *The Journal of Antibiotics* **2017,** *70* (4), 366-377.

12. Zhang, S.; Chen, J.; Shi, W.; Cui, P.; Zhang, J.; Cho, S.; Zhang, W.; Zhang, Y., Mutation in clpC1 encoding an ATP-dependent ATPase involved in protein degradation is associated with pyrazinamide resistance in Mycobacterium tuberculosis. *Emerging Microbes & Infections* **2017,** *6* (1), 1-2.

13. Hanna, C. C.; Hermant, Y. O.; Harris, P. W.; Brimble, M. A., Discovery, Synthesis, and Optimization of Peptide-Based Antibiotics. *Accounts of Chemical Research* **2021,** *54* (8), 1878-1890.

14. Harris, P. W.; Cook, G. M.; Leung, I. K.; Brimble, M. A., An Efficient Chemical Synthesis of Lassomycin Enabled by an On-Resin Lactamisation–Off-Resin Methanolysis Strategy and Preparation of Chemical Variants. *Australian Journal of Chemistry* **2016,** *70* (2), 172-183.

15. Lear, S.; Munshi, T.; Hudson, A.; Hatton, C.; Clardy, J.; Mosely, J.; Bull, T.; Sit, C.; Cobb, S., Total chemical synthesis of lassomycin and lassomycin-amide. *Organic & Biomolecular Chemistry* **2016,** *14* (19), 4534-4541.

16. Kreutzer, A. G.; Salveson, P. J.; Yang, H., Standard Practices for Fmoc-Based Solid-Phase Peptide Synthesis in the Nowick Laboratory (Version 1.6. 3). **2018**.

17. Han, Y.; Zhang, M.; Lai, R.; Zhang, Z., Chemical modifications to increase the therapeutic potential of antimicrobial peptides. *Peptides* **2021,** *146*, 170666.

18. Lau, J. L.; Dunn, M. K., Therapeutic peptides: Historical perspectives, current development trends, and future directions. *Bioorganic & Medicinal Chemistry* **2018,** *26* (10), 2700-2707.

19. Vijayadas, K. N.; Nair, R. V.; Gawade, R. L.; Kotmale, A. S.; Prabhakaran, P.; Gonnade, R. G.; Puranik, V. G.; Rajamohanan, P. R.; Sanjayan, G. J., Ester vs. amide on folding: a case study with a 2-residue synthetic peptide. *Organic & Biomolecular Chemistry* **2013,** *11* (48), 8348-8356.

20. Stéphane, V. O., Werbitzky; Thomas, Z.,On-resin peptide cyclization. 2011.

21. Walensky, L. D.; Bird, G. H., Hydrocarbon-stapled peptides: principles, practice, and progress: miniperspective. *Journal of Medicinal Chemistry* **2014,** *57* (15), 6275-6288.

22. Prasasty, V.; Radifar, M.; Istyastono, E., Natural peptides in drug discovery targeting acetylcholinesterase. *Molecules* **2018,** *23* (9), 2344.

23. Teixidó, M.; Albericio, F.; Giralt, E., Solid-phase synthesis and characterization of N-methyl-rich peptides. *The Journal of Peptide Research* **2005,** *65* (2), 153-166.

24. Zhang, S.; Govender, T.; Norström, T.; Arvidsson, P. I., An improved synthesis of Fmoc-N-methyl-α-amino acids. *The Journal of Organic Chemistry* **2005,** *70* (17), 6918-6920.

25. Wade, J. D.; Bedford, J.; Sheppard, R. C.; Tregear, G. W., DBU as an N alpha-deprotecting reagent for the fluorenylmethoxycarbonyl group in continuous flow solid-phase peptide synthesis. *Peptide Research* **1991,** *4* (3), 194-199.

Chapter 3

The synthesis of lassomycin-amide peptide derivatives conjugated to lipophilic molecules

3.1. Introduction

The conjugation of peptides into lipophilic acids, such as fatty acids (e.g., palmitic acid) and polycyclic-caged molecules (e.g., adamantane carboxylic acid), is well reported. This strategy increases the hydrophobicity of the peptides and improves interaction and binding to the lipid-rich bacterial cell membrane, thus leading to improved antibacterial activity. [1-3]

In general, antimicrobial peptides (AMPs) are cationic and have a high affinity for bacterial cell membranes. Due to their amphipathic nature, they electrostatically interact with anionic surfaces and bind to phospholipid-rich membrane regions through hydrophobic forces.[4] The amphiphilicity of AMPs results from their ability to possess hydrophilic and hydrophobic regions. Peptide conjugation to lipophilic acids has been found to improve the hydrophobic interactions and thus enhance cell membrane disruption caused by AMPs resulting in the formation of pores, thereby increasing membrane permeability and peptide penetration.[3] Increased membrane permeability can promote the passing of more peptides through the membrane to reach their specific target inside the cell and thus result in improved activity. The conjugation of AMPs to lipophilic acids also increases cytotoxicity, which results in cell death, increases the AMPs' half-life[2], and improves peptide stability through self-association.[5] Furthermore, adamantane can bind to the pores of cellular ion channels and cause a blockage that inhibits the passage of crucial ions, thus acting as a "bullet".[6-8] The conjugation of fatty acids to antimicrobial peptides also minimizes the risks against bacterial resistance.[9] The *N*-terminus of peptides is the most preferred area to conjugate lipophilic molecules since it has resulted in better activity, as Storck *et al.,* demonstrated, where several peptides conjugated with fatty acids of different lengths were tested against various pathogens.[10]

The *Mycobacterium tuberculosis* cell envelope is waxy and rich in complex lipids that include the mycolic acids, which are covalently bound to the arabinogalactan-peptidoglycan layer, and these act as a hydrophobic protecting barrier against antibiotic entry.[11] Hence the

need for lipophilic molecules that facilitate the membrane permeability of lassomycin-amide peptide derivatives. The composition of the *Mycobacterium tuberculosis* cell envelope is presented in **Figure 3.1** below.[12]

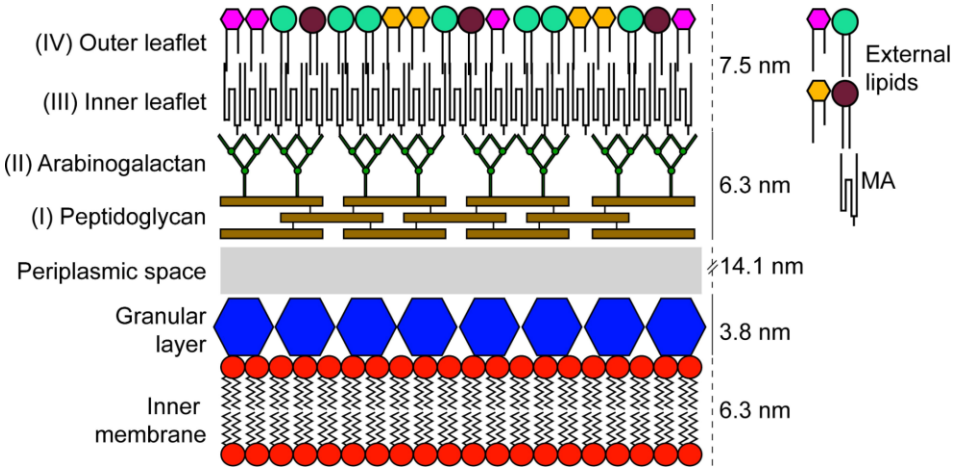

Figure 3.1: A representation of the *Mycobacterium tuberculosis* cell envelope, licensed under the Creative Commons Attribution 4.0 International License, CC BY 4.0.

3.2. The conjugation of lassomycin derivatives to fatty acids

Pep-1-NNA and Pep-2-NNA are lassomycin derivatives discussed in detail in Chapter 2. This chapter further explores their conjugation derivatization to linear fatty acids and caged structured lipid acids such as palmitic acid and adamantane carboxylic acid. Pep-1-NNA-Ada and Pep-2-NNA-Ada were formed by coupling adamantane onto the *N*-terminus of the peptide sequences. In contrast, Pep-2-NNA-Pal was formed by attaching palmitic acid onto the *N*-terminus of Pep-2-NNA. Reference linear forms of Pep-1-NNA-Ada and Pep-2-NNA-Ada were also formed by removing the disulfide bridge to study the cyclized derivatives' behaviour and the cyclic ring's role. **Figure 3.2** below shows the structures of the peptide derivatives discussed in this chapter, and **Table 3.1** below shows the variances in their sequences.

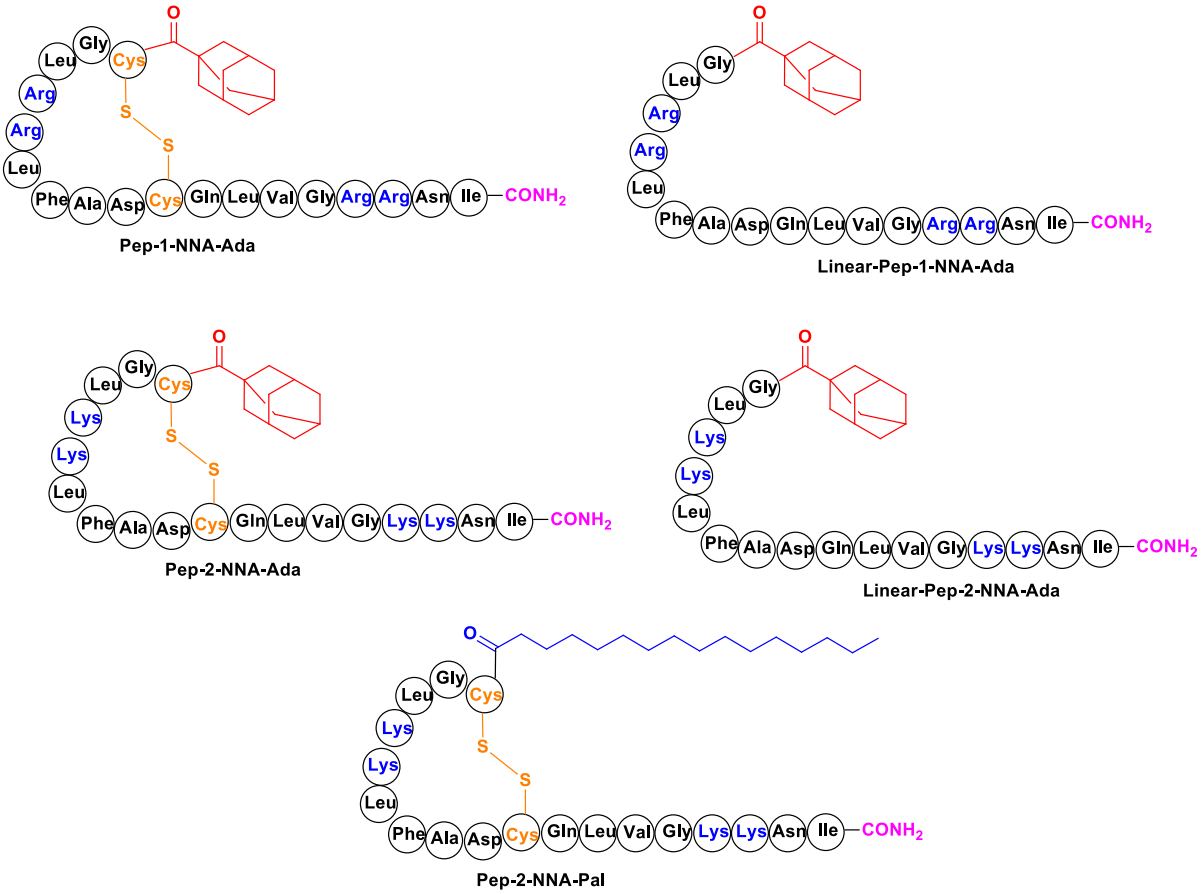

Figure 3.2: Structures of lassomycin peptide derivatives conjugated to adamantane and palmitic acid fatty acids.

Table 3.1: Illustrating the sequences and modifications of lassomycin derivatives conjugated to fatty acids. Ada = Adamantane and Pal = Palmitic acid.

Item no.	Peptide derivative	Sequence	Modification
1	Pep-1-NNA-Ada	INRRGVLQCDAFLRRLGC-Ada	Pep-1-NNA conjugated with adamantane
2	Linear Pep-1-NNA-Ada	INRRGVLQDAFLRRLG-Ada	Pep-1-NNA-Ada without cysteine disulfide bridge
3	Pep-2-NNA-Ada	INKKGVLQCDAFLKKLGC-Ada	Pep-2-NNA conjugated with adamantane
4	Linear Pep-2-NNA-Ada	INKKGVLQDAFLKKLG-Ada	Pep-2-NNA-Ada without cysteine disulfide bridge
5	Pep-2-NNA-Pal	INRRGVLQCDAFLRRLGC-Pal	Pep-2-NNA conjugated with Palmitic acid

Pep-1-NNA and Pep-2-NNA are cationic amphiphiles, and their overall positive charges are due to arginine and lysine residues, respectively. Adamantane and palmitic acid were conjugated to the *N*-terminus of Pep-1-NNA and Pep-2-NNA derivatives by acylation. These moieties were chosen based on their ability to improve potency and selectivity and reduce side reactions as reported in previous studies.[6, 13]

One of the highly hydrophobic AMPs drawbacks reported is their tendency to become non-selective towards bacterial and human cell membranes. We hypothesize that the overall positive charge of the lassomycin derivatives will increase their affinity for the acidic bacterial membrane and not mammalian cells, thereby improving selectivity.

3.3. Synthesis

All the peptides discussed in this thesis were synthesized via the Fluorenylmethyloxycarbonyl (Fmoc-) solid phase peptide synthesis (SPPS) strategy on the Fmoc-protected Rink Amide 4-methylbenzhydrylamine (MBHA) resin as a solid support.[14] The rink amide resin was first pre-swelled in dimethyl formamide (DMF) for 3 hours before use. The resin was then transferred to a reaction vessel fitted with a fritted resin support and washed with DMF (3×5 mL) followed by DCM (3×5 mL the solvent was removed by vacuum filtration.

3.3.1. Fmoc removal:

The Fmoc-protected resin was treated with a 20% piperidine solution in DMF (v/v) for 2 x 5 min to expose the free amino group (-NH_2) and allow for the aminoacylation with an incoming amino acid. The reagents were removed by filtration under vacuum. The resin was washed with DMF (3×5 mL) followed by DCM (3×5 mL to remove contaminants and side products.

3.3.2. Amino acids

All the amino acids used in the synthesis of each peptide derivative were commercially purchased and are Fmoc-protected temporarily at the amine (NH_2) group and permanently protected with acid labile side chain protecting groups such as butyloxycarbonyl (Boc), tert-

butyloxycarbonyl (OtBu) and trityl (Trt). Examples of Alanine, lysine, and cysteine are presented below in **Figure 3.3**.

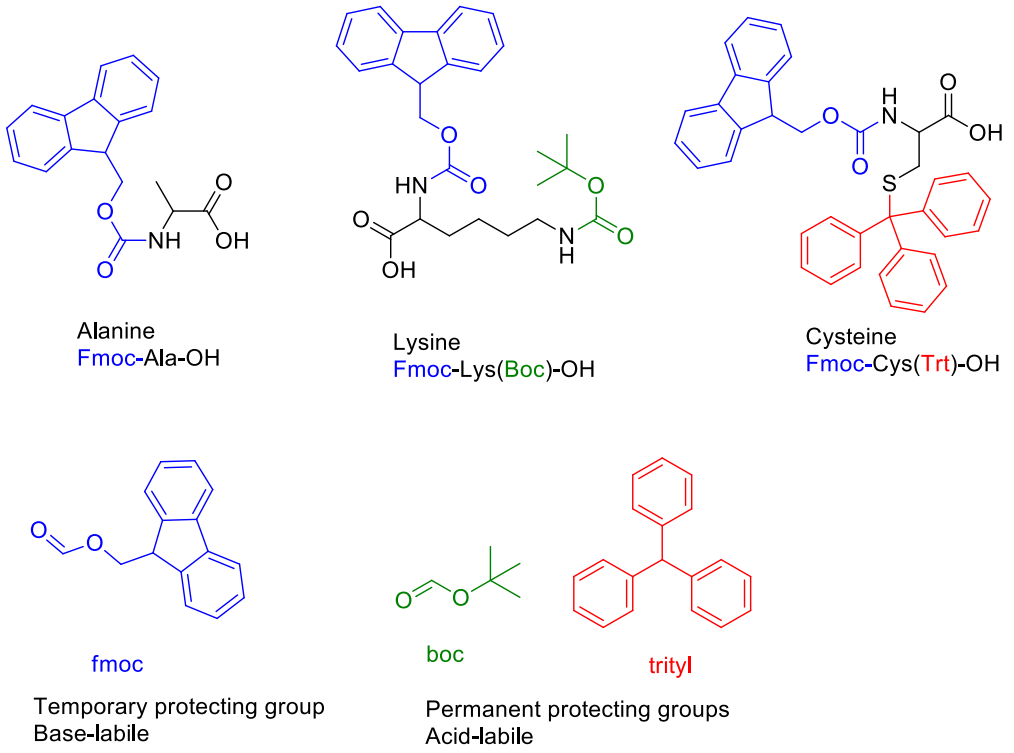

Figure 3.3: Amino acids and their protecting groups

3.3.3. Attachment of the first amino acid to the resin and peptide chain elongation

The first amino acid (6mL, 0.2 M) was attached to the newly deprotected resin by the addition of a solution of oxymapure (0.2 M) coupling reagent and diisopropylcarbodiimide (DIC, 0.2 M) at a 1:1:1 equivalence to the resin. The amino acid was coupled twice for 35 minutes to ensure successful aminoacylation and washed with DCM and DMF in-between couplings, and the waste was filtered out using vacuum filtration. The amino acid attached to the resin linker forms the C-terminus of the peptide upon cleavage and is dependent on the peptide derivative sequence. The peptide resin was then treated with 20% piperidine to remove the Fmoc group. The second amino acid (6 mL, 0.2M) was mixed with oxymapure and DIC, and the mixture was added twice to the peptide-resin for at least 35 minutes each time. The aminoacylation and Fmoc removal steps were repeated until all the amino acids in the peptide sequence were added. Washings were done in-between steps with DMF (3×5 mL) followed by DCM (3×5 mL).

3.3.4. Attachment of adamantane and palmitic acid

After synthesizing each peptide, a mixture of oxyma pure, diisopropyl carbodiimide, and the respective fatty acid (0.2 M), 1-adamantane carboxylic acid or palmitic acid were added twice for 1 hour to the newly Fmoc deprotected peptide-resin. Washings were done in-between steps with DMF (3×5 mL) followed by DCM (3×5 mL).

3.3.5. Peptide cleavage from resin and permanent protecting groups using trifluoroacetic acid (TFA) and cyclization

The peptides were cleaved from the resin linker, and the permanent protecting groups were removed by acidolysis with a 95% trifluoroacetic acid (TFA) cocktail with 2.5% triisopropylsilane (TIS) and 2.5% water. The peptides were precipitated using diethyl ether, and the supernatant was decanted after centrifuging. The peptides were then washed four times with ether. TIS and water function as scavengers for the cleaved protecting groups as these can irreversibly attack the peptide backbone and alkylate it, which may lead to the formation of impurities and low yields. The cleavage time for each peptide was at least 3 hours. Each cyclic peptide was cyclized overnight using 20% DMSO and analyzed using High-Performance Liquid Chromatography coupled to Mass Spectroscopy (HPLC-MS).

3.3.6. Peptide analysis using High-Performance Liquid Chromatography coupled to Mass Spectroscopy (HPLC-MS)

A small amount of each derivative was dissolved in HPLC-grade solvents and analyzed using HPLC-MS to determine successful synthesis. A Thermo Scientific Dionex Ultimate 3000 UHPLC instrument coupled to a Bruker Compact Q-TOF mass spectrometer was used to analyze the peptides and determine purity. The compounds were separated on a Phenomenex XB-C18 column (5 µm, 100 Å, 250 mm × 21.2 mm), and the flow rate was set at 0.3 mL/min. The mass spectrometry analysis was performed using a positive mode electrospray ionization source (ESI). A two-buffer system was employed, Buffer A consisted of 0.1 % formic acid/H_2O (v/v), and Buffer B consisted of 0.1 % formic acid/acetonitrile (v/v).

3.4. Results and Discussion

All the peptides were analysed using LCMS, which revealed that adamantane and palmitic acid were successfully conjugated to their respective derivatives, and selected spectra of the crude peptides are shown in **Figure 3.4** below. The LCMS data for all the derivatives are recorded in **Table 3.2** below, showing each derivative's observed mass and retention time.

Table 3.2: Presentation of the LCMS data of lipid acids conjugated peptides. Pep-2-NNA-Ada was analysed using an LC gradient method of 5 – 95% acetonitrile for 10 minutes, while the rest of the peptides were analysed using the same gradient over 15 minutes.

Compound	Calculated Mass	Observed Mass	Molecular Ion	Retention Time (min)
Pep-1-NNA-Ada	2250,2354 $C_{99}H_{167}N_{33}O_{23}S_2$ Uncyclized	1127.6006	$[M+2H]^{2+}$	9.63 – 9.76
	2248,2198 $C_{99}H_{165}N_{33}O_{23}S_2$ Cyclized	1126.6106	$[M+2H]^{2+}$	9.93 – 10.18
Linear Pep-1-NNA-Ada	2044,2170 $C_{93}H_{157}N_{31}O_{21}$	1024.1152	$[M+2H]^{2+}$	8.11 – 8.17
		2246.2427	$[M+H]^{+}$	9.84 – 9.98
	1882,1126 $C_{82}H_{143}N_{31}O_{20}$ No adamantane	1884.1402	$[M+H]^{+}$	7.82 – 7.91
Pep-2-NNA-Ada	2136,1952 $C_{99}H_{165}N_{25}O_{23}S_2$ Cyclized	1069.6104	$[M+2H]^{2+}$	13.42 – 13.49
	2138,2108 $C_{99}H_{167}N_{25}O_{23}S_2$ Uncyclized	1070.6201	$[M+2H]^{2+}$	13.59 – 13.82
Linear Pep-2-NNA-Ada	1960,1986 $C_{93}H_{157}N_{25}O_{21}$	981.5949	$[M+2H]^{2+}$	9.38
Pep-2-NNA-Pal	2214,3360 $C_{104}H_{183}N_{25}O_{23}S_2$	1108.0785	$[M+2H]^{2+}$	16.09 – 16.33
		1117.0838	$[M+H_2O+H]^{2+}$	

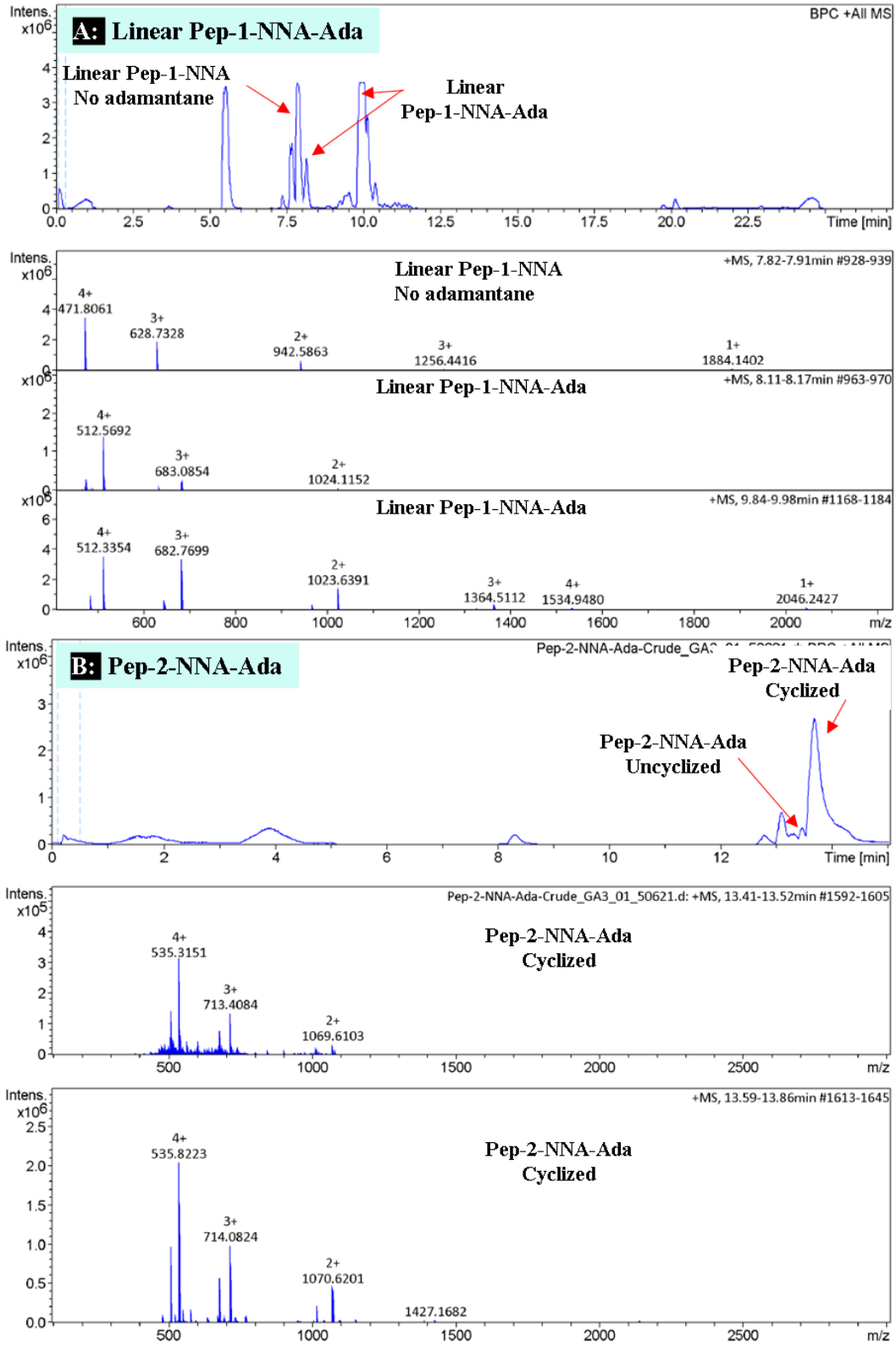

Figure 3.4: Selected LCMS spectra of peptides conjugated to lipid acids, including that of **A:** Linear Pep-1-NNA-Ada and **B:** Pep-2-NNA-Ada.

Pep-1-NNA-Ada, Linear Pep-1-NNA-Ada, Linear Pep-2-NNA-Ada, and Pep-2-NNA-Pal were analysed using an LC gradient method of 5 – 95% acetonitrile for 15 minutes while Pep-2-NNA-Ada analysed using the same gradient over 10 minutes.

3.4.1. Effect of the lipid molecules on the hydrophobicity of peptides

The order of separation of peptides during purification and analysis with reversed-phase HPLC depends on their interaction with the mobile phase and non-polar stationary phase, where they are separated in the order of increasing hydrophobicity.[15] The presence of adamantane and palmitic acid increased the hydrophobicity of the peptides and caused them to elute at a delayed retention time as they were retained longer on the non-polar C-18 stationary phase of the LC column. This was further demonstrated in the analysis of Linear Pep-1-NNA-Ada, where the conjugate was eluted between T_{R1}: 8.11 – 8.17 min and T_{R2}: 9.84 – 9.98 min, while the adamantane-free Linear Pep-1-NNA due to incomplete coupling was eluted at an earlier retention time range of T_R: 7.82 – 7.91 min (**Table 3.2**). In order to ensure complete acylation of adamantane to the resin-bound peptide during synthesis, a mixture of oxymapure coupling reagent and diisopropyl carbodiimide (DIC) was used, and this has been reported to have a similar coupling effect as HATU, which is superior to HBTU. However, the presence of adamantane-free peptide may suggest that coupling times that are longer than 1 hour may be required for complete and successful conjugation.

3.4.2. Adamantane versus palmitic acid

The LCMS analysis of the crude products of Pep-2-NNA conjugated with adamantane carboxylic acid and palmitic acid revealed that Pep-2-NNA-Pal was eluted with 95% acetonitrile (v/v) while Pep-2-NNA-Ada was eluted between 80 – 70% of acetonitrile (v/v). The behavior of Pep-2-NNA-Ada is discussed in detail in the next section (**3.4.1. (b)**). Pep-2-NNA-Pal was found to be more hydrophobic than all the adamantane-conjugated peptides listed in **Table 3.2**, and this is because palmitic acid (Log P = 5.77) is more lipophilic than adamantane (Log P = 2.37).[16] Log P measures the lipophilicity (hydrophobicity) of molecules. A study by Arnush *et. al.*, reported that the conjugation of lysine-based cationic ultrashort peptides to palmitic acid enhanced biological activity across several bacterial species. In contrast, the peptides conjugated to shorter lipophilic molecules (including

adamantane) were inactive.[16] Palmitic acid conjugated Pep-2-NNA was less soluble in water and acetonitrile HPLC grade solvents than adamantane conjugated peptides and required DMSO to dissolve. Furthermore, Pep-2-NNA-Pal had a lower response to mass spectrometry detection when compared to adamantane-based conjugates, and a few drops of formic acid were added before LCMS analysis to improve ionization.

3.4.3. Linear versus cyclized adamantane conjugated peptide derivatives and the effect of the disulfide bridge

The LCMS results also revealed that cyclized adamantane carboxylic acid conjugated peptides were eluted at a higher acetonitrile percentage than their linear counterparts. Cyclized peptide compounds are characterized by a loss of -2 Da on the mass spectrum when compared to uncyclized derivatives of the same sequence resulting from a loss of 2 protons ($-2H^+$) due to the oxidation of the thiol groups on the sidechains of cysteine residues to form a disulfide bond. Pep-2-NNA-Ada (T_R: 13.59 – 13.82 min) and Pep-1-NNA-Ada (T_R: 9.93 – 10.18 min) were eluted from 64% acetonitrile gradient while the linear adamantane-peptide conjugates were eluted between 53 – 65 %. Therefore, the presence of non-polar cysteine residues increases the hydrophobicity of peptides. Furthermore, it was also observed that uncyclized Pep-1-NNA-Ada, due to incomplete oxidation of cysteine residues, was eluted earlier than the cyclized peptide-conjugate (T_R: 9.63 – 9.76 min) but later than the Linear Pep-1-NNA-Ada. This effect was also observed in the analysis of Pep-2-NNA-Ada. However, free cysteine amino acid residues contain thiol groups (R-SH) and are reportedly more hydrophobic than the oxidized disulfide bonded cystine (R-S-S-R)[17]. Therefore uncyclized peptides should be more retained and eluted after they are cyclized.[18] The cyclization of peptides results in a stabilized and restricted structure and thus influences structural conformations, which may influence their interaction with the non-polar stationary phase.[19] Peptide cyclization can limit random conformations and provide a stable conformation with the hydrophobic regions better positioned for interactions. It is reported that the organic HPLC solvents such as acetonitrile, ion pairing agent, and the non-polar stationary phase may influence the conformation of the peptides leading to secondary structure stabilization.[15]

The incomplete cyclization of Pep-1-NNA-Ada and Pep-2-NNA-Ada may be due to the bulky nature of adamantane, which may interfere with the formation of the cyclic ring.

3.4.4. Adamantane conjugated Pep-2-NNA-Ada

Adamantane carboxylic acid was successfully conjugated to Pep-2-NNA-Ada as revealed by LCMS analysis shown in **Figure 3.4 (B)**. Interestingly, it was observed that the crude peptide was not eluted during the standard gradient of 5 – 95% acetonitrile (v/v) but was eluted when the acetonitrile was decreasing from 79.8 – 70%. This unusual behavior was also observed during the analysis of the purified Pep-2-NNA-Ada using LCMS, as shown in **Figure 3.5** below. Since this was not observed with the other adamantane-conjugated peptides, future studies need to be carried out to understand such behaviour, which may help improve the prep-HPLC methods, which may lead to better peak separation and increased purity and yields.

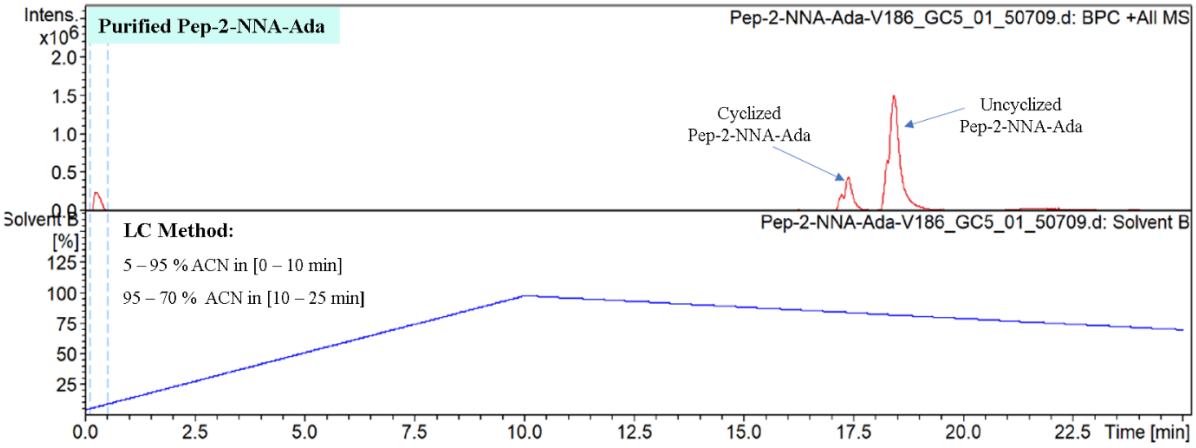

Figure 3.5: The LCMS of purified Pep-2-NNA-Ada.The peaks represent the cyclized and uncyclized Pep-2-NNA-Ada derivative. The blue line represents the LC method (through line B) that was used to obtain the peptide spectrum.

The purification of Pep-2-NNA-Ada using reversed-phase prep-HPLC was challenging due to the poor separation of peaks that resulted in the co-elution of the peptide with the contaminants. Several method modifications were done to improve purification, which resulted in a significant loss of peptide (yield < 1%). This may be due to the presence of adamantane, which has increased the peptide's hydrophobicity and affinity for the stationary phase, thus causing the peptide to be strongly retained in the column. Pep-2-NNA-Ada was eluted when the percentage of acetonitrile was 81 – 95% (v/v). Poor peptide solubility may have also contributed to poor yields due to the presence of adamantane. DMSO had to be used to initially dissolve the peptide, on which a minimum amount of water or acetonitrile

was added to avoid peptide precipitation. Unconjugated Pep-2-NNA dissolves completely in water.

Despite the difficulties encountered during purification, Pep-2-NNA-Ada was regarded as a better adamantane-conjugated lassomycin derivative due to its cleaner LCMS spectrum and the presence of less contaminants, while Pep-1-NNA-Ada had the most impurities. This may be because Pep-2-NNA-Ada consists of lysine residues instead of arginine and lysine, enabling efficient coupling and fewer truncated peptides. It was also observed that Pep-2-NNA-Ada was co-eluting with a deleted sequence impurity corresponding to a missing leucine residue in the peptide sequence (loss of 113 Da); therefore, the coupling times may be increased to ensure successful aminoacylation. The oxymapure coupling reagent and diisopropyl carbodiimide were used to couple each amino acid during peptide synthesis.

3.5. Conclusion

All the peptides were successfully conjugated to adamantane and palmitic acid lipophilic acids; however, their synthesis and purification was challenging due to their relatively longer peptide chain sequences.

Arginine-based adamantane-conjugated peptide derivatives could make better lipopeptides due to their highly basic nature, increasing their affinity for the acidic bacterial membrane. However, arginine is a ‘difficult’ amino acid to couple during peptide synthesis as it has a sterically hindered guanidine side chain protected by a bulky Pbf group, and its coupling reaction results in highly contaminated products. Incomplete aminoacylation of arginine to an adjacent amino acid may result in the formation of impurities such as truncated and deleted sequences. This was also observed in the study reported in Chapter 2. Lysine is a better substitute for arginine since it can still maintain the basicity of the peptides and has a less sterically hindered Boc sidechain protecting group; thus, its use during peptide synthesis results in less formation of contaminations. Pep-2-NNA-Ada, formed by replacing all the arginine residues with lysine, had better LCMS results with a cleaner spectrum due to less contaminants and successful adamantane conjugation. Pep-2-NNA-Ada was also observed to have better properties than the rest of the conjugated derivatives and will be further investigated for antimicrobial activity and cytotoxicity.

Although both adamantane and palmitic acid were successfully conjugated to the peptides, they both had challenges. However, adamantane is easier to use as it is more soluble and more responsive to detection by HPLC-MS. More studies may be required to find better ways to dissolve palmitic acid derivatives, which may result in improved purity and yield. Longer cyclization times may be required to ensure the complete cyclization of adamantane-based peptides. Palmitic acid does not appear to hinder the cyclization in Pep-2-NNA-Pal.

The cyclization of lipophilic conjugated peptides may influence their behaviour regarding the effect of hydrophobicity. Lastly, adding two cysteine residues and their oxidation contribute to increased hydrophobicity of peptides, as observed with the early retention times of linear peptides compared to the cyclized peptides retained longer in the non-polar stationary phase.

References

1. Malina, A.; Shai, Y., Conjugation of fatty acids with different lengths modulates the antibacterial and antifungal activity of a cationic biologically inactive peptide. *Biochemical Journal* **2005,** *390* (3), 695-702.

2. Gao, X.; De Mazière, A.; Beard, R.; Klumperman, J.; Hannoush, R. N., Fatty acylation enhances the cellular internalization and cytosolic distribution of a cystine-knot peptide. *Iscience* **2021,** *24* (11), 103220.

3. Artur Schmidtchen, M. P., Martin Malmsten, Effect of hydrophobic modifications in antimicrobial peptides. *Advances in Colloid and Interface Science* **2013**.

4. Zhang, Q.-Y.; Yan, Z.-B.; Meng, Y.-M.; Hong, X.-Y.; Shao, G.; Ma, J.-J.; Cheng, X.-R.; Liu, J.; Kang, J.; Fu, C.-Y., Antimicrobial peptides: mechanism of action, activity and clinical potential. *Military Medical Research* **2021,** *8*, 1-25.

5. Avrahami, D.; Shai, Y., A new group of antifungal and antibacterial lipopeptides derived from non-membrane active peptides conjugated to palmitic acid. *Journal of Biological Chemistry* **2004,** *279* (13), 12277-12285.

6. W. Zhan, G. G., Z. Liu, X. Liu, L. Xu, M. Wang, H.-D. Xu, R. Tang, J. Cao, X. Sun, G. Liang, Enzymatic Self-Assembly of Adamantane-Peptide Conjugate for Combating Staphylococcus aureus Infection. *Advanced Healthcare Materials* **2023**.

7. Wanka, L.; Iqbal, K.; Schreiner, P. R., The lipophilic bullet hits the targets: medicinal chemistry of adamantane derivatives. *Chemical Reviews* **2013,** *113* (5), 3516-3604.

8. Rosenberg, M. R.; Casarotto, M. G., Coexistence of two adamantane binding sites in the influenza A M2 ion channel. *Proceedings of the National Academy of Sciences* **2010,** *107* (31), 13866-13871.

9. Suzana K. Straus, R. E. W. H., Mode of action of the new antibiotic for Gram-positive pathogens daptomycin: Comparison with cationic antimicrobial peptides and lipopeptides. *Biochimica et Biophysica Acta* **2006,** (1758), 1215 - 1223.

10. Storck, P.; Umstätter, F.; Wohlfart, S.; Domhan, C.; Kleist, C.; Werner, J.; Brandenburg, K.; Zimmermann, S.; Haberkorn, U.; Mier, W., Fatty acid conjugation leads to length-dependent antimicrobial activity of a synthetic antibacterial peptide (Pep19-4LF). *Antibiotics* **2020,** *9* (12), 844.

11. Batt, S. M.; Minnikin, D. E.; Besra, G. S., The thick waxy coat of mycobacteria, a protective layer against antibiotics and the host's immune system. *Biochemical Journal* **2020,** *477* (10), 1983-2006.

12. Vincent, A. T.; Nyongesa, S.; Morneau, I.; Reed, M. B.; Tocheva, E. I.; Veyrier, F. J., The mycobacterial cell envelope: a relict from the past or the result of recent evolution? *Frontiers in Microbiology* **2018,** *9*, 2341.

13. Alexander F. Chu-Kung a, R. N. a., Kristen N. Bozzelli a, Matthew Tirrell, Chain length dependence of antimicrobial peptide–fatty acid conjugate activity. *Journal of Colloid and Interface Science* **2010**.

14. Kreutzer, A. G.; Salveson, P. J.; Yang, H., Standard Practices for Fmoc-Based Solid-Phase Peptide Synthesis in the Nowick Laboratory (Version 1.6. 3). **2018**.

15. Erckes, V.; Steuer, C., A story of peptides, lipophilicity and chromatography–back and forth in time. *RSC Medicinal Chemistry* **2022,** *13* (6), 676-687.

16. Arnusch, C. J.; Ulm, H.; Josten, M.; Shadkchan, Y.; Osherov, N.; Sahl, H.-G.; Shai, Y., Ultrashort peptide bioconjugates are exclusively antifungal agents and synergize with cyclodextrin and amphotericin B. *Antimicrobial Agents and Chemotherapy* **2012,** *56* (1), 1-9.

17. Nagano, N.; Ota, M.; Nishikawa, K., Strong hydrophobic nature of cysteine residues in proteins. *FEBS letters* **1999,** *458* (1), 69-71.

18. Johnson, M.; Liu, M.; Struble, E.; Hettiarachchi, K., Characterization of cyclic peptides containing disulfide bonds. *Journal of Pharmaceutical and Biomedical Analysis* **2015,** *109*, 112-120.

19. Thakkar, A.; Trinh, T. B.; Pei, D., Global analysis of peptide cyclization efficiency. *American Chemical Society Combinatorial Science* **2013,** *15* (2), 120-129.

Chapter 4

The synthesis of short-chain lassomycin derivatives-fatty acid conjugates

4.1. Introduction

Cationic antimicrobial peptides (AMPs) are a promising class of antibiotic candidates with a low propensity for the formation of bacterial resistance and an ability to eliminate multi-drug-resistant bacteria.[1] Despite these attractive properties, AMPs have had limited clinical success largely due to their large structural sizes that can pose challenges with the administration, bioavailability, toxicity, and stability compared to currently used antibiotics which are smaller in size.[2-3] Antimicrobial peptides usually comprise amino acid chain lengths ranging from 15 – 50 residues.[3] Several studies have reported that when reducing the peptide chain length, several factors, including hydrophobicity, net positive charge, and amphiphilicity, play a significant role in the antimicrobial activity of peptides than the position of the amino acids in the peptide sequence.[3-4] Reducing the length of the peptides may lead to an ease of passage through the complex bacterial cell membrane and especially into the non-lipid regions of the inner membrane portion, which can increase antibacterial activity as observed in the studies conducted by Liu *et al.* and Niidome *et al.*[1, 4] Furthermore, decreasing the peptide chain length also causes a reduction in the hemolytic activity against human erythrocytes and thus minimizing toxicity towards human cells.[1]

In this chapter, we explore the effects of modifying lassomycin peptide derivatives by shortening their chain lengths. Furthermore, the short-chain derivatives will be conjugated to lipophilic molecules such as palmitic acid and adamantane carboxylic acid to increase their hydrophobicity.

4.2. The design of Tail-2-NN, Ring-2-NNA and Ring-2-NN

The short-chain peptide derivatives discussed in this chapter were derived from the Pep-2-NNA and Pep-2-NN lassomycin peptides, which are discussed in detail in Chapter 2. These lassomycin derivatives were previously synthesized in our research group. They had good antimicrobial activities against the *Mycobacterium tuberculosis* cells and were consequently selected for further modification by shortening the peptide sequences. The sequences of the tail portion of these lassomycin peptides are similar and were used to form the Tail-2-NN short-chain peptide, while Ring-2-NNA and Ring-2-NN were formed using the cyclic ring sequences of Pep-2-NNA and Pep-2-NN, respectively. A map showing the design for shorter lassomycin peptides is illustrated in **Scheme 4.1** below.

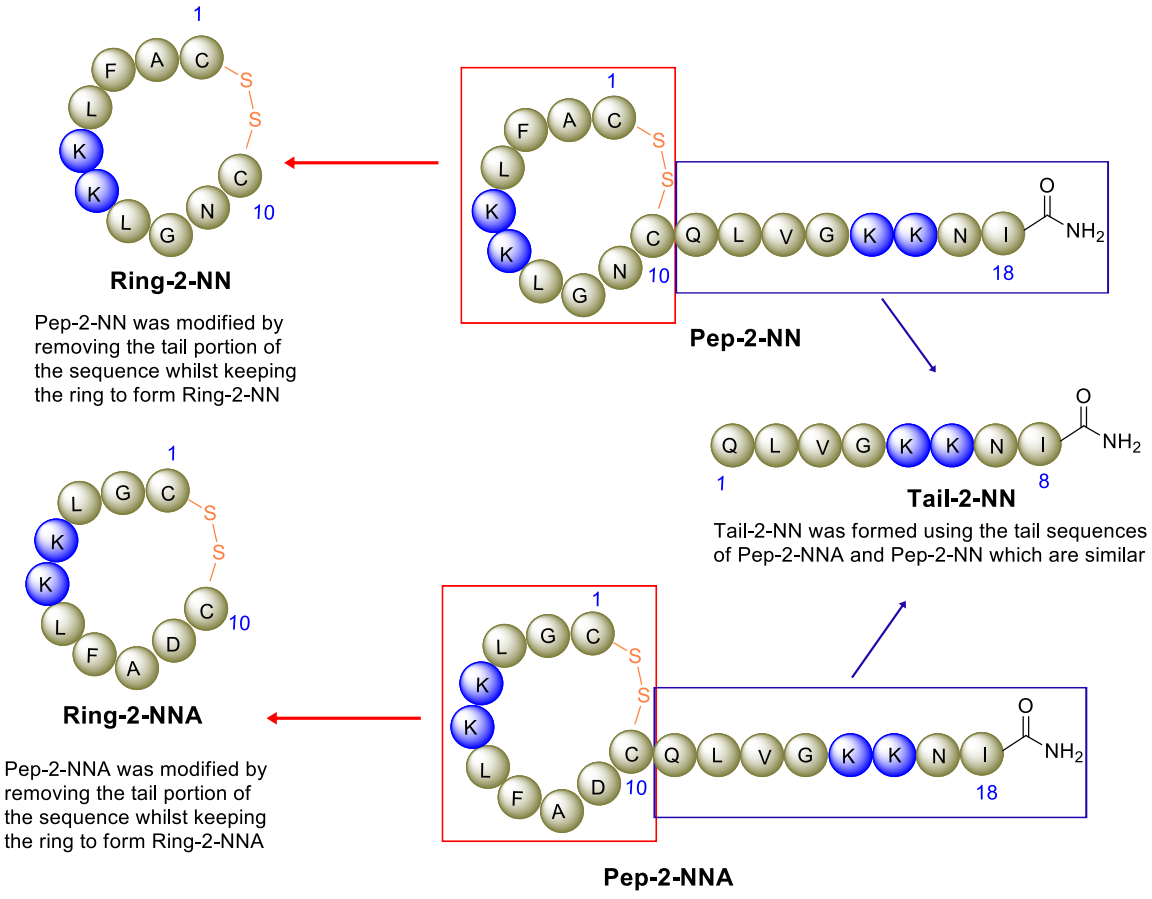

Scheme 4.1: The design of short-chain lassomycin peptides Ring-2-NNA (from Pep-2-NNA), Ring-2-NN (from Pep-2-NN), and Tail-2-NN from the tail sequences of both Pep-2-NNA and Pep-2-NN.

Although Pep-2-NN and Pep-2-NNA have moderate-good activity, they are both large peptides due to their longer sequences of 18 amino acids. Longer peptides are vulnerable to the risk of contamination by impurities during synthesis, and thus the yield and purity of peptides decrease with increasing chain length.[5-6] Therefore, shortening the peptide chain length can result in improved yields and may be cost-effective as it can reduce the amount of solvents/reagents and waste generated during synthesis due to reducing the number of coupling steps required to synthesize the peptide.

The sequences and molecular structures of Ring-2-NNA, Ring-2-NN, and Tail-2-NN short-chain peptide derivatives are shown in **Figure 4.1**, below. The order of amino acids in the sequences of the ring and tail derivatives was not altered to minimize possible negative impacts resulting from removing residues that may be crucial for a bactericidal effect. Ring-2-NNA and Ring-2-NN were cyclized by forming a disulfide bond between two cysteine residues inserted at positions **C1** and **C10** in the sequences.

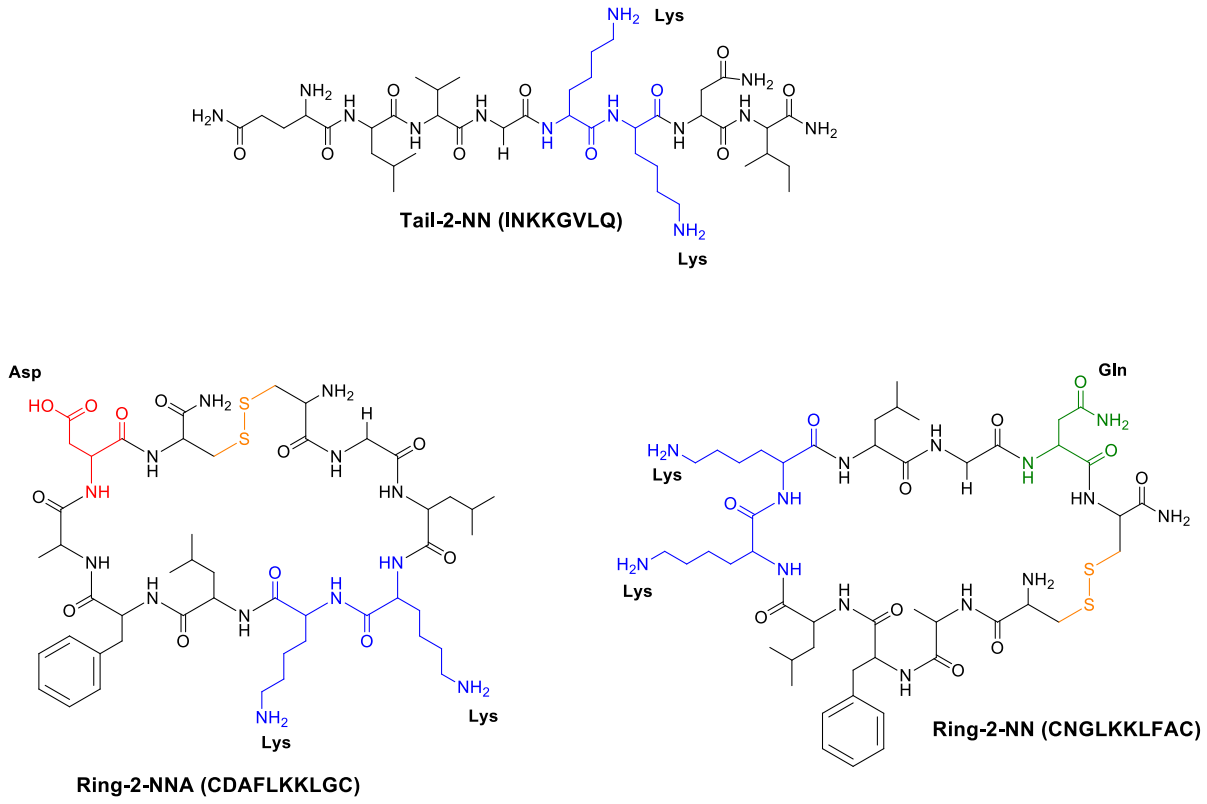

Figure 4.1: Shortened lassomycin-amide peptide derivatives. Lysine residues are highlighted in blue and contribute to the peptides' overall net charge and basicity. Ring-2-NNA contains aspartic acid, which is substituted by glutamine in Ring-2-NN.

4.2.1. Synthesis

All the peptides discussed in this chapter were synthesized using the Fmoc solid phase peptide synthesis (SPPS) protocol presented in Chapter 3. Each peptide derivative was formed by adding a mixture of each amino acid (6 mL, 0.2 M), k-oxyma (0.2 M) coupling reagent, and diisopropyl carbodiimide (DIC, 0.2 M) at 1:1:1 equivalence to a growing resin-bound peptide. The amino acids were coupled twice for 35 minutes to ensure successful aminoacylation. A solution of 20% piperidine in DMF (v/v) was used to remove Fmoc before the aminoacylation of the next incoming amino acid. Washings were done in-between steps with DMF (3×5 mL) followed by DCM (3×5 mL), and the waste was filtered out using vacuum filtration. A cocktail mixture of 95% TFA with 2.5% water and 2.5% triisopropylsilane (TIS) was used to cleave the peptides from the resin and permanent protecting groups from the side chains.

4.2.2. Results and Discussion

After the cleavage of the peptides using TFA, the crude products were dissolved in HPLC-grade solvents and analysed using LCMS, revealing that all the peptides were successfully synthesized. The peptides were then purified using reversed-phase semi-preparatory HPLC. The purification of the peptides unexpectedly was challenging due to the poor separation of peaks resulting in the co-elution of the peptides with contaminants. This led to the peptides' re-purification multiple times to improve purity. However, peptide product yield was lost due to method development and modification. The LCMS results are presented in **Figure 4.2** and the peptide sequences, masses obtained after purification and percentage yields of each derivative are presented in **Table 4.1**, below.

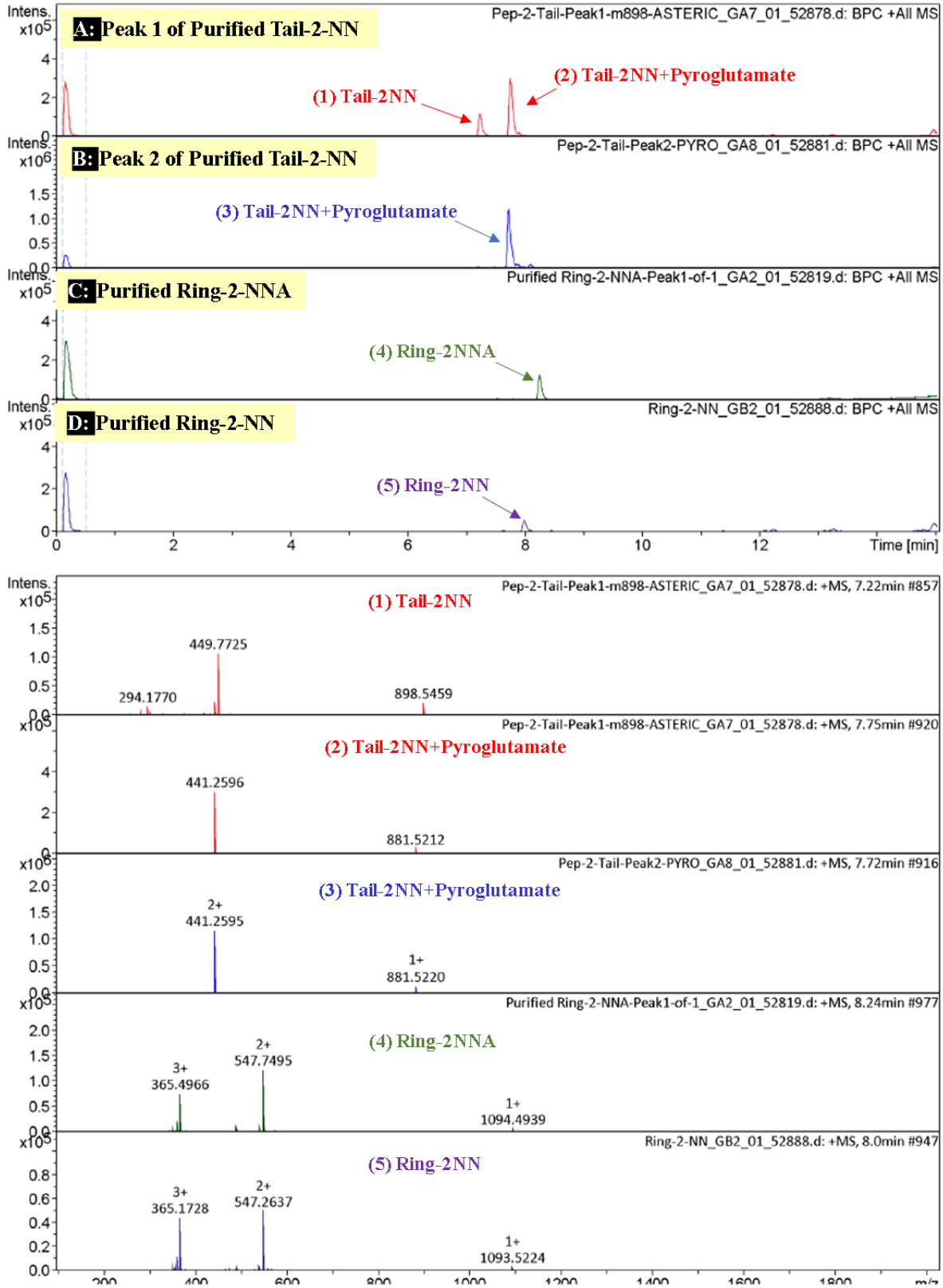

Figure 4.2: The LCMS spectra of purified peptides (A) – (B) Tail-2-NN; (C) Ring-2-NNA and (D) Ring-2-NN obtained by operating at a gradient of 5 – 95% acetonitrile (v/v) in 10 minutes.

Table 4.1: Summary of the results obtained for Peak 1 and Peak 2 during the purification of Tail-2-NN

Compound	Calculated Mass	Observed Mass/ Molecular Ion	Retention Time (min)	Obtained Mass (mg)	%Yield
Tail-2-NN* INKKGVLQ	897,5760 $C_{40}H_{75}N_{13}O_{10}$	898.5458 $[M+H]^+$	7.23	3.3 mg	13%
Tail-2-NN* Pyroglutamate (Δm = -17 Da)	880,5494 $C_{40}H_{72}N_{12}O_{10}$	881.5212 $[M+H]^+$	7.75		
Tail-2-NN-Pyroglutamate** (Δm = -17 Da)	880,5494 $C_{40}H_{72}N_{12}O_{10}$	881.5225 $[M+H]^+$	7.72	2.6 mg	11%
Ring-2-NNA CDAFLKKLGC	1094.5253 $C_{48}H_{78}N_{12}O_{13}S_2$	1094.4932 $[M+H]^+$	8.24	0.5 mg	1.7%
Ring-2-NN: Cyclized CNGLKKLFAC	1092,5572 $C_{48}H_{80}N_{14}O_{11}S_2$	1093.5221 $[M+H]^+$	8.00	46.9 mg	48%

* Obtained as Peak 1 during the purification of Tail-2-NN
** Obtained as Peak 2 during the purification of Tail-2-NN

Tail-2-NN

The purification of Tail-2-NN was achieved by employing an HPLC gradient starting from 5% acetonitrile, and when it reached 38% (v/v), it was set to ramp up to 45% acetonitrile over 9 minutes, upon which 2 peaks were collected and analysed using LCMS. The first peak (Peak 1) of Tail-2-NN (898.5458 Da, $[M+H]^+$) was co-eluted with a mass of 881.5225 Da ($[M+H]^+$) between 7.23-7.75 minutes, which was analysed and attributed to a sequence that had undergone a pyroglutamate side-reaction at the *N*-terminus glutamine residue. Tail-2-NN-pyroglutamate was then eluted alone in the second peak (Peak 2) at a retention time of 7.72 minutes.

An LCMS gradient method of 5 – 95% acetonitrile over 10 minutes was used to analyse the fractions collected during the purification of Tail-2-NN. The obtained spectra are presented in **Figure 4.2A-B,** and the data is recorded in **Table 4.1** above. The final mass obtained for the Tail-2-NN/pyroglutamic acid was 5.9 mg. Further purification would have resulted in peptide loss; hence the peptide was subjected to a protease assay study against the *Mycobacterium tuberculosis* caseinolytic protease. Tail-2-NN has an inhibitory effect on the ClpP protease activity, and this is discussed further in section 4.4. Due to time constraints, the peptide could not be resynthesized.

The formation of pyroglutamate in Tail-2-NN

The formation of the pyroglutamic acid, also known as pyrrolidone carboxylate, is usually a spontaneous conversion process that commonly occurs at the *N*-terminus glutamine and results in the loss of the primary amine (**Scheme 4.2**), and thus the acidity of the peptide (or biological molecule) increases.[7] This process results in a mass change of -17 Da and an increased retention time which can be attributed to increased hydrophobicity as the peptide-pyroglutamate is retained longer in the non-polar stationary phase as seen in the LCMS spectra presented in **Figure 4.2A-B**. The formation of pyroglutamic acid can occur under acidic conditions, which favour the leaving group, or basic conditions, which increase the nucleophilicity of the attacking amino group.[8-9] Glutaminyl cyclase is an enzyme found in plants, animals, and humans that can catalyse pyroglutamic acid formation in proteins and peptides with *N*-terminal glutamine or glutamic acid.[7]

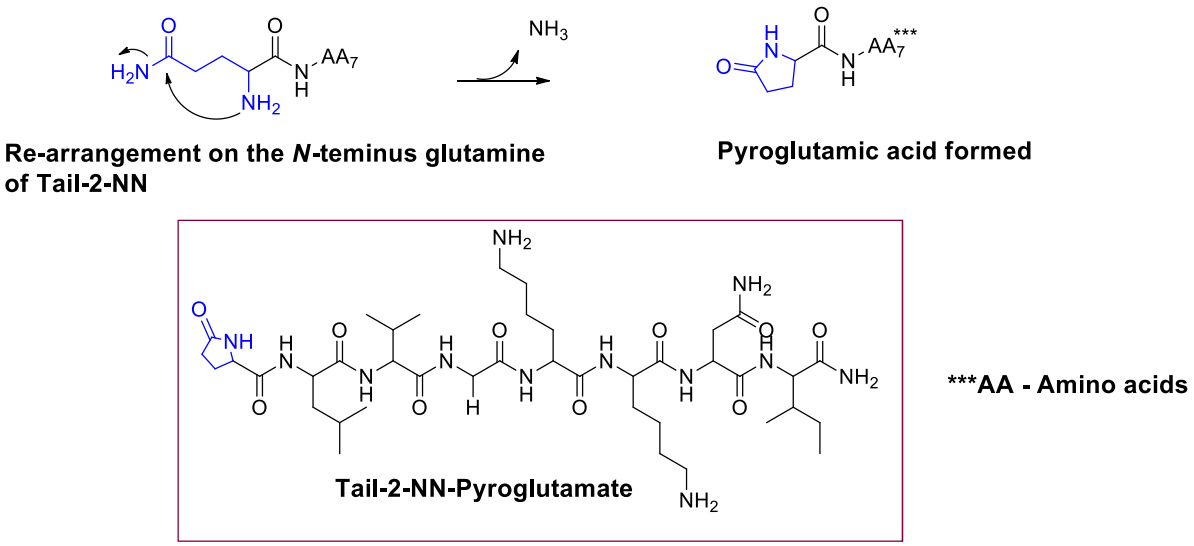

Scheme 4.2: Illustrating the formation of Tail-2-NN pyroglutamate.

Ring-2-NNA and Ring-2-NN

Both Ring-2-NNA and Ring-2-NN were cyclized using 20% DMSO in water (v/v) overnight, which was confirmed by LCMS analysis. The peptides were purified with reversed phase HPLC where Ring-2-NNA was eluted between 48 – 54% acetonitrile (v/v) while Ring-2-NN was eluted between 43% – 45% acetonitrile (v/v). Multiple re-purifications were performed due to poor peaks separation. The final masses obtained for Ring-2-NNA and Ring-2-NN

were 1.1 mg (1.7% yield) and 46.9 mg (48% yield), respectively. Ring-2-NN was subjected to circular dichroism studies and was found to be 58.8% alpha helix and 33.1% antiparallel with 5.8% turn motif, discussed further in **section 4.4**.

The hydrophobicity of the peptides

Upon analysis of the peptide derivatives using an LCMS gradient method of 5 – 95% acetonitrile in 10 minutes, it was observed that Tail-2-NN (T_R = 7.23 – 7.75 min) was the least hydrophobic peptide as it was eluted earlier than Ring-2-NN (T_R = 8.00 min) and Ring-2-NNA (T_R = 8.24 min). The cyclic ring peptides have similar amino acid residues in their sequences, which are positioned in opposite directions, and also, the aspartic acid in Ring-2-NNA was replaced with asparagine in Ring-2-NN. According to the online calculator software[10] (**Table 4.2**), Ring-2-NN is more hydrophilic than Ring-2-NNA, which may be due to the presence of the amide group on the side chain of asparagine which is more polar than the carboxylic side chain of aspartic acid.

Table 4.2: Properties of short-chained lassomycin derivatives (Tail-2-NN, Ring-2-NNAand Tail-2NN) including peptide chain length, derived by the number of amino acids; hydrophobicity; a ratio of hydrophilic residues; and the overall charge at pH 7.0 determined by the number of charged residues. AAs: amino acids; TNR: total number of residues. Pep-2-NNA and Pep-2-NN are included as references.

Peptide derivative/ Sequence	Peptide length (No. of Aas)	Hydro-philicity	Ratio of hydrophilic residues /TNR	Net charge at pH 7.0
Short-chained peptide derivatives				
Tail-2-NN/ INKKGVLQ	8	0.16 (+)	50%	3.00
Ring-2-NN/ CNGLKKLFAC	10	-0.24 (-)	30%	2.91
Ring-2-NNA/ CDAFLKKLGC	10	0.04 (+)	30%	1.91
Longer-Chained peptide derivatives				
Pep-2-NN/ INKKGVLQCNGLKKLFAC	18	-0.06 (+)	39%	4.91
Pep-2-NNA/ INKKGVLQCDAFLKKLGC	18	0.09 (+)	39%	3.91

The basicity of the peptides

All derivatives maintained some basicity due to the two lysine residues' presence in their respective sequences. However, this is a significant reduction from the basicity of Pep-2-

NNA and Pep-2-NN. Tail-2-NN is the most basic derivative of the short-chained peptides due to its net charge of 3.00 at a pH of 7.0. The properties of the peptides are summarized in **Table 4.2** above. The basicity of Ring-2-NNA is significantly decreased due to the presence of aspartic acid, a negatively charged polar amino acid. Aspartic acid is found in the original sequence of the natural lassomycin peptide and was replaced by the asparagine amino acid in Ring-2-NN. Basicity plays an important role in the bactericidal activities of antimicrobial peptides as it has been shown to improve membrane permeability and activity by increasing the binding affinity of the peptide to the negatively charged bacterial membrane, including that of *Mycobacterium tuberculosis*.

The basicity and hydrophobicity of the peptides are the most significant factors due to the proposed mechanism, which suggests that lassomycin binds to the ClpC1 acidic *N*-terminal domain. Furthermore, cyclic peptides such as acyldepsipeptides are reported to bind to the hydrophobic pockets of the Clp protease; hence, relating the activity of the synthesized peptides to their basicity and hydrophobicity is crucial. Ring-2-NN is more basic than Ring-2-NNA and Tail-2-NN; therefore, it might have more affinity for the highly acidic region targeted by lassomycin and thus improve the bactericidal effect. Additionally, Ring-2-NN is cyclic and can therefore be assumed to be more stable than Tail-2-NN against protease degradation. This phenomenon may also explain the bactericidal activities observed for the longer-chained peptides, whereby Pep-2-NN was more active than Pep-2-NNA and its isomers (explained more in Chapter 2). Although both peptides have a similar chain length and the same hydrophilicity ratio, Pep-2-NN is slightly more basic than Pep-2-NNA.

In conclusion, lassomycin and its derivatives, Pep-2-NN and Pep-2NNA, are significantly longer peptides that must be shortened without negatively impacting the bactericidal effects. Also, understanding their intrinsic properties may help direct a path for further modifications. In the next section, the shortened peptides are further derivatized by conjugation to fatty acids to improve membrane permeability.

4.3. Conjugation of fatty acids onto the shortened peptides

4.3.1. Background information

The short-chain peptides were further modified by conjugation to palmitic acid and adamantane lipid molecules. These were analysed with the LCMS to study their structure-activity relationship. This section studies and discusses the combined effect of reducing the peptide chain length and conjugation to a lipid molecule. The lipid acids enhance the peptides' hydrophobic interactions with the lipid-rich bacterial cell membrane while reducing the size of the peptides helps improve permeability and passage, especially in non-lipid surfaces. The combined effect of peptide chain-length reduction and increased hydrophobicity may enhance antimicrobial activity. Reducing the peptide chain length may also help improve their pharmacodynamics and pharmacokinetics, thus making them more attractive to pharmaceutical companies. A detailed introduction of the two hydrophobic moieties is presented in detail in Chapter 3. Palmitic acid and adamantane carboxylic acid were coupled to the *N*-terminus of Tail-2-NN, Ring-2-NNA, and Tail-2-NN derivatives derivative, and their structures are presented in **Figure 4.3** below.

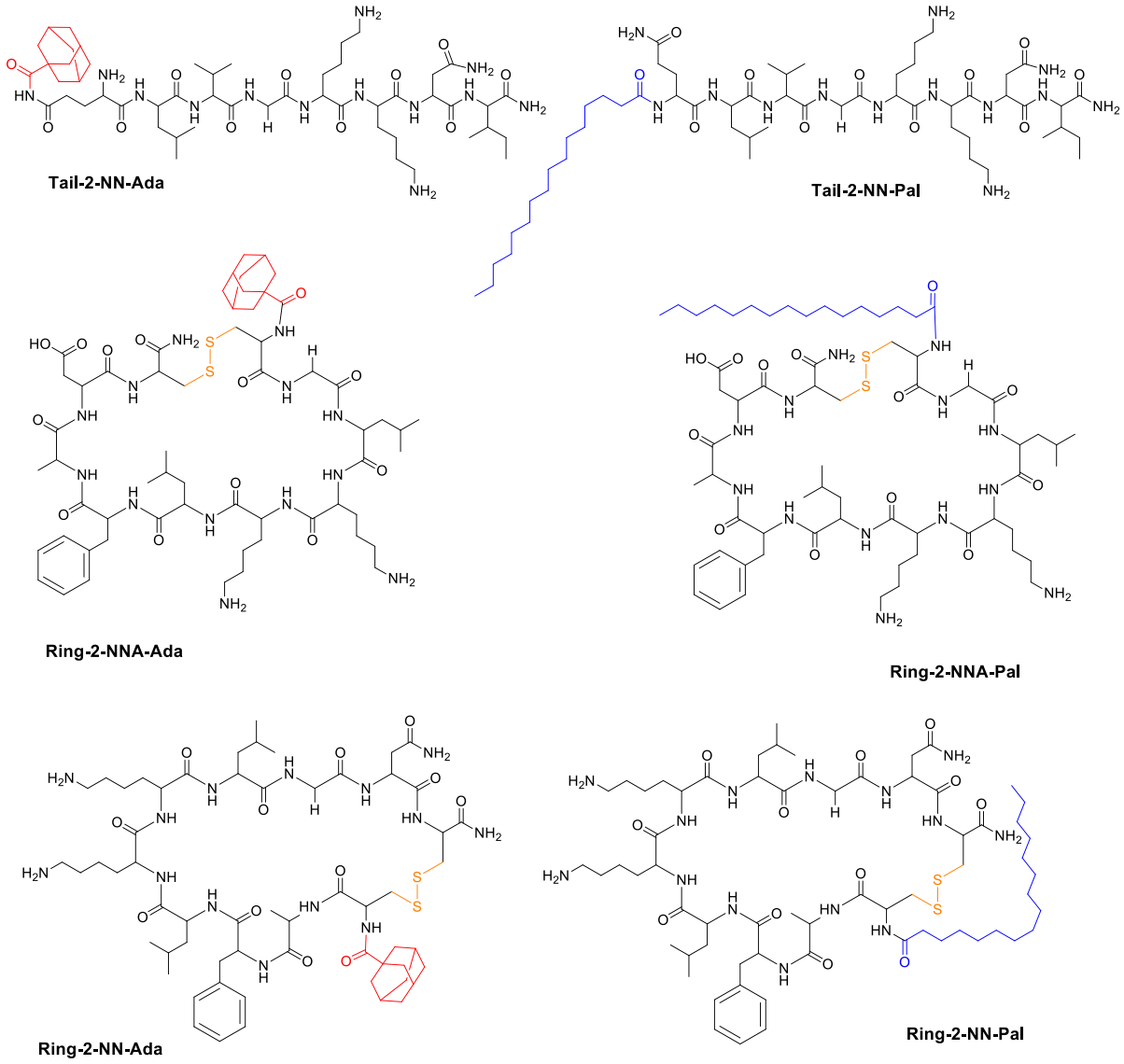

Figure 4.3: The structures of short peptides conjugated to hydrophobic palmitic acid and adamantane groups.

4.3.2. Synthesis:

Tail-2-NN, Ring-2-NN, and Ring-2-NNA short-chained peptides were synthesized following the method presented earlier in this Chapter in section 4.2.2. Palmitic acid (0.2 M) or adamantane carboxylic acid (0.2 M) mixed with k-Oxyma (0.2 M) and DIC (0.2 M) was coupled twice for 60 minutes to a newly Fmoc-deprotected resin-bound peptide. The peptides were then cleaved using TFA, purified using prep-HPLC, and analysed using reversed-phase LCMS.

4.3.3. Results

Purification using Prep-HPLC

All the peptides were successfully synthesized; however, purification was challenging due to poor separation of peaks that led to the co-elution of the peptides with impurities resulting in multiple re-purifications that led to significant product loss and negligible yields. The difficulty with the purification of the peptides was noticeably greater for the lipid conjugates compared to those unconjugated, which are discussed in **section 4.2**. This was attributed to poor solubility and strong retention to the column's stationary phase resulting from conjugation to lipid molecules, including palmitic acid and adamantane carboxylic acid. Only Ring-2-NNA-Ada was successfully purified and was obtained at a yield of 5% (1.7 mg) and a purity > 95%. Ring-2-NNA-Ada was thus used in a ClpP protease assay study, where it was revealed that it had an inhibitory effect against ClpP activity. All the fractions collected during purification were analysed using LCMS; the spectra are presented in **Figure 4.4** and **Figure 4.5**, and the data is recorded in **Table 4.3**. The peptide-lipid conjugates were analysed utilizing a gradient method of 5 – 98% acetonitrile (v/v) over 10 minutes for Ring-2-NNA and Ring-2-NN and 12 minutes for Tail-2-NN.

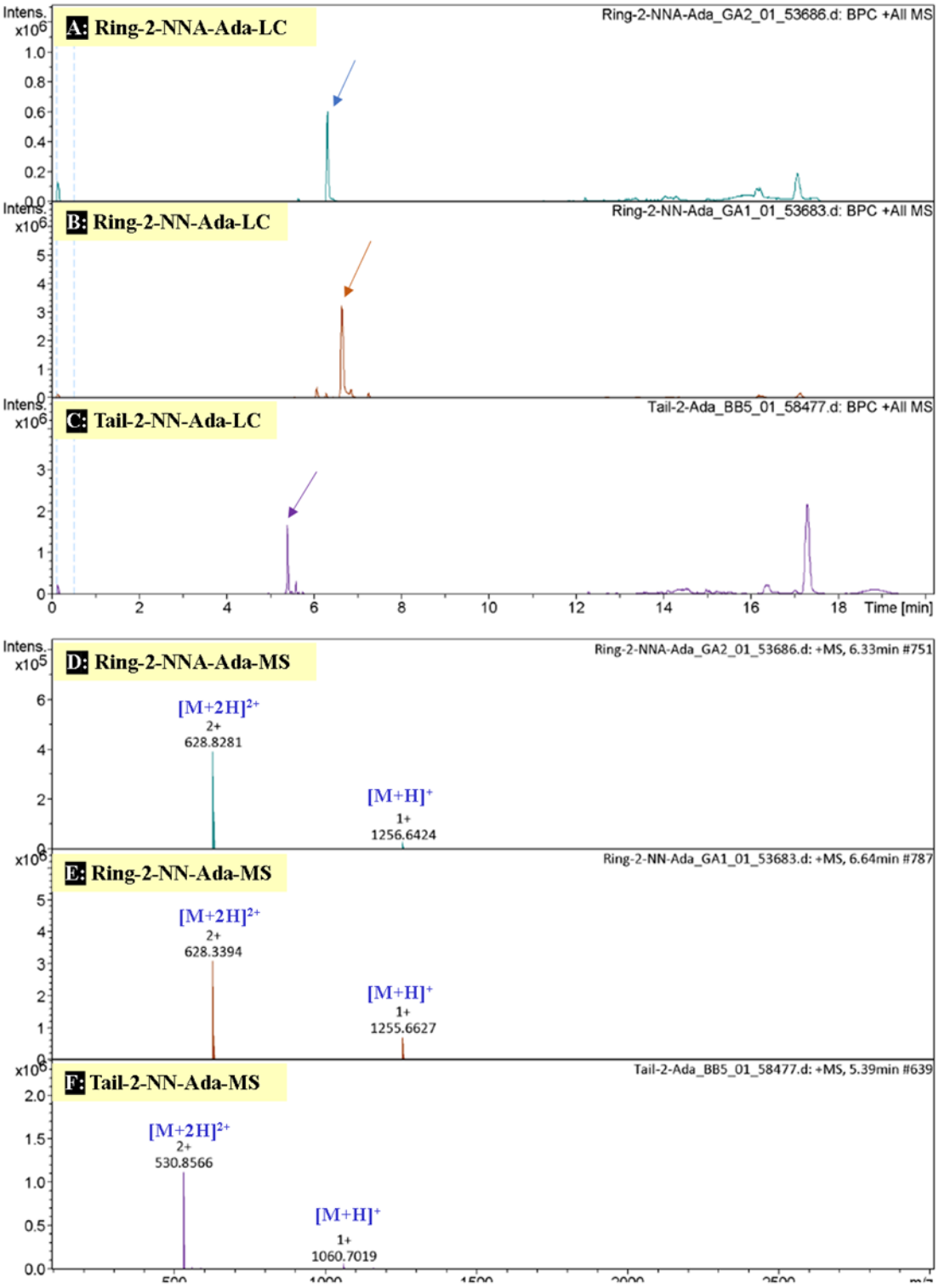

Figure 4.4: The LCMS spectra of adamantane conjugated (A, D) Ring-2-NNA, (B, E) Ring-2-NN, and (C,F) Tail-2-NN. A gradient of 5 – 98% acetonitrile (v/v) over 10 minutes (Ring-2-NNA and Ring-2-NN) and 12 minutes (Tail-2-NN) was employed for the analysis of the peptide-lipid conjugates.

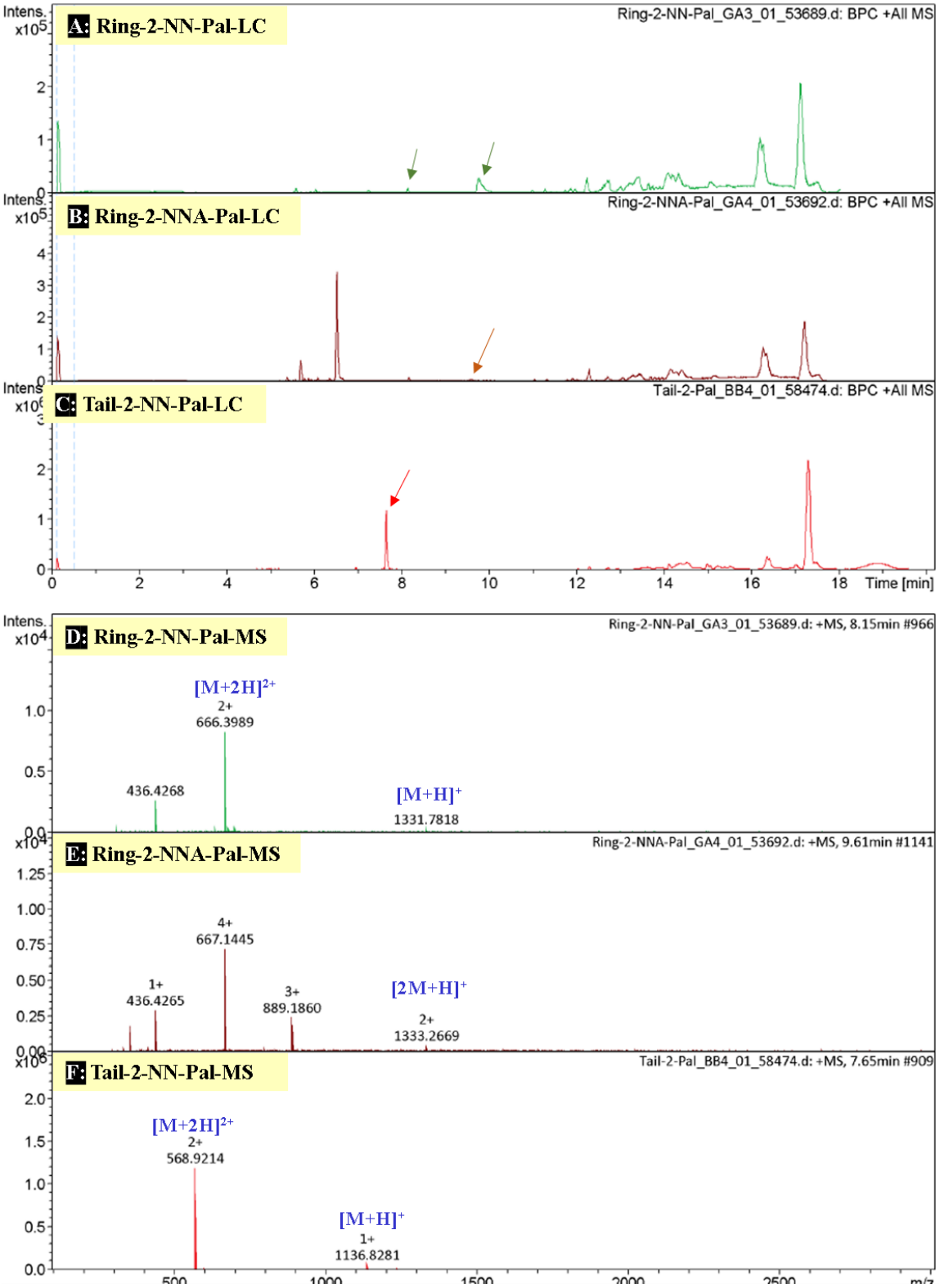

Figure 4.5: The LCMS spectra of palmitic acid conjugated (**A, D**) Ring-2-NNA, (**B, E**) Ring-2-NN, and (**C, F**) Tail-2-NN. A gradient of 5 – 98% acetonitrile (v/v) over 10 minutes (Ring-2-NNA and Ring-2-NN) and 12 minutes (Tail-2-NN) was employed for the analysis of the peptide-lipid conjugates.

Table 4.3: LCMS data of short-chained lassomycin derivatives conjugated to hydrophobic molecules, palmitic acid, and adamantane carboxylic acid.

Compound	Calculated Mass	Observed Mass	Molecular Ion	Retention Time (min)
Tail-2-NN-Ada	1059,6805 $C_{51}H_{89}N_{13}O_{11}$	1060.7019	$[M+H]^+$	5.39
Ring-2-NNA-Ada	1255,6457 $C_{59}H_{93}N_{13}O_{13}S_2$	1256.6424	$[M+H]^+$	6.64
Ring-2-NN-Ada	1254,6617 $C_{59}H_{94}N_{14}O_{12}S_2$	1255.6627	$[M+H]^{2+}$	6.33
Tail-2-NN-Pal	1135,8057 $C_{56}H_{105}N_{13}O_{11}$	1136,8281	$[M+H]^+$	7.65
Ring-2-NNA-Pal	1331,7709 $C_{64}H_{109}N_{13}O_{13}S_2$	1333.2669	$[2M+H]^+$	9.61
Ring-2-NN-Pal	1330,7869 $C_{64}H_{110}N_{14}O_{12}S_2$	1331.7818	$[M+H]^+$	8.15
		1332.7853	$[2M+H]^+$	9.75

Adamantane versus palmitic acid

The conjugation of the peptides to palmitic acid increased their affinity to the stationary phase, resulting in the peptides-lipid conjugates being eluted at higher acetonitrile concentrations (65 – 96%, v/v) as shown in **Table 4.4** below, which revealed that Ring-2-NNA-Pal is the most hydrophobic derivative. Adamantane-peptide conjugates showed better LCMS results than those conjugated to palmitic acid, which had poor ionization and detection, resulting in low peak intensities, as shown in **Figure 4.5** above. Small amounts of formic acid were added to the samples to improve ionization and detection during analysis. It was also observed that the conjugation of fatty acids to Tail-2-NN prevented the formation of the pyroglutamate side reaction.

Table 4.4: The percentage of acetonitrile (v/v) observed when the lipid-conjugated peptides are eluted during analysis with LCMS. The large amount observed for Ring-2-NNA-Pal suggests that it is more lipophilic than the rest of the lipid conjugated peptides

	Adamantane conjugation	**Palmitic acid conjugation**
Tail-2-NN	46 – 48%	65 – 67%
Ring-2-NN	63 – 65%	79 – 80%
Ring-2-NNA	65 – 68%	93 – 96%

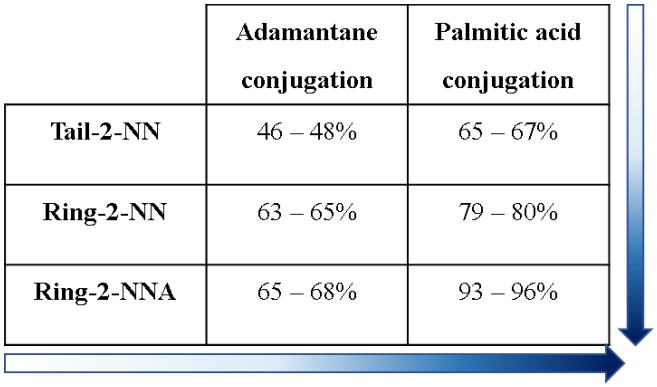

Studying the behaviour of lassomycin derivatives with various modifications is important as it leads to a better understanding of the nature of lassomycin, a complex antimicrobial peptide. Further investigation is required to help improve the purity and peptide yield to test for antimicrobial activity and toxicity which require at least 95% purity. The lower yield obtained from the peptides' purification is unexpected and may be improved by changing the column and solvents employed to obtain better peak separation.

4.4. Circular dichroism (CD) and ClpP-ATPase studies

4.4.1. Circular dichroism studies of selected lassomycin derivative

The secondary structures of peptides and other biological molecules, such as proteins, are usually formed by non-covalent interactions such as hydrogen bonding and van der Waals forces with the peptide backbone, including alpha-helices and beta-sheets beta-turns and beta-hairpins.[11-12] Circular dichroism is a spectroscopic technique used to determine the secondary structure of biological molecules and their folding properties (i.e., structural conformation).[13-14] Ring-2-NN was subjected to circular dichroism (CD) studies along with Pep-2-NN and Pep-Lys-NN, as shown in **Figure 4.6** below, discussed in detail in Chapter 2. Pep-Lys-NN is a highly basic and cationic peptide due to the presence of eight lysine residues and is active against *Bacillus subtilis*, which shares a similar caseinolytic protease targeted by lassomycin.

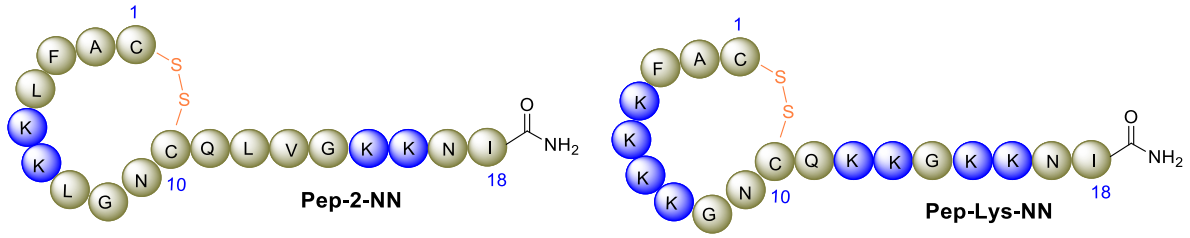

Figure 4.6: The structures of Pep-2-NN and Pep-Lys-NN lassomycin-amide derivatives

The CD measurements of the peptides were recorded on a JASCO spectrometer instrument at 25 °C. The results were generated from the Beta Structure Selection (BeStSel) online software provided by Micsocai *et al.*[15] and are recorded in **Table 4.5** below.

Table 4.5: Summary of the data from the circular dichroism study of Ring-2-NN.

	Secondary structure		
Peptide	**Alpha helix**	**Antiparallel**	**Turn**
Ring-2-NN	58.8%	33.1%	-
Pep-2-NN-2	47%	53%	-
Pep-2-NN-3	44.1%	55.9%	-
Pep-Lys-NN	25.9%	68.4%	5.8%

The analysis of the CD measurements reveals that the secondary structure of Ring-2-NN mostly comprised the alpha-helix (58.8%) followed by the antiparallel beta-sheets (33.1%). However, the most dominant conformation of the peptides is the antiparallel beta-sheets found in higher proportions in Pep-Lys-NN. The alpha-helix conformation results from the peptide backbone stabilization caused by intramolecular hydrogen bonding between a carbonyl oxygen and an amide hydrogen of a residue that is four amino away in the sequence.[11]

Parallel and antiparallel beta-sheets are formed through intermolecular (and sometimes intramolecular) hydrogen bonding between the carbonyl oxygens of one strand and the amide hydrogens of adjacent strands.[11] Antiparallel beta-sheets are formed when the hydrogen bonds are aligned, and these are more energetically favoured and thus more stable than parallel beta-sheets, as demonstrated in **Figure 4.7** below. The high propensity of the peptides to form beta-sheets may be influenced by the presence of a cyclic ring[16] held together by a disulfide bond. The formation of beta-sheet may increase the risk of peptide aggregation during synthesis and thus lead to a difficult synthesis and thus lead to poor yields.[17]

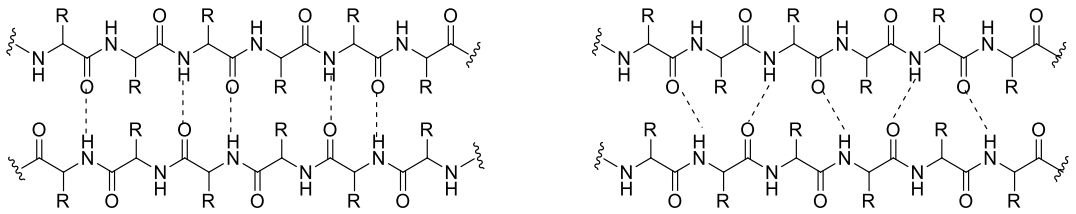

Figure 4.7: An illustration showing the difference between antiparallel and parallel beta-sheets.

A small proportion of Pep-Lys-NN is a turn motif absent in other peptides. Beta-turns are the most common turn motifs connecting successive antiparallel beta-strands through hydrogen bonding between the amide hydrogens and the carbonyl oxygens.

This study suggests that lassomycin derivatives are stabilized by the antiparallel beta sheets followed by the alpha-helix.

4.4.2. ClpP-ATPase study

Selected lassomycin peptide derivatives were subjected to a ClpP-Assay study to investigate their influence on the proteolytic activity of the caseinolytic protease (ClpP or ClpP1P2). The

procedure of the assays involves utilizing ClpP to cleave ZPKM-AMC, a short peptide conjugated to a fluorophore, to measure the output fluorescence. The 7-amino-4-methylcoumarin (AMC) is a highly fluorescing compound that generates fluorescence with a peak at 441 nm ±100 and excitation at 341 nm ±100. The ZPKM-AMC conjugate has a low fluorescent coefficient. The peptidase activity of ClpP is determined by the presence of free AMC, which is measured by a fluorescence spectrophotometer. The emission was read at 415-445 nm and excitation at 365 nm.

The fluorescence results against the reaction time for ClpP activity are recorded in **Table 4.6** below. The results represent the influence of lassomycin peptide analogues on ClpP activity while using DMSO as a control. Negative values indicate the inhibition of peptidase activity. In contrast, positive values indicate that the derivatives could activate the proteolytic activities of the ClpP protease, increasing the cleavage of ZPKM-AMC.

The analysis of the results shows that under normal circumstances and without the influence of the peptides, the ClpP activity increases with time, as observed in the control reaction, as illustrated in **Graph 4.1** below. The results also reveal that all the peptides, excluding Ring-2-NN, managed to inhibit the activity of ClpP. This aligns with the mode of action employed by the natural lassomycin, which kills *Mycobacterium tuberculosis* by inhibiting ClpP activity. Lassomycin also kills TB by activating the ATPase activity of the caseinolytic enzyme (ClpC1).

Table 4.6: The results of a ClpP-Assays study of lassomycin-amide derivatives against the caseinolytic enzyme.

Peptides	Tail-2-NN	Ring-2-NN	Compound X	Pep-2-NN	Ring-2-NNA-Ada
Percentage inhibition	-13	85	-89	-79	-61

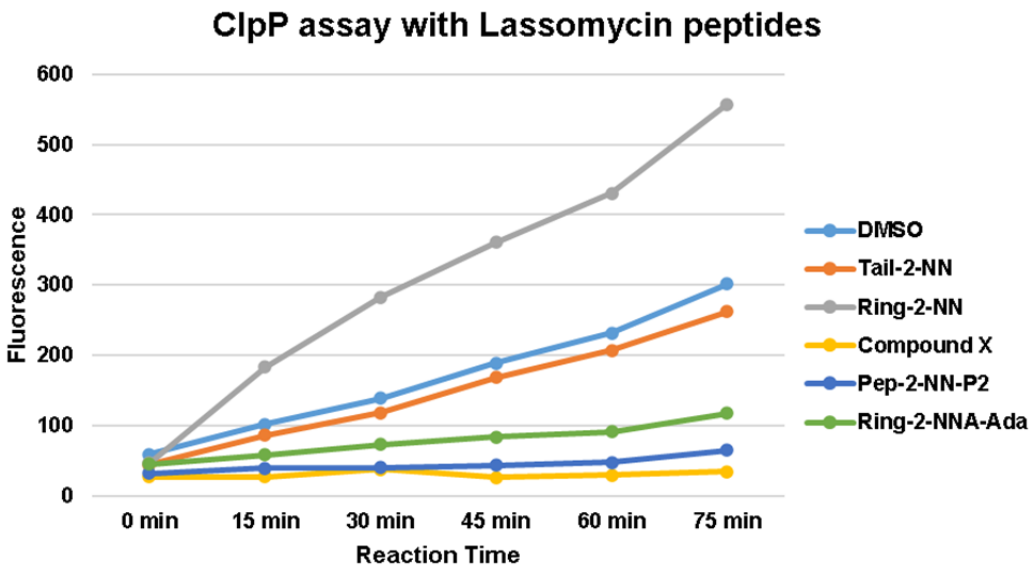

Graph 4.1: Illustrating the influence of the peptides against ClpP peptidase activity with time.

Further analysis of the results also shows that the presence of a tail in the form of amino acids (Pep-2-NN) or lipophilic moiety (Ring-2-NNA-Ada) may influence the inhibition effect of the peptide derivatives. Pep-2-NN and Ring-2-NNA-Ada have an inhibition effect, while the Ring-2-NN without the tail moiety has an activating effect. Furthermore, Ring-2-NN had a high proportion of alpha-helix in its secondary structure than Pep-2-NN. Hence, the secondary structure may also influence the effect of the peptides when interacting with the ClpP protease and therefore cause the peptides to bind at different protease sites.

The assay study also shows that the peptide size may not limit the action of lassomycin derivatives against *Mtb*. An appropriate proportion of amphiphilicity, hydrophobicity, and overall charge plays a significant role in the activity of antimicrobial peptides, as discussed in the introduction section.

Compound X showed a greater peptidase inhibition than all the peptides, however, its structure has not yet been determined but is believed to be a truncated sequence and was obtained during the synthesis and purification of Pep-2-NN. Further investigations will be conducted to determine the composition and structure of Compound X, which will be achieved through techniques such as NMR.

Further investigations on the secondary structure of the rest of the peptides will be done in the future in order to study their behaviour.

4.5. Conclusion

Lassomycin-amide short peptides and their corresponding lipid-conjugated derivatives were successfully synthesized and characterized by LCMS, however, challenges were encountered during the purification that led to a significant loss of yield. Ring-2-NNA and its lipid conjugates were more retained by the stationary phase than Ring-2-NN and its lipid conjugate during analysis using LCMS. This behaviour was attributed to the glutamine polar amide group present in Ring-2-NN. The conformation of the peptides due to stabilization caused by the presence of a disulfide bond was also observed to have some influence on the behaviour of the peptides, which may be crucial in understanding the nature and behaviour of peptides which may help improve synthesis and purification with better yields.

The peptides conjugated to adamantane have better LCMS results than those conjugated to palmitic acid. This may be because palmitic acid is more hydrophobic and has poor solubility, which affects its purification and analysis using HPLC and LCMS. The conjugation of lipid molecules to Tail-2-NN also prevented the formation of the pyroglutamate impurity. In the future, further investigations may be done in order to improve the solubility of the palmitic conjugated peptides.

CD measurements showed that the lassomycin peptide derivatives are stabilized by antiparallel beta turns followed by alpha-helix. This may have made the peptides more vulnerable to the risk of aggregation formation during synthesis, thus resulting in poor yields. Ring-2-NN exhibited a high proportion of the alpha-helix conformation and was found to have an activating effect on the ClpP proteolytic effect compared to the other derivative, which inhibited peptidase activity, including Pep-2-NN. CD measurements revealed that Pep-2-NN had almost equal proportions of antiparallel and alpha-helix conformations.

References

1. Niidome, T.; Matsuyama, N.; Kunihara, M.; Hatakeyama, T.; Aoyagi, H., Effect of chain length of cationic model peptides on antibacterial activity. *Bulletin of the Chemical Society of Japan* **2005,** *78* (3), 473-476.

2. Haug, B. E.; Stensen, W.; Stiberg, T.; Svendsen, J. S., Bulky nonproteinogenic amino acids permit the design of very small and effective cationic antibacterial peptides. *Journal of Medicinal Chemistry* **2004,** *47* (17), 4159-4162.

3. Strøm, M. B.; Haug, B. E.; Skar, M. L.; Stensen, W.; Stiberg, T.; Svendsen, J. S., The pharmacophore of short cationic antibacterial peptides. *Journal of Medicinal Chemistry* **2003,** *46* (9), 1567-1570.

4. Liu, Z.; Brady, A.; Young, A.; Rasimick, B.; Chen, K.; Zhou, C.; Kallenbach, N. R., Length effects in antimicrobial peptides of the (RW) n series. *Antimicrobial Agents and Chemotherapy* **2007,** *51* (2), 597-603.

5. Loose, C. R.; Langer, R. S.; Stephanopoulos, G. N., Optimization of protein fusion partner length for maximizing in vitro translation of peptides. *Biotechnology Progress* **2007,** *23* (2), 444-451.

6. Wang, S.; Ishii, Y., Revealing protein structures in solid-phase peptide synthesis by 13C solid-state NMR: Evidence of excessive misfolding for Alzheimer's β. *Journal of the American Chemical Society* **2012,** *134* (6), 2848-2851.

7. Liu, Y. D.; Goetze, A. M.; Bass, R. B.; Flynn, G. C., N-terminal glutamate to pyroglutamate conversion in vivo for human IgG2 antibodies. *Journal of Biological Chemistry* **2011,** *286* (13), 11211-11217.

8. F. Nguyen, A.; S. Schill, M.; Jian, M.; J. LiWang, P., The effect of N-terminal cyclization on the function of the HIV entry inhibitor 5P12-RANTES. *International Journal of Molecular Sciences* **2017,** *18* (7), 1575.

9. Hudson, D. Protecting groups for asparagine and glutamine in peptide synthesis. 1990.

10. https://www.bachem.com/knowledge-center/peptide-calculator/ (accessed 12 May 2023).

11. Caporale, A.; Adorinni, S.; Lamba, D.; Saviano, M., Peptide–Protein Interactions: From Drug Design to Supramolecular Biomaterials. *Molecules* **2021,** *26* (5), 1219.

12. Rehman, I.; Kerndt, C. C.; Botelho, S., *Biochemistry, Tertiary Protein Structure*. **2017**.

13. Andrews, S. S.; Tretton, J., Physical principles of circular dichroism. *Journal of Chemical Education* **2020,** *97* (12), 4370-4376.

14. Greenfield, N. J., Using circular dichroism spectra to estimate protein secondary structure. *Nature Protocols* **2006,** *1* (6), 2876-2890.
15. Micsonai, A.; Moussong, E.; Wien, F.; Boros, E.; Vadászi, H.; Murvai, N.; Lee, Y.-H.; Molnár, T.; Réfrégiers, M.; Goto, Y., BeStSel: webserver for secondary structure and fold prediction for protein CD spectroscopy. *Nucleic Acids Research* **2022,** *50* (W1), W90-W98.
16. Epand, R. M.; Vogel, H. J., Diversity of antimicrobial peptides and their mechanisms of action. *Biochimica et Biophysica Acta (BBA)-Biomembranes* **1999,** *1462* (1-2), 11-28.
17. Paradís-Bas, M.; Tulla-Puche, J.; Albericio, F., The road to the synthesis of "difficult peptides". *Chemical Society Reviews* **2016,** *45* (3), 631-654.

Chapter 5

Synthesis of Silver nanoparticles (AgNPs)-peptide conjugates

5.1. Introduction

5.1.1. Background

Nanotechnology is a rapidly growing field due to its vast applications in various sectors, such as the industrial and agricultural sectors as well as the medical field (nanomedicine), where nanotechnology is employed in the prevention, treatment, and diagnosis of diseases.[1] In this study, we evaluate the properties of nanomaterials by conjugating silver nanoparticles to promising antimycobacterial peptides synthesized in our group and reported in Chapters 2-4.

Silver (Ag) has long been used for medical treatment due to its effective bactericidal properties against numerous disease-causing bacteria.[1] Silver nanoparticles (AgNPs) with a diameter that is less than 100 nm are important due to their bactericidal and anticancer properties and wound-healing abilities. The application of silver nanoparticles in wound healing includes its use in dressings, drug delivery, and tissue scaffolding. Silver nanoparticles are preferred over free silver (Ag) due to their larger surface area, which causes them to have greater exposure to microbes.[1] Silver nanoparticles are found to be relatively non-toxic towards humans and have been reported to have a high antimicrobial effect against both MDR and non-MDR strains of *Mycobacterium tuberculosis*.[2-3] Silver nanoparticles employ various mechanisms to cause TB cell death, including membrane destruction and denaturing resulting from the accumulation of AgNPs on the peptidoglycan layer.[4-5] Moreover, AgNPs release silver ions (Ag^{+}) which can interact with the cell wall and disrupt the bacterial envelope, causing the generation of reactive oxygen species that interrupt DNA processes, denature the ribosome, and inhibit protein synthesis.[4]

5.1.2. General synthesis of AgNPs

Currently, the three main cost-effective ways utilized to produce silver nanoparticles include physical, chemical synthesis, and biological methods, which are mostly environmentally

friendly.[1] The biological synthesis of silver nanoparticles involves using organisms (e.g., algae, fungi, bacteria, and yeast) as capping, reducing, or stabilizing agents. Chemical synthesis of silver nanoparticles is mostly preferred due to its convenience and simplicity. The general procedure to form silver nanoparticles involves using a silver salt precursor, a reducing, capping, and stabilizing agent. Silver nitrate ($AgNO_3$) is the most used precursor and acts as a source of silver ions (Ag^+), while sodium borohydride ($NaBH_4$) and trisodium citrate (TSC) act as reducing and capping agents.[1] During synthesis, silver ions (Ag^+) are released from the nitrate salt and receive electrons from the reducing agent, and are converted to the metallic form (Ag^0), which begins to cluster (nucleate) with the progression of time and form agglomerates (illustrated in **Figure 5.1** below). Stabilizing agents such as polyvinylpyrrolidone (PVP) and starch can be used to stabilize nanoparticles and minimize the rate of formation of clusters.

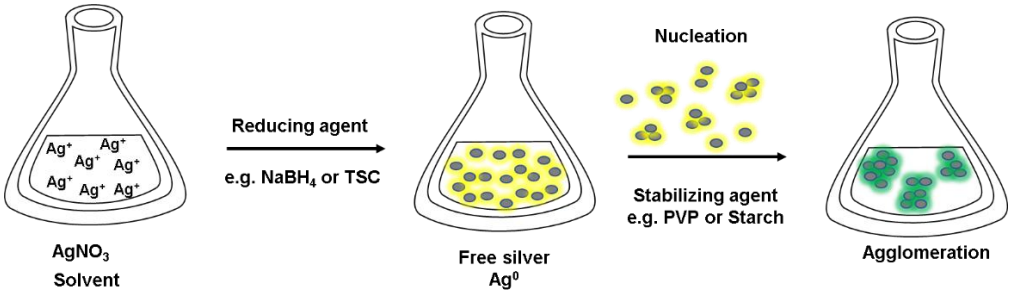

Figure 5.1: The general chemical synthesis method of silver nanoparticles from silver nitrate and the progression to agglomeration.

Sodium borohydride is a stronger reducing agent and usually produces silver nanoparticles with an average size range of 5 – 20 nm compared to trisodium citrate, which usually produces nanoparticles with an average size range of 60 – 100 nm.[1] It is very challenging to produce nanoparticles with an actual size; thus, an additional step is required to prevent aggregation.

5.1.3. Characterization using TEM and UV-Vis spectroscopy

Transmission electron microscopy (TEM) imaging and ultraviolet-visible (UV-Vis) spectroscopy techniques were utilized to monitor and characterize metal nanoparticles. The TEM was used to generate images of NPs at a sub-nanometer resolution[6] and also to

determine the particle sizes, morphology, and distribution (i.e., dispersion or agglomeration) of the NPs.[7]

Ultraviolet-visible (UV-Vis) spectroscopy is the most commonly utilized characterization technique for metallic NPs and is usually used to monitor the reaction and stability of nanoparticles. The surface plasmon resonance (SPR) is formed due to the movement of electrons between the valence and conduction bands in metallic nanoparticles when they absorb and scatter light at specific wavelengths. [8-9] The valence and conduction bands of metal NPs are very close to each other. The generated SPR band depends on the silver nanoparticles' shape and size, which depend on the method used to synthesize them.[8] Silver nanoparticles have a characteristic SPR peak with strong absorption in the visible region that ranges between 380 – 450 nm.[10]

5.2. Synthesis

The silver nanoparticles were synthesized in-house, and the employed methods are discussed below in detail.

Method 1:

In method 1, the silver nanoparticles were synthesized by mixing water (60 mL) and glycerol (40 mL), which was stirred vigorously and heated to 97°C. Silver nitrate (34 mg, 2 nM) was added to the glycerol-water mixture, which was then stirred for 5 minutes, which resulted in the mixture changing to a light orange-brown colour. Trisodium citrate (13 mg, 2 nM) was added to the mixture and allowed to stir for 20 minutes, and a pale-yellow colour was observed. After that, the mixture was allowed to cool for 10 -15 minutes without stirring. After cooling, it was observed that the solution's colour had turned to an undesired dark yellow-green, indicating a possible formation of agglomeration.

Method 2:

In method 2, the silver nanoparticles were prepared by transferring water (20 mL) into a conical flask, and the temperature was cooled and kept at 0°C using an ice bath. A magnetic stirrer was used to vigorously stir the water at a speed of 500 revolutions per minute (RPM). Sodium borohydride (1.52 mg, 2mM) was added, followed by trisodium citrate (5.11 mg, 1 mM), which was left to mix for 5 minutes. Concurrently, silver nitrate (2.72 mg, 2 mM) was

dissolved in 8 mL distilled water and then transferred to the mixture in a drop-wise manner with continuous stirring, which was stopped after all the silver nitrate solution was transferred. The colour of the mixture changed to yellow, indicating the formation of silver nanoparticles which were then washed using 2 mM of TSC and centrifuged at 10,000 RPM, and the supernatant was separated from the precipitate. The supernatant was decanted but not discarded as it had the desired yellow colour, and the precipitate was obtained as very fine, dark particles.

5.3. Results and Discussion

Silver nitrate ($AgNO_3$) was used as a source of silver metal in both methods, which was then reduced using trisodium citrate (TSC) in glycerol-water (in **method 1**) and sodium borohydride ($NaBH_4$) in an aqueous solution (in method 2). TSC was used as a stabilizing agent for the nanoparticles in both methods. The colour of the colloidal solution of nanoparticles produced from **Method 1** was dark green, indicating the formation of agglomeration (clustering)[11], while those from **Method 2** had a golden-yellow colour which indicated a successful formation of NPs.[12] The colours of silver nanoparticle colloids are used to monitor their stability, and their description is presented in **Figure 5.2**.

5.3.1. UV-Vis results

After the synthesis, the nanoparticles from each method were analysed using UV-Vis spectrophotometry, and the recorded SPR absorption peaks are presented in **Figure 5.2** below. A broad SPR absorption band at 432 nm around the longer wavelength region was observed for the nanoparticles synthesized using **Method 1**, which indicated the formation of agglomeration (clustering) of the particles. Meanwhile, a strong SPR absorption band around 388 nm was observed for the nanoparticles synthesized using **Method 2**, which confirmed the successful conversion of Ag^+ to Ag^0, which was closer to the characteristic band for spherical silver nanoparticles (400 nm). The SPR bands for silver nanoparticles are presented in **Figure 5.2**.

After synthesis using **Method 2**, it was noticed that the stability of the silver nanoparticles was short-lived, and the colour changed from yellow to dark-green within a few days, and thus the method was amended to include washing the final colloidal product with a solution

of TSC. The mixture was then centrifuged to separate the precipitate (AgNPs-NN) and the supernatant (AgNPs-NN1) samples which were analysed using UV-Vis where SPR absorption bands were recorded to be 387 nm and 390 nm, respectively (shown in **Figure 5.2C**). Silver nanoparticles were present in both the AgNPs-NN and AgNPs-NN1 samples. This additional washing step was noticed to prolong the stability of silver nanoparticle samples which were monitored over two weeks using UV-Vis, and the yellow colour was maintained in both samples. This may be due to the excess presence of citrate ions which surround the NPs and form strong repulsive forces around them, thus reducing the chances of clustering. Silver nanoparticles are generally unstable in solution.[13] The results of all the samples analysed with UV-Vis are recorded in **Table 5.1**.

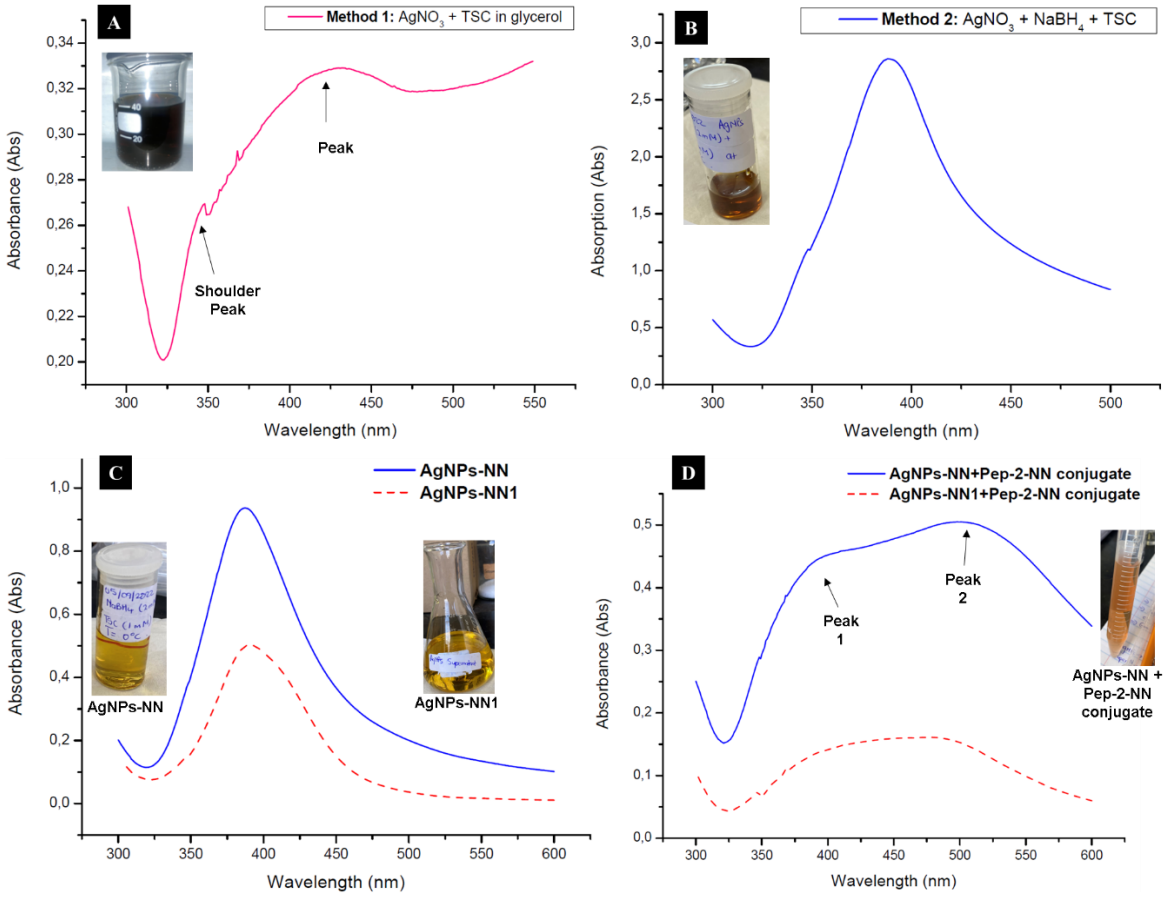

Figure 5.2: The UV-Vis spectra of silver nanoparticles synthesized with method 1 **(A)** and method 2 **(B)**. from which the UV-Vis spectra of **(C)** AgNPs-NN (precipitate, blue smooth line) and AgNPs-NN1 (supernatant, red dashed line) which were synthesized using $NaBH_4$ (2 mM) as a reducing agent and was capped using 1 mM TSC and (**D**) Pep-AgNPs-NN (blue smooth line) and Pep-AgNPs-NN1 (red dashed line) nanoparticle-peptide conjugates.

Table 5.1: The observed colour of each sample of silver nanoparticles as well as the SPR band as determined by the UV-Vis analysis.

Sample	Colour of final product	UV-Vis SPR band
Method 1 AgNPs	Dark green	348 (shoulder Peak), 432
Method 2 AgNPs	Golden yellow	388
AgNPs-NN	Yellow	387
AgNPs-NN1	Yellow	390

5.3.2. Conjugation of silver nanoparticles to peptide derivatives

Antimicrobial peptides and silver nanoparticles are promising agents for developing new antimicrobial drug treatments due to their ability to effectively combat drug-resistant pathogens.[5, 13] The combination of silver nanoparticles with antibiotics or antimicrobial peptides has been reported to result in a synergistic effect and enhanced antimicrobial activity.[5] Moreover, the conjugation of peptides to AgNPs increases the stability and bioavailability of the peptides and nanoparticles.[13-14] Nanoparticles can act as a delivery system when conjugated to antimicrobial peptides.[14]

Silver nanoparticles have a strong affinity for sulfur[4], and their conjugation to peptides containing cysteine in their sequences usually results in favourable nanoparticle-peptide interactions.[13] Pal *et al.* reported that the disulfide bonds present in antimicrobial peptides were preserved and not disrupted upon conjugation to silver nanoparticles[13], however, other studies suggest Ag-induced cleavage of the disulfide bond upon conjugation to AgNPs.[15] Disulfide bonds in AMPs are important as they stabilize the peptide structure and thus impact the peptide's function and activity.[13] This section explores the conjugation of silver nanoparticles to Pep-2-NN lassomycin peptide derivative (**Figure 5.3**).

Pep-2-NN was conjugated to the silver nanoparticles by dissolving approximately 2.7 mg of peptide in 5 mL of distilled water and the solution was mixed with AgNPs-NN (5 mL) and AgNPs-NN1 (5 mL) at 4°C to form Pep-AgNPs-NN and Pep-AgNPs-NN1 conjugates, respectively. The peptide-AgNP conjugates were analysed with UV-Vis and TEM.

The SPR bands of the peptide-AgNP conjugates were noticed to have shifted and appeared around 502 nm in the longer wavelength region (red-shift), with the peak more apparent in

Pep-AgNPs-NN than Pep-AgNPs-NN, however, a similar spectral trend is noticed in both samples. UV-Vis results are recorded in **Table 5.2** below. The red-shift of the SPR peak may have resulted from the agglomeration of the NPs due to the displacement of citrate ions by the larger-sized peptide.

Pep-2-NN interacts with the AgNPs through the cysteine thiol groups, as illustrated in **Figure 5.3B**. The colour of the nanoparticles spontaneously changed to reddish-brown upon peptide conjugation, which was attributed to agglomeration. A weak SPR band around 394 nm could indicate that the nanoparticles are also present as nanospheres.

The silver nanoparticles are more likely to react with the disulphide bridge of Pep-2-NN upon conjugation and cause some conformational changes. The change in the conformation of peptides and proteins from helical to beta sheets when conjugated to nanoparticles is outlined in detail in a mini-review by Duran *et al.* Pep-2-NN CD measurements showed the presence of 53% antiparallel beta sheets. Hence the agglomeration observed with the nanoparticles can be hypothesized to be caused by beta sheets formation, and low peptide concentrations should be investigated in the future.

Table 5.2: The observed colour of each sample of silver nanoparticles and the SPR band as determined by the UV-Vis analysis.

Sample	Colour of the final product	UV-Vis SPR band
Pep- AgNPs-NN conjugation	Reddish-brown	394, 502
Pep-AgNPs-NN1 conjugation	Reddish-brown	-

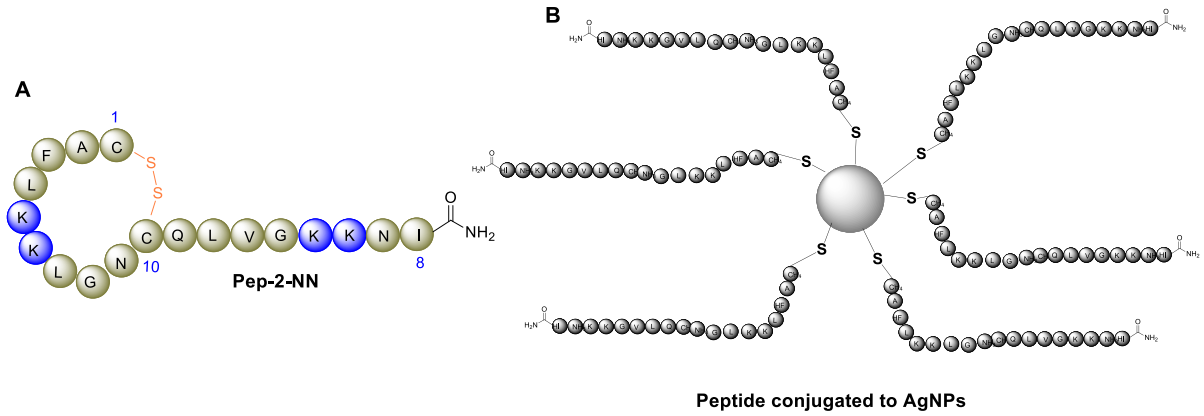

Figure 5.3: (A) represents the structure of Pep-2-NN, and **(B)** illustrates the interaction between the peptide-NPs conjugates.

5.3.3. Transmission Electron Microscopy (TEM) imaging results

The AgNPs-NN and AgNPs-NN1 nanoparticles and their peptide conjugates were analysed using Transmission Electron Microscopy (TEM) imaging to determine their size and shape. The TEM images reveal that the morphology of AgNPs-NN and AgNPs-NN silver nanoparticles and their respective peptide conjugates are spherical, as shown in **Figure 5.4** below.

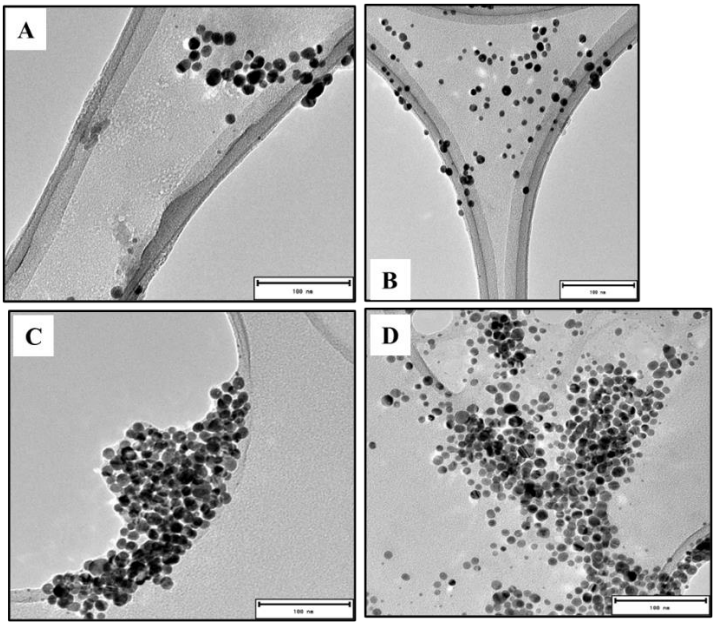

Figure 5.4: TEM images of **(A)** AgNPs-NN, **(B)** AgNPs-NN1, and Pep-2-NN conjugates of **(C)** AgNPs-NN and **(D)** AgNPs-NN1.

The size distribution of the nanoparticles was determined by measuring the diameter of the particles on the TEM images using the ImageJ software. The histogram of the particle size distribution for each sample is presented in **Figure 5.5,** and the data is recorded in **Table 5.3** below. The average sizes of AgNPs-NN and AgNPs-NN silver nanoparticles were 9 ± 2 nm and 7 ± 2 nm, respectively. AgNPs-NN1 was obtained as part of the supernatant and had a smaller size than AgNPs-NN, which was suspended at the bottom as "precipitates." Therefore, the washing and centrifuging step can be used to separate sizes. After conjugation to Pep-2-NN, the sizes of the nanoparticles increased to 12 ± 3 for Pep-AgNPs-NN and 9 ± 2 for AgNPs-NN1. The slight increase in the average size of the silver nanoparticles conjugated to Pep-2-NN is still within a reasonable range and may be due to aggregation, as observed with the red-shifting of the SPR band observed around 502 nm. The spherical shape morphology was still retained after conjugation, as seen in the TEM images in **Figure 5.4C-D**. The TEM images also show that the silver nanoparticles AgNPsNN and AgNPs-NN1 are more dispersed, while the NPs-peptide conjugates are more clustered, confirming agglomeration. AgNPs-NN1 and its peptide conjugate have smaller sizes than AgNPs-NN and its respective conjugate, and this is because AgNPs-NN1 was saved as part of the supernatant during the washing step. At the same time, the slightly denser particles were pulled to the bottom during centrifugation. In order to reduce agglomeration, a dilute concentration of the peptides will be investigated, and a linker between the silver and the peptide will be introduced.

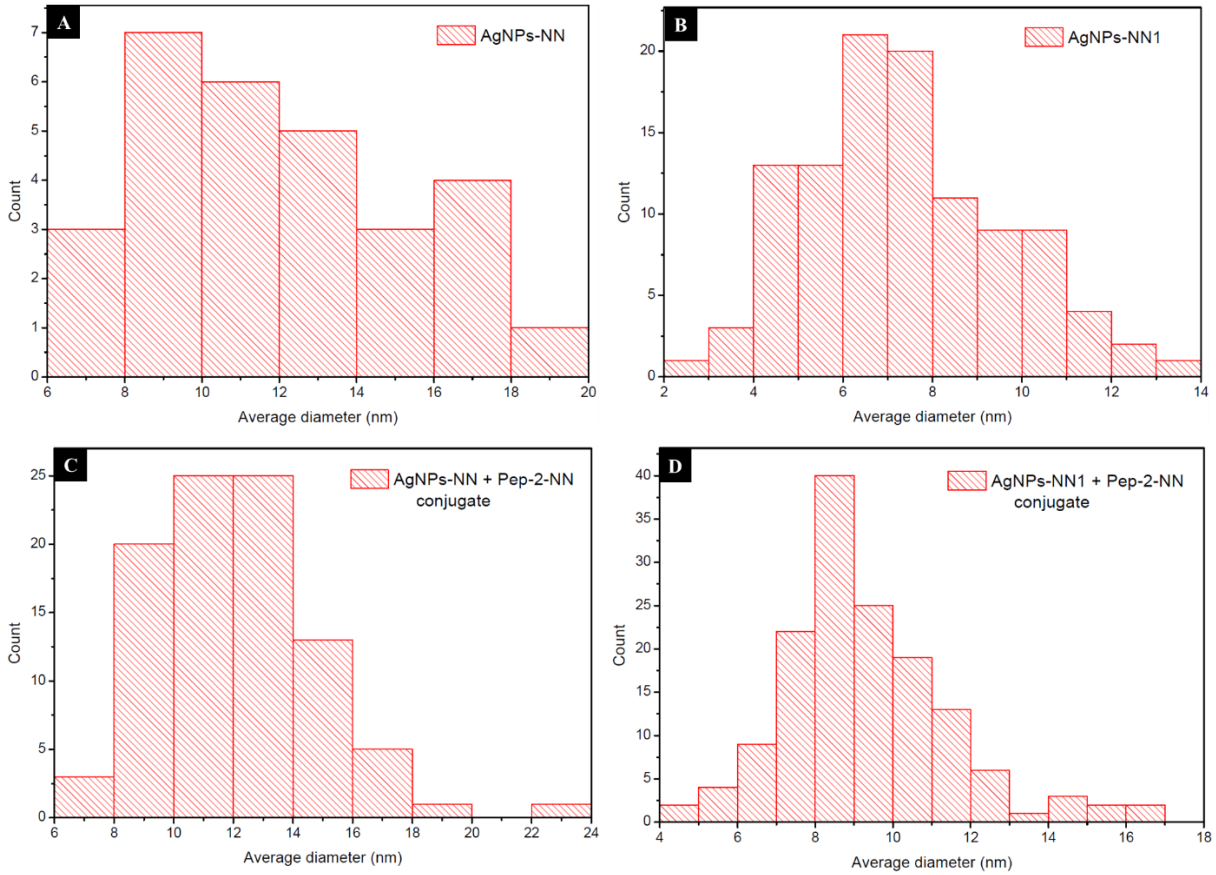

Figure 5.5: Histogram showing the size distribution of AgNPs-NN1 **(A)**, AgNPs-NN1 **(B),** silver nanoparticles-peptide conjugates, Pep-AgNPs-NN **(C)** and Pep-AgNPs-NN1 **(D)**.

Table 5.3: The average size of AgNPs-NN and AgNPs-NN1 nanoparticles and their Pep-2-NN conjugates.

Sample	Average diameter (nm)
AgNPs-NN	9 ± 2
AgNPs-NN1	7 ± 2
AgNPs-NN + Pep-2-NN (Pep-AgNPs-NN)	12 ± 3
AgNPs-NN1 + Pep-2-NN (Pep-AgNPs-NN1)	9 ± 2

5.4. Conclusion

Silver nanoparticles were successfully synthesized using sodium borohydride and trisodium citrate (TSC) and characterized by UV-Vis and TEM analysis. Colour change was used to monitor the synthesis of the NPs and their stability while in storage. The colour of the nanoparticles remained yellow for over two weeks, indicating that the nanoparticles were stable. A yellow colour indicated a successful formation of the nanoparticles, and the undesired agglomeration caused the colour to change to green. The silver nanoparticles were centrifuged after the washing step, which resulted in the separation of the NPs according to size, with smaller particles transferred to the supernatant (7 ± 2 nm), while the larger-sized particles (9 ± 2 nm) remained in the bottom "precipitates." TEM imaging revealed that the nanoparticles were spherical, which was also corroborated by the SPR absorption bands around 400 nm for AgNPs-NN and AgNPs-NN1 when analysed using the UV-Vis. Pep-2-NN was successfully conjugated to the nanoparticles, and the conjugates maintained the spherical morphology. However, there was evidence of aggregation which resulted in a slight increase of the particle size to 12 ± 3 nm for Pep-AgNPs-NN and 9 ± 2 nm for Pep-AgNPs-NN1. The UV-Vis also showed a red-shift of the SPR band for the peptide-NPs conjugates. In order to reduce agglomeration, a dilute concentration of the peptides will be investigated in the future, and a linker between the silver and the peptide will be introduced. The conjugates will also be examined for antimicrobial activity.

References

1. Almatroudi, A., Silver nanoparticles: Synthesis, characterisation and biomedical applications. *Open Life Sciences* **2020,** *15* (1), 819-839.

2. Lara, H. H.; Ayala-Núnez, N. V.; Ixtepan Turrent, L. d. C.; Rodríguez Padilla, C., Bactericidal effect of silver nanoparticles against multidrug-resistant bacteria. *World Journal of Microbiology and Biotechnology* **2010,** *26*, 615-621.

3. Morones, J. R.; Elechiguerra, J. L.; Camacho, A.; Holt, K.; Kouri, J. B.; Ramírez, J. T.; Yacaman, M. J., The bactericidal effect of silver nanoparticles. *Nanotechnology* **2005,** *16* (10), 2346.

4. Yin, I. X.; Zhang, J.; Zhao, I. S.; Mei, M. L.; Li, Q.; Chu, C. H., The antibacterial mechanism of silver nanoparticles and its application in dentistry. *International Journal of Nanomedicine* **2020**, 2555-2562.

5. Zharkova, M. S.; Golubeva, O. Y.; Orlov, D. S.; Vladimirova, E. V.; Dmitriev, A. V.; Tossi, A.; Shamova, O. V., Silver nanoparticles functionalized with antimicrobial polypeptides: benefits and possible pitfalls of a novel anti-infective tool. *Frontiers in Microbiology* **2021,** *12*, 3881.

6. Winey, M.; Meehl, J. B.; O'Toole, E. T.; Giddings Jr, T. H., Conventional transmission electron microscopy. *Molecular Biology of the Cell* **2014,** *25* (3), 319-323.

7. Gamboa, S. M.; Rojas, E.; Martínez, V.; Vega-Baudrit, J., Synthesis and characterization of silver nanoparticles and their application as an antibacterial agent. *International Journal of Biosensors & Bioelectronics* **2019,** *5*, 166-173.

8. Wu, C.; Zhou, X.; Wei, J., Localized surface plasmon resonance of silver nanotriangles synthesized by a versatile solution reaction. *Nanoscale Research Letters* **2015,** *10* (1), 1-6.

9. Mavani, K.; Shah, M., Synthesis of silver nanoparticles by using sodium borohydride as a reducing agent. *International Journal of Engineering Research & Technology* **2013,** *2* (3), 1-5.

10. Yerragopu, P. S.; Hiregoudar, S.; Nidoni, U.; Ramappa, K.; Sreenivas, A.; Doddagoudar, S., Chemical synthesis of silver nanoparticles using tri-sodium citrate, stability study and their characterization. *International Research Journal of Pure and Applied Chemistry* **2020,** *21* (3), 37-50.

11. Badi'Ah, H.; Seedeh, F.; Supriyanto, G.; Zaidan, A. Synthesis of silver nanoparticles and the development in analysis method, IOP Conference Series: Earth and Environmental Science, IOP Publishing: 2019; p 012005.

12. Hamedi, S.; Ghaseminezhad, S. M.; Shojaosadati, S. A.; Shokrollahzadeh, S., Comparative study on silver nanoparticles properties produced by green methods. *Iranian Journal of Biotechnology* **2012**, 10 (3).

13. Pal, I.; Brahmkhatri, V. P.; Bera, S.; Bhattacharyya, D.; Quirishi, Y.; Bhunia, A.; Atreya, H. S., Enhanced stability and activity of an antimicrobial peptide in conjugation with silver nanoparticle. *Journal of Colloid and Interface Science* **2016,** *483*, 385-393.

14. Dijksteel, G. S.; Ulrich, M. M.; Middelkoop, E.; Boekema, B. K., Lessons learned from clinical trials using antimicrobial peptides (AMPs). *Frontiers in Microbiology* **2021,** *12*, 616979.

15. Kato, R.; Uesugi, M.; Komatsu, Y.; Okamoto, F.; Tanaka, T.; Kitawaki, F.; Yano, T.-a., Highly stable polymer coating on silver nanoparticles for efficient plasmonic enhancement of fluorescence. *American Chemical Society Omega* **2022,** *7* (5), 4286-4292.

Chapter 6

Structural elucidation of lassomycin-amide peptide derivatives

6.1. Introduction

Lassomycin-amide derivatives, Pep-2-NN and Pep-2-NNA, have been shown to possess acceptable potency against *Mycobacterium tuberculosis* (*Mtb*), the causative agent of tuberculosis (Chapter 2). This chapter discusses the structural elucidation of Pep-2-NN using one-dimensional (1D) and two-dimensional (2D) Nuclear Magnetic Resonance (NMR) spectroscopy. Computational studies were used to predict the stable structural conformations of the peptides. Circular dichroism (CD) spectroscopy was used to determine the secondary structure of selected lassomycin-amide derivatives, including Pep-2-NN.

Structures of biological molecules play a significant role in their function, and several techniques can be used as effective structural determination tools. These include X-ray crystallography, circular dichroism, Fourier transform infrared (FTIR), and Nuclear Magnetic Resonance (NMR) spectroscopy.[1-2] X-ray diffraction and NMR are the two main tools utilized to get structural details at a molecular level.[3] However, NMR is usually preferred over X-ray diffraction in peptide studies due to its ability to reveal information about the three-dimensional (3D) structure of biological molecules in solution by utilizing experiments that can reveal through-bond and space interactions.[1, 4] On the other hand, X-ray crystallography is more challenging and involves using a peptide that is in a single crystal form with an appropriate size obtained in a process that usually requires highly pure and water soluble peptides.[1, 5] One of the challenges that arise in NMR studies is the limitation due to the mass of the peptide as the order of difficulty in NMR increases with molecular size, and this is because larger molecules have slower tumbling rates and shorter NMR signal relaxation times, a problem not experienced with X-ray crystallography.

Since proteins/peptides are almost entirely composed of protons and carbons, NMR provides a wealth of information about the primary structure and all levels of the higher-order structure (HOS) responsible for the correct folding and the 3D shape.[2] One-dimensional NMR includes proton (^{1}H) and carbon (^{13}C) NMR experiments, primarily used to determine the structure of

small – medium molecules and insufficient for large-sized molecules, which may result in overlapping signals. Hence, nuclear Overhauser Effect (NOE) NMR parameters are useful in obtaining the 3-dimensional or tertiary structure of larger peptide molecules.[3] In addition to scalar, through-bond interactions, NOE experiments use through-space interactions mediated mainly by dipolar interactions.[3] NOE is also a function of ωτc where ω is the spectrometer frequency and τc is the rotational correlation time of the molecule, and this relation is expressed as; NOE = $(1/r^6)\times f(\tau c)$.[3] However, NOE enhancement decreases with increasing molecular size and hence the increase in the rotational correlation time (τc).[3]

Scalar (or through-bond) interactions in NMR studies can be determined by using correlation spectroscopy (COSY) and total correlation spectroscopy (TOCSY) experiments which can generate spectra consisting of protons connected through covalent bonding. In a TOCSY experiment, the interacting hydrogen atoms are confined in the amino acid residue involving the amide proton (NH), alpha-proton (αH) connected to the α-carbon, and the hydrogen atoms in the sidechain. Interacting protons generate a spin system unique to each amino acid residue in the peptide. The fingerprint amide region of the NMR spectra plays a crucial role in residue assignment and shows the connection within a spin system of an amino.

Furthermore, the Nuclear Overhauser effect (NOE) experiment can detect long-range and through-space interactions between amino acid residues that are far apart in a sequence, thus establishing the folding patterns with the peptide's sequence.[1] Chemical shifts and scalar coupling constants are usually used to determine the secondary structure of peptides as they can reveal the nature of the amino acids and their coupling interactions. The cross-peak intensities in a NOESY spectrum can be used to estimate the distance between the interacting amino acids. One of the major drawbacks of 2-D NMR is the limitation of peptide molecular weight whereby above an upper limit of approximately 10 kDa, the analysis may result in severe resonance overlap that may result in undesirable results.[1] Hence the need for the Rotating frame Overhauser Enhancement Spectroscopy (ROESY) experiment, which can be used in the place of NOESY to determine the structure of peptides. It can show the correlation between neighbouring residues and through-space interaction at higher mass ranges.[6] Another challenge that can arise with NMR involves the overlapping of resonance signals in a peptide that contains a large number of different conformations, thus resulting in poor elucidation.[3]

Two-dimensional NMR experiments such as Heteronuclear Single Quantum Coherence (HSQC) and Heteronuclear Multiple Bond Correlation (HMBC) involve the interaction between proton and carbon atoms within a residue resulting in the generation of NMR spectra with ^{1}H – ^{13}C correlations. HSQC experiments determine proton-carbon single bond correlations (^{1}J-coupling) where the hydrogen atom is directly bonded to the carbon. Contrary to HSQC, HMBC determines correlations between protons and carbons that may not be directly attached and are separated by two – three covalent bonds. Furthermore, ^{1}H – ^{13}C HMBC correlations in conjugated systems can also occur on atoms up to four bonds away.

Herein all the NMR experiments were used to determine the 3D structure of Pep-2-NN.

6.2. Experimental procedure

Nuclear magnetic resonance experiments:

The peptide (39.5 mg) was dissolved in 0.5 mL deuterated dimethyl sulfoxide (DMSO), and the following NMR experiments were acquired: ^{1}H COSY, [^{1}H, ^{1}H] TOCSY, [^{1}H, ^{13}C] HSQC, [^{1}H, ^{1}H] HMBC and [^{1}H, ^{1}H] ROESY. Instrument settings and specifications are outlined in detail in Chapter 8.

Circular dichroism studies:

Selected peptides, namely Pep-2-NN, Ring-2-NN, and Pep-Lys-NN (shown in **Figure 6.1**), were subjected to circular dichroism, where each peptide sample was dissolved in distilled water and diluted to a concentration of 100 μM. The CD measurements of the peptides were recorded on a JASCO spectrometer instrument at 25°C, and the spectra were generated from the Beta Structure Selection (BeStSel) online software provided by Micsocai *et al.*[7]

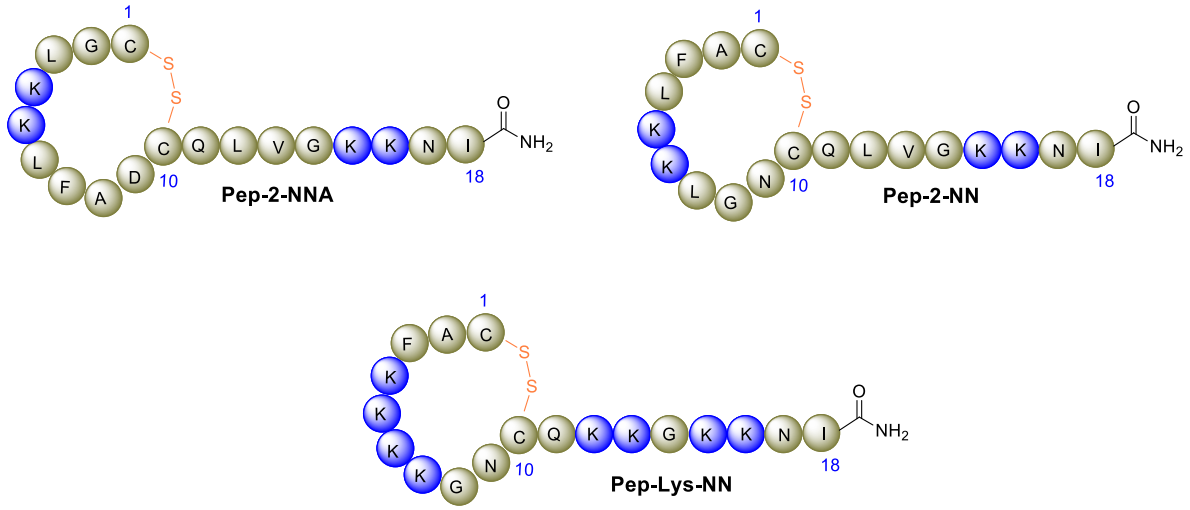

Figure 6.1: The structures of Pep-2-NNA, Pep-2-NN, and Pep-Lys-NN

6.3. Results and Discussion

6.3.1. Prediction by computational analysis

The extended peptides were modelled by the LEAP module of the Amber18 GPU program.[8] The Amber ff19SB force field was applied in the construction of the peptides. The disulfide bond between the cysteine residues (Cys1 and Cys10) in both peptides was modelled using the bond command in tleap.

6.3.1.1. Structure prediction using the Ramachandran plot

The Ramachandran tool uses three backbone torsion (or dihedral) angles, namely phi (Ψ), psi (ϕ), and omega (ω), obtained from two neighbouring chemical bonds to determine the three-dimensional structure of peptides.[9] The side chains of amino acids are also defined by chi (χ) torsion angles.[9] **Figure 6.2** illustrates the torsion angles used to determine the peptides' secondary structure. The omega (ω) angle is usually not very variable and, therefore, typically adopts a trans (rarely cis) conformation; hence polypeptide folding is mainly defined by free rotation around N–Cα and Cα–C bonds represented by φ and ψ torsion angles, respectively as bond lengths and bond angles remain invariant.[3, 9] The Ramachandran plots usually uses the ϕ and ψ backbone angles.[9] In Ramachandran, only particular regions tend to be accessible, resulting in highly populated clusters that represent the secondary structure elements.

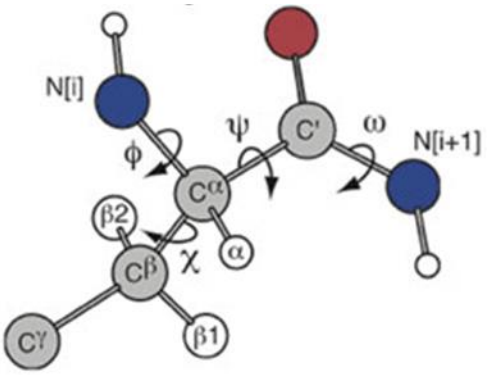

Figure 6.2: The illustration of a peptide showing torsion angles that define the protein backbone and sidechains, including phi (Ψ), psi (ϕ), and omega (ω).[9] The modified image is obtained under the Creative Commons Attribution 4.0 International License, CC BY 4.0.

A Ramachandran plot was generated for Pep-2-NN and Pep-2-NNA peptides to predict their secondary structures during analysis. It was observed that the arrangement of amino acids directly influences the folding and conformation of the secondary structure elements. The Ramachandran plot of the peptides presented in **Figure 6.3** shows that the population analysis of the phi (Ψ) – psi (ϕ) dihedral angles tend to be highly clustered in the right-handed α-helical region. Therefore, the predicted peptides consist of an alpha-helix structure. Furthermore, the beta (β) sheet conformation was observed in the plot, as represented by the signals in the right-handed β-sheet quadrant, also seen in **Figure 6.3**.

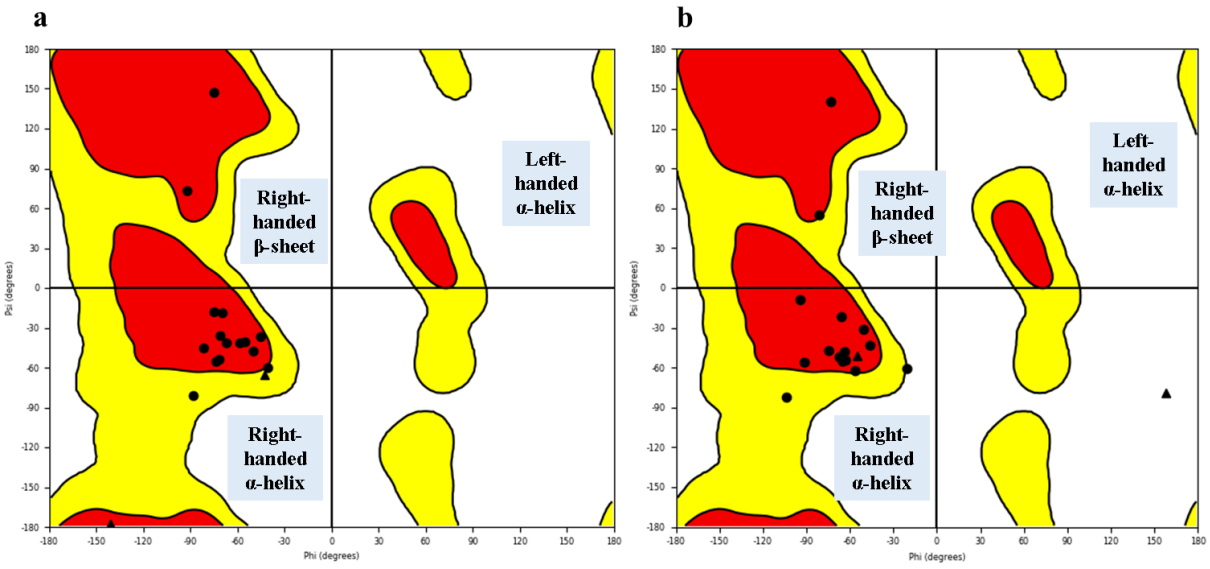

Figure 6.3: The Ramachandran plots showing the distribution of the peptides' phi (Ψ) and psi (ϕ) dihedral angles. The amino acids distribution shows a majority in the α-helix allowed region. The red region represents the favored region, the yellow represents the allowed region, and the white represents the disallowed region.

6.3.1.2. Molecular Dynamics simulations

Molecular dynamics (MD) simulations were conducted on the peptides to assess their potential energy and stability, which was analysed using the root-mean-square deviation (RMSD) of the backbone αC in the peptide chain. Furthermore, the RMSD clustering was used to locate the lowest energy-minimized peptide from the MD trajectories. The peptides were pre-minimized to remove any possible clashes between amino acid residues before the molecular dynamics (MD) simulations were performed. Full geometry optimization and gradual heating without restraints were performed on the peptides. The RMSD plot (**Figure 6.4A**) revealed that cyclized lassomycin derivatives, Pep-2-NN and Pep-2-NNA, were stable with marginal variations. Furthermore, it was noticed that the potential energy (**Figure 6.4B**) aligned with the predicted α-helix folded state of the peptides. The studies revealed that the α-helical conformation was stable throughout the MD simulation. The predicted 3D structures of Pep-2-NN and Pep-2-NNA are shown in **Figure 6.4C** and **D**, respectively.

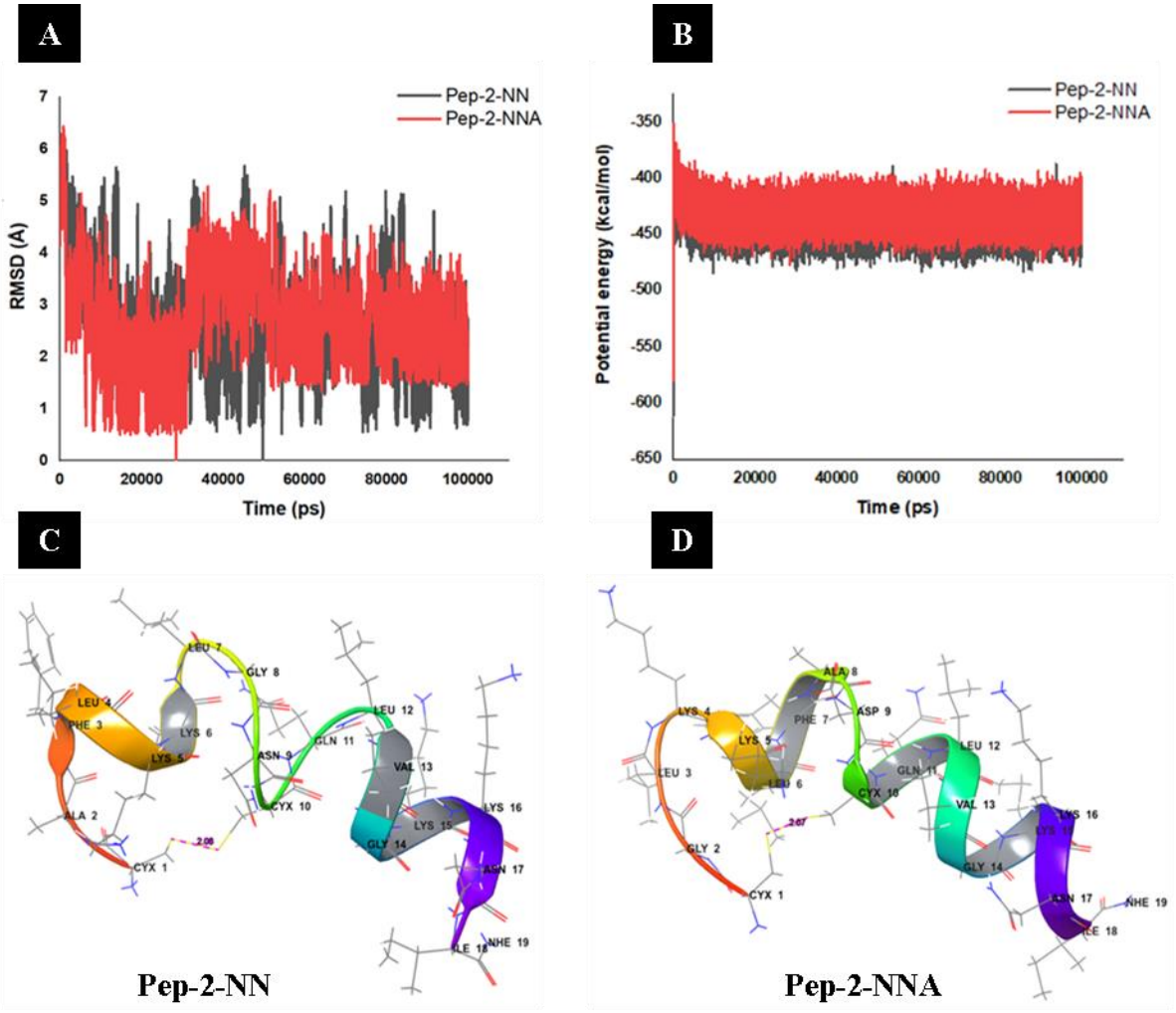

Figure 6.4: The **(A)** RMSD plots and **(B)** potential energy profiles for Pep-2-NN and Pep-2-NNA over 100ns MD simulations at 325K and the lowest-energy minimized predicted 3D structures for **(C)** Pep-2-NN and **(D)** Pep-2-NNA.

Furthermore, the structural alignment of the peptides was carried out to determine the structural similarities regarding their folded states, revealing that Pep-2-NN and Pep-2-NNA have minor discrepancies in the disulfide bond region and the secondary structural elements in the loop region. The loop conformation in peptides is formed by hydrogen bonding interactions. The structural elucidation also revealed that the loop region in Pep-2-NN extended from Leu7 to Leu12, i.e., leucine residues at positions 7 and 12. In contrast, Pep-2-NNA only extended from Asp9 (aspartic acid) to Cys10 (cysteine), as shown in **Figure 6.5**. Despite the observed discrepancies, the disulfide bond lengths of Pep-2-NN and Pep-2-NNA were within the acceptable range of 2.08 and 2.07, respectively (as shown in **Figure 6.5**).

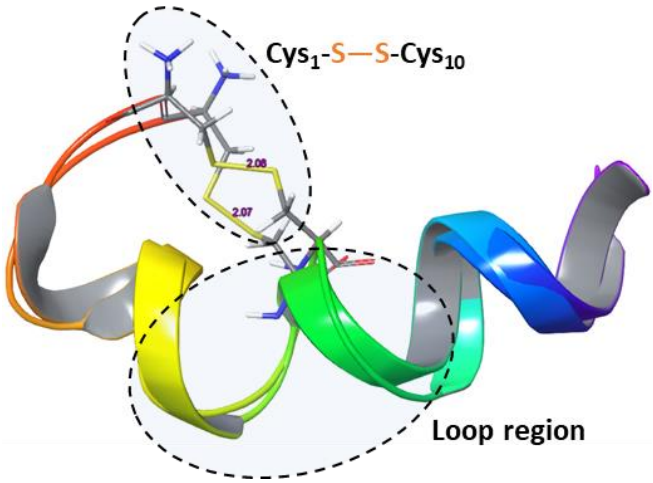

Figure 6.5: Structural alignment of Pep-2-NN and Pep-2-NNA conformers. The circled regions show minor discrepancies in the disulfide region and the secondary structural elements in the loop region.

The computational studies also revealed that there is a possible interaction between Phe3 and Ile18 in Pep-2-NN, shown in **Figure 6.6A**. However, NMR studies on the peptide (presented in section 6.3.3) reveal that Ile interacts with Lys5 and Lys 6, which are not that far apart from Phe3. This may suggest that the C-terminus of the sequence is closer to the ring and not far away. This may occur in two possible scenarios, firstly, the tail may be tightly packed against the cyclic ring, or secondly, it might be threading inside the ring. The tail is likely to be threaded inside the ring whilst the Phe3 acts as a 'steric plug' interacting with isoleucine to prevent unthreading. On the other hand, the Phe3 residue in Pep-2-NNA, is far from the Ile18 side chain as shown in **Figure 6.6B**. In the future, the MD simulation time and the temperature will be prolonged to retrieve more conformations.

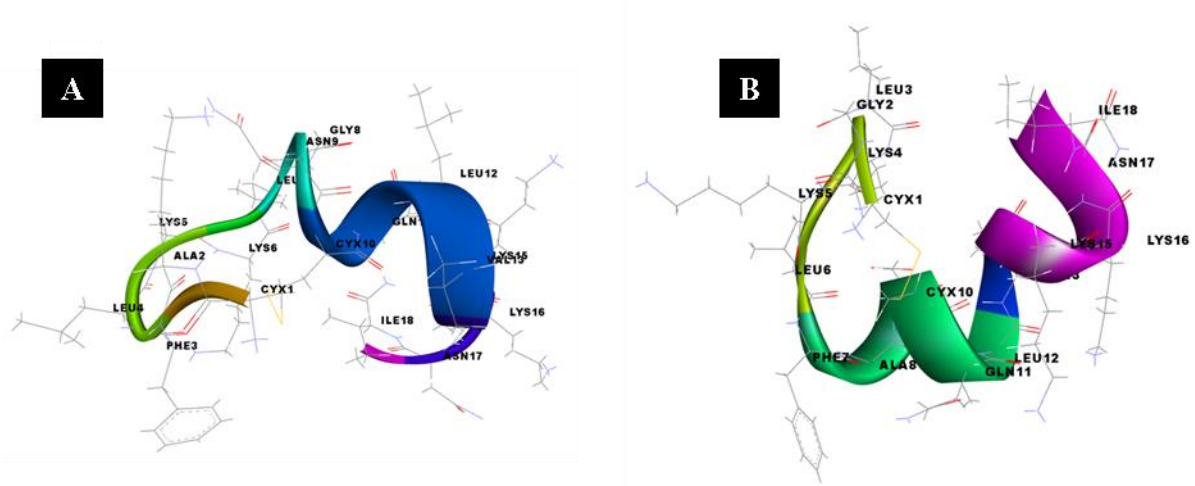

Figure 6.6: The snapshots of **(A)** Pep-2-NN and (**B**) Pep-2-NNA secondary structures from a 100ns MD simulated at 340K as predicted by computational modeling.

6.3.2. Characterization by Circular Dichroism

The secondary structures of Pep-Lys-NN and Pep-2-NN derivatives were investigated and determined with circular dichroism. Each peptide sample was dissolved in distilled water and diluted to a concentration of 100 μM. It was not easy to obtain good measurements at concentrations less than 100 μM. Since Pep-Lys-NN and Pep-2-NN are completely soluble in water, they were therefore dissolved in it for CD measurements. Furthermore, water was selected over organic solvents, most of which can result in structural changes, such as ethanol and trifluoroethanol (TFE), which can induce the formation of helices. The CD measurements of the peptides were recorded on a JASCO spectrometer instrument at 25°C, and the spectra were generated from the Beta Structure Selection (BeStSel) online software provided by Micsocai *et al.*[7] The BeStSel software can determine the composition of the secondary structure of the analysed peptide and the data is presented in **Figure 6.7** and **Table 6.1**.

CD measurements revealed that a major proportion of the peptides adopted an antiparallel conformation (over 50%), followed by the alpha-helix and a beta-turn to a small degree. According to the CD measurements, the structures of Pep-2-NN-2 (53% antiparallel) and Pep-2-NN-3 (55.9% antiparallel) were slightly different, although they were obtained from the same sample during purification with HPLC, eluting at different retention times. Therefore, this might suggest that the conformation of the peptides due to structural differences may influence their interaction with the stationary phase. Moreover, during the cyclization step of Pep-2-NN, the linear peptide was treated with 20% DMSO in water (v/v) and may have influenced the folding and, thus, the conformation of the peptides. It is suggested that during the biosynthesis of lassomycin, macrolactam cyclization occurs after the full peptide has been synthesized and folded in a manner that results in the threading of the tail, thus forming the lasso structure.

The antiparallel beta sheets can also be attributed to the cyclic ring amino acids, which can form sheets within the ring. Furthermore, the lasso peptide structure of the antimicrobial peptide microcin J25 has been reported to be stabilized by two short double-stranded antiparallel β-sheets.[4] The computational studies showed that long-range interaction between Phe 3 and Ile-18 might be attributed to the knotting effect stabilized by antiparallel sheets.

When compared to Pep-Lys-NN, which was formed by replacing selected non-polar amino residues with charged polar lysine, Pep-2-NN lacks the presence of a turn motif, and this may

suggest that the nature of the amino acid in the sequence may have a direct impact on the peptide secondary structure. This may be in agreement with the computational modelling studies performed on the peptides, which indicated that the arrangement of the amino acid residues directly influences the folding and conformation of the secondary structure elements. Ultimately, the majority of the structure of Pep-2-NN is antiparallel, and therefore it can be postulated that the lassomycin-amide derivatives have the propensity to form antiparallel – to – alpha-helix structures.

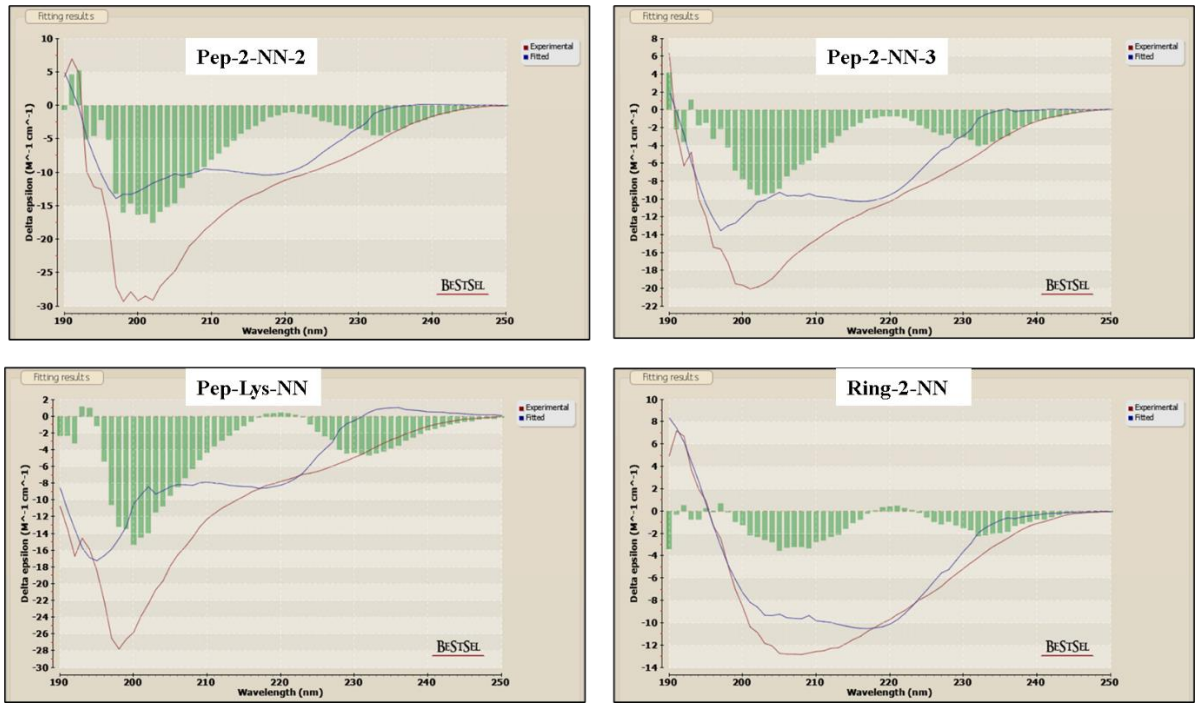

Figure 6.7: The CD measurements and the composition of the secondary structures of Pep-Lys-NN, Ring-2-NN and Pep-2-NN conformers as determined using the BestSel online software.

Table 6.1: The secondary structure of lassomycin derivatives Ring-2-NN, Pep-2-NN, and Pep-Lys-NN as determined by circular dichroism (CD) studies.

	Secondary structure		
Peptide	**Alpha helix**	**Antiparallel**	**Turn**
Ring-2-NN	58.8%	33.1%	-
Pep-2-NN-2	47%	53%	-
Pep-2-NN-3	44.1%	55.9%	-
Pep-Lys-NN	25.9%	68.4%	5.8%

6.3.3. Characterization by NMR

The structure of Pep-2-NN was elucidated using the [^{1}H, ^{1}H] COSY, [^{1}H, ^{1}H] TOCSY, [^{1}H, ^{13}C] HSQC, [^{1}H, ^{1}H] HMBC and [^{1}H, ^{1}H] ROESY experiments. Pep-2-NN is a relatively longer peptide consisting of 18 amino acids, as presented in **Figure 6.8** below. The isoleucine residue at position 18 (Ile18) is at the C-terminus of the peptide chain, while the amidated Cys1 is located at the N-terminus. Some residues of Pep-2-NN, such as glycine, asparagine, leucine, and cysteine, are repeated and positioned at different sites within the sequence, resulting in overlapping resonance signals.

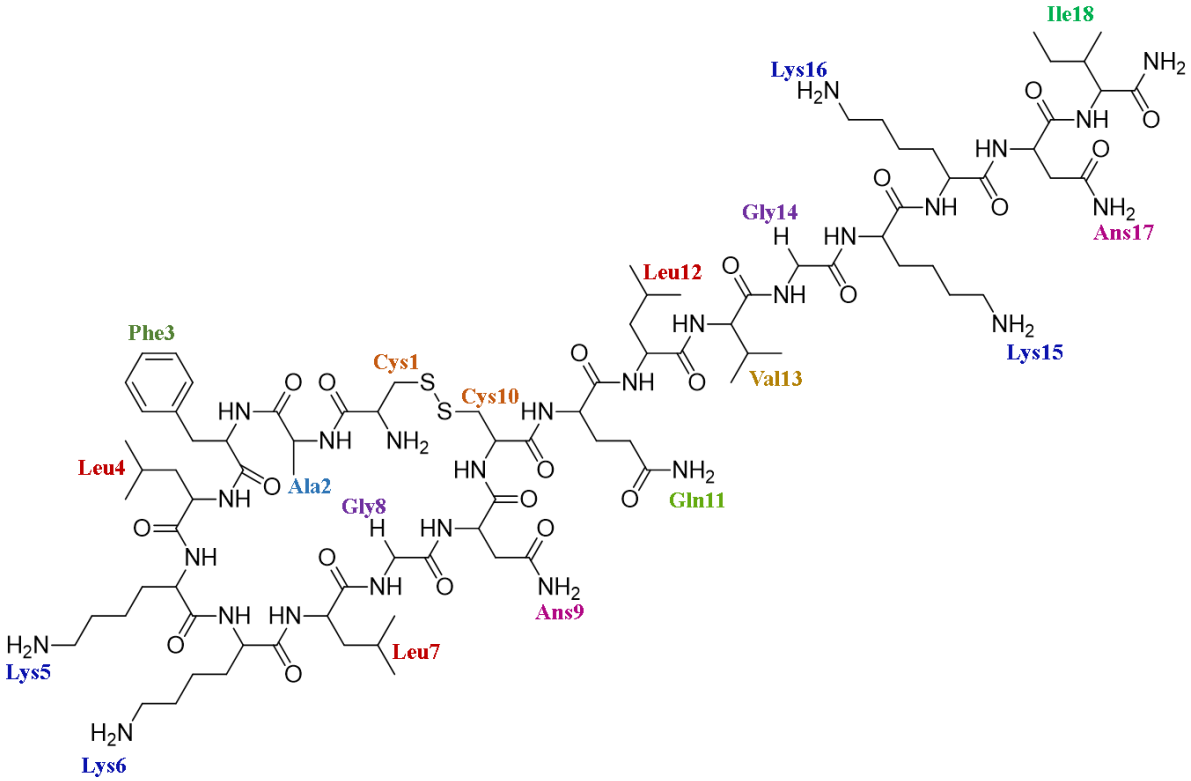

Figure 6.8: The molecular structure of Pep-2-NN

1D NMR spectral analysis of Pep-2-NN

A one-dimensional (1D) ^{1}H NMR of Pep-2-NN (dissolved in dimethyl sulfoxide solvent (DMSO-d6)) was obtained and is shown in **Figure 6.9**. The amide protons (NH) appeared downfield between 7.55 ppm and 8.40 ppm in the chemical shift (δ) scale recorded in parts per million (ppm). The alpha-carbon protons (αH) resonance signals appeared between 3.65

ppm – 4.55 ppm. The amide and alpha protons play a vital role in residue assignment, and they form the NH-αH fingerprint region on the 2D COSY and TOCSY experiments, which show spin systems unique to each amino acid. The aliphatic region, including β- (beta), γ- (gamma), and δ- (sigma) protons appeared upfield between 1.16 – 3.11 ppm. The carbon (^{13}C) NMR is presented in the supplementary information.

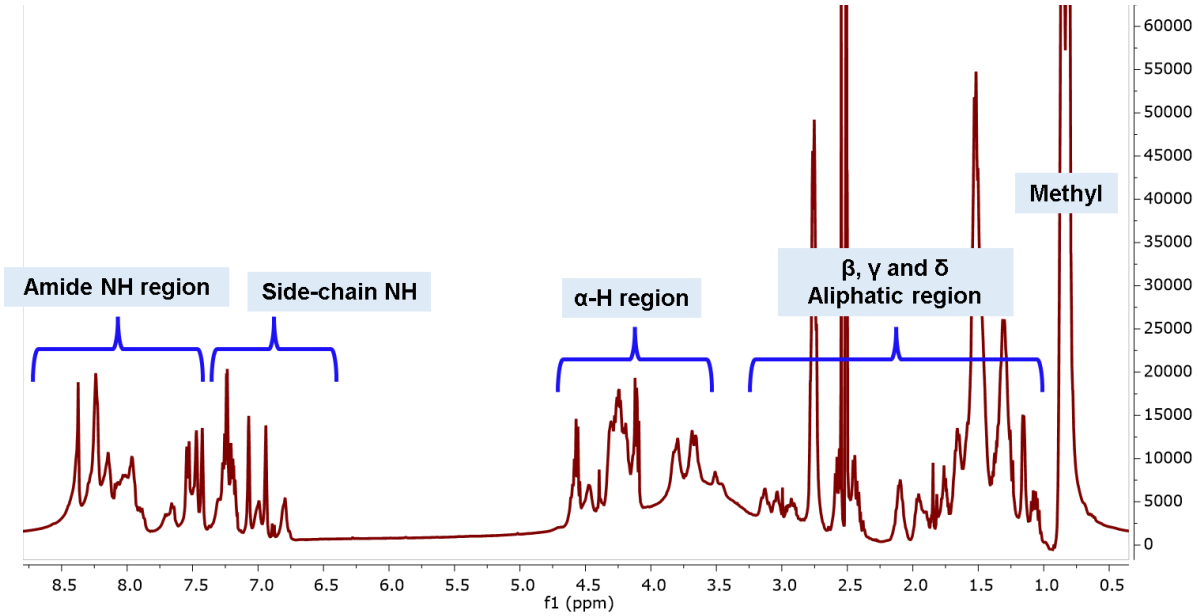

Figure 6.9: ^{1}H NMR spectrum of Pep-2-NN

The amino acid residues of Pep-2-NN were assigned by examining the correlation spectroscopy (COSY), total correlation spectroscopy (TOCSY), and the Rotating Frame Overhauser Enhancement Spectroscopy (ROESY) experiments.

6.3.3.1. Residue assignment of Pep-2-NN using COSY, TOCSY, HSQC and HMBC

The TOCSY fingerprint region for Pep-2-NN is shown in **Figure 6.10**, and the assignments are presented in **Table 6.2**. The COSY spectrum is presented in the supplementary section.

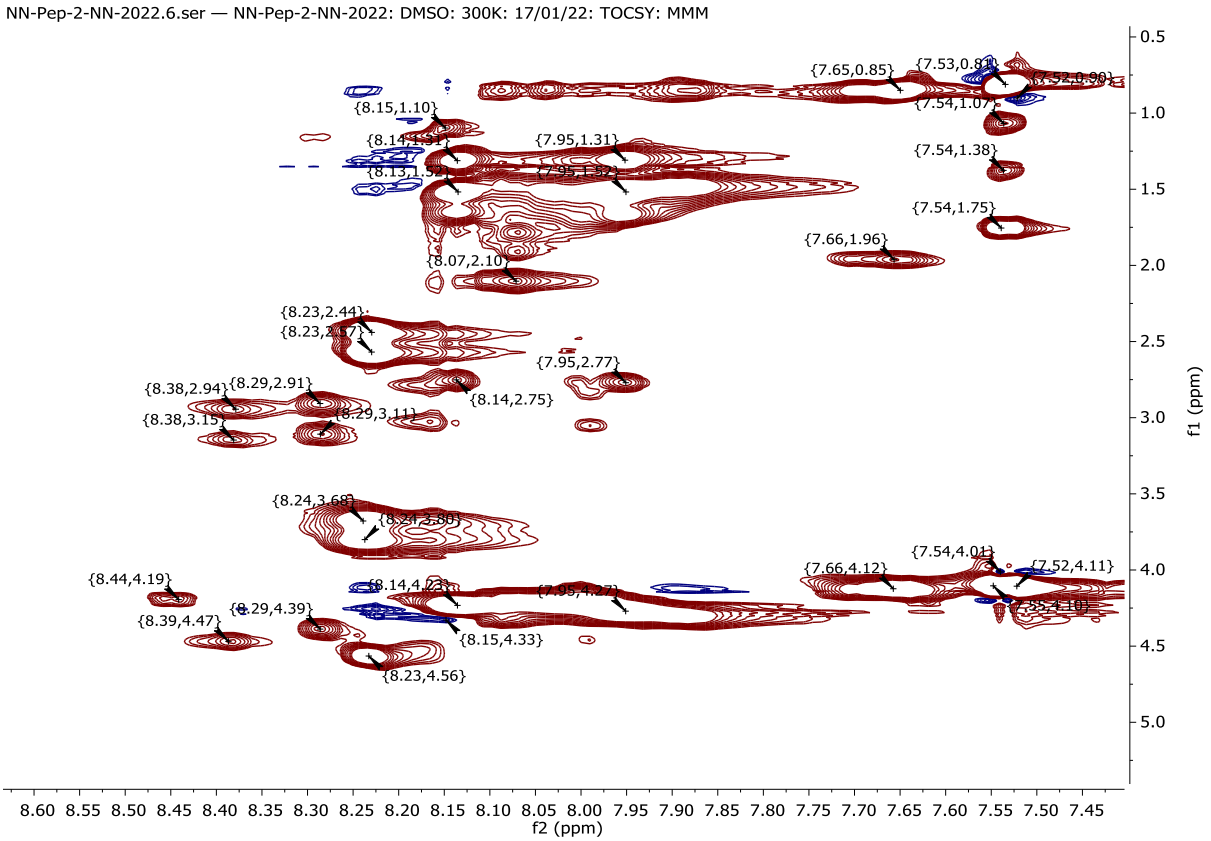

Figure 6.10: TOCSY fingerprint region of Pep-2-NN between 7.50 ppm – 8.40 ppm

Glycine contains an AX spin system[10] comprising the amide proton (NH) and the alpha protons (Hα1 and Hα2) only and has no sidechain. Glycine was one of the least challenging residues to assign in the peptide. The sequence of Pep-2-NN contains two glycine residues, namely, Gly8 and Gly14. The COSY spectrum showed a correlation between the amide proton (NH) at a chemical shift of δ = 8.25 ppm and alpha-protons (αH1 and αH2) at 3.67 ppm and 3.80 ppm, and these were in close proximity with another glycine spin system with NH = 8.21 ppm, αH1 = 3.68 ppm and αH2 = 3.81 ppm. A sequential walk on the ROESY spectrum, discussed in the next section, revealed that the first spin system (NH=8.25) belongs to Gly14 (ROESY correlation to Lys15/16) while the second spin (NH=8.21) belongs to Gly8. The TOCSY spectrum also clearly shows the spin pattern of the glycine residues. The Heteronuclear Single Quantum Coherence Spectroscopy (HSQC) experiment was used to establish the connection between directly bound proton and carbon molecules by correlating ^{1}H and ^{13}C NMR chemical shifts and was used to assign the alpha-carbon (Cα) bonded to αH and the results are presented in **Table 6.2**. The [^{1}H, ^{13}C] HSQC clearly shows that both

glycine α-protons are connected to a carbon signal resonating at 42.30 ppm (Cα), although they are overlapping.

The amide proton of alanine was found to resonate at a chemical shift of 8.44 ppm which was found to correlate with an αH signal at 4.18 ppm on the COSY spectrum. The αH correlated to a signal resonating at 1.16 ppm, which was determined to be the βH belonging to the methyl group of the sidechain of alanine. The unique spin pattern of alanine was also confirmed and established by the TOCSY.

Valine, leucine, and isoleucine amino acid residues contain sidechains of branched saturated hydrocarbons of varying lengths without the presence of functional groups. Valine (Val13) contains the simplest and shorter chain length that consists of an amide proton resonating at 7.65 ppm with the αH, βH, and γ(H1, H2) resonating at 4.12 ppm, 1.97 ppm, and 0.85 ppm, respectively as determined using COSY and TOCSY spectra. The gamma-protons of the methyl groups of valine were overlapping. The alpha-carbon of valine was determined with HSQC, which showed the correlation between the αH and αC at (4.12, 57.51) ppm. Valine beta-carbon was also determined at (1.97, 30.98) ppm. Isoleucine (Ile18) contains unique chemical environments of the three residues, including an amide proton resonating at 7.55 ppm, αH at 4.10 ppm, βH at 1.75 ppm, γH at 1.38 ppm, δH at 1.07 ppm and εH at 0.81 ppm which were determined using the COSY spectrum and validated by the TOCSY spectrum. The αC of Ile18 resonated at 51.57 ppm, as determined using the HSQC.

The peptide sequence contains three leucine residues at different positions, namely, Leu4, Leu7, and Leu12. The leucine spin systems were one of the most challenging residues to characterize using a combination of COSY, TOCSY, and ROESY. The signals of the amide protons of the leucine residues were in close range because they are similar in structure, although they are at different positions in the peptide sequence. The NH-αH-δH or (NH, αH, βH) correlation peaks of leucine were assigned at the chemical shift of (7.89, 4.30, 1.47) ppm for Leu12, (8.09, 4.20, 1.48) ppm for Leu7 and (8.03, 4.22, 1.51) ppm. The spin system of Leu12 displayed a correlation between the βH and δH, which appeared at a chemical shift of 0.86 ppm. The ROESY was used to determine the position of each leucine residue by its connection to their immediate neighbouring residues. Furthermore, the alpha-carbon of Leu12 Cα was assigned to the chemical shift of 51.66 ppm using the HSQC spectrum.

Asparagine, cysteine, and phenylalanine have a similar AMX spin system consisting of three resonance signals arising from the αH, βH1 and βH2 in addition to the amide protons.[10] Pep-

2-NN contains two asparagine (Asn 17 and Asn 9) and two cysteine (Cys10 and Cys1) residues whose positions in the peptide sequence were determined by the ROESY experiment due to the neighbouring (adjacent) amino acids.

Since Phe3 contains a phenyl ring, the Heteronuclear Multiple Bond Correlation (HMBC) experiment was used to determine the protons that showed a correlation to aromatic carbons. The aromatic carbon atoms usually appear between 110 – 170 ppm in the ^{13}C spectrum, while the aromatic protons appear around 6 – 9 ppm. Several protons appeared to be correlated with aromatic carbon molecules in the HMBC spectrum, including resonance signals at 7.20 ppm, 7.18, and 6.88 ppm correlating to 126.3 ppm, 129.5 ppm, and 132.5 ppm, respectively, which were assigned to the aromatic carbons (ArCs) of Phe3. Furthermore, 129.5 ppm (ArC) correlated to signals at 3.11 ppm and 2.90 ppm, which were assigned to the βH1 and βH2 of Phe3. Also, the αH of Phe3 (4.38 ppm) was correlated to 157.1 ppm (ArC), which correlated with 7.20 ppm. The HSCQ spectrum clearly shows the connection between 6.88 ppm and 114.9 ppm (ArC). Thus the chemical environment of Phe3 was established. The COSY and TOCSY spectra showed a correlation between 6.88 ppm and 7.18 ppm. A correlation between the aromatic ring protons (AA'XX'M spin pattern system) and the NH, αH, and βHs (AMX spin system) cannot be established with COSY and TOCSY, and thus the ROESY experiment was used. The ROESY spectrum showed a clear correlation between 7.20 ppm to 4.38 ppm (αH), 2.90 ppm (βH1), and 3.11 (βH2).

The NH-αH-β(H1&H2) spin patterns of Cys1 and Cys10 were assigned using TOCSY. The signals resonating at 7.99 ppm (NH), 4.46 ppm (αH), 3.05 ppm (βH1), and 2.84 ppm (βH2) were assigned to Cys1 while 8.39 ppm (NH), 4.47 ppm (αH), 3.14 ppm (βH1) and 2.94 ppm (βH2) were assigned to Cys10. The COSY spectrum was also used to determine the resonance signal correlations. The alpha-protons of Cys1 and Cys10 are very close and were correlated to an αC appearing at δ = 50.10 ppm with the HSQC spectrum. The position of each cysteine was determined with the ROESY sequential walk, which revealed the residue's neighbouring amino acids.

The NH-αH spin systems for Asn17 and Asn 9 appeared at (8.24, 4.56) ppm and (8.23, 4.59) ppm, respectively. The beta-protons for Asn17 were assigned to 2.44 ppm (βH1) and 2.57 ppm (βH2), while those of Asn9 appeared at the chemical shifts of 2.46ppm (βH1) and 2.58 ppm(βH2). Their positions were assigned using the ROESY sequential walk described below. The Gln11 protons appeared at 8.07 ppm (NH), 4.19 ppm (αH), 1.91 ppm (βH1), 1.79 ppm

(βH2), and 2.10 ppm (γH). The αC of Gln 11 was assigned at 49.32 ppm. Pep-2-NN contains four lysine residues in its sequence, and overlapping signals were observed for Lys5/6 and Lys15/16. The NH-αH-βH1-βH2-γH-δH spin patterns of Lys15/16 and Lys5/6 were assigned at (7.95, 4.25, 1.52, 1.66, 1.31, 2.77) ppm and (8.13, 4.23, 1.64, 1.52, 1.31, 2.75) ppm, respectively.

Table 6.2: NMR chemical shifts (ppm) for amino acid residues in Pep-2-NN obtained from TOCSY NMR and ROESY assignment showing through-space correlation between residues in Pep-2-NN

Residue number	Known Residue	NH	αH	αC	βH	γH	δH	εH	COSY	ROESY correlation/ Residue	Long range/ Correlation residue
18	**Ile**	7.55	4.10	51.57	1.75	1.38	1.07	0.81	(7.55, 4.10) (4.10, 1.75) (1.75, 1.38) (1.38, 1.07) (1.07, 0.81	**Asn17** (7.55. 8.24), (7.55, 4.56), (7.55, 2.44), (7.55, 2.57), (8.24, 0.85), (7.47, 2.57), (7.47, 2.44)	**Lys5/6** (2.75, 1.07), (7.42, 1.75), (4.10, 7.42), (4.10, 7.07), (4.10, 1.75)
17	**Asn**	8.24	4.56		2.44, 2.57	7.47 6.94			(7.47, 6.94) (8.24, 4.56) (2.56, 2.44) (2.56, 2.57)	**Ile18, Lys16** (8.24, 4.25) (4.56, 2.77) (4.56, 1.52)	
16/15	**Lys**	7.95	4.25		1.52, 1.66	1.31	2.77	7.42 7.07	(7.95, 4.27) (4.25, 1.66) (4.25, 1.52) (1.52, 1.31) (7.42, 7.07)	**Asn17 Gly14** (7.95, 3.80) (7.95, 3.67)	**Cys1**(3.05, 2.77) **Cys10** (2.77, 8.39), (2.77, 4.47) **Ala2**(1.16 with 2.77) **Phe3**(1.52 with 2.90)
14	**Gly**	8.25	3.67, 3.80	42.30					(8.25, 3.67) (8.25, 3.80)	**Lys15/16 Val13** (8.25, 4.12)	
13	**Val**	7.65	4.12	57.51	1.97	0.85			(7.65, 4.12) (4.12, 1.97) (1.97, 0.85)	**Gly14 Lue12** (7.65, 4.30)	**Phe3**(7.65, 4.12) (0.85, 7.20) **Lys5/6**(7.42, 7.07) **Lys5/6**(8.24, 7.65) **Cys10**(8.39, 7.65), (4.47, 0.85)
12	**Leu**	7.89	4.30	51.66	1.47	0.86			(7.89, 4.30)	**Val13 Gln11** (7.89,4.19)	
11	**Gln**	8.07	4.19	49.32	1.78, 1.91	2.10	7.27 6.79		(7.27, 6.79)	**Leu14 Cys10** (8.07, 4.47)	**Lys15/16**(2.78, 1.78) **Leu7**(4.20, 1.91), (4.20, 2.10), (4.20, 1.16)
10	**Cys**	8.39	4.47	50.10	2.94, 3.14				(8.39, 4.47)	**Gln11 Asn9** (8.23, 4.59)	**Leu12** (7.89) **Lys15/16**(7.95 with 8.39)

Residue number	Known Residue	NH	αH	αC	βH	γH	δH	εH	COSY	ROESY correlation/ Residue	Long range/ Correlation residue
									(4.47, 2.94) (4.47, 3.14)	**Cys10**(3.14, 3.05), (3.05, 2.94)	**Val13**(4.47, 4.12), (4.47, 0.84), (4.47, 0.85)
9	**Asn**	8.23	4.59		2.46, 2.58	7.47 6.94			(4.59, 2.46) (7.47, 6.94)	**Cys10**	**Lys15/16**(4.59, 4.25) **Lys5/6**(8.23, 1.65)
8	**Gly**	8.21	3.68, 3.81	42.30					(8.21, 3.68) (8.21, 3.81)	**Overlap**	
7	**Leu**	8.09	4.20		1.48				(8.09, 4.20)	**Lys5/6**(4.20, 2.75)	**Gln11**(4.20, 1.91), (4.20, 2.10), (4.20, 1.16)
5/6	**Lys**	8.13	4.23		1.64, 1.52	1.31	2.75	7.42 7.07	(7.42, 7.07)	**Leu7** **Leu4**(8.03, 4.23)	**Val13** (1.97) with 2.75 **Asn9**(8.23 with 1.64) 8.13 with 7.95 2.75, 4.11
4	**Leu**	8.03	4.22	53.22	1.51				(4.22, 1.51)	**Lys5/6** **Phe3**(8.03, 4.38), (4.38, 1.51)	**Ile18**(4.30, 0.81) **Lys15/16**(1.51, 1.66)
3	**Phe**	8.29	4.38	55.17	2.90, 3.11	7.20	6.88 7.18		(4.38, 2.90) (7.18, 6.88)	**Leu4** **Ala2**(8.29, 1.16) (7.20, 1.16), (7.18, 4.18)	**Val13**(7.66, 4.12), (0.85, 7.20) **Lys15/16**(6.88, 7.07), (1.52, 2.90)
2	**Ala**	8.44	4.18	49.32	1.16				(8.44, 4.18) (4.18, 1.16)	**Phe3**	**Lys16/15**(4.18, 4.25)
1	**Cys**	7.99	4.46	50.10	2.84, 3.05				(7.99, 4.46) (4.46, 2.96)	**Cys10**(3.14, 3.05) (3.05, 2.94)	**Lys15/16**(3.04, 2.76)

6.3.3.2. ROESY sequential walk of Pep-2-NN

A ROESY sequential walk is used to determine the correlations between neighbouring amino acids in a peptide. The connection of amino acid residues in the Pep-2-NN peptide sequence was determined using a ROESY spectrum. NOE sequential walk can be performed by moving from the NH-αH spin system of the first residue (i) to the αH of the second residue (i+1) to give (NH(i), αH(i+1) correlation in the spectrum.

A ROESY sequential walk was successfully performed on the amino acids of the tail sequence, from Ile18 through to Gly8 of the ring portion in the sequence (i.e., Ile18-Asn17-Lys16-Lys15-Gly14-Val13-Leu12-Gln11-Cys10-Asn9-Gly8) as shown in **Figure 6.11**. Ile18 correlated with all the protons of the neighbouring Asn17 residue, including the γNH_2 proton signals at 7.42 ppm and 7.07 ppm. Asn17 was connected to Lys16/15 because of the correlations observed between the asparagine amide proton NH at 4.56 ppm with lysine βH (1.52 ppm) and δH (2.77 ppm) protons. The amide proton of Lys16/15 (7.95 ppm) correlated to the Gly14 αH1 at 3.67 ppm and αH2 at 3.80 ppm. Gly14 was connected to the αH of Val13 due to a correlation signal observed between 8.25 ppm and 4.12 ppm. Valine also correlated with Leu12 at (7.65, 4.30) ppm. This process was repeated until Cys10/Asn9 were connected in the cyclic ring. Gly8 is the next residue from Asn9, however, the connection to Leu7 was lost due to signal overlap with Gly14.

Inside the peptide ring, the sequence Leu7-Lys5/6-Leu4-Phe3-Ala2 was elucidated with the ROESY experiment. The αH of Leu showed a correlation to the δH of Lys5/6 (4.20, 2.75) ppm. Amide proton of lysine (8.03 ppm) correlated with 4.23 ppm belonging to the αH of Leu4. The αH of Phe3 (4.38 ppm) showed a correlation to the amide proton of Leu4 (NH = 8.03 ppm), and the amide proton of phenylalanine correlated to βH (1.16 ppm) of Ala2. Unfortunately, a correlation peak between Ala2 and Cys1 was not found. However, the mass spectrometry results reveal that the full peptide was synthesized. Therefore, the absence of the Ala2/Cys1 signal may be due to poor resolution of the ROESY spectrum and overlapping signals.

In order to prove that the peptide was cyclized, Cys1 and Cys10 protons should show a correlation to each other through-space using an NOE experiment such as ROESY, proving that the amino acids are in proximity. The ROESY spectrum shows that the βH of Cys1 (δ =

3.05 ppm) is correlated with βH1 (3.14 ppm) and βH2 (2.94 ppm) of Cys10 suggesting that the residues are in close range and that the peptide is cyclised.

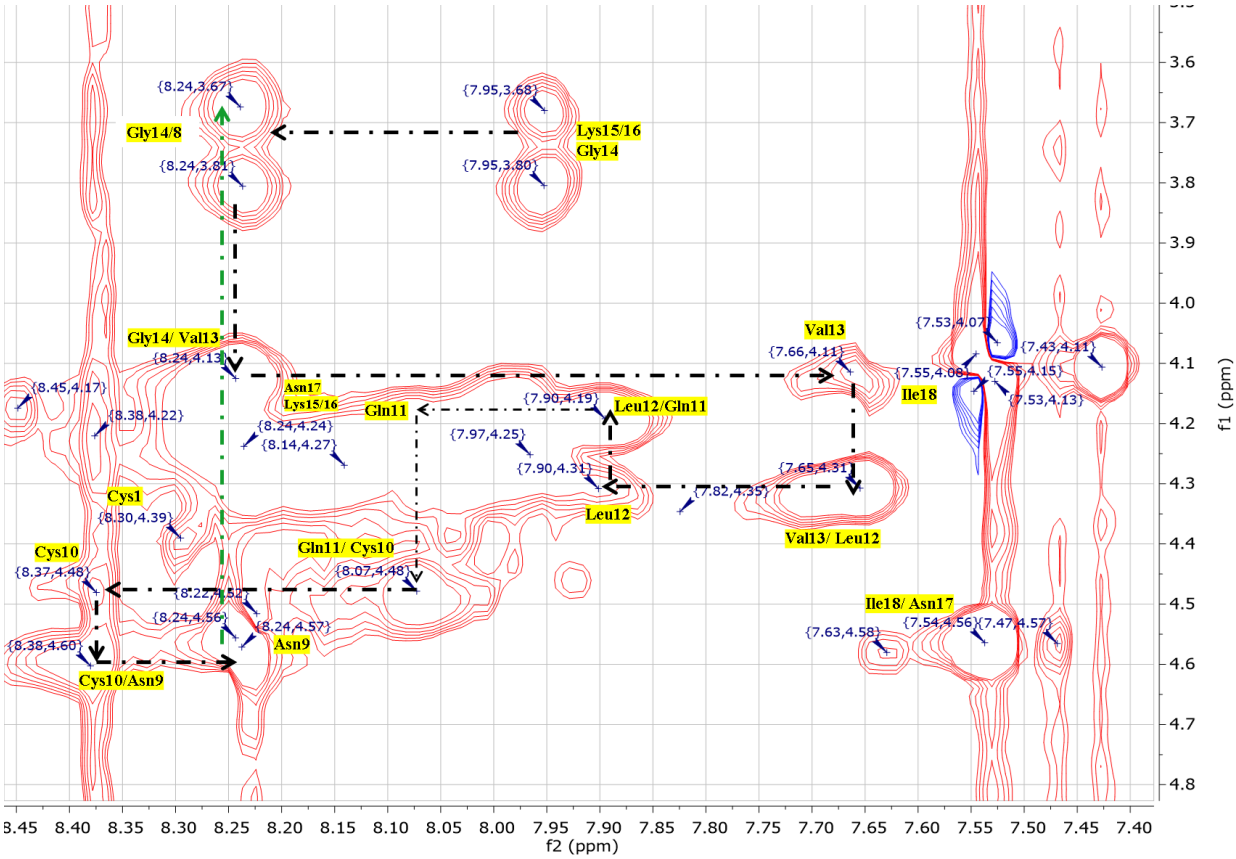

Figure 6.11: A ROESY sequential walk of Pep-2-NN showing the connection of the amino acid residues in the INKKGVLQCNG portion of the sequence in the chemical shift region of 7.40 – 8.50 ppm.

6.3.3.3. Long-range ROESY correlations

Since the peptide has been shown to be cyclic, the next step was to investigate if it has a threaded (knotted) conformation by determining long-range ROESY correlations and thus elucidating the structure of Pep-2-NN. Long-range correlations show that residues of the tail portion, including I*KK*VL* (where the asteric represents missing residues in the tail sequence of the peptide), are in proximity to the residues in the cyclic ring. C-terminal Ile18 correlated with Lys6/5 and Leu4 and Lys16/15 showed correlations with Ala2, Phe3, Cys10 and Cys1. Furthermore, Val13 and Leu12 showed correlations with Cys10 and Cys1. The alpha-proton of Ile18 (4.10 ppm) correlated with signals at 7.42 ppm (εH1) and 7.07 ppm (εH2) that belong to the lysine sidechain NH_2. Due to overlapping signals, whether Ile18 interacts with lysine at position 6 or 5 in the cyclic ring cannot be specified. Most of the tail

residues that can interact with the cyclic ring amino acids are located mostly on the left side of the ring, considering the structure of Pep-2-NN as presented in **Figure 6.12**.

All the long-range ROESY correlation peaks for Pep-2-NN are recorded in **Table 6.2**. Cys10 correlated with the amide protons of Val13 (7.65 ppm) and Leu12 (7.89 ppm). From the information discussed thus far, it is possible that the tail could be tightly packed around the left side of the cyclic ring. However, the correlation between Gln11/Gly14 suggests that these residues are in proximity, and thus the peptide may have formed a bight (knot or loop) encasing Val13 and Leu12, and the tail might not be tightly packed around the ring but threaded inside. The proposed Pep-2-NN structure is illustrated in **Figure 6.12**.

ROESY correlation between Lys15/16 and Leu4, Phe3, and Ala2 may suggest that the sidechain of the residues may act as 'steric plugs' that interact with lysine to hold the tail inside the ring to prevent unthreading. The ROESY also showed a correlation between Gln11 and Lys16/15; thus, glutamine may also contribute to holding the tail in place and inside the ring. Lastly, the interaction between Cys10 with Val13 and Leu12 may suggest that the loop region is slightly leaning towards the left side of the cyclic ring, illustrated by the blue arrow in **Figure 6.12**.

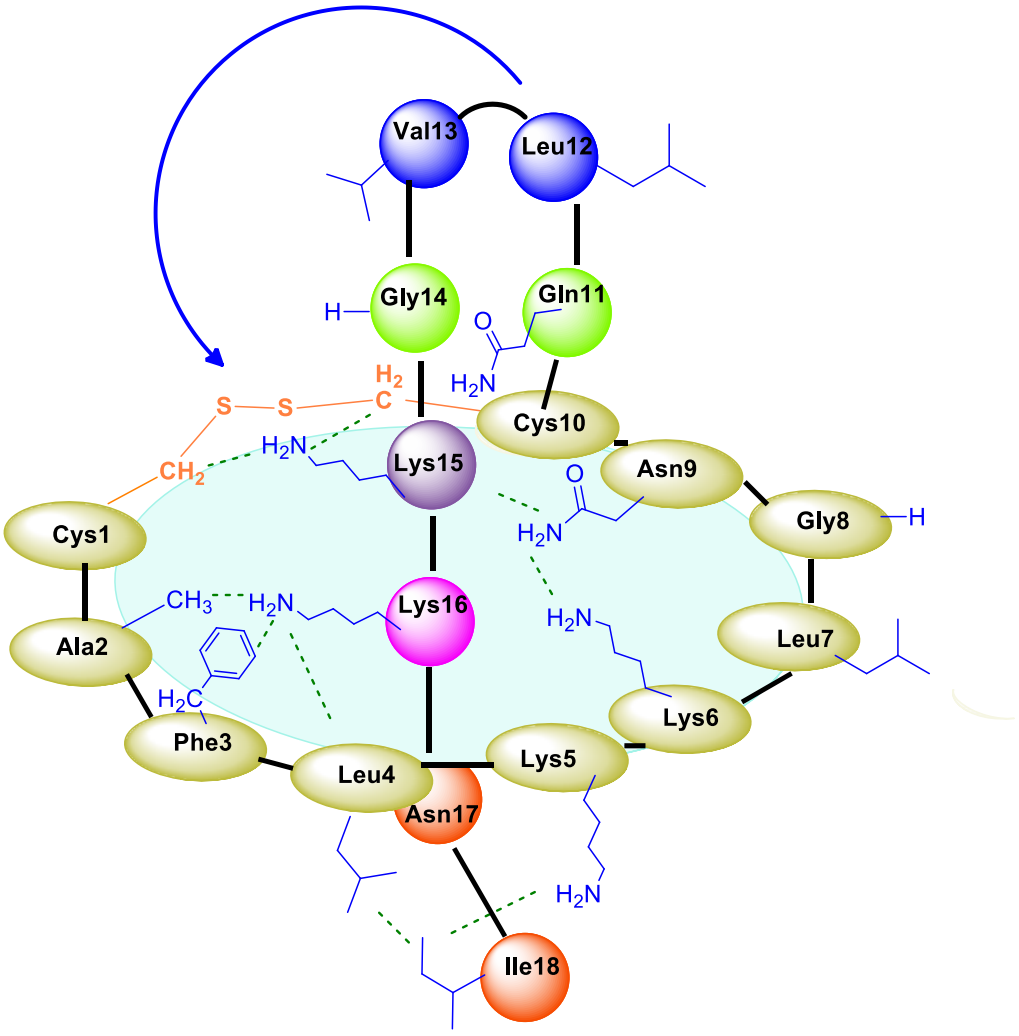

Figure 6.12: The structure of Pep-2-NN as determined by NMR analysis using sequential and long-range [1H, 1H] ROESY, residue assignment with ^{1}H COSY, [^{1}H, ^{1}H] TOCSY, [^{1}H, ^{13}C] HSQC and [^{1}H, ^{1}H] HMBC spectra. Green dotted lines represent through-space interaction between residues. The blue arrow represents the leaning direction of the loop towards the left side of the cyclic ring. The light blue disc represents the plane of the peptide ring in order to distinguish residues below and above the ring.

[^{1}H, ^{1}H] COSY, [^{1}H, ^{1}H] TOCSY, [^{1}H, ^{13}C] HSQC, [^{1}H, ^{1}H] HMBC and [^{1}H, ^{1}H] ROESY spectra are shown as supplementary information in the appendices section.

6.4. Conclusion

The circular dichroism studies revealed that most of the analysed lassomycin derivatives, including Pep-2-NN, are stabilized by antiparallel beta-sheets, which could be attributed to the cyclic ring formed through disulfide bonds. The computational studies also showed that the disulfide bond stabilizes Pep-2-NN and Pep-2-NNA. Ring-2-NNA, which does not have the tail portion of Pep-2-NN, exists mostly in an alpha-helical conformation followed by antiparallel beta sheets. The highly basic Pep-Lys-NN showed a presence of a beta-turn motif which is absent in the other peptides.

Although the Ramachandran plots predicted that the Pep-2-NN and Pep-2-NNA peptides mostly consisted of an α-helical structure, the circular dichroism studies showed that almost 50% structure of Pep-2-NN was comprised of the α-helix conformation. The Ramachandran plot also revealed that there was a minimal presence of β-sheets in the peptides, which were revealed by CD studies to be in a rather higher proportion of up to 56%. The computational studies also predicted the formation of loop secondary structures extending from Leu7 to Leu12 in Pep-2-NN and Asp9 to Cys10 in Pep-2-NNA.

The computational studies revealed that the disulfide bridge length was within an acceptable range for Pep-2-NN and Pep-2-NNA, thus proving to be a successful alternative to the rather challenging lactam bridge found in the original parent peptide sequence.

While the computational studies revealed that there was a possible interaction between Ile18 of the tail and Phe3 of the cyclic ring, NMR showed that Ile18 rather interacted with Lys5 and possibly Lys6, which are also part of the ring and not far from Phe3. Therefore, this shows that the C-terminus of the peptide sequence is in close approximation to the ring as opposed to away from the ring and one of the conformations that can allow such an interaction is a knotted (threaded) structure. The possibility that the tail portion is tightly packed around the ring is disputed by the interaction of Gly14 and Gln11, which suggest that a loop was formed that allows the tail to thread inside the ring.

The NMR study suggests a knotted threaded conformation where the tail passes through the ring and is stabilized by the sidechain of Phe3 and Ala, which acts as ‘plugs’ to hold the tail in place. Lysine residues in the ring also interacted with Ile, which may also stabilise the tail.

In the future, an NMR instrument with a higher resolution and longer experiment times will be used to improve the quality of the spectra and alleviate signal overlapping.

References

1. Gomathi, L.; Subramanian, S., Elucidation of secondary structures of peptides using high resolution NMR. *Current Science* **1996**, 553-567.

2. Hwang, T.-L.; Batabyal, D.; Knutson, N.; Wikström, M., Use of the 2D 1H-13C HSQC NMR methyl region to evaluate the higher order structural integrity of biopharmaceuticals. *Molecules* **2021,** *26* (9), 2714.

3. Raghothama, S., NMR of peptides. *Journal of the Indian Institute of Science* **2010,** *90* (1), 145-161.

4. Xie, X.; Marahiel, M. A., NMR as an effective tool for the structure determination of lasso peptides. *ChemBioChem* **2012,** *13* (5), 621-625.

5. Spencer, R. K.; Nowick, J. S., A newcomer′ s guide to peptide crystallography. *Israel Journal of Chemistry* **2015,** *55* (6-7), 698-710.

6. Jeannerat, D.; Furrer, J., NMR experiments for the analysis of mixtures: beyond 1D 1H spectra. *Combinatorial Chemistry & High Throughput Screening* **2012,** *15* (1), 15-35.

7. Micsonai, A.; Moussong, E.; Wien, F.; Boros, E.; Vadászi, H.; Murvai, N.; Lee, Y.-H.; Molnár, T.; Réfrégiers, M.; Goto, Y., BeStSel: webserver for secondary structure and fold prediction for protein CD spectroscopy. *Nucleic Acids Research* **2022,** *50* (W1), W90-W98.

8. Lee, T.-S.; Cerutti, D. S.; Mermelstein, D.; Lin, C.; LeGrand, S.; Giese, T. J.; Roitberg, A.; Case, D. A.; Walker, R. C.; York, D. M., GPU-accelerated molecular dynamics and free energy methods in Amber18: performance enhancements and new features. *Journal of Chemical Information and Modeling* **2018,** *58* (10), 2043-2050.

9. van der Wel, P. C., Dihedral Angle Measurements for Structure Determination by Biomolecular Solid-State NMR Spectroscopy. *Frontiers in Molecular Biosciences* **2021,** *8*, 791090.

10. B Hughes, A., Amino Acids. Peptides and Proteins in Organic Chemistry. *Volume 5. Analysis and Function of Amino Acids and Peptides*. Wiley-VCH Verlag & Co. KGaA: 2012.

Chapter 7

Conclusion and future work

The project aimed to design and synthesize lassomycin derivatives targeting the *Mycobacterium tuberculosis* (*Mtb*) caseinolytic protease enzyme.

Pep-2-NN and Pep-2-NNA are lassomycin derivatives that demonstrated activity against *Mtb,* with the former possessing potency that is similar to that of ethambutol with a Minimum Inhibitory Concentration (MIC) of 9.87 μg/mL after 7 days of incubation. Furthermore, a dose-response cytotoxicity study against Human T cells (MT4 cells) showed that at the MIC concentration of Pep-2-NN, over 50% of cells were still viable. The cationic lassomycin derivative, Pep-Lys-NN, was able to only target and kill *Bacillus subtilitis* (*B. subtilitis*) in a study that featured a small pool of bacterial pathogens, including *Escherichia coli*, *Pseudomonas aeruginosa,* and *Staphylococcus aureus*. This was because *B. subtilitis* shares a similar caseinolytic protease to that of *Mycobacterium tuberculosis*. Thus, the lassomycin derivatives demonstrate the ability to selectively target microbes that possess the caseinolytic protease similar to that of the *mycobacterium*. Due to the obtained results, it can be concluded that certain common modifications, such as the replacement of the macrolactam bond with a disulfide bond and the amidation of the C-terminus can be performed on the lassomycin derivatives without negatively impacting their function and activity.

The next step involved the conjugation of the lassomycin derivatives to lipophilic molecules in order to improve cell membrane permeability and thus improve potency. Pep-1-NNA, Pep-2-NNA, and their linear analogues missing the cysteine residues and the disulfide bond were successfully conjugated to palmitic acid and 1-adamantane carboxylic acid lipophilic molecules. Adding these lipophilic molecules increased their hydrophobicity, which was monitored and analysed using liquid chromatography-mass spectrometry (LCMS). The study also revealed that the palmitic conjugated Pep-2-NNA was the most hydrophobic derivative, deduced from the higher retention time during LCMS analysis. Peptide hydrophobicity plays an important role during the peptide's interaction with the lipid-rich bacterial cell envelope. Although the peptide derivatives were successfully conjugated to the lipophilic molecules, their synthesis and purification were challenging due to their longer sequences that resulted in

poor yields and purity. Pep-1-NNA and Pep-2-NNA are relatively larger peptides that consist of 18 amino acid residues, and their purification led to co-elution with impurities during HPLC purification. Hence the action to design derivatives with shorter sequence lengths was undertaken. This led to the exploration and synthesis of shorter-chained peptide derivatives, including Ring-2-NN and Ring-2-NNA derived from the cyclic ring sequences of Pep-2-NN and Pep-2-NNA, respectively. Tail-2-NN was also synthesized and was derived from the tail sequences of Pep-2-NN and Pep-2-NNA, which are similar. Adamantane and palmitic acid were also coupled to the shorter-chain peptides to study the effect of decreasing the peptide chain length while increasing lipophilicity. These peptides were successfully synthesized and purified using preparative High-Performance Liquid Chromatography (HPLC). Although the synthesis was less challenging with a shorter synthetic time due to reduced chain lengths, challenges were also observed during HPLC purification, to a smaller extent when compared to longer-chained derivatives.

Lassomycin is known to target the caseinolytic enzyme (ClpC1) of *Mtb*; however, a caseinolytic protease (ClpP1P2 or ClpP) Assay was performed on selected lassomycin derivatives in order to study their interaction with the protease. The Assay study revealed that all the peptides, namely, Tail-2-NN, Pep-2-NN, Compound X, and Ring-2-NNA-Ada (Ring-2-NNA that is coupled to adamantane), except for Ring-2-NN, possessed an inhibiting effect against the protease activity. Compound X possessed the highest inhibitory effect against ClpP. However, Compound X is an impurity that is usually obtained during the synthesis and purification of Pep-2-NN and its amino acid composition is not yet determined. Interestingly, Ring-2-NN had an activating effect that increased proteolytic activity. Since all the peptides that showed the inhibitory effect have a tail sequence or tail-like moiety (in the case of Ring-2-NNA-Ada), this may suggest that a tail-like structure may be required in order to cause the inhibitory effect. The information obtained from the protease study may suggest that the peptide derivatives can be successfully shortened without compromising their activity. Furthermore, the peptides' tail and ring portion may play a role in the overall peptide activity. In the future, Nuclear Magnetic Resonance studies (NMR) will be utilized to determine the structure of Compound X. In addition, more short-chained derivatives, including those conjugated to lipophilic groups, will be studied against the protease. Lastly, the activating action of Ring-2-NN will be explored further as another possible mode of action of lassomycin and its derivatives.

Silver nanoparticles (AgNPs) were successfully synthesized using silver nitrate as a source of silver ions, sodium borohydride as a reducing agent, and trisodium citrate as a capping and stabilizing agent. The formation of the AgNPs was monitored by a colour change and ultraviolet-visible (UV-vis) spectrophotometry and analysed using Transmission Electron Microscopy (TEM) imaging to determine their size and shape. The absorption band for the nanoparticles was obtained along the acceptable range of 400 nm. TEM imaging revealed that the nanoparticles had a spherical morphology, and the size of the nanoparticles was between the range of 7 ± 2 nm and 9 ± 2 nm. Pep-2-NN was successfully conjugated to the silver nanoparticles and maintained the spherical morphology; however, there was evidence of aggregation which resulted in a slight increase of the particle size to 9 ± 2 nm and 12 ± 3 nm. The UV-Vis also showed a red shift of the absorption band for the peptide-NPs conjugates. In order to reduce agglomeration, a dilute concentration of the peptides will be investigated in the future, and a linker between the silver and the peptide will be introduced. Also, the conjugates will be examined for antimicrobial activity.

The secondary structure of the peptides was determined using circular dichroism (CD) spectroscopy which revealed that the derivatives are mostly stabilized by anti-parallel beta sheets as observed for Pep-2-NN and Pep-Lys-NN, followed by the alpha-helix and a beta-turn to a lesser extent. Ring-2-NN had a higher proportion of alpha-helix (58.8%), followed by anti-parallel beta sheets. In the future, more lassomycin derivatives will be subjected to CD studies, and various buffer systems will be employed to study their secondary structures.

Structure elucidation of Pep-2-NN was determined using two-dimensional (2-D) NMR, which could show a possible lasso conformation. The COSY and TOCSY experiments were utilized for residue assignments with the assistance of HSQC, ROESY, and HMBC experiments. A ROESY sequential walk was successfully demonstrated for neighbouring amino acid residues. Long-range ROESY correlations were attributed to a lasso structure and revealed that the tail amino acids were threaded inside the cyclic ring whilst other residues like phenylalanine acted as ‘steric plugs’ to prevent unthreading. Furthermore, computational studies predicted a possible interaction between Phe3 in the ring sequence and the Ile18 of the tail, suggesting a knotted lasso structure. In addition, Ile18 had a long-range ROESY correlation with the lysine residues in the ring, not far from Phe3. In order to confirm the observed interactions, Pep-2NN will be further analysed using an 800 MHz NMR spectrometer at Prof K Petzold’s labs.

In future studies, the interaction (dissociation constant (K_D)) between lassomycin derivatives and the caseinolytic enzyme (ClpC1) will be investigated using Mass Spectrometry (MS). D-amino acids will be incorporated into the peptide sequences to improve protease stability.

Chapter 8

Experimental procedures

8.1. Materials

Reagents and solvents

The reagents used to synthesize the peptides include the rink amide MBHA resin, Fmoc protected amino acids, coupling reagents such as Hexafluorophosphate Azabenzotriazole Tetramethyl Uronium (HATU), Hydroxybenzotriazole (HOBt), OxymaPure and K-Oxyma, which were purchased from DLD Scientific. Diisopropylethylamine (Dipea), piperidine, trifluoroacetic acid (TFA), triisopropylsilane (TIS), formic acid, *N, N'*-Diisopropylcarbodiimide (DIC), thionyl chloride, 1,2-Ethanedithiol (EDT), and acetic acid (AcOH) were purchased from Sigma Aldrich and Pyramid Scientific.

Solvents such as dimethylformamide (DMF), dimethyl sulfoxide (DMSO), diethyl ether, methanol, and acetonitrile were purchased from Sigma Aldrich, Radchem, and Pyramid Scientific. Dichloromethane (DCM) was dried upon distillation over calcium hydride.

8.2. Methods

8.2.1. General procedure for peptide synthesis

All the peptides were synthesized via the Fluorenylmethyloxycarbonyl (Fmoc-) solid phase peptide synthesis (SPPS) strategy on the Fmoc-protected rink Amide 4-methylbenzhydrylamine (MBHA) resin as a solid support. Firstly, the rink amide resin was pre-swelled in dimethyl formamide (DMF) for 3 hours before use. The resin was then transferred to a reaction vessel fitted with a fritted resin support and washed twice with DMF/ DCM/DMF, and the solvent was removed by vacuum filtration.

8.2.1.1. Fmoc removal

The resin was treated with a 20% piperidine solution in DMF (v/v) for 2 x 5 min, and the generated waste was removed by filtration under vacuum. The piperidine solution was used to irreversibly cleave the base-labile Fmoc- group and expose the free amino group (NH_2) to allow aminoacylation with incoming amino acid. The resin was then washed with DMF/DCM/DMF to remove contaminants and side products.

8.2.1.2. Attachment of the first amino acid to the resin and peptide elongation

All the amino acids used for the synthesis of peptides are Fmoc protected. The first amino acid (AA_1) attached to the resin depends on the individual peptide sequence and is either cysteine or isoleucine. The amino acid (0.2 M, 0.6 mL) was activated into an active ester by mixing with OxymaPure (0.2 M) and DIC (0.2 M) at a 1:1:1 equivalence. The mixture was then transferred to the reaction vessel containing the resin-linker, coupled twice for 35 min, and washed with DCM (3 X 5 mL) and DMF (3 X 5 mL) in between couplings, and the waste was filtered out using vacuum filtration. The resin-bound amino acid (Fmoc-AA_1-resin) was treated with 20% piperidine and washed with DMF. The second amino acid (AA_2) (0.2 M) in the peptide sequence was mixed with OxymaPure and DIC at a 1:1:1 equivalence and was attached to give Fmoc-AA_1-AA_2-resin. The aminoacylation and Fmoc removal steps were repeated until all the amino acids in the peptide sequence were added. Washings were done in-between steps with DMF (3×5 mL) followed by DCM (3×5 mL). K-Oxyma was sometimes used as a substitution for OxymaPure as they behave similarly.

8.2.1.3. Attachment of lipophilic molecules

Some peptides, including Ring-2-NN, Ring-2-NNA, and Tail-2-NN, were coupled to 1-adamantane carboxylic acid or palmitic acid lipophilic molecules at the C-terminus in order to increase their hydrophobicity character. After the synthesis of each peptide, a mixture of OxymaPure (0.2 M), diisopropyl carbodiimide (0.2 M), and the respective fatty acid (0.2 M), 1-adamantane carboxylic acid or palmitic acid were added twice for 1 hour each time to the newly Fmoc deprotected resin-bound peptide. Washings were done in-between steps with

DMF (3×5 mL) followed by DCM (3×5 mL). All the peptides discussed in this thesis are presented in **Table 8.1** below.

Table 8.1: Peptide derivatives discussed in the thesis with their corresponding sequences. Lysine (K) and arginine (R) residues contribute to the overall basicity of the peptides and are written in violet and blue colours, respectively.

Item no.	Peptide derivative/ Sequence	Item no.	Peptide derivative/ Sequence
1.	**Pep-1-NN** INRRGVLQCNGLRRLFAC	13.	**Ring-2-NN** CNGLKKLFAC
2.	**Pep-1-NNA** INRRGVLQCDAFLRRLGC	14.	**Ring-2-NN-Ada** CNGLKKLFAC- Ada
3.	**Pep-1-NNA-Ada** INRRGVLQCDAFLRRLGC-Ada	15.	**Ring-2-NN-Pal** CNGLKKLFAC- Pal
4.	**Linear Pep-1-NNA-Ada** INRRGVLQDAFLRRLG-Ada	16.	**Ring-2-NNA** CDAFLKKLGC
5.	**Pep-2-NN** INKKGVLQCNGLKKLFAC	17.	**Ring-2-NNA-Ada** CDAFLKKLGC- Ada
6.	**Pep-2-NNA** INKKGVLQCDAFLKKLGC	18.	**Ring-2-NNA-Pal** CDAFLKKLGC- Pal
7.	**Pep-2-NNA-Ada** INKKGVLQC-DAFLKKLGC-Ada	19.	**Pep-Lys-NN** INKKGKKQCNGKKKKFAC
8.	**Linear Pep-2-NNA-Ada** INKKGVLQDAFLKKLG-Ada	20.	**Pep-Lys-NNA** INKKGKKQCDAFKKKKGC
9.	**Pep-2-NNA-Pal** INKKGVLQC-DAFLKKLGC-Pal	21.	**Pep-1-NN-Lys** INRRGKKQCNGKRRKFAC
10.	**Tail-2-NN** INKKGVLQ	22.	**Pep-1-NNA-Lys** INRRGKKQCDAFKRRKGC
11.	**Tail-2-NN-Ada** INKKGVLQ- Ada	23.	**Pep-Ala-NN** INAAGVLQCNGLAALFAC

Item no.	Peptide derivative/ Sequence
12.	**Tail-2-NN-Pal** INKKGVLQ- Pal

Item no.	Peptide derivative/ Sequence
24.	**Pep-Ala-NNA** INAAGVLQCDAFLAALGC

8.2.1.4. The TFA-cleavage of the permanent protecting groups

After synthesis, the resin-bound peptides were thoroughly washed with DCM and dried under a vacuum. The peptides were cleaved from the resin linker, and the permanent protecting groups were removed by acidolysis with a cocktail of 95% trifluoroacetic acid (TFA), 2.5% triisopropylsilane (TIS), and 2.5% water. The peptides were precipitated using diethyl ether, and the mixture was transferred to centrifuge tubes and centrifuged at 5000 rpm for 5 minutes, and the ether/TFA solution was decanted. The peptides were then washed four times with ether. The cleavage time for each peptide was at least 3 hours. The peptides were obtained as powder products.

8.2.1.5. Cyclization using DMSO

After the cleavage of the peptides with TFA, the crude products were dried and cyclized overnight by treatment with 20% dimethyl sulfoxide (DMSO) in water (v/v).

8.2.1.6. Loading capacity of the resin after the first amino acid attachment

The loading capacity of the resin was determined using the following procedure:

After attaching the first amino acid to the resin, about 5 – 10 mg of resin-bound amino acid was dried and transferred to an Eppendorf tube in duplicate samples and treated with a 20% solution of piperidine in DMF (v/v). The tubes were shaken for 20 minutes at 90 rpm to remove the Fmoc protecting group from the amino acid. The mixture was then centrifuged at 5000 rpm for 2 min. Approximately 100 µl of the mixture was transferred into a tube containing 10 mL of DMF, and the solution was analyzed using a UV-Vis spectrophotometer. A quartz cuvette with a pathlength of 0.1 nm was used. Each sample was scanned in

triplicates, and the absorbance was observed at 301 nm wavelength. DMF was used as a blank solvent.

Calculations

Loading capacity was calculated using the formula below, where **A** is the absorbance (Abs), and **w** is the weight of the resin (mg).

Loading capacity = 101 (**A**) / 7.8 (**w**)

The loading capacity was also used to determine the peptide yield using the formula below:

Theoretical mass = Loading capacity (mmol/g) x mass of resin (g) x peptide exact mass (g/mol)

∴ Peptide yield = Actual yield/ Theoretical yield.

8.2.2. General procedure for the synthesis of silver nanoparticles

8.2.2.1. Synthesis of silver nanoparticles

Method 1:

Silver nanoparticles were synthesized by mixing water (60 mL) and glycerol (40 mL), which was stirred vigorously and heated to 97 °C. Silver nitrate (34 mg, 2 nM) was added to the glycerol-water mixture and stirred for 5 minutes. Trisodium citrate (13 mg, 2 nM) was added to the mixture and allowed to stir for 20 minutes, and a pale-yellow colour was observed. After that, the mixture was allowed to cool for 10 -15 minutes without stirring.

Method 2:

Silver nanoparticles were prepared by transferring water (20 mL) into a conical flask, and the temperature was cooled and kept at 0 °C using an ice bath. A magnetic stirrer was used to vigorously stir the water at 500 revolutions per minute (RPM) speed. Sodium borohydride (1.52 mg, 2mM) was added, followed by trisodium citrate (5.11 mg, 1 mM), which was left to mix for 5 minutes. Concurrently, silver nitrate (2.72 mg, 2 mM) was dissolved in 8 mL distilled water and then transferred to the mixture drop-wise with continuous stirring, which

was stopped after all the silver nitrate solution was transferred. The colour of the mixture changed to yellow, indicating the formation of silver nanoparticles which were then washed using 2 mM of TSC and centrifuged at 10,000 RPM, and the supernatant was separated from the precipitate. The supernatant was decanted but not discarded as it had the desired yellow colour, and the precipitate was obtained as very fine, dark particles.

8.2.2.2. Conjugation of Pep-2-NN to silver nanoparticles

Pep-2-NN was conjugated to the silver nanoparticles by dissolving approximately 2.7 mg of peptide in 5 mL of distilled water, and the solution was mixed with the synthesized silver nanoparticles AgNPs-NN (5 mL) and AgNPs-NN1 (5 mL) at 4 °C to form Pep-AgNPs-NN and Pep-AgNPs-NN1 conjugates, respectively. The peptide-AgNP conjugates were analysed with UV-Vis and TEM.

8.2.3. ClpP-ATPase study

Selected lassomycin peptide derivatives were subjected to a ClpP-Assay study to investigate their influence on the proteolytic activity of the caseinolytic protease (ClpP or ClpP1P2). The assay measures the fluorescence generated when the ClpP cleaves the ZPKM-AMC, a short peptide conjugated to a fluorophore. The 7-amino-4-methylcoumarin (AMC) is a highly fluorescing compound that generates fluorescence with a peak at 441 nm ±100 and excitation at 341 nm ±100. The ZPKM-AMC conjugate has a low fluorescent coefficient. The peptidase activity of ClpP was determined by the presence of free AMC, which is measured by a fluorescence spectrophotometer. The emission was read at 415-445 nm and excitation at 365 nm.

8.3. Instrumentation techniques

8.3.1. Peptide analysis using High-Performance Liquid Chromatography coupled to Mass Spectroscopy (HPLC-MS)

A small amount of each derivative was dissolved in HPLC-grade solvents and analyzed using an HPLC-MS to determine successful synthesis. A Thermo Scientific Dionex Ultimate 3000

UHPLC instrument coupled to a Bruker Compact Q-TOF mass spectrometer was used to analyze the peptides and determine purity. The compounds were separated on a Phenomenex XB-C18 column (5 μm, 100 Å, 250 mm × 21.2 mm), and the flow rate was set at 0.3 mL/min. The mass spectrometry analysis was performed using an electrospray ionization source (ESI) in positive mode. A two-buffer system was employed, Buffer A consisted of 0.1 % formic acid/H_2O (v/v), and Buffer B consisted of 0.1 % formic acid/acetonitrile (v/v).

8.3.2. Purification with preparatory High-Performance Liquid Chromatography (HPLC)

The synthesized peptide derivatives were purified using semi-preparative HPLC, carried out on an Agilent 1260 Infinity semi-preparative instrument via reverse-phase chromatography. A Phenomenex Kinetex XB-C18 column (5 μm, 100 Å, 250 mm × 21.2 mm) was used to separate the compounds, and the flow rate was set at 15 mL/min. The compounds were detected at wavelengths of 215 nm and 254 nm. For the mobile phase, two-buffer systems consisting of 0.1% formic acid/H_2O (v/v) (Buffer A) and 0.1 % formic acid/acetonitrile (v/v) (Buffer B) were utilized. Unless stated otherwise, the peptide derivatives were eluted using a gradient method of 5 – 95% Buffer B for 10 min.

8.3.3. Circular dichroism measurements

Selected peptide derivatives, including Pep-2-NN conformers, Pep-Lys-NN and Ring-2-NN, were subjected to circular dichroism (CD) studies. Each peptide was dissolved in water to a concentration of 100 μM. The CD measurements of the peptides were recorded on a JASCO J-1500 CD spectrometer instrument at 20 °C between a range of 190 – 260 nm. The spectra were recorded at 0.5 nm intervals with 8 scans at a 200 nm/min scanning speed. The quartz cuvette used had a 0.2 nm pathlength and a 5.0 nm bandwidth. The absorption value was measured as molar ellipticity per residue (deg.cm^2.dmol^{-1}). The signals obtained were converted to mean residue ellipticity [θ] using the equation below:

$[\theta] = (MRW \times \theta)\ 10 \times d \times c$ obtained in deg.cm^2.dmol^{-1} units.

where *MWR* is the mean residue weight, θ the observed ellipticity in degrees, *c* is the peptide concentration in g/mL, and *d* is the pathlength in cm. The spectra were generated from the Beta Structure Selection (BeStSel) online software provided by Micsocai *et al.*[1]

8.3.4. Analysis using UV-Vis spectroscopy

The analysis of silver nanoparticles was conducted using an Agilent Technologies Cary Series UV-Vis spectrophotometer with a Quartz cuvette of 1cm optical length.

8.3.5. Analysis using TEM microscopy

Transmission electron microscopy (TEM) images of silver nanoparticles and conjugated peptides were obtained from the FEI Tecnai-12 microscopy at an electron acceleration voltage of 200 KV and beam sport size of 10-100 nm.

8.3.6. Nuclear magnetic resonance spectroscopy (NMR)

About 35.9 mg of Pep-2-NN was dissolved in 0.5 mL deuterated dimethyl sulfoxide (DMSO-d6) and was analysed using Nuclear Magnetic Resonance (NMR) spectroscopy. The proton and carbon NMR spectra (^{1}H NMR and ^{13}C NMR, respectively) were recorded on a Bruker Avance 300 MHz, Bruker Avance 400 MHz, and Bruker III 500 MHz spectrometer. The NMR chemical shift (δ) values are reported in parts per million (ppm) relative to dimethyl sulfoxide (DMSO-d) at 2.49 ppm and 39.52 ppm for the proton and carbon NMR, respectively. The NMR chemical shifts were referenced against the internal standard, tetramethylsilane (TMS, 0.00 ppm). The spectra were analysed in the first order, and the coupling constant (J) values were reported as Hertz (Hz). The multiplicity of signals is expressed as; s=singlet, br s=broad singlet, d=doublet, dd=double doublet, t=triplet, q=quartet, m=multiplet.

The secondary structure of Pep-2-NN was elucidated using two-dimensional (2-D) NMR spectroscopy. 2-D NMR spectra, including COSY, ^{13}C-HSQC, TOCSY, NOESY, and ROESY experiments, were recorded at 300K on a 500 MHz NMR Bruker III spectrometer. The first ROESY experiments were recorded with a mixing time of 200 ms, while TOCSY was

recorded with a mixing time of 70 s; each increment was the sum of 32 scans with a relaxation delay of 2.0 s; 2048 data points were collected per experiment.

References:

1. Micsonai, A.; Moussong, E.; Wien, F.; Boros, E.; Vadászi, H.; Murvai, N.; Lee, Y.-H.; Molnár, T.; Réfrégiers, M.; Goto, Y., BeStSel: webserver for secondary structure and fold prediction for protein CD spectroscopy. *Nucleic Acids Research* **2022,** *50* (W1), W90-W98.

Appendices

Contents

Appendix I: Supplementary information for Chapter 3

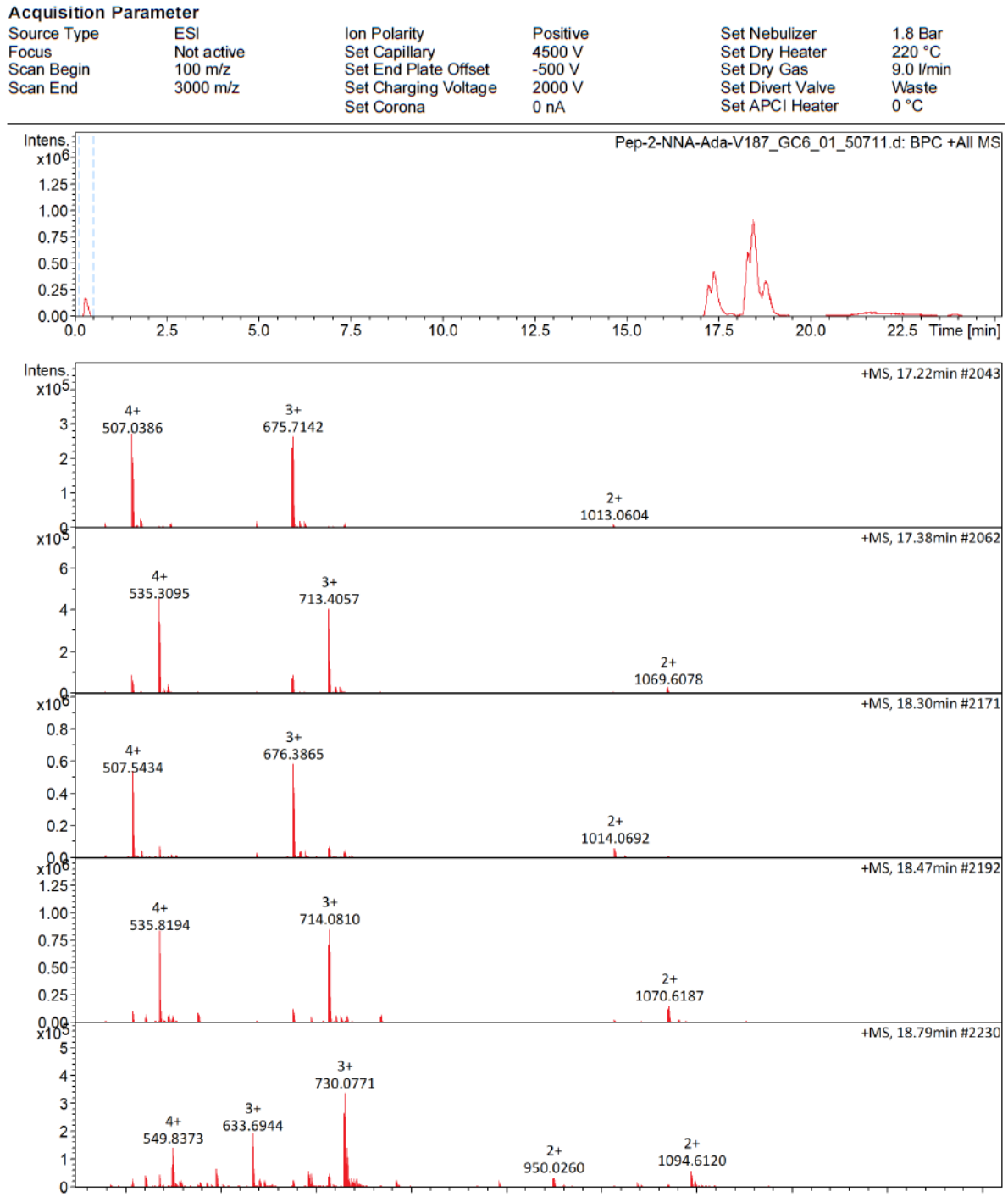

Figure S1-1: LCMS of Pep-2-NNA-Ada

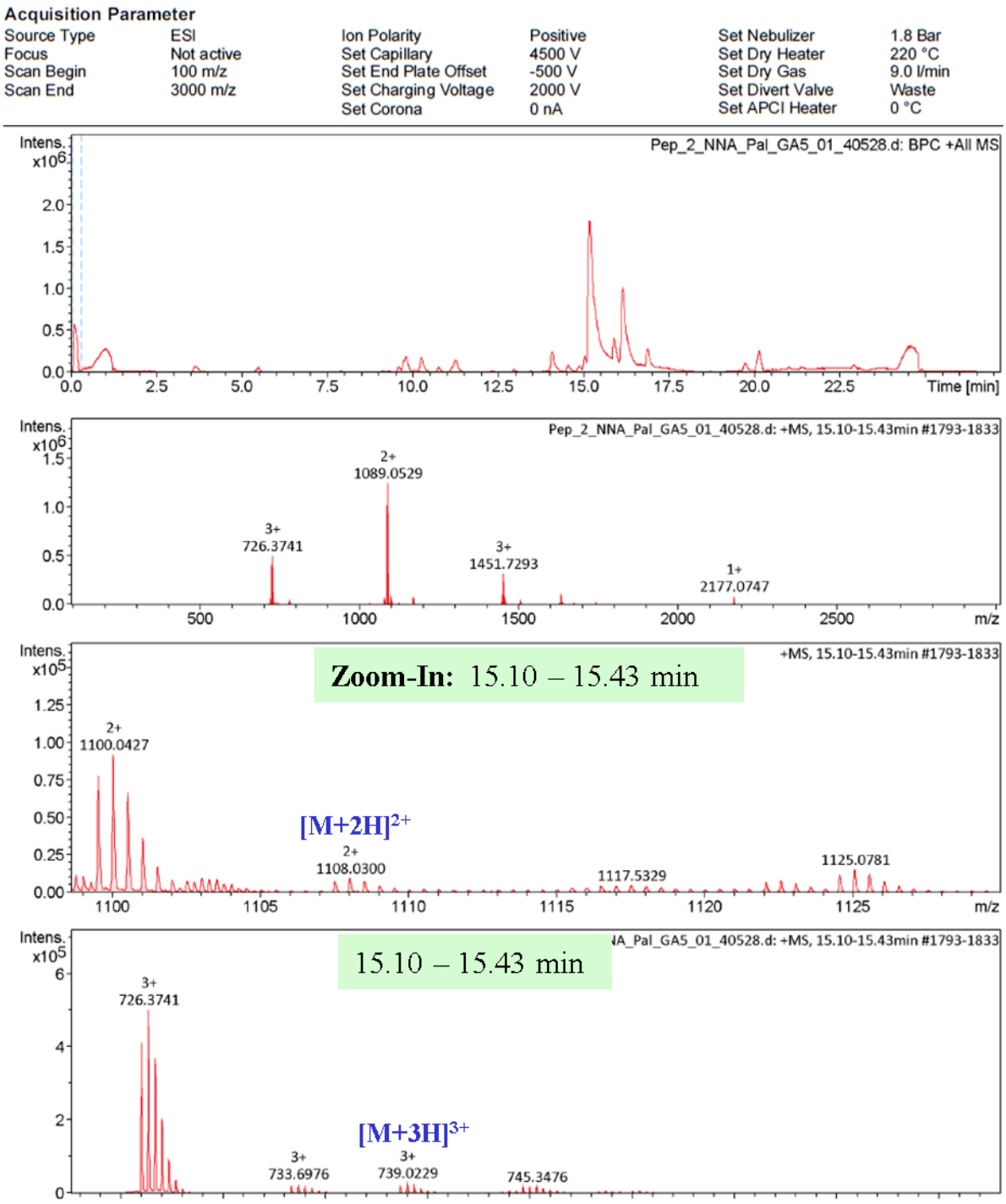

Figure S1-2: LCMS of Pep-2-NNA-Pal

Acquisition Parameter

Source Type	ESI	Ion Polarity	Positive	Set Nebulizer	1.8 Bar
Focus	Not active	Set Capillary	4500 V	Set Dry Heater	220 °C
Scan Begin	100 m/z	Set End Plate Offset	-500 V	Set Dry Gas	9.0 l/min
Scan End	3000 m/z	Set Charging Voltage	2000 V	Set Divert Valve	Waste
		Set Corona	0 nA	Set APCI Heater	0 °C

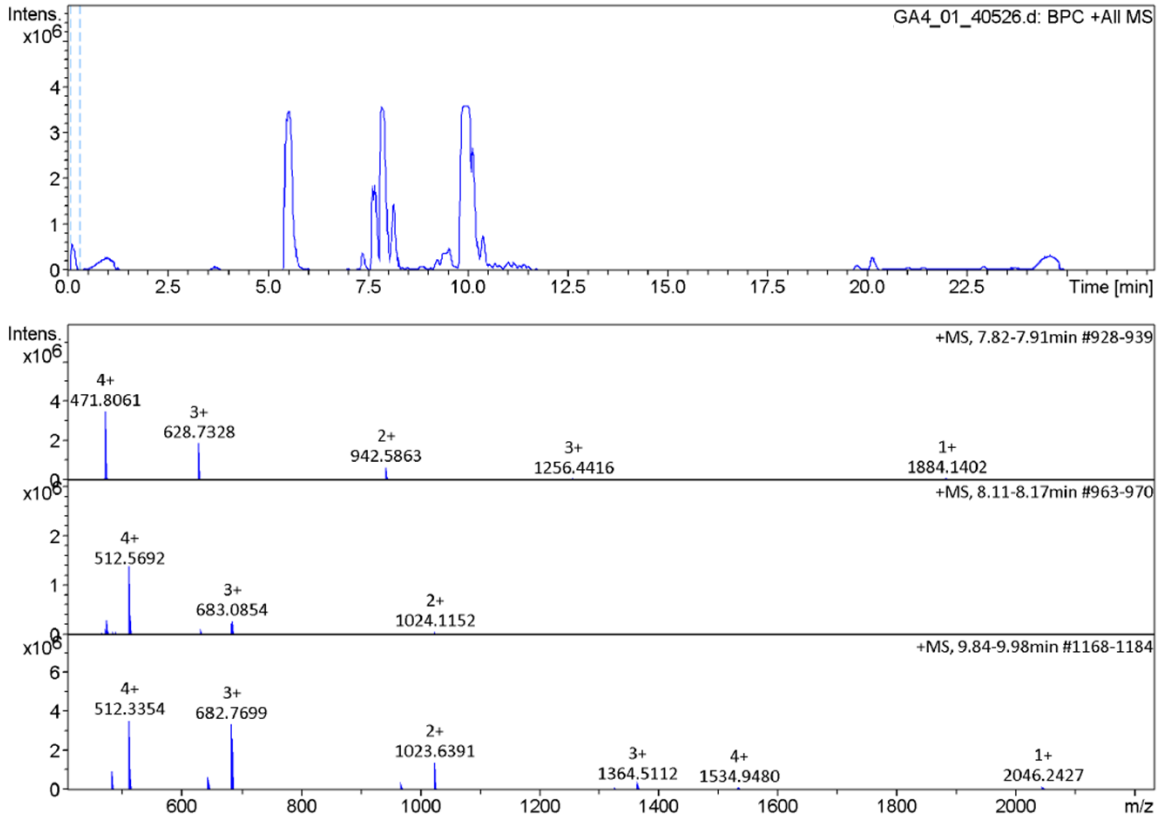

Figure S1-3: LCMS of Linear Pep-1-NNA-Ada

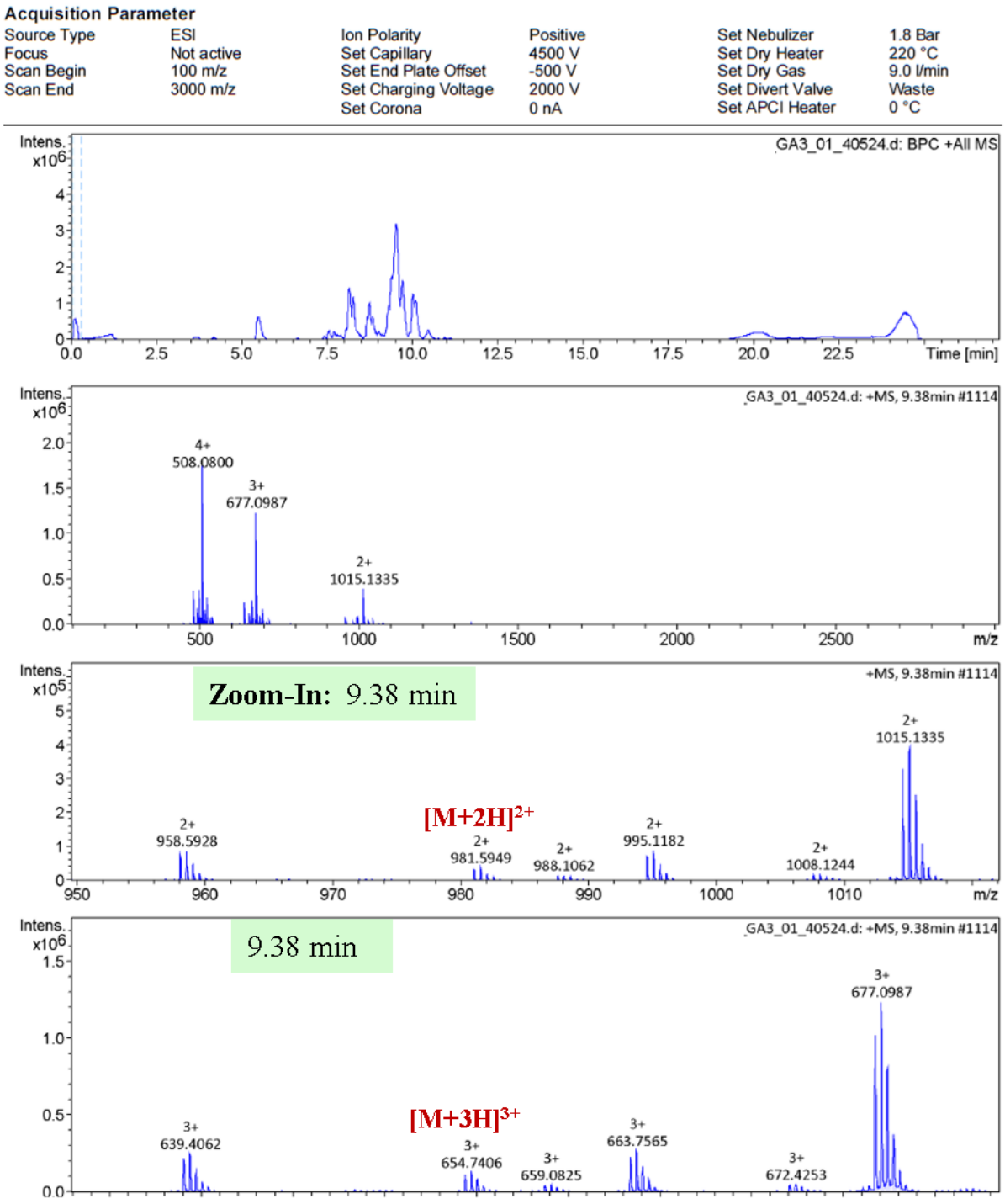

Figure S1-4: LCMS of Linear Pep-2-NNA-Ada

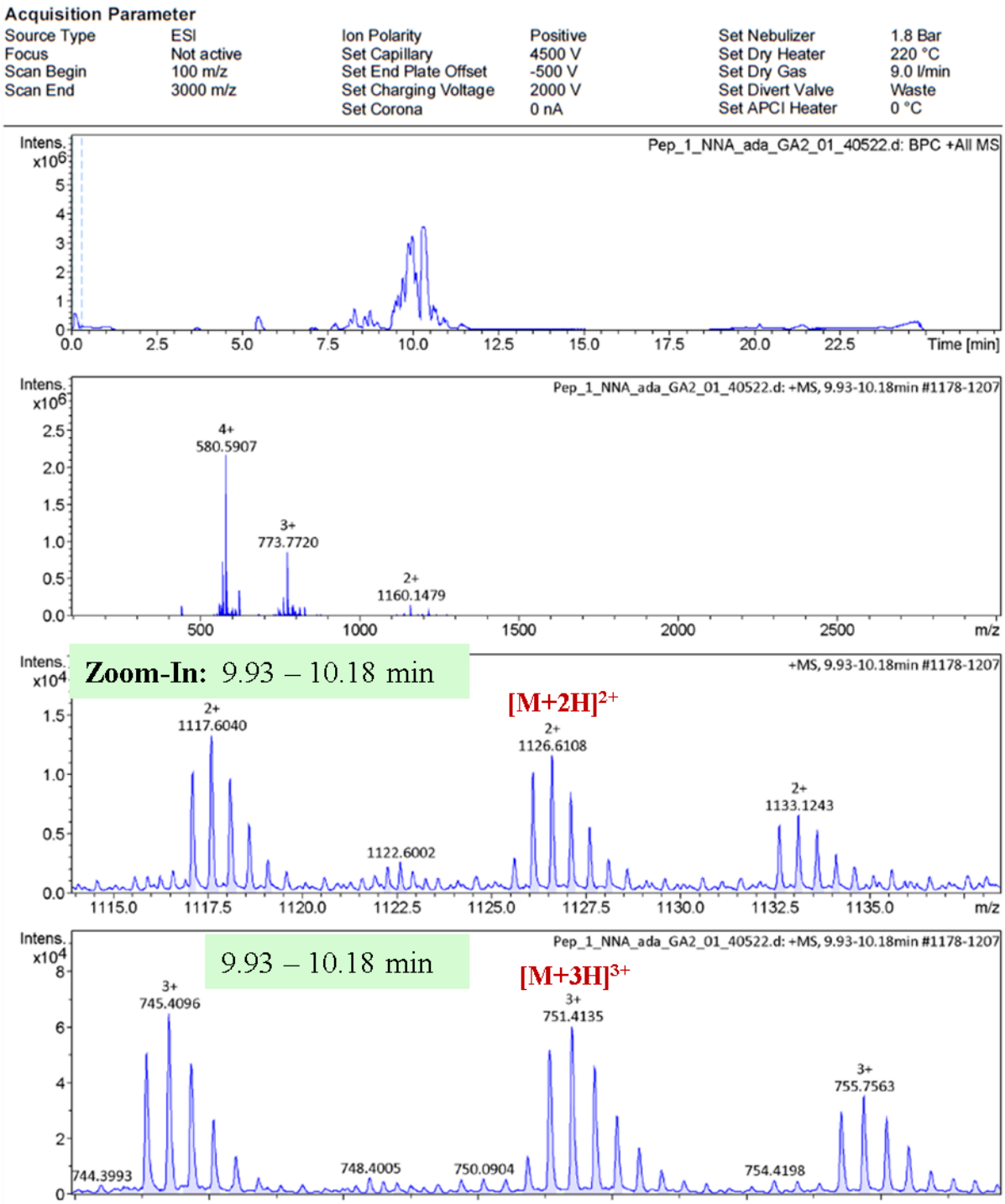

Figure S1-5: LCMS of Pep-1-NNA-Ada

Appendix II: Supplementary information for Chapter 4

Acquisition Parameter

Source Type	ESI	Ion Polarity	Positive	Set Nebulizer	1.8 Bar
Focus	Not active	Set Capillary	4500 V	Set Dry Heater	220 °C
Scan Begin	100 m/z	Set End Plate Offset	-500 V	Set Dry Gas	9.0 l/min
Scan End	3000 m/z	Set Charging Voltage	2000 V	Set Divert Valve	Waste
		Set Corona	0 nA	Set APCI Heater	0 °C

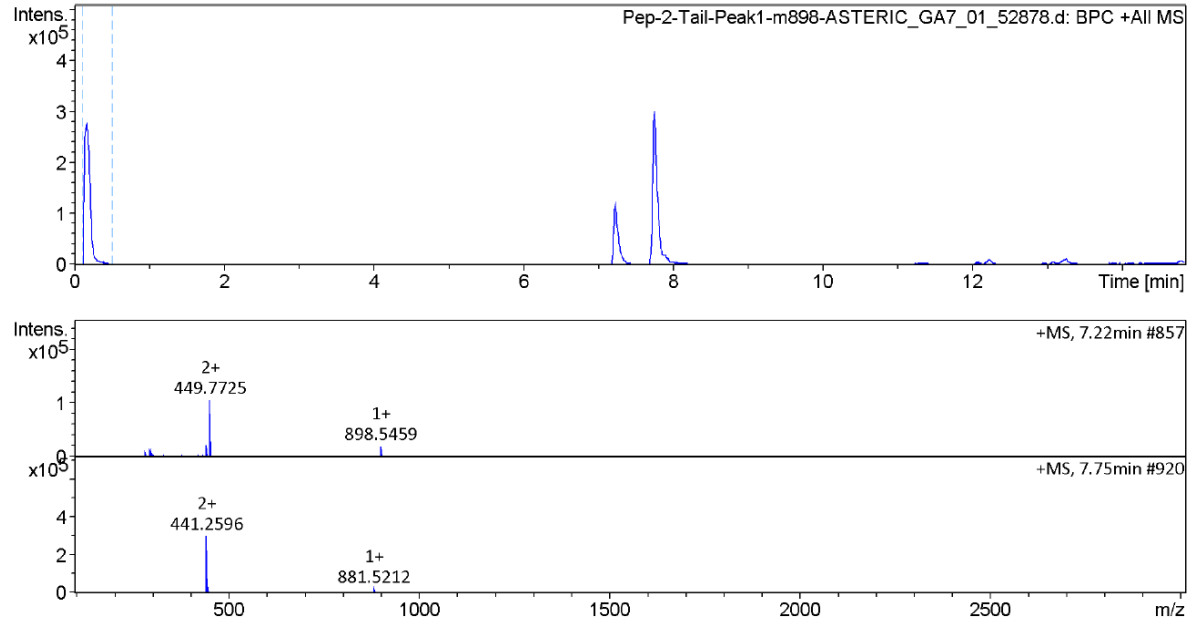

Figure S2-1: LCMS of Tail-2-NN Peak 1

Acquisition Parameter

Source Type	ESI	Ion Polarity	Positive	Set Nebulizer	1.8 Bar
Focus	Not active	Set Capillary	4500 V	Set Dry Heater	220 °C
Scan Begin	100 m/z	Set End Plate Offset	-500 V	Set Dry Gas	9.0 l/min
Scan End	3000 m/z	Set Charging Voltage	2000 V	Set Divert Valve	Waste
		Set Corona	0 nA	Set APCI Heater	0 °C

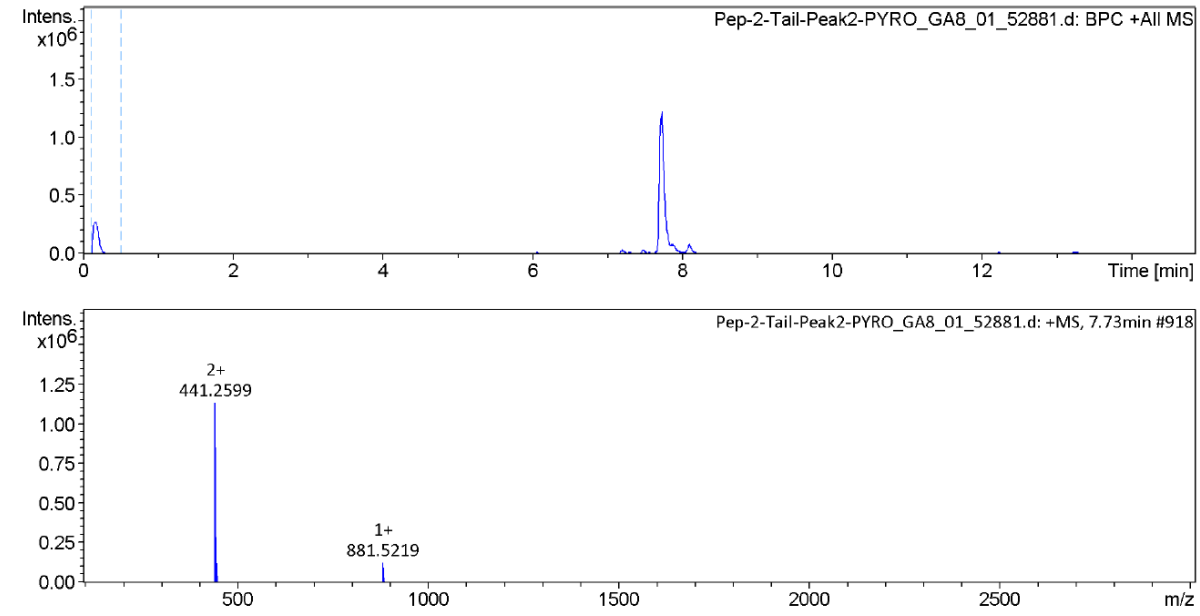

Figure S2-2: LCMS of Tail-2-NN Peak 2

Acquisition Parameter

Source Type	ESI	Ion Polarity	Positive	Set Nebulizer	1.8 Bar
Focus	Not active	Set Capillary	4500 V	Set Dry Heater	220 °C
Scan Begin	100 m/z	Set End Plate Offset	-500 V	Set Dry Gas	9.0 l/min
Scan End	3000 m/z	Set Charging Voltage	2000 V	Set Divert Valve	Waste
		Set Corona	0 nA	Set APCI Heater	0 °C

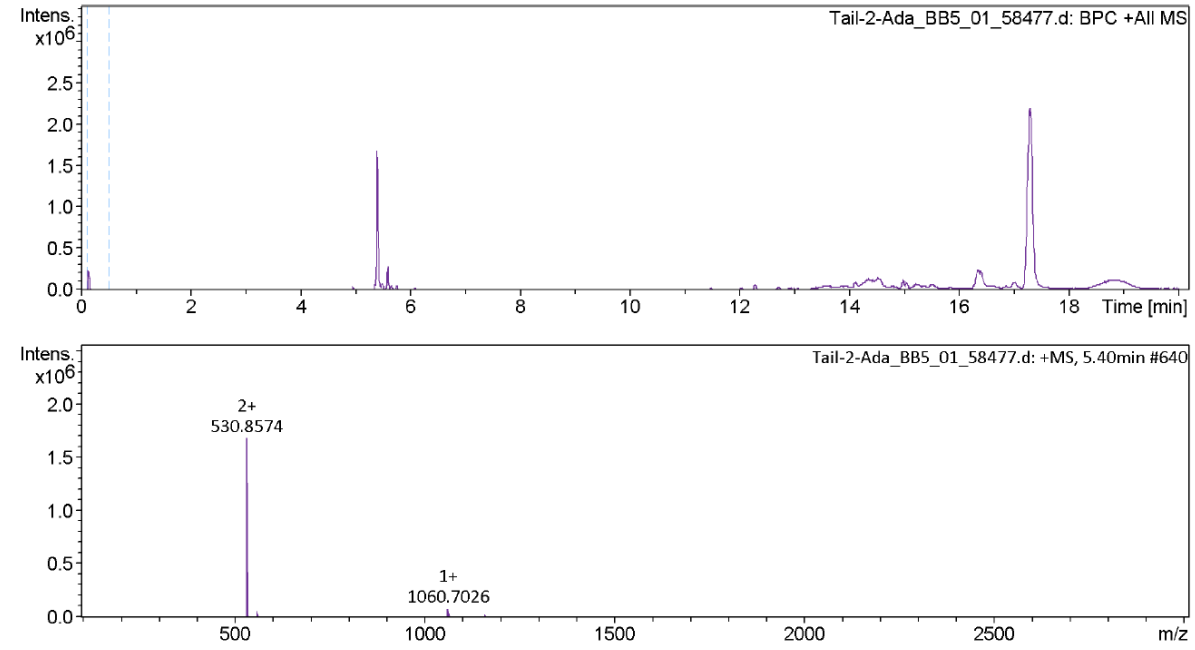

Figure S2-3: LCMS of Tail-2-NN-Ada

Acquisition Parameter

Source Type	ESI	Ion Polarity	Positive	Set Nebulizer	1.8 Bar
Focus	Not active	Set Capillary	4500 V	Set Dry Heater	220 °C
Scan Begin	100 m/z	Set End Plate Offset	-500 V	Set Dry Gas	9.0 l/min
Scan End	3000 m/z	Set Charging Voltage	2000 V	Set Divert Valve	Waste
		Set Corona	0 nA	Set APCI Heater	0 °C

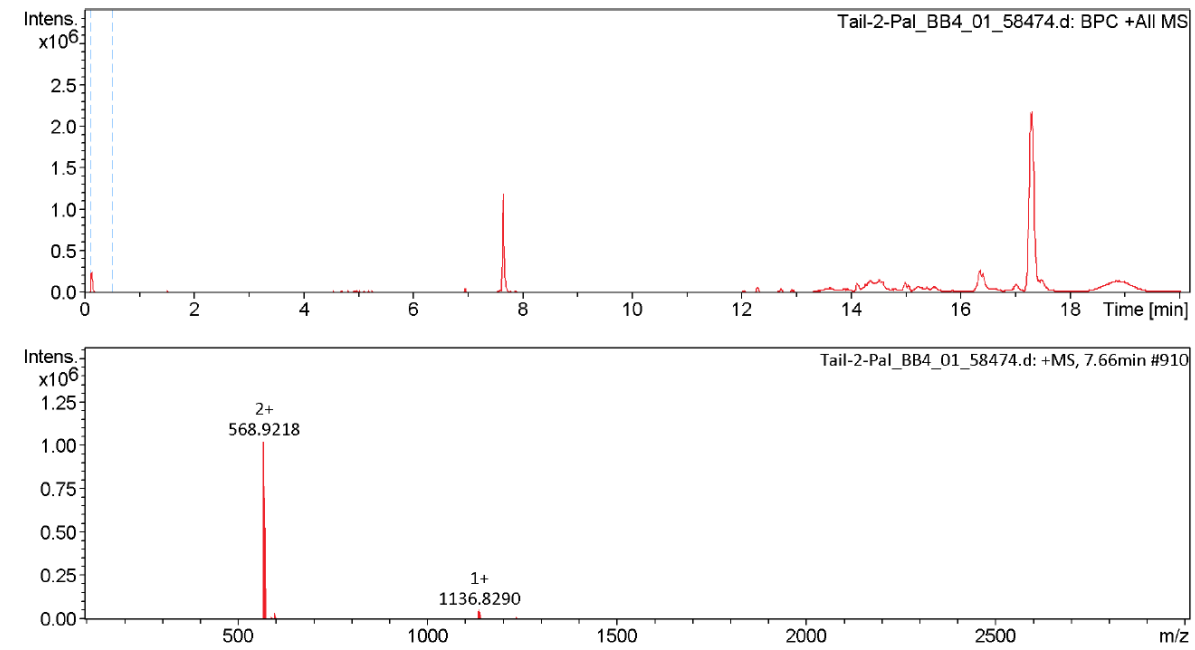

Figure S2-4: LCMS of Tail-2-NN-Pal

Acquisition Parameter

Source Type	ESI	Ion Polarity	Positive	Set Nebulizer	1.8 Bar
Focus	Not active	Set Capillary	4500 V	Set Dry Heater	220 °C
Scan Begin	100 m/z	Set End Plate Offset	-500 V	Set Dry Gas	9.0 l/min
Scan End	3000 m/z	Set Charging Voltage	2000 V	Set Divert Valve	Waste
		Set Corona	0 nA	Set APCI Heater	0 °C

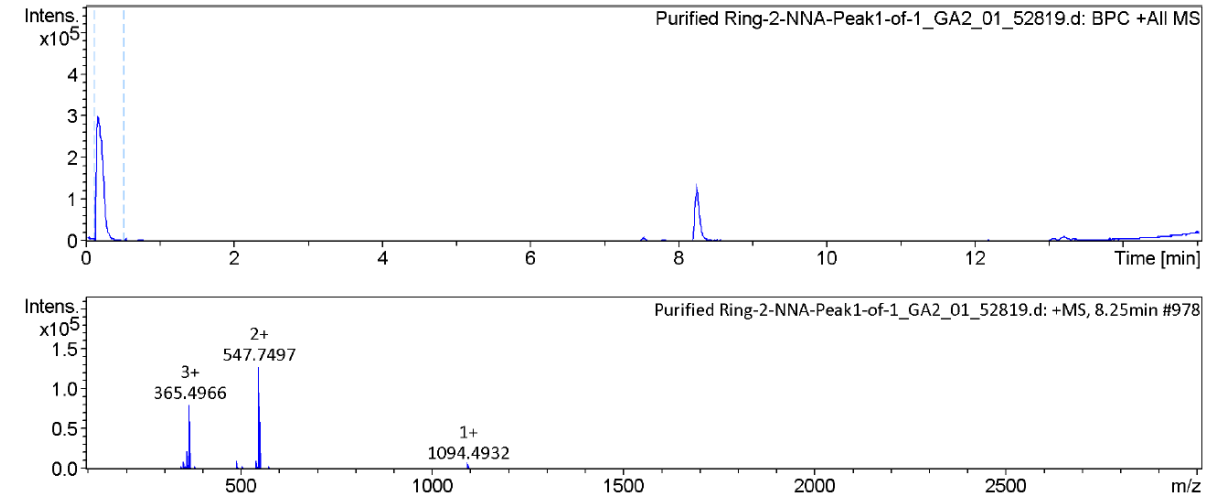

Figure S2-5: LCMS of Ring-2-NNA

Acquisition Parameter

Source Type	ESI	Ion Polarity	Positive	Set Nebulizer	1.8 Bar
Focus	Not active	Set Capillary	4500 V	Set Dry Heater	220 °C
Scan Begin	100 m/z	Set End Plate Offset	-500 V	Set Dry Gas	9.0 l/min
Scan End	3000 m/z	Set Charging Voltage	2000 V	Set Divert Valve	Waste
		Set Corona	0 nA	Set APCI Heater	0 °C

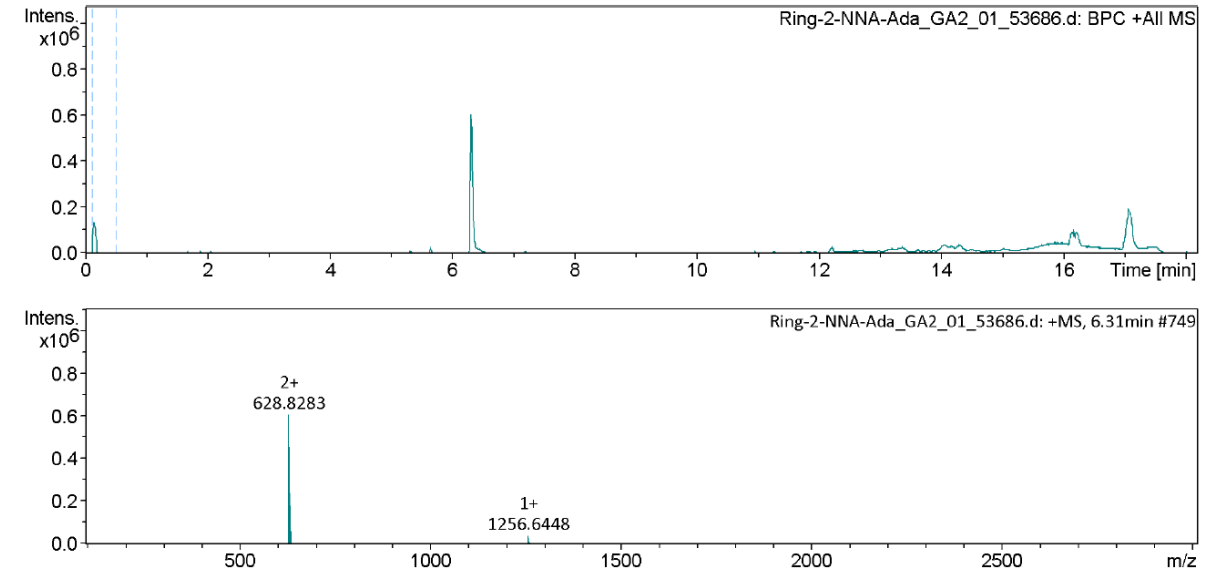

Figure S2-6: LCMS of Ring-2-NNA-Ada

Acquisition Parameter

Source Type	ESI	Ion Polarity	Positive	Set Nebulizer	1.8 Bar
Focus	Not active	Set Capillary	4500 V	Set Dry Heater	220 °C
Scan Begin	100 m/z	Set End Plate Offset	-500 V	Set Dry Gas	9.0 l/min
Scan End	3000 m/z	Set Charging Voltage	2000 V	Set Divert Valve	Waste
		Set Corona	0 nA	Set APCI Heater	0 °C

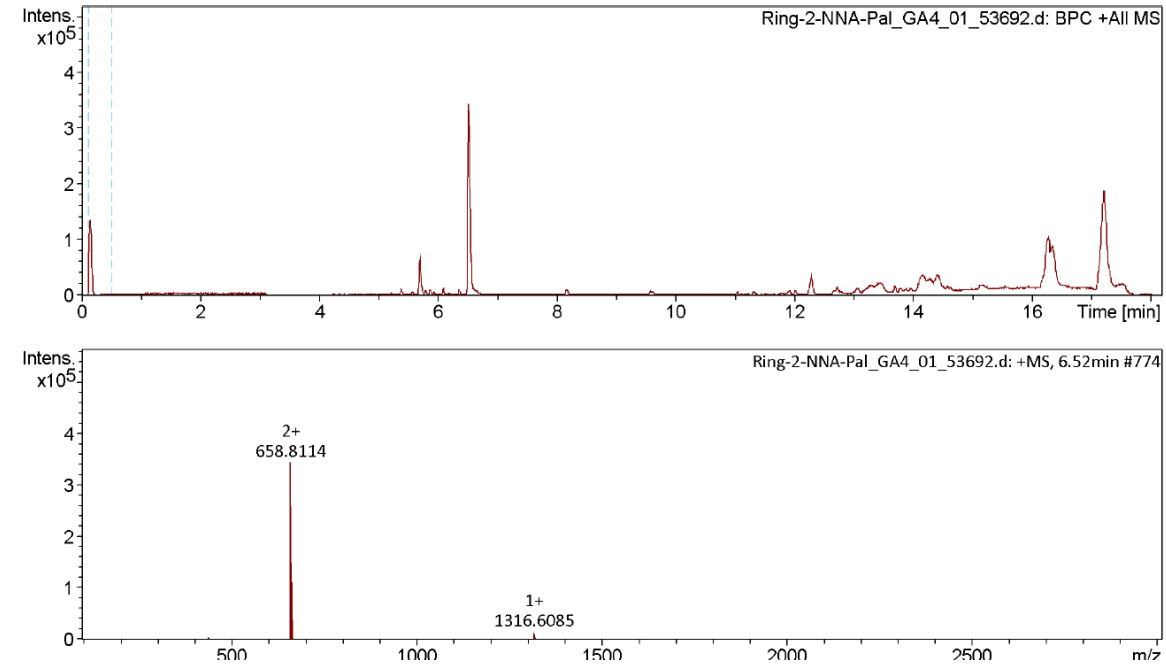

Figure S2-7: LCMS of Ring-2-NNA-Pal

Acquisition Parameter

Source Type	ESI	Ion Polarity	Positive	Set Nebulizer	1.8 Bar
Focus	Not active	Set Capillary	4500 V	Set Dry Heater	220 °C
Scan Begin	100 m/z	Set End Plate Offset	-500 V	Set Dry Gas	9.0 l/min
Scan End	3000 m/z	Set Charging Voltage	2000 V	Set Divert Valve	Waste
		Set Corona	0 nA	Set APCI Heater	0 °C

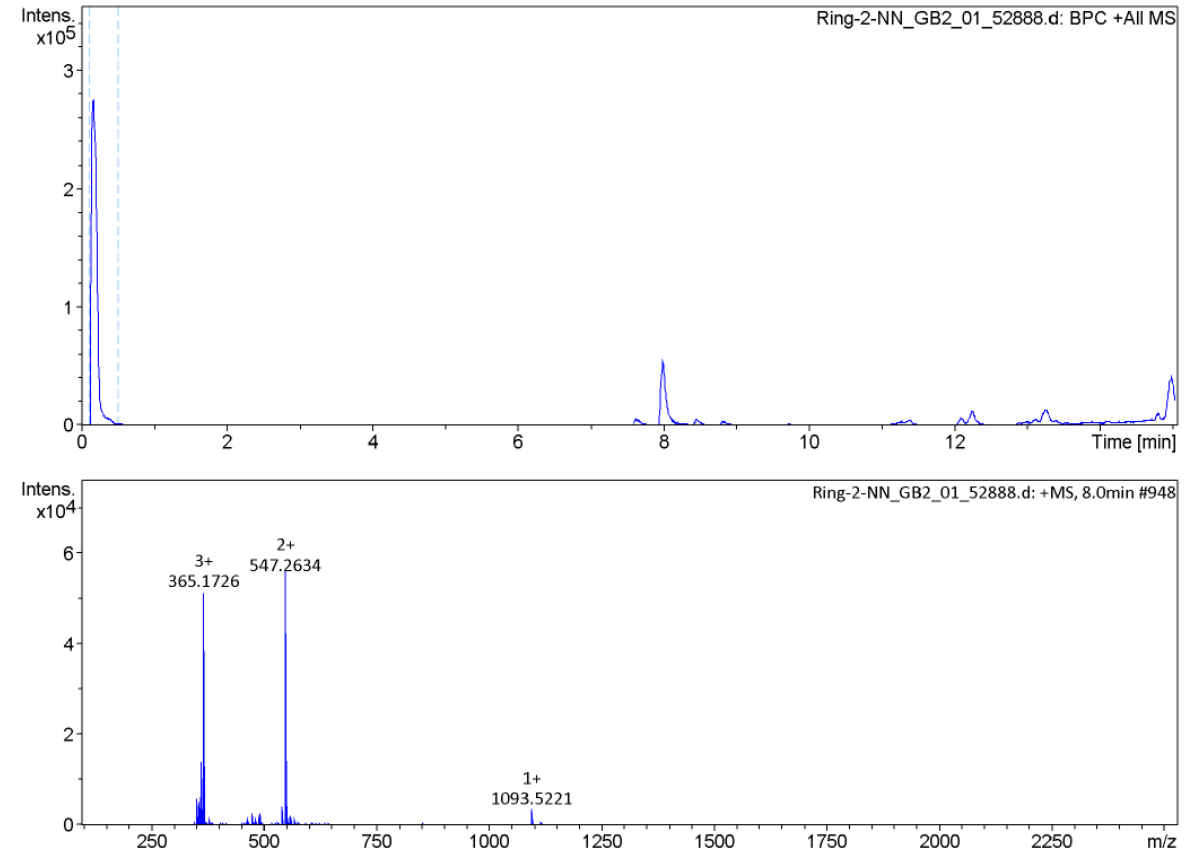

Figure S2-8: LCMS of Ring-2-NN

Acquisition Parameter

Source Type	ESI	Ion Polarity	Positive	Set Nebulizer	1.8 Bar
Focus	Not active	Set Capillary	4500 V	Set Dry Heater	220 °C
Scan Begin	100 m/z	Set End Plate Offset	-500 V	Set Dry Gas	9.0 l/min
Scan End	3000 m/z	Set Charging Voltage	2000 V	Set Divert Valve	Waste
		Set Corona	0 nA	Set APCI Heater	0 °C

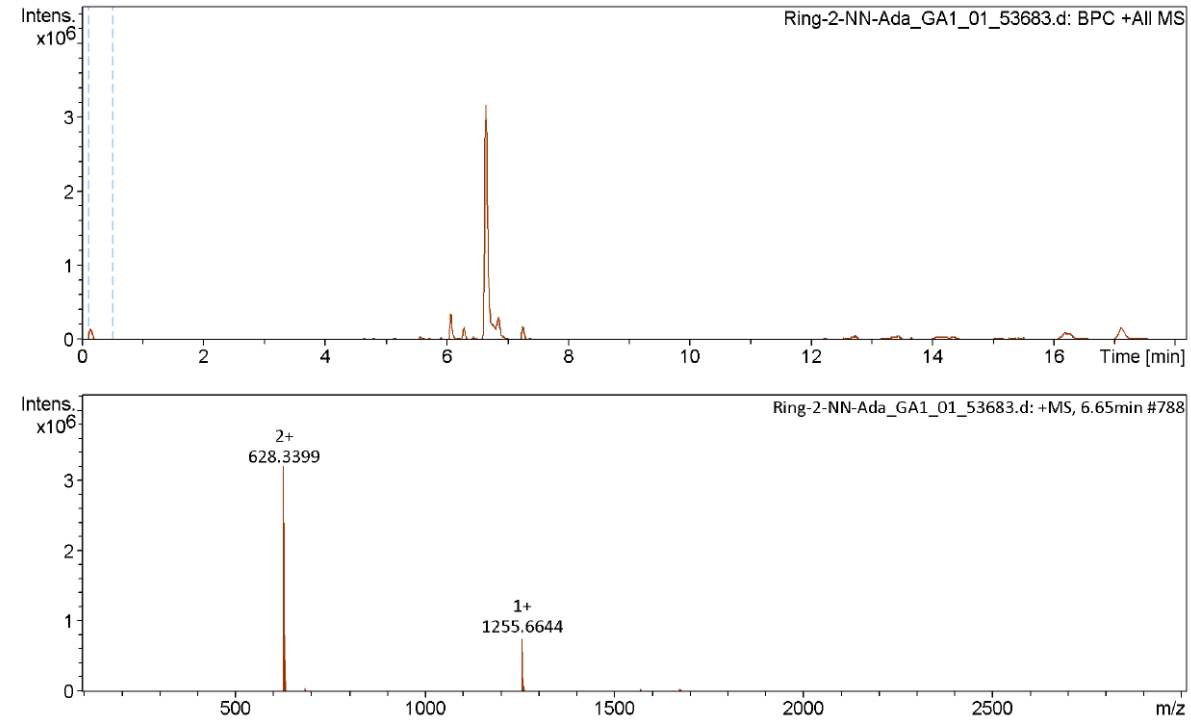

Figure S2-9: LCMS of Ring-2-NN-Ada

Acquisition Parameter

Source Type	ESI	Ion Polarity	Positive	Set Nebulizer	1.8 Bar
Focus	Not active	Set Capillary	4500 V	Set Dry Heater	220 °C
Scan Begin	100 m/z	Set End Plate Offset	-500 V	Set Dry Gas	9.0 l/min
Scan End	3000 m/z	Set Charging Voltage	2000 V	Set Divert Valve	Waste
		Set Corona	0 nA	Set APCI Heater	0 °C

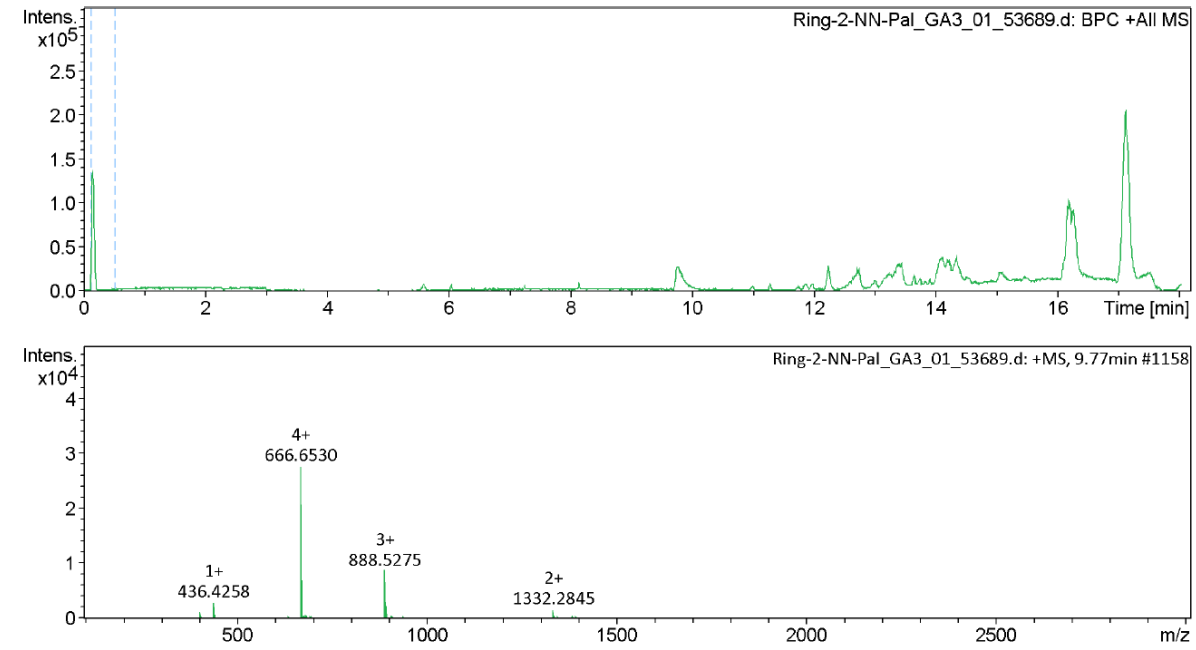

Figure S2-10: LCMS of Ring-2-NN-Pal

Appendix III: Supplementary information for Chapter 6

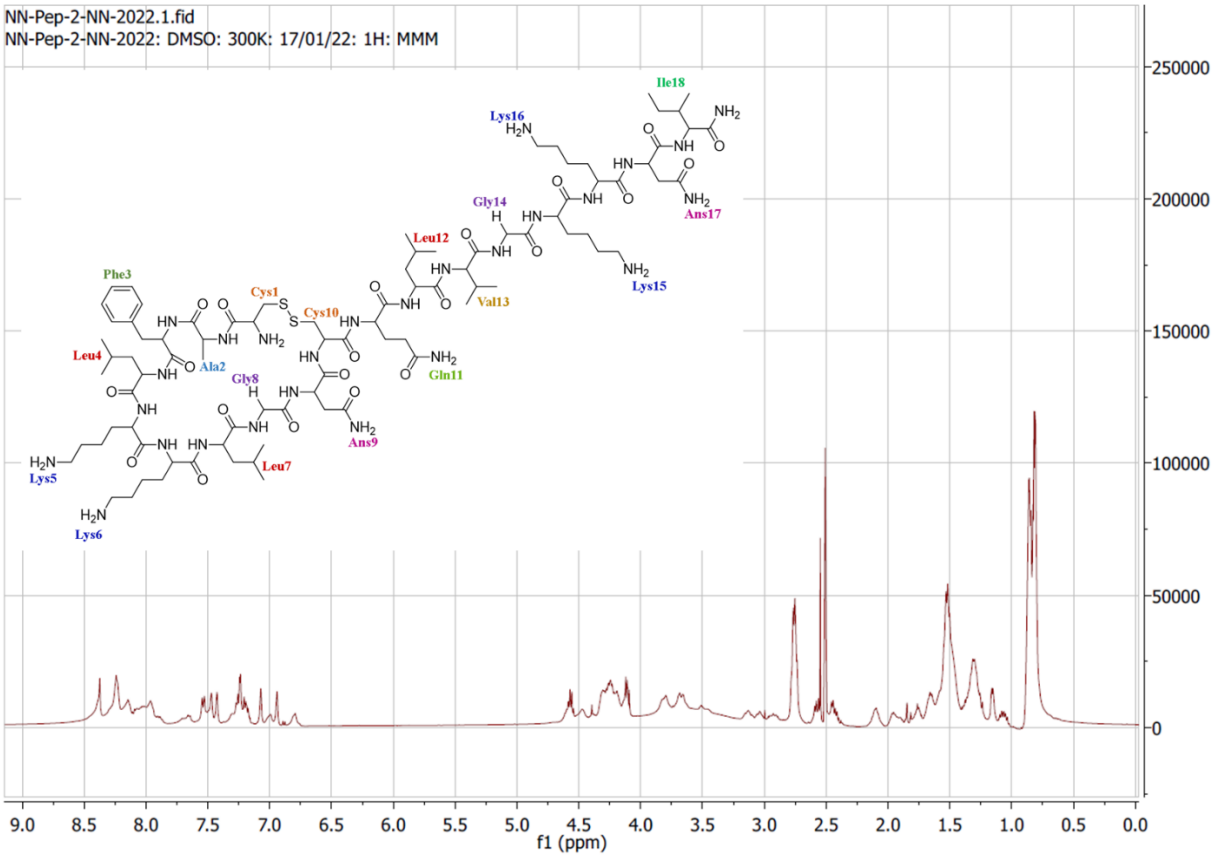

Figure S3-1: ^{1}H NMR spectrum of Pep-2-NN

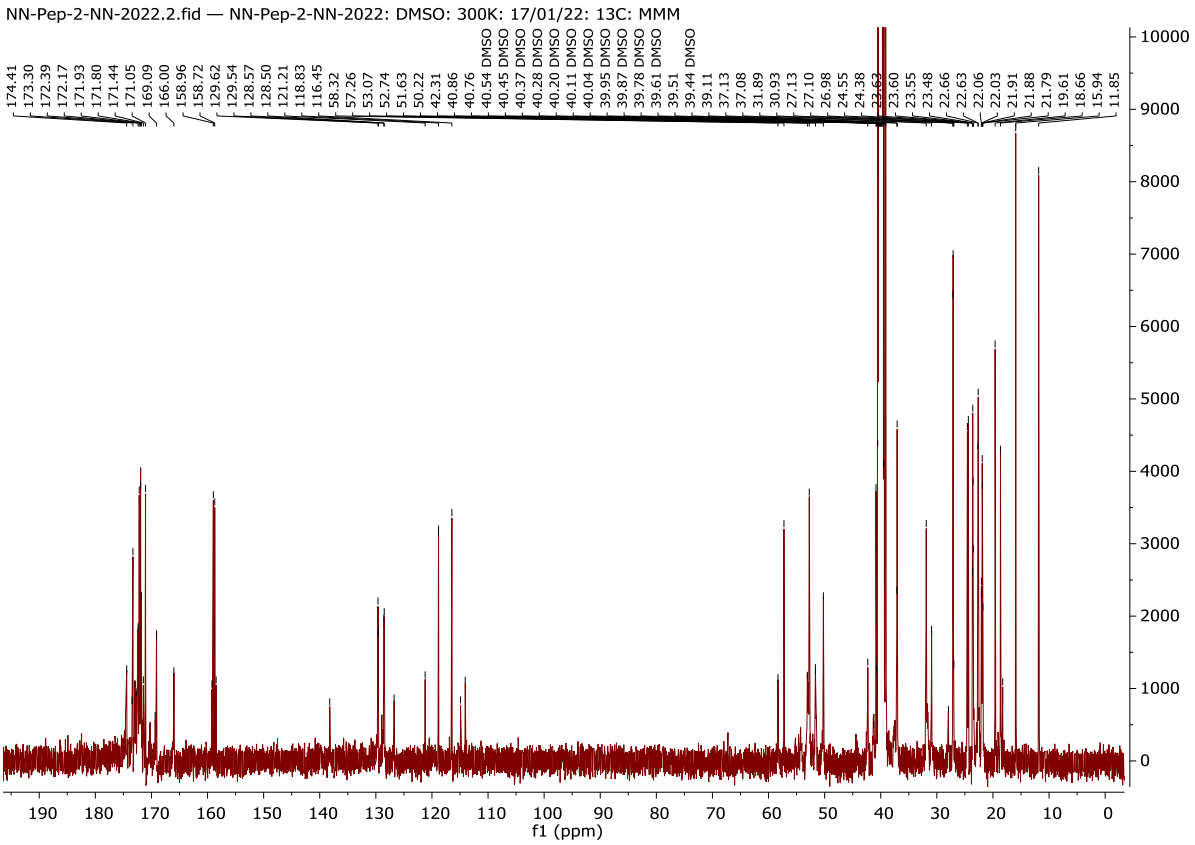

Figure S3-2: ^{13}C NMR spectrum of Pep-2-NN

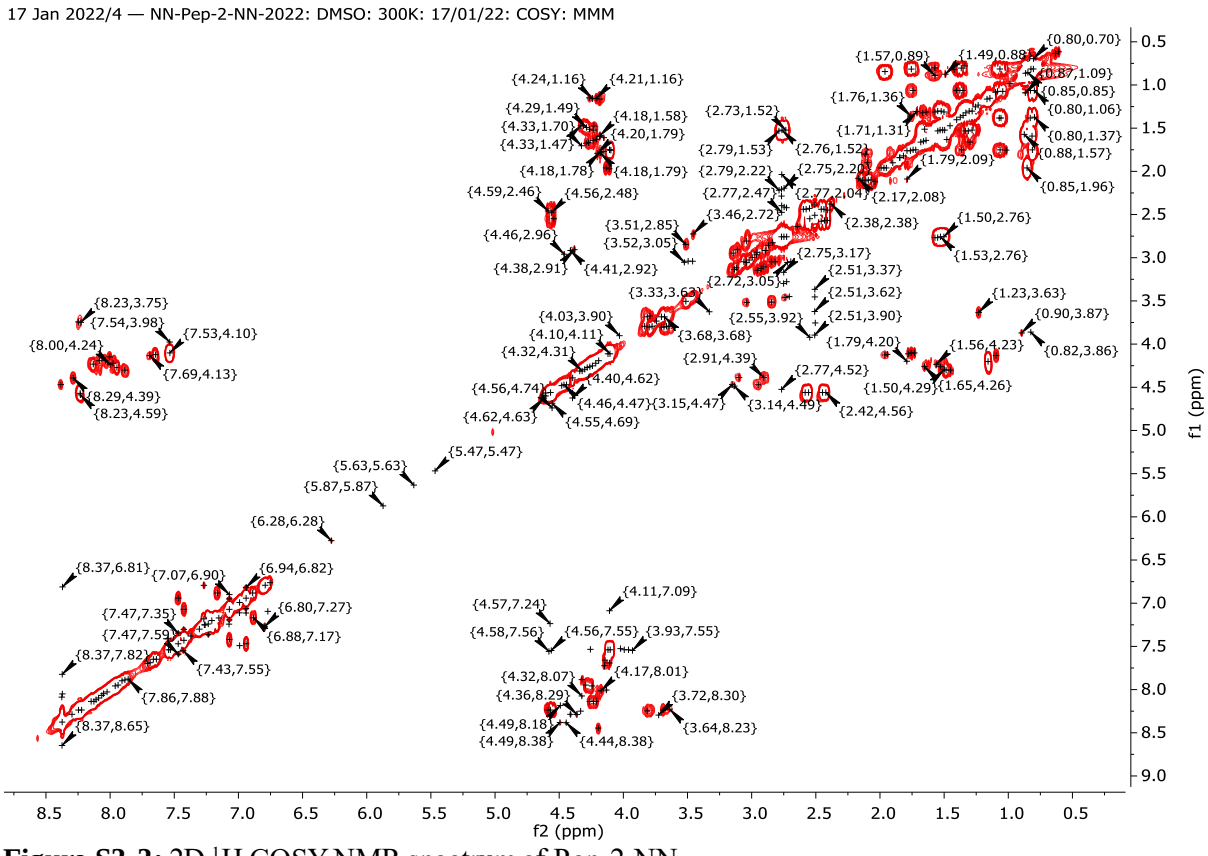

Figure S3-3: 2D ^{1}H COSY NMR spectrum of Pep-2-NN

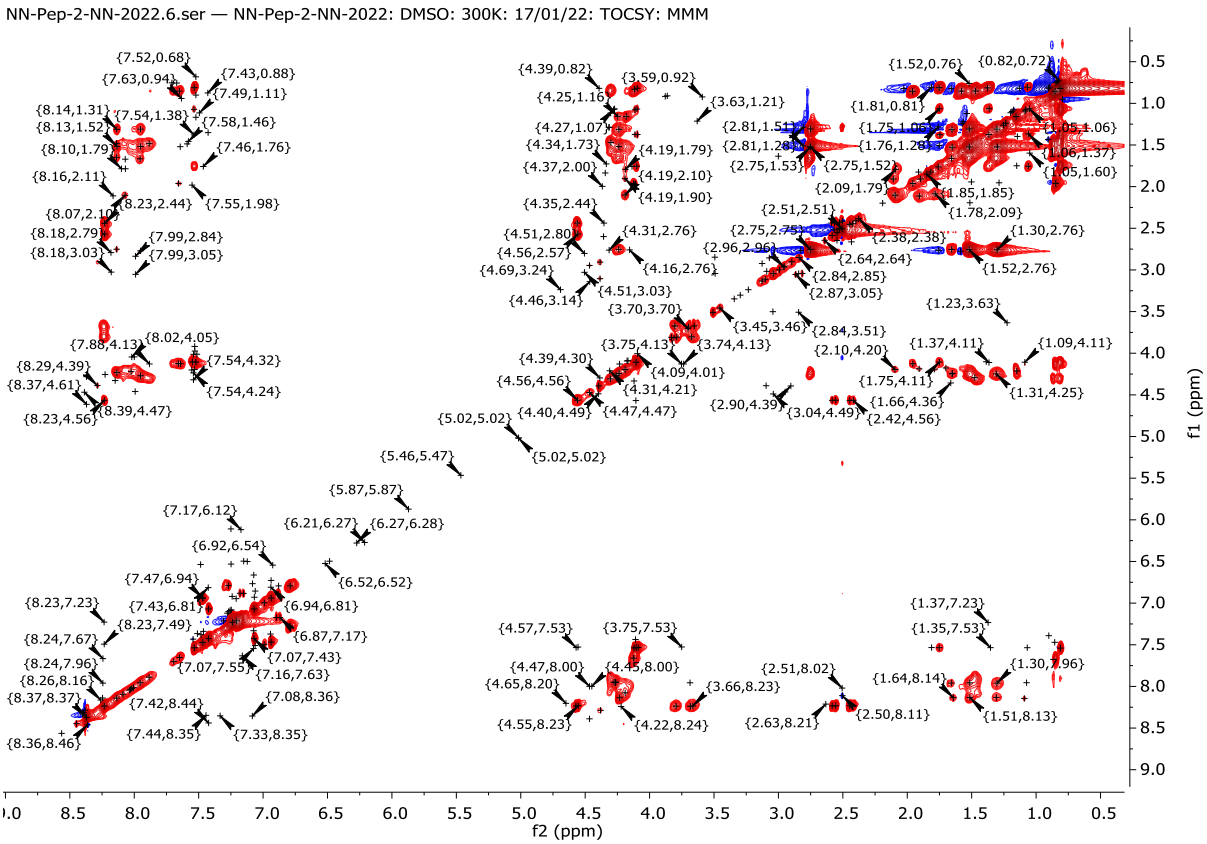

Figure S3-4: [^{1}H, ^{1}H] TOCSY spectrum of Pep-2-NN

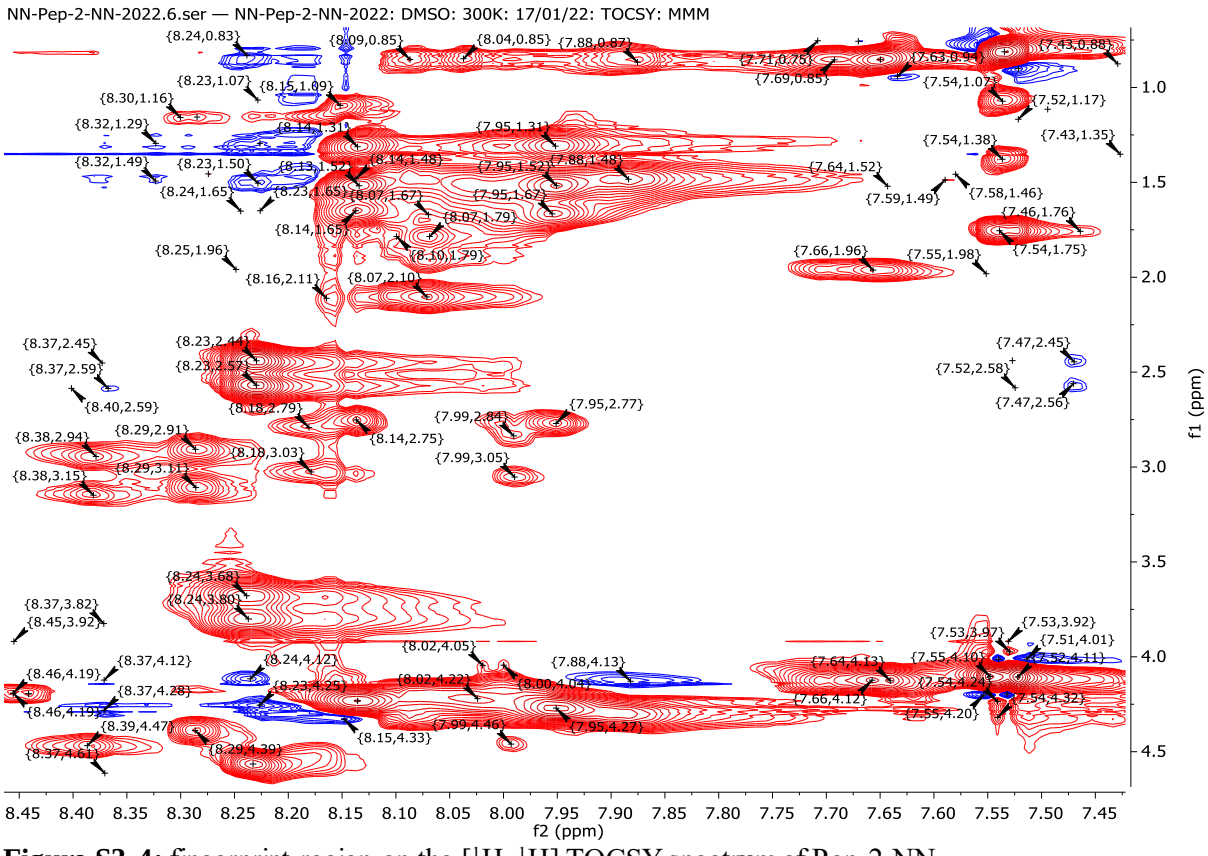

Figure S3-4: fingerprint region on the [^{1}H, ^{1}H] TOCSY spectrum of Pep-2-NN

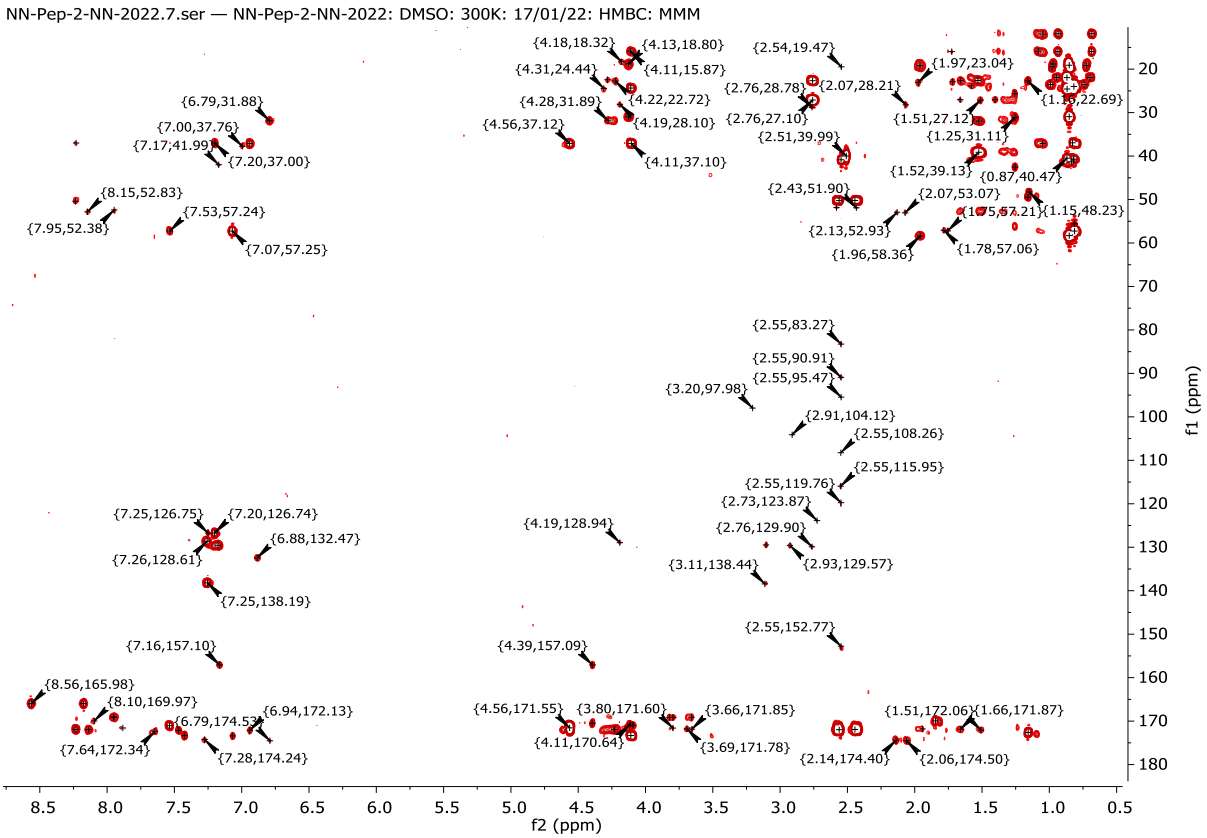

Figure S3-5: [^{1}H, ^{13}C] HMBC NMR spectrum of Pep-2-NN

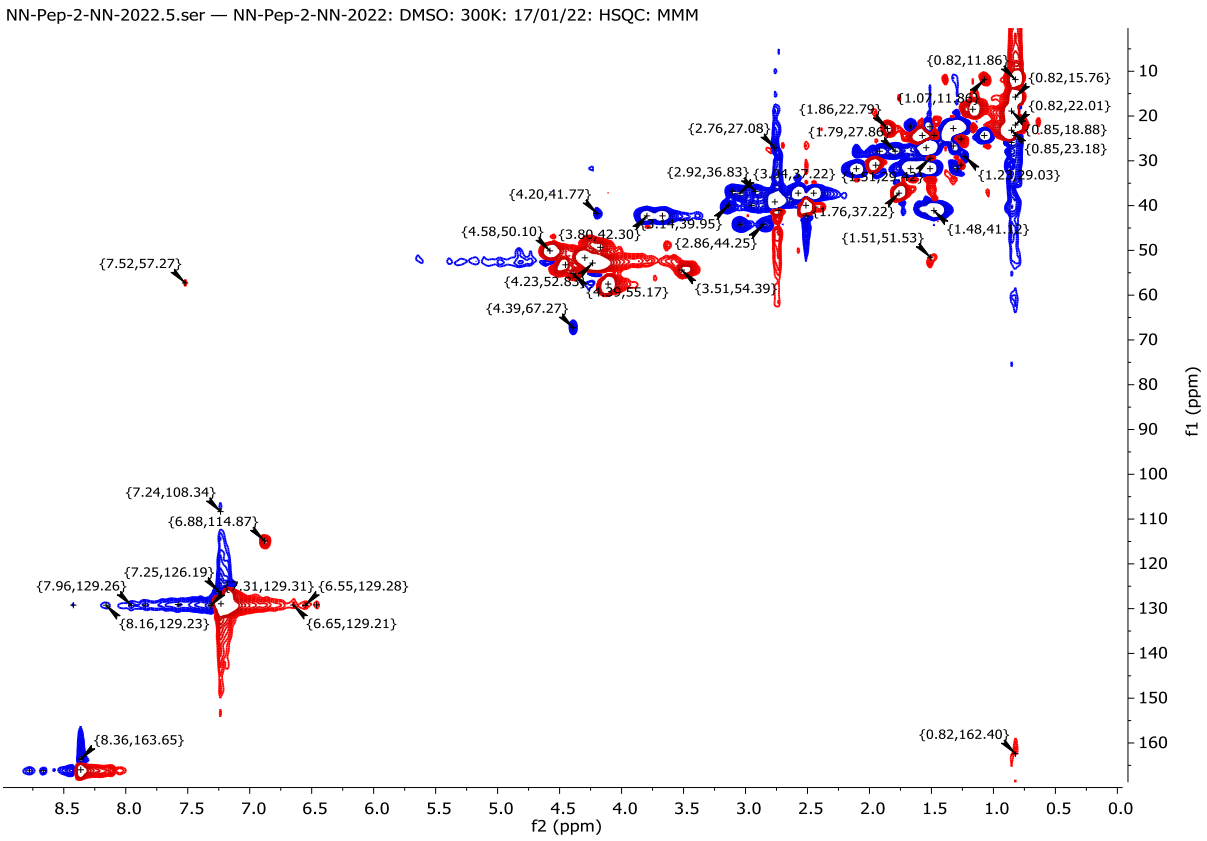

Figure S3-6: ^{13}C HSQC NMR spectrum for Pep-2-NN

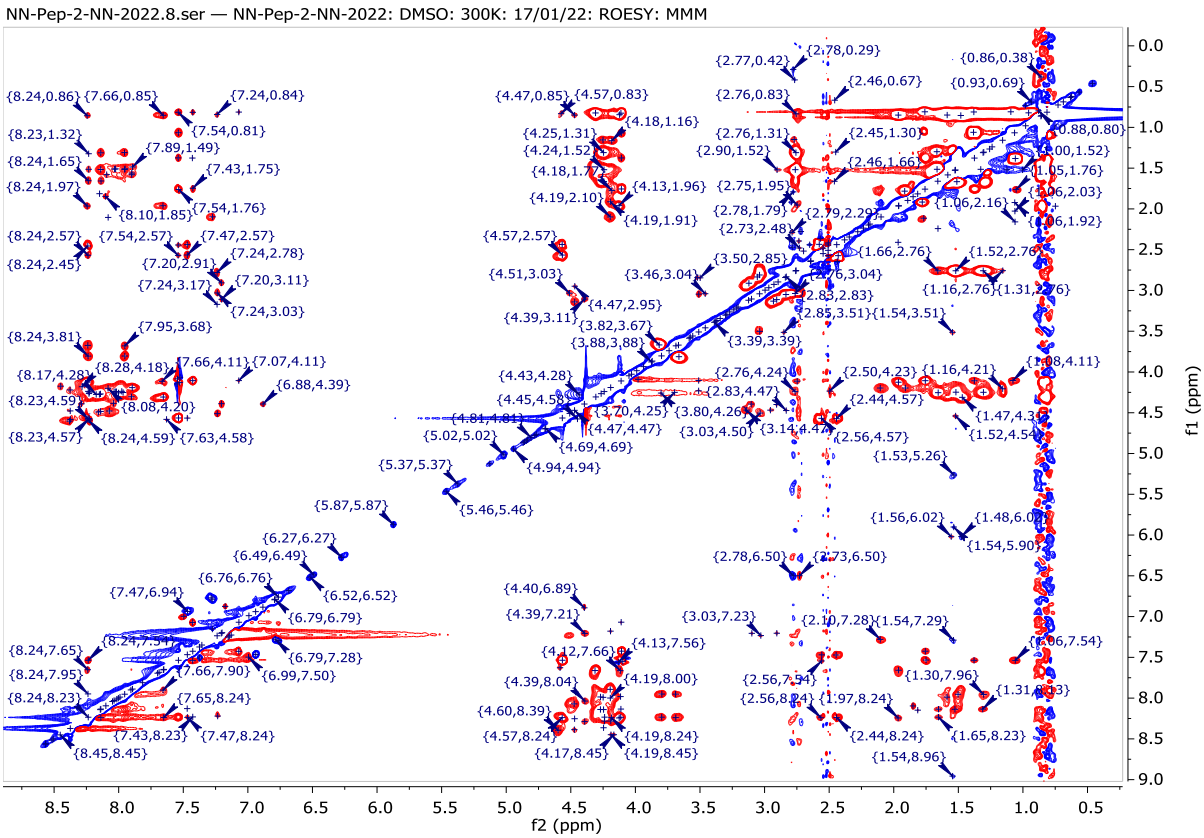

Figure S3-6: 2D [^{1}H, ^{1}H] ROESY NMR spectrum of Pep-2-NN

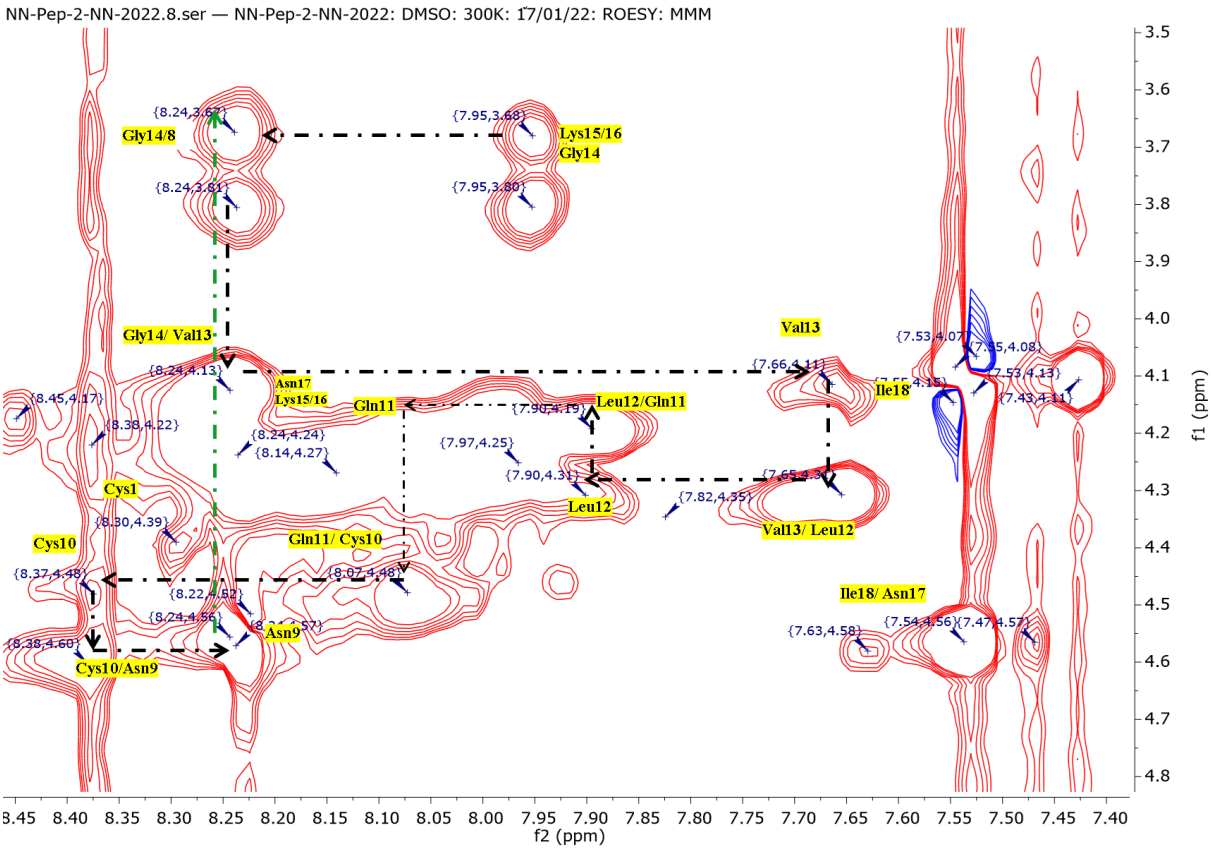

Figure S3-7: Sequential walk on 2D [1H, 1H] ROESY NMR spectrum of Pep-2-NN

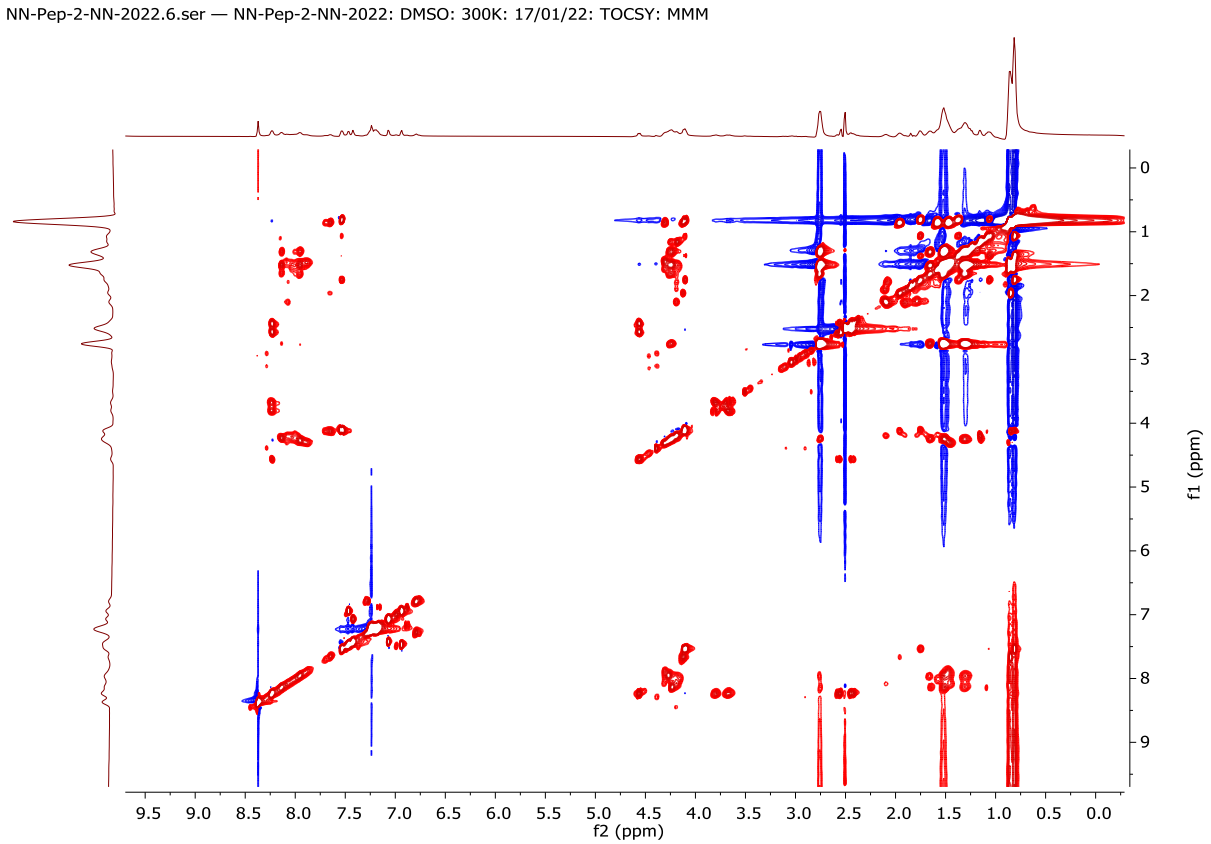

Figure S3-8: 2D NOESY NMR spectrum of Pep-2-NN

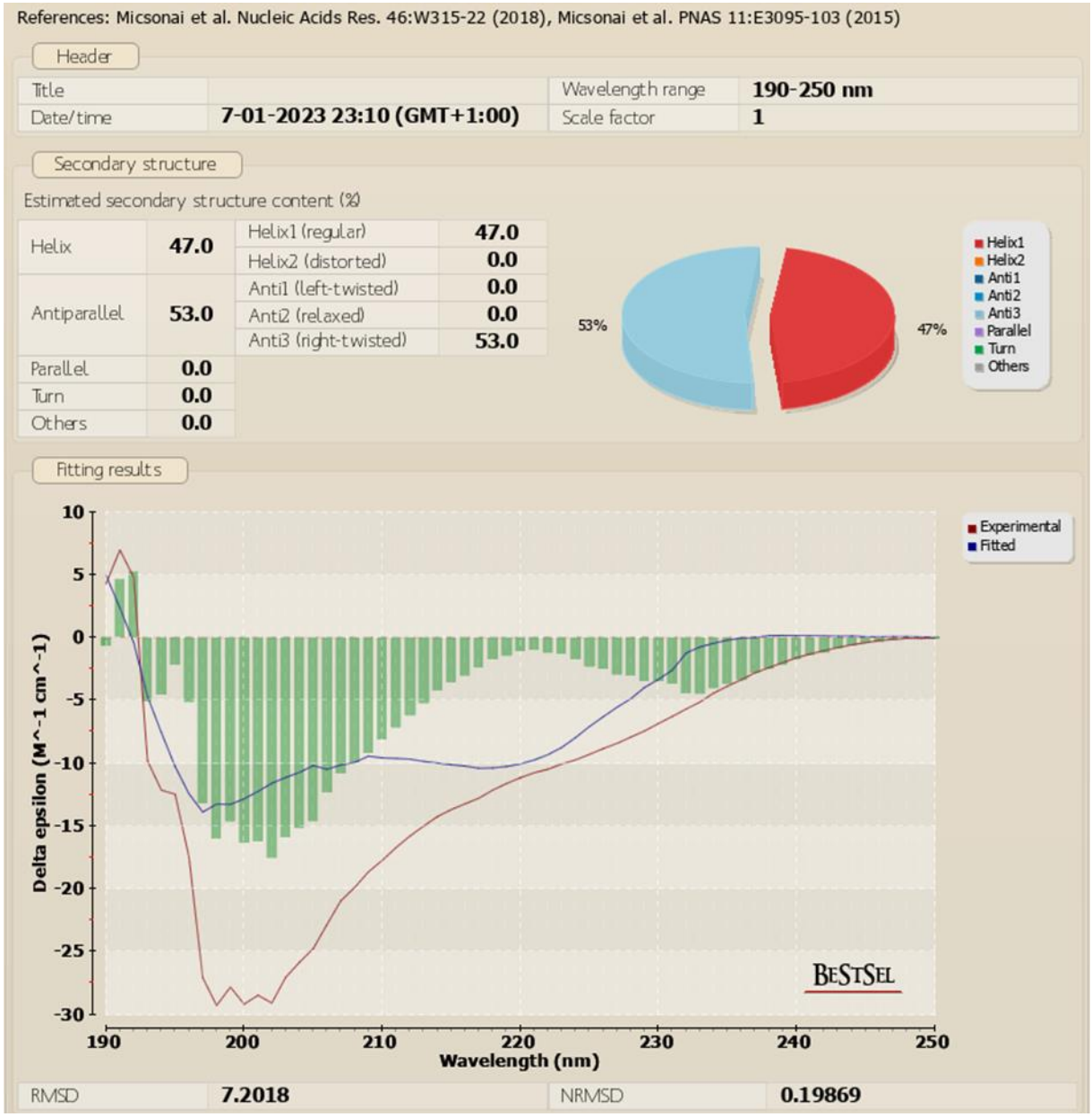

Figure S3-9: CD spectrum of Pep-2-NN-2

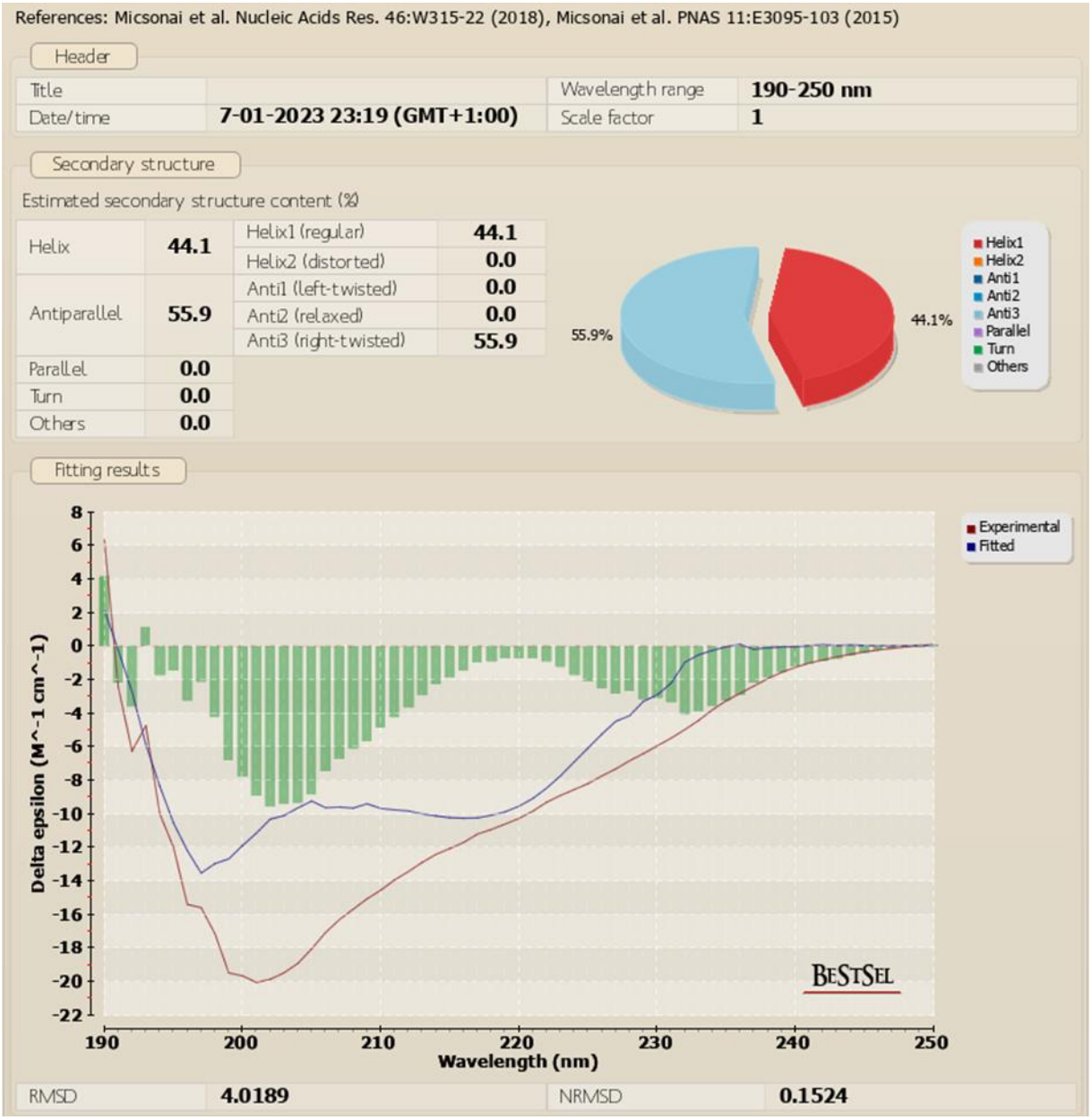

Figure S3-10: CD spectrum of Pep-2-NN-3

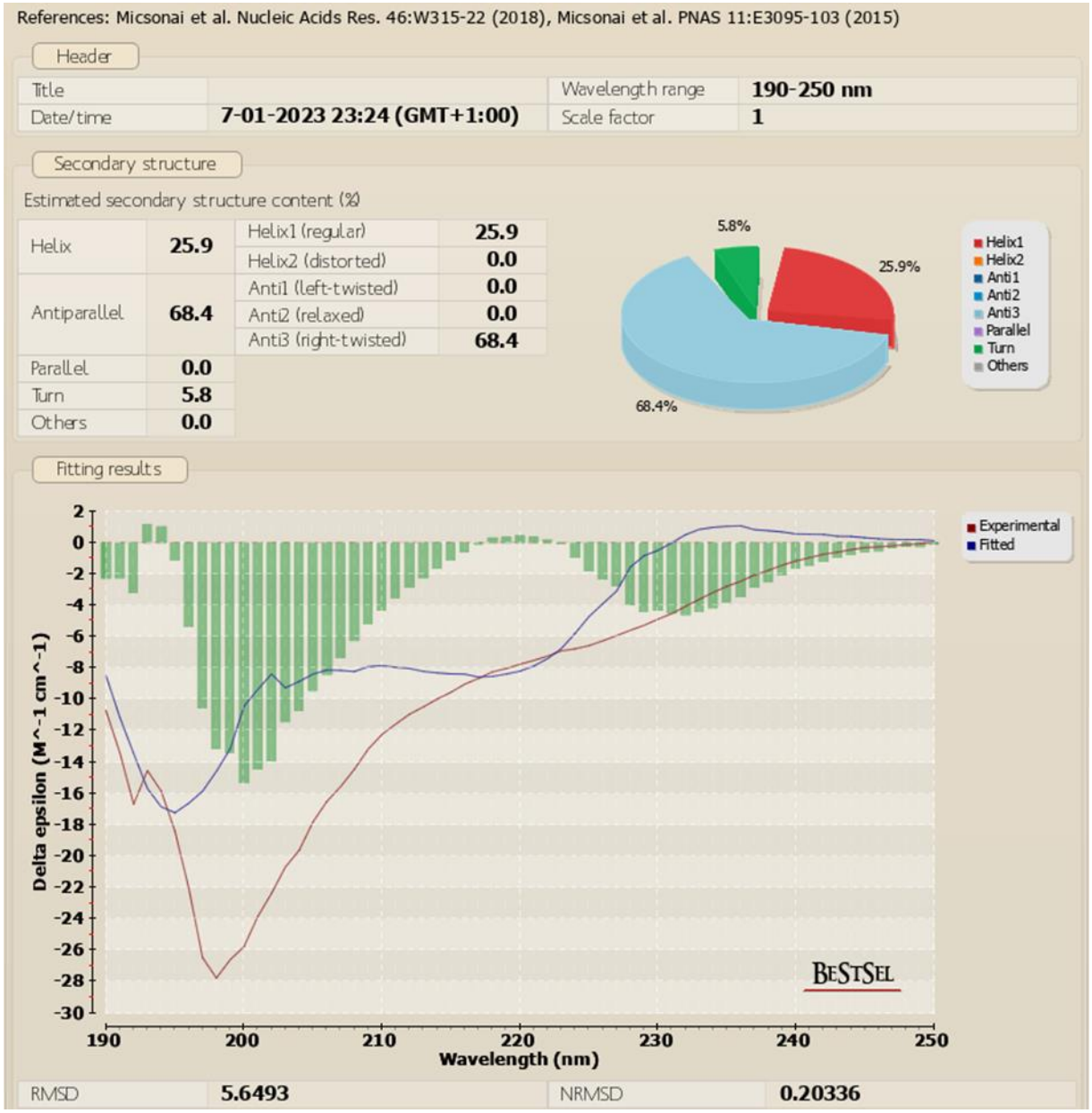

Figure S3-11: CD spectrum of Pep-Lys-NN

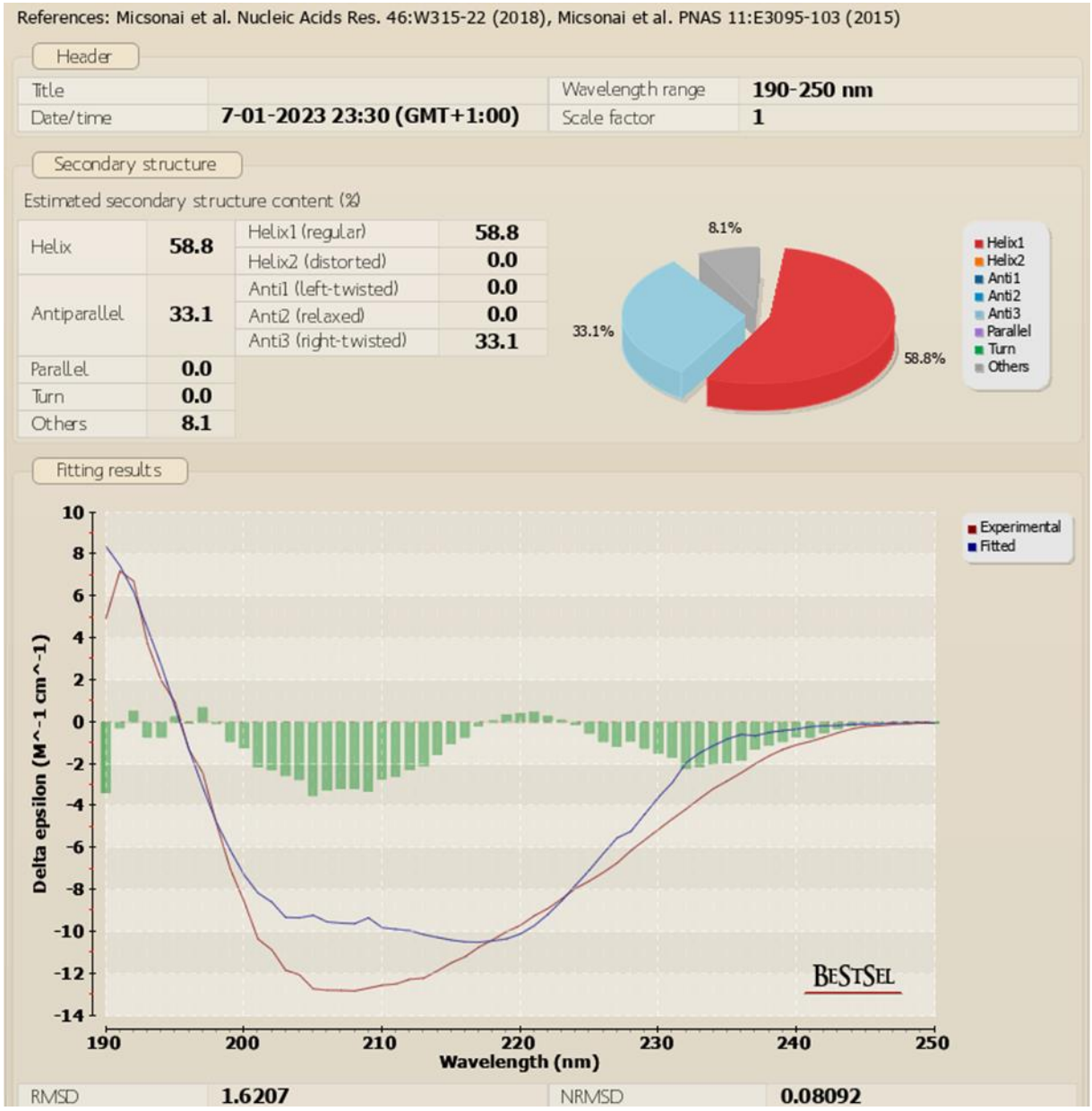

Figure S3-12: CD spectrum of Ring-2-NN